Modelling Heat Transfer during Chilling and Freezing of Packaged Foods in Industrial Refrigeration Facilities

A thesis

submitted in partial fulfilment

of the requirements for the degree

of

Doctor of Philosophy in Engineering

at

The University of Waikato

by

DUY HOANG

THE UNIVERSITY OF
WAIKATO
Te Whare Wānanga o Waikato

2020

ABSTRACT

Industrial refrigeration equipment companies are continuously looking for ways to optimise the design of chilling and freezing tunnels in order to minimise food quality loss and increase the energy efficiency of the equipment. However, possibilities for dedicated experimental tests of the industrial operations are limited due to a large amount of food product involved while the number of design variables to be considered is high. A cost-effective alternative to experiments is numerical modelling. The main goal of this research was to simulate heat transfer of packaged food products in a chilling and freezing tunnel. Computational fluid dynamics (CFD) models were developed to improve prediction in industrial cheese chilling and chicken freezing. The industrial cheese chilling model was developed based on six blocks of agar that mimic the product arrangement and airflow pattern of a cheese chiller; while the chicken freezing model represents the first case of a CFD freezing model where the geometry was derived empirically via computed tomography scan data. The model predictions were validated by experimental temperature histories generated as part of the study. Once validated, the model was used to investigate the cooling heterogeneity and the effect of different operating conditions on the processing time. In addition to the CFD model, a simple heat transfer simulation based on the one-dimensional finite difference method was developed for industrial users. Thermal property models in the literature were also reviewed to propose the most suitable choice for thermal processing calculations.

Acknowledgements

Firstly, I would like to thank my supervision team, without them I could not have completed this project:

- Dr. James Carson (Chief supervisor). Thanks James for your patience, encouragement, mentoring and always available to support me throughout my PhD journey.
- Dr. Simon Lovatt (Co-supervisor). Thank you for your invaluable advice and guidance which I am truly grateful for.
- Dr. Jamal Olatunji (Co-supervisor). Thank you for your valuable comments and suggestions. Your carefully and detailed reviewed helped improve the clarity of the text.

I would like to thank Shane Leath and Robert Wieliczko at AgResearch Ltd, Robert Kemp of Robert Kemp Consulting Ltd, and Ross Clarke and Dave Smitheram, both formerly at MilMeq, for your assistance and support when I conducted the experiments.

Thanks to the School of Engineering, Waikato University for providing me a great place to work.

I would like to thank Vietnamese government for their financial support

I would like to thank my parents, friends for their support and encouragement

My final and most heartfelt acknowledgement must go to my wife who takes care of my son on her own to let me focus on my PhD study. Thank you for your unconditional support and encouragement.

TABLE OF CONTENTS

Abstract i

Acknowledgements ii

List of Figures vii

List of Tables xii

Nomenclature xiv

1 Introduction 1

2 Literature review 4

2.1 Introduction 4

2.2 Modes of heat transfer during the forced-air chilling and freezing 4

2.3 Food properties 6

2.4 Modelling heat transfer of foods chilling and freezing 7

2.4.1 Analytical solutions 8

2.4.2 Empirical solutions. 9

2.4.3 Numerical solutions 12

2.5 CFD methodology. 14

2.5.1 Pre-processing 15

2.5.2 Solving 15

2.5.3 Post-processing 16

2.6 CFD modelling approach to simulate packaged products 16

2.6.1 Porous medium modelling 17

2.6.2 Direct computational fluid dynamics simulations 18

2.7 Application of CFD to foods chilling and freezing 18

2.8 Summary 21

2.9 Research objectives 23

3 Improved prediction of thermal property of foods 24

3.1 Introduction 24

3.2 Specific heat and enthalpy 24

3.2.1 Specific heat 24

3.2.2 Enthalpy 28

3.3. Thermal conductivity 29

3.3.1 Single-step method 29

3.3.2 Multi-step methods 31
3.4. Relative quantity of frozen water 35
3.5 Comparison of model predictions against measured data. 37
3.5.1 Enthalpy 37
3.5.2 Thermal conductivity 39
3.6. Conclusions 42
4 Numerical heat transfer model for industrial chilling installations. 43
4.1 Introduction 43
4.2 Experimental study 44
4.2.1 Objective 44
4.2.2 Experimental system 44
4.3 CFD model for six blocks of agar chilling 49
4.3.1 Introduction 49
4.3.2 Geometrical model 50
4.3.3 Transport phenomena and governing equations in the forced air cooling 50
4.3.4 Numerical setup 53
4.3.5 Results 56
4.3.6. Conclusion 62
5 A simple heat transfer simulation for the forced-air chilling of food products.. 63
5.1 Introduction 63
5.2 Experimental system 63
5.3 Numerical solution 66
5.4 Thermal properties and heat transfer coefficient model 70
5.5 Results 71
5.5.1 Comparison of measured and predicted product temperatures 72
5.5.2 Comparison of experimental and numerical cooling times 75
5.6 Conclusions 76
6 Experimental study on the forced air freezing of whole chicken and bulk packed chicken drumsticks 78
6.1 Introduction 78
6.2 The industrial chicken freezing 78
6.3 Experimental system 80
6.4 Experimental design 82

6.4.1 Temperature measurement 82
6.4.2 Air velocity and pressure measurement 87
6.5 Experimental procedure 87
6.6 Experimental results 88
6.6.1 Average temperature of chicken breast and chicken cavity per tray 88
6.6.2 Temperature profile of individual chickens within a tray 91
6.6.3 The cooling air temperature profile in the whole chicken freezing trials 95
6.6.4 The average temperature profile of chicken drumsticks per tray 96
6.6.5 Comparison of cooling rate between regular and irregular packing of drumsticks 97
6.6.6 Comparison of cooling times of regularly packed drumsticks with and without liner bag 98
6.6.7 Temperature profile of individual drumsticks within a tray..... 100
6.6.8 The cooling air temperature profiles in the chicken drumsticks freezing experiments 103
6.7 Conclusions 105
7 Numerical modelling of the forced air freezing of bulk packed whole chickens and chicken drumsticks 107
7.1 Introduction 107
7.2 Geometrical model 109
7.2.1 Reconstruction of bulk packed chicken products geometrical model. 109
7.2.2 The cardboard tray and the polyliner model..... 114
7.2.3 The completed computational domain 117
7.3 Mesh generation 118
7.4 Transport equations 123
7.5 Numerical model 125
7.5.1 Thermal properties of materials 125
7.5.2 Boundary and operating conditions 128
7.5.3 Numerical solution 128
7.6 Numerical model validations 129
7.6.1 Comparison of the numerical and measured average temperature history of chickens per tray. 130
7.6.2 Comparison of the numerical and measured SECT of a tray of chickens 132

7.6.3 Comparison of the numerical and measured temperature history of individual chickens within a tray. 133
7.6.4 Comparison of the numerical and measured average temperature history of chicken drumsticks per tray. 136
7.6.5 Comparison of the numerical and measured SECT of a tray of drumsticks 139
7.6.6 Comparison of the numerical and measured temperature histories of individual drumsticks within a tray. 140
7.7 Analysis 142
7.7.1 Temperature distribution 142
7.7.2 Airflow distribution 144
7.7.3 Effect of operating conditions on freezing time 146
7.8 Conclusions 148
8 General conclusions and future study 150
8.1 General conclusions 150
8.2 Future study 153
9 References 155
Appendices 167
Published papers 167

List of Figures

Figure 3.1 Plots of two different relative quantity of frozen water models (Eqs 3.34 and 3.35) with T_f = 272.15K, x_p = 0.2, x_{wo} = 0.75 36
Figure 3.2: Comparision between experimental data (Pham et al., 1994) and enthalpy predictions for lean lamb 38
Figure 3.3. Comparison between experimental data (Willix et al., 1998) and the thermal conductivity predictions for lean beef..... 39
Figure 3.4: Comparison between thermal conductivity data (Cogné et al., 2003) and predictions of Dul'nev and Novikov's model for ice-cream. The predicted results depict in the lines and the experimental data depict in the points. 42

Figure 4.1 The industrial cheese chilling tunnel (photo courtesy of Milmeq)..... 44
Figure 4.2 a) Products arrangement in the industrial cheese chiller. b) Experimental domain 45
Figure 4.3: Six blocks of agar arrangement 46
Figure 4.4: a) Polystyrene Test Tunnel and b) the transition section 47
Figure 4.5: Thermocouples position in the six blocks of agar chilling trials (not to scale) 47
Figure 4.6: The process of inserting a multi-thermocouple probe in a block of agar: a) half-full block of agar, b) full block of agar in a plastic box..... 48
Figure 4.7: Image of a surface temperature's thermocouple..... 48
Figure 4.8: a) DANTEC anemometer and b) inclined fluid manometer 49
Figure 4.9: The computational domain of the six blocks agar chilling 50
Figure 4.10: Comparison between predicted and experimental temperature of two tested blocks at the inlet velocity of 1 m s^{-1} 57
Figure 4.11: Comparison between predicted and experimental temperature of two tested blocks at the inlet velocity of 3 m s^{-1} 57
Figure 4.12: Comparison between predicted and experimental temperature of two tested blocks at the inlet velocity of 4.5 m s^{-1} 58
Figure 4.13: *SHTC* of two test blocks of agar at the inlet air velocity of 4.5 m s^{-1}60
Figure 4.14: Temperature difference of the two test blocks at the same positions at the inlet air velocity of 4.5 m s^{-1} 61

Figure 4.15: Temperature distribution for a) vertical symmetry plane and b) horizontal symmetry plane of the two test blocks agar after 4.5 hours (half cooling time) at the velocity inlet of 4.5 m s^{-1} 62

Figure 5.1: Experimental system for a single block of agar chilling..... 64
Figure 5.2: The modified PTT with a transition section for the single block of agar experiment..... 64
Figure 5.3: a) The test sample, and b) a single block of cheese in the chilling tunnel..... 65
Figure 5.4: Thermocouples position in the single block of cheese chilling trial... 66
Figure 5.5: The finite different scheme..... 68
Figure 5.6: "Prognosis-correction" regime to determine T_{ij} 70
Figure 5.7: Plots of the temperature predictions of CFM, FPM with experimental data for a single block of cheese at the inlet velocity of 1.0 m s^{-1}..... 73
Figure 5.8: Plots of the temperature predictions of CFM, FPM with experimental data for a single block of cheese at the inlet velocity of 4.4 m s^{-1}..... 73
Figure 5.9: Plots of the temperature predictions of CFM, FPM with experimental data for a single block of agar at the inlet velocity of 1 m s^{-1} 74
Figure 5.10: Plots of the temperature predictions of CFM, FPM with experimental data for a single block of agar at the inlet velocity of 4 m s^{-1} 74

Figure 6.1: Typical trays used by the chicken processors (photo courtesy of Milmeq)..... 79
Figure 6.2: Chicken on the conveyors before entering the freezing tunnel (photo courtesy of Milmeq)..... 79
Figure 6.3: A typical freezing tunnel configuration (photo courtesy of Milmeq). 80
Figure 6.4: Experimental system for chicken freezing trials 80
Figure 6.5: Close fit of the transition section to the original tunnel: a) front view, b) back view, c) inside the PTT..... 81
Figure 6.6: The cardboard tray in the chicken freezing trials: a) without polyliner, b) with polyliner. 81
Figure 6.7: Chickens arrangement in a tray a) excluding and b) including the thermocouples..... 83
Figure 6.8: The completed chicken tray for freezing trials..... 84

Figure 6.9: Bulk packed chicken drumsticks arrangements: a) regularly arranged drumsticks with liner bag, c) randomly arranged drumsticks with liner bag, c) regularly arranged drumsticks without liner bag..... 85
Figure 6.10: Chicken drumsticks distribution: a) the bottom and second layer, b) the third and top layer 86
Figure 6.11: Thermocouple placement in chicken drumsticks 87
Figure 6.12: The plots of average temperature per tray of chicken breast and chicken cavity during the freezing trial at three tested air velocities. Error bars indicate standard deviation..... 90
Figure 6.13: Comparison of experimental chicken breast and chicken cavity temperature of individual chicken in the freezing experiment at the inlet air velocity of 2.5 m s^{-1}. Error bars indicate experimental uncertainty 93
Figure 6.14: The maximum temperature difference profiles of chicken breast and chicken cavity within a tray..... 94
Figure 6.15: The cooling air temperature profiles in whole chicken freezing experiments a) at the air velocity of 1 m s^{-1}, b) at the air velocity of 2.5 m s^{-1} and c) at the air velocity of 4.5 m s^{-1} 96
Figure 6.16: Average temperature profiles of chicken drumsticks per tray in the regular arrangement freezing experiments..... 97
Figure 6.17: Cooling histories of regularly packed and randomly packed drumsticks at different air velocities..... 98
Figure 6.18: Cooling histories of regularly packed drumsticks with and without the liner bag..... 99
Figure 6.19: Cooling profile of individual drumsticks within a tray in freezing experiment at the inlet air velocity of a) 1.0 m s^{-1}, b) 2.5 m s^{-1} and c) 4.3 m s^{-1}. 102
Figure 6.20: The maximum differences in temperatures between individual chicken drumsticks within a tray at different air velocities. 103
Figure 6.21: The cooling air temperature profiles in regular packed drumsticks freezing experiments a) at the air velocity of 1 m s^{-1}, b) at the air velocity of 2.5 m s^{-1} and c) at the air velocity of 4.3 m s^{-1} 105

Figure 7.1: Scanning process of a chicken tray..... 110
Figure 7.2: Surface reconstruction model of whole chickens a) top view, b) perspective view, c) left side view and d) front view 111

Figure 7.3: Surface reconstruction model of bulk packed chicken drumsticks a) top view, b) perspective view, c) right side view and d) front view 111
Figure 7.4: The workflow to create a 3D model from CT images 112
Figure 7.5: Geometrical model of bulk-packed whole chickens..... 113
Figure 7.6: Geometrical model of bulk packed chicken drumsticks 113
Figure 7.7: Photo of a) the real, and b) the geometrical model construction of the cardboard tray..... 114
Figure 7.8: a, c) a real tray of whole chickens, b) top view and d) isometric view of 3D model of a tray of chicken containing polyliner..... 116
Figure 7.9: a, c) a real tray of drumsticks, b) top view and c) isometric view of 3D model of a tray of drumsticks containing polyliner..... 116
Figure 7.10: Computational domain of a) bulk-packed whole chickens, b) chicken drumsticks in the forced-air freezing model 118
Figure 7.11: a) Mesh of the chickens and air region inside the polyliner b) gap between chickens and polyliner..... 121
Figure 7.12: a) Mesh of the drumstick and air region inside the polyliner b) gap between drumsticks and polyliner 122
Figure 7.13: Position of virtual breast sensors in chicken model..... 130
Figure 7.14: Predicted and experimental average temperature of chicken breast and chicken cavity at the air velocity of a) 1 m s^{-1}, b) 2.5 m s^{-1} and c) 4.5 m s^{-1} 132
Figure 7.15: Predicted and experimental temperature history of individual a) chicken breasts and b) chicken cavities at the air velocity of 1 m s^{-1}. The numerical temperatures are depicted in red continuous lines; measured values are depicted in blue dash lines 134
Figure 7.16: Predicted and experimental temperature history of individual a) chicken breasts and b) chicken cavities at the air velocity of 2.5 m s^{-1}. The numerical temperatures are depicted in red continuous lines, measured values are depicted in blue dash lines 135
Figure 7.17: Predicted and experimental temperature history of individual a) chicken breasts and b) chicken cavities at the air velocity of 4.5 m s^{-1}. The numerical temperatures are depicted in red continuous lines, measured values are depicted in blue dash lines 136
Figure 7.18: Position of virtual sensors in the drumstick model..... 137

Figure 7.19: Predicted and experimental average temperature of chicken drumsticks per tray at the air velocity of a) 1 m s^{-1}, b) 2.5 m s^{-1} and c) 4.3 m s^{-1}. The numerical temperatures are depicted in red continuous lines, measured values are depicted in blue dash lines. 139
Figure 7.20: Predicted and experimental temperature history of individual drumsticks within a tray at the air velocity of 1 m s^{-1}. The numerical temperatures are depicted in red continuous lines, measured values are depicted in blue dash lines 140
Figure 7.21: Predicted and experimental temperature history of individual drumsticks within a tray at the air velocity of 2.5 m s^{-1}. The numerical temperatures are depicted in red continuous lines, measured values are depicted in blue dash lines 141
Figure 7.22: Predicted and experimental temperature history of individual drumsticks within a tray at the air velocity of 4.3 m s^{-1}. The numerical temperatures are depicted in red continuous lines, measured values are depicted in blue dash lines 141
Figure 7.23: a) Location of vertical and horizontal cross-sectional area b) temperature distribution on chicken surfaces, temperature contour along the c) vertical cross-sectional area and d) horizontal cross-sectional area. Results were taken at the air velocity of 2.5 m s^{-1} after 13 hours freezing (average HCT)..... 143
Figure 7.24: a) Location of vertical and horizontal cross-sectional area b) temperature distribution on drumstick surfaces, temperature contour along the c) vertical cross-sectional area and d) horizontal cross-sectional area. Results were taken at the air velocity of 2.5 m s^{-1} after 13 hours freezing (average HCT)..... 144
Figure 7.25: Contour along the vertical plane of airflow in the wind tunnel for the drumstick model at the inlet air velocity of 2.5 m s^{-1} 145
Figure 7.26: Contours along the vertical plane of airflow inside the liner bag of a) chicken model and b) drumstick model. Results were taken at the air velocity of 2.5 m s^{-1} after 13 hours freezing (average HCT) 145
Figure 7.27: Effect of operating conditions on freezing time of bulk-packed whole chickens..... 147
Figure 7.28: Effect of operating conditions on freezing time of bulk-packed drumsticks 147

List of Tables

Table 1.1 Number of refrigeration systems in operation worldwide in food preservation application (Du-pont, 2019) 2

Table 3.1: Specific heat capacity and density of major food components as a function of temperature T (°C) (-40 ⩽ T ⩽ 150°C) (Choi & Okos, 1986) 26
Table 3.2 Thermal conductivities and densities of major food components as a function of temperature T (°C) (-40 ⩽ T ⩽ 150°C) (ASHRAE, 2006; Carson, 2011; Choi & Okos, 1986) 31
Table 3.3 Comparision of the mean absolute relative errors between predicted and experimental enthalpy data (Pham et al., 1994) of foods over temperature ranged from -40°C to 40°C. 38
Table 3.4 Comparison of the absolute relative errors between predicted and experimental thermal conductivity values (Willix et al., 1998) for non-porous foods 40
Table 3.5 Comparison of the absolute relative errors between predicted and experimental thermal conductivity values for ice cream (Cogné et al., 2003)..... 41

Table 4.1: Material thermo-physical properties 53
Table 4.2. Effect of different mesh size on average *SHTC* of two test blocks of agar. 55
Table 4.3: Mean absolute temperature difference at different locations and testing conditions. 59

Table 5.1 Thickness of packaging materials and air gap. 71
Table 5.2 The calculated heat transfer coefficient and Biot number for each experiment 72

Table 6.1: The SECT of a tray of chicken in a freezing trial at different air velocities 91
Table 6.2: Experimental SECT of the tray of drumsticks 99

Table 7.1: Element size in the whole chicken model and drumstick model 118

Table 7.2: Effect of different mesh size on the volume-average temperature of chicken after 20 hours freezing in the chicken model 119
Table 7.3: Effect of different mesh size on the volume-average temperature of drumstick after 20 hours freezing in the drumstick model 119
Table 7.4 Thermal properties of air and packaging materials..... 126
Table 7.5: Comparison between predicted and experimental enthalpy data for whole chicken and chicken drumsticks. The experimental enthalpy data was obtained from Riedel (1957) 127
Table 7.6: Comparison between predicted and experimental thermal conductivity data for whole chicken and chicken drumsticks. The experimental thermal conductivity data was taken from Sweat et al. (1973)..... 127
Table 7.7 Experimental and predicted SECT of a tray of chicken at different air velocities 133
Table 7.8 Experimental and predicted SECT of a tray of drumsticks at different air velocities 139

Nomenclature

A	heat transfer area, m^2
Bi	Biot number
c	specific heat capacity, J kg^{-1} K^{-1}
C	volumetric heat capacity, J m^{-3} K^{-1}
D_H	hydraulic diameter, m
E	equivalent heat transfer dimensionality or shape factor
F	view factor
Fo	Fourier number
g	acceleration due to gravity, m s^{-2}
H	enthalpy, J kg^{-1}
k	thermal conductivity, W m^{-1} K^{-1}
L	characteristic length, m
L_f	latent heat of water solidification /fusion, J kg^{-1}
L_o	latent heat of fusion of water at 0°C = 333.6×10^3 J/kg^{-1}
M	molecular weight
x	mass fraction of food items
T	temperature, K or °C
Y	dimensionless temperature
v	volumetric fraction of food items
t	time, s
P	static pressure, Pa
Pr	Prandtl number
R	half-thickness of the shortest dimension, m
Ra	Rayleigh number
Re	Reynolds number
Gr	Grashof number
u	velocity, m s^{-1}
V	object volume, m^3
x	position, m

Greek letter

ω	relative quantity of frozen water
ρ	density, kg m^{-3}

δ	relative error
β	volumetric thermal expansion coefficient, K^{-1}
μ	dynamic viscosity, kg m^{-1} s^{-1}
v	kinematic viscosity, m^2 s^{-1}

Subscripts

a	air
ash	ash
b	bound water
CHO	carbohydrate
e	effective property
f	initial freezing point
fa	fat
F	freezing point
fi	fiber
i	i^{th} component
ice	ice
ME1	Maxwell-Eucken model with air is dispersed phase
ME2	Maxwell-Eucken model with air is continuous phase
p	protein
r	reference
w	water
wo	total water
s	solid
u,np	unfrozen, non-porous foods
f,np	frozen, non-porous foods

Chapter 1

Introduction

Refrigeration is crucial for the food sector because it ensures the preservation of perishable foodstuffs. The main food refrigeration processes include chilling and freezing. Competing with other preservation technologies such as salting, smoking, canning and drying, the application of chilling and freezing has several advantages. Firstly, they are the most satisfactory methods for preserving the quality of fresh foods during long storage periods (Arthey, 1993), and secondly they are some of the most flexible and easiest to implement processes with a wide variety of equipment for several different food products.

The refrigerated food market is one of the largest and most dynamic sectors of the food industry. In developed countries, the annual consumption of frozen food is about 50 kg for each person (IIR, 2013). Valued at USD 219.9 billion in 2018, the frozen-food market is expected to grow 30% by 2023 (Markets and Markets, 2018). Currently, there are around 5 million refrigerated vehicles in service worldwide, including vans, trucks, semi-trailers or trailers (Cavalier & Tassou, 2011). Furthermore, the volume dedicated to cold storage in the world accounted for 616 million m^3 in 2018, representing around 50,000 cold stores with an increase of 34% over 2012 (Salin, 2018). In order to illustrate the importance of refrigeration in food preservation, Table 1.1 summarises the number of refrigeration systems in operation worldwide in this application (Du-pont, 2019).

However, the food cold chain requires further development as food waste and resulting economic loss is still significant (Du-pont, 2019). According to the International Institute of Refrigeration (IIR), nearly 20% of the global food supply is lost due to the absence of refrigeration (IIR, 2009). The FAO estimates that food production will have to increase globally by 50% from 2012 to 2050 (FAO, 2018) and refrigeration plays a vital role in reducing food wastage.

Table 1.1 Number of refrigeration systems in operation worldwide in food preservation application (Du-pont, 2019)

Sector	Equipment	Number of units in operation
Domestic refrigeration	Refrigerators and freezers	2 billion
Commercial refrigeration	Commercial refrigeration equipment (including condensing units, stand-alone equipment and supermarket systems)	120 million
Refrigerated transport	Refrigerated vehicles (vans, trucks, semi-trailers or trailers)	5 million
	Refrigerated containers ("reefers")	1.2 million
Refrigerated storage	Cold stores	50,000

Two key performance parameters for refrigeration processes are the time required for the product to cool to the target temperature, and the quantity of energy required. Currently, the design of refrigeration equipment is based heavily on experience, while some designers also make use of modelling software. A reliable heat transfer model can be of considerable help in optimising a process and investigating the consequences of design changes (James, Ketteringham, Palpacelli, & James, 2009)

The industrial partner of this project is Milmeq Ltd. (now part of H&C Automated Solutions), a refrigeration equipment design and build company providing chilling and freezing equipment to food producers around the world. It designs and builds chilling and freezing tunnels incorporating both single retention time (SRT) tunnels and multiple retention time (MRT) tunnels. The design process for these products is based on a mix of experience and refrigeration model predictions from Food Product Modeller™ (FPM), software that us used to evaluate chilling, freezing, thawing and heating processes for a variety food products (MIRINZ). Milmeq Ltd approached the University of Waikato with the desire to increase their modelling capability, particularly with regards to airflow behavior within the refrigerated space and the effects of void spaces within the packaging on cooling rates.

The aim of this research is to simulate heat transfer not only in the packaged product itself but also in the airspace, the pallet, and the support structures. Heat transfer throughout the entire refrigeration space will be modelled rather than simply within the food product with a single layer of packaging, which is a limitation of FPM. The simulated results can provide a fundamental understanding of local airflow and energy transport mechanisms within packages, information that can be used for optimising the design of chilling and freezing tunnels.

Two case studies chosen for this research were cheese chilling and chicken freezing. Cheese accounts for one-third of New Zealand dairy export earnings and contributes to around 8% of GDP (DCANZ, 2018). In 2018, New Zealand cheese production was 385,000 tons, of which 322,000 tons (84%) was exported valued at NZ$ 1.9 billion (Lee-Jones, 2019). Chicken meat is today the most consumed meat in New Zealand. It overtook beef as the country's number one animal protein in the late 1990s and its consumption has increased dramatically since then. Today, the average New Zealander eats close to 40 kg of chicken meat each year – over twice the amount consumed 20 years ago (Stafford, 2017). In the past decade, New Zealand chicken meat exports have grown from almost nothing to over NZ$100 million in 2016 (MBIE, 2017).

This study will develop a heat transfer model for cheese chilling and chicken freezing, with a focus on the effect of airflow behavior in the large-scale cheese chilling system and effects of air voids within chicken packages on cooling and freezing rate. These factors have been identified as the greatest sources of uncertainty facing designers of industrial refrigeration equipment, such as Milmeq Ltd.

Chapter 2
Literature review

2.1 Introduction

This literature review begins with a review of modes of heat transfer and modelling techniques in foods chilling and freezing, and the food properties input to the heat transfer model. Next, two computational fluid dynamic (CFD) modelling approaches, including porous medium modelling and direct modelling are considered with an emphasis on advantages and disadvantages of each approach and the suitability of each for the modelling work of this research. An overview of CFD applications is presented and current knowledge gaps are identified and discussed. Finally, the specific research aims of the thesis are presented.

2.2 Modes of heat transfer during the forced-air chilling and freezing

Heat transfer between a food product and its environment can occur in several ways, namely conduction, convection and radiation. Within solid bodies, heat transfer is described by Fourier's conduction equation (Cengel & Ghajar, 2011):

$$\rho c \frac{\partial T}{\partial t} = \nabla \left(k_s \nabla T \right) + q_v \tag{2.1}$$

where ρ (kg m^{-3}) is the density, c (J kg^{-1} K^{-1}) is the specific heat capacity, k_s (W m^{-1} K^{-1}) is the thermal conductivity of food, T (K) is the product's temperature, t (s) is time and q_v (W m^{-3}) is the volumetric heat generation.

Heat transported towards the product surface is then carried away by convection and radiation. The energy balance at the product surface is given by Eq. 2.2:

$$-k_s \frac{\partial T}{\partial n} = q_{conv} + q_{rad} \tag{2.2}$$

where q_{conv} and q_{rad} (W m^{-2}) are the convection and radiation heat fluxes respectively, and n is the outward normal to the product surface. The left-hand side of Eq. 2.2 is the conduction heat flux within the product.

Convection describes the heat transfer between a solid object (e.g. the food product) and a moving fluid (e.g. air). The rate of convection heat transfer is often expressed by Newton's Law of Cooling (Eq. 2.3) that incorporates the complexity of heat transfer through the boundary layer formed at the surface of an object by a single parameter *h*:

$$q_{conv} = h\left(T_s - T_a\right) \tag{2.3}$$

where h (W m^{-2} K^{-1}) is the convective heat transfer coefficient, T_s and T_a (K) are the product's surface and cooling air temperature.

The *h* value relates the heat flux normal at the food surface to the temperature difference between the fruit surface and a reference temperature, usually the refrigerated air temperature. Amongst other factors, the *h* value depends on the geometry of the product, the properties of the surrounding fluid, the flow pattern and the degree of turbulence (Pham, 2014). Several empirical Nusselt-Reynolds-Prandtl correlations exist to approximate the surface averaged *h* value as a function of food geometry, fluid velocity and product stacking pattern (Alvarez & Flick, 1999; Becker & Fricke, 2004). In these correlations, the food geometry is often assumed to be either spherical or cylindrical, or else specific shape factors are employed for other geometries. The stacking pattern in a package is typically assumed to be a packed bed organised according to a certain configuration (Alvarez & Flick, 1999). These correlations represent a surface-averaged *h* value estimation. However, the convective transfer coefficient is directly related to the local thickness of the boundary layer on the product surface. Thus, the *h* value varies with location on the food surface. Since food surfaces are often curved, flow separation can occur and a wake can develop. In these regions, the *h* value cannot be analysed analytically and must be calculated numerically (Kondjoyan, 2006).

All matter above absolute zero temperature emits electromagnetic waves from its surface via radiation to the surroundings (Datta, 2002), resulting in a transfer of energy. Compared to the other heat transfer mechanisms, radiation does not require a physical medium for its propagation (Singh & Heldman, 2009). Thermal radiation

emitted by a food product can be calculated with the Stefan-Boltzmann equation (Eq. 2.4):

$$q_{rad} = \sigma \varepsilon F \left(T_s^4 - T_a^4 \right) \tag{2.4}$$

where σ (W m^{-2} K^{-4}) is the Stefan-Boltzmann constant, $\sigma = 5.67 \times 10^8$ W m^{-2} K^{-4}, F is the view factor, and ε is the emissivity of the food product.

In addition to convection and radiation, heat can be extracted from the product surface by moisture evaporation. However, for cheese or chicken products encased within a polyliner, any moisture evaporated from surface can be assumed to condense back on cool surfaces within the polyliner. Therefore, the latent heats of evaporation and condensation of moisture are assumed to equal and opposite to each other providing no significant net contribution to the overall heat balance.

The total rate of heat transfer of fresh produce is a combination of the different heat transfer mechanisms discussed above. In general, it is assumed that conduction is the only significant mode of heat transfer within the food product while radiation and convection are assumed to occur at the product surface, essentially serving as boundary conditions for the conduction problem.

2.3 Food properties

Before the processing time and heat load can be calculated, thermal property data must be available as an input. The relevant physical properties of the food are enthalpy, specific heat, density and thermal conductivity. The selection of a suitable thermal property dataset is a key factor for obtaining accurate predictions of a heat transfer model. Tocci and Mascheroni (1994) investigated freezing times of a meat ball by a numerical method using three different sets of thermal properties. The authors concluded that a change in the thermal properties dataset made the average error between predicted freezing time and experimental data shift from -0.92% to 13.23%. With recent advances in numerical analyses, the accuracy of any model of a thermal process can be limited more by reliable thermal properties input data than by the model formulation or the solution process (Datta, 2007b).

Measured thermal property data is available from a number of sources for minimally processed foods such as meat, dairy and horticultural produce (ASHRAE, 2006; Houska et al., 1997; Houska et al., 1994; Rahman, 2009). However, when comparing data for similar foods measured by different authors, it is not uncommon to encounter conflicting and widely variable data, and the composition, origin, processing conditions, and structure of the foods are often not well documented (Carson, 2017; Kent et al., 1984; Nesvadba, 2005; Singh & Sarkar, 2005). This observation, coupled with the lack of data for many foods, particularly those which are highly processed, demonstrates the need for models that may be used to predict thermal properties from chemical composition data and temperature.

There are many thermal property models in the literature, particularly for predicting thermal conductivity; however, many of these are purely empirical, which can limit their range of applicability. Others have theoretical bases but contain empirical parameters whose values must be obtained by experimentation (Carson, Wang, North, & Cleland, 2016). A number of food engineering and refrigeration handbooks contain guidelines for thermal property prediction, such as (ASHRAE, 2006; Rahman, 2009; Rao, Rizvi, & Datta, 2005; Wang & Curtis, 2012); however, these focus more on providing a methodology for thermal property prediction than attempting to demonstrate that the models recommended for use are suitable for any particular purpose. Modelling the thermal properties of frozen foods in particular can be unreliable if unsuitable models are used, because the ratio of the thermal conductivity of frozen water to that of other component materials is relatively larger than the ratio of the thermal conductivity of unfrozen water to that of the other components and the uncertainty of the thermal conductivity prediction increases as the difference between thermal conductivities of the components increases (Carson, Lovatt, Tanner, & Cleland, 2006; Cheng & Vachon, 1969). Therefore, accurate thermal properties models are essential for a heat transfer model to produce a suitable prediction.

2.4 Modelling heat transfer of foods chilling and freezing

Many researchers have proposed different models to simulate heat transfer during chilling and freezing processes. These models can be divided into analytical, empirical and numerical solutions. The choice of technique depends on the

objectives of the modellers and the technical means at their disposal. Analytical techniques produce exact results provided their underlying assumptions are fulfilled, which is rarely the case. Their main usefulness is in providing benchmark results for the verification of other methods. Empirical formulas are derived with the objective of providing quick answers, requiring minimal computational power, with sufficient accuracy for most industrial users. These can be used only in situations similar to those used to derive and validate the empirical formulas. Numerical methods can, in principle, provide near-exact predictions for a wide variety of scenarios, although in practice their accuracy is limited by inadequate knowledge of the problem's parameters (product properties, geometry, flow characteristics; (Pham, 2008), as discussed in Section 2.3.

2.4.1 Analytical solutions.

For chilling of foods of simple, regular geometry with constant thermal properties, constant external conditions, uniform initial conditions, no internal heat generation, and only convection at the boundary, there are analytical solutions (Carslaw & Jaeger, 1959). For example, for an infinite slab geometry:

$$Y = \frac{T - T_a}{T_{in} - T_a} = \sum_{i=1}^{\infty} \frac{2\mathrm{Bi} \times \cos\left(\lambda_i \frac{r}{R}\right) \sin\left(\lambda_i\right)}{\mathrm{Bi}(\mathrm{Bi}+1)+\lambda_i^2} \exp(-\lambda_i^2 \mathrm{Fo}) \tag{2.5}$$

where λ_i are the roots of:

$$\lambda \tan \lambda = \mathrm{Bi} \tag{2.6}$$

$$\mathrm{Fo} = \frac{kt}{\rho c R^2} \tag{2.7}$$

$$\mathrm{Bi} = \frac{hR}{k} \tag{2.8}$$

and Y is the dimensionless temperature; T, T_i, T_a (K) are the product temperature, initial temperature and cooling air temperature, respectively; R (m) is the half-thickness of the slab; and r (m) is the distance from the center.

Newman (1936) showed that the solutions for regular, multidimensional objects can be obtained using the product rule. For example, for the three-dimensional rectangular brick shape, it is the product of the slab solutions in the three orthogonal dimensions:

$$Y = Y_x \,.\, Y_y \,.\, Y_z \tag{2.9}$$

For a high value of Fo (e.g., Fo > 0.2), Eq. 2.5 and the equivalents for infinite cylinders and sphere geometries can be simplified to the first term of the series.

For food freezing, an analytical solution is Plank's equation. For one-dimensional geometries, the equation to predict the time to freeze is:

$$t_f = \frac{V}{A_s R}\frac{L_f}{\left(T_f - T_a\right)}\left(\frac{R}{h} + \frac{R^2}{2k}\right) \tag{2.10}$$

where t_f (s) is the freezing time, V (m^3) and A_s (m^2) are volume and heat transfer area of the food item, T_f and T_a (K) are the initial freezing and cooling air temperatures, respectively, and L_f (J kg^{-1}) is the latent heat of freezing. The derivation of Plank's equation requires the following simplifications: unique phase change temperature, physical homogeneity, isotropic and regular shape, sensible heat effects are negligible relative to latent heat effects, constant heat transfer coefficient, h, and constant thermal conductivity, k. The net effect is that freezing time predictions are typically up to 50% too low (Wang, Pham, & Cleland, 2010).

2.4.2 Empirical solutions.

Empirical models can be obtained by carrying out a range of experiments in pilot plants where processing conditions can be accurately controlled. They involve some empirical parameters obtained by curve-fitting experimental data. This approach provides valuable data on the system performance but may lack a generalized theoretical description of the process. However, the experimental approach is indispensable in validating analytical solutions due to the simplifying assumptions that are required (Wang et al., 2010).

For chilling, empirical prediction approaches are grouped in two main categories: methods based on simplifying one-dimensional analytical solutions (Eq. 2.5) using *j* and *f* factors; and methods based on equivalent heat transfer dimensionality.

Many researchers have used the first term approximation of the infinite series analytical solutions, but these have limited the ranges of applicability (i.e. $Fo > 0.2$ and $Y < 0.7$). The prediction equation becomes (ASHRAE, 2006; Pham, 2002):

$$Y = j \exp\left(-2.303 \frac{t}{f} \right) \tag{2.11}$$

where t (s) is the cooling time, j (lag factor) is a measure of the lag between the onset of cooling and the exponential decrease in the temperature of the food, and f (s) is the time required to obtain a 90% reduction in the fractional unaccomplished temperature difference.

Equations are available for calculating j and f for basic shapes (slab, cylinder and sphere). Pflug (1965) plotted these solutions on a graph. Ramaswamy, Lo, and Tung (1982) and Lacroix and Castaigne (1987) gave approximate solutions that can be computed with a calculator.

For complex or irregular shapes, the most comprehensive methods is that of Lin et al. (1993, 1996a, 1996b). The formulas are long and involve many variables but are simple to implement on a spreadsheet.

Another empirical approach to predict cooling rate is using a shape factor called equivalent heat transfer dimensionality (E) to account for the geometry of food products (Cleland & Earle, 1982). The E compares the total heat transfer to the heat transfer through the shortest dimension. An expression for estimating E of irregularly shaped food items as a function of Biot number was also developed.

For freezing, most empirical freezing time prediction methods are based on Plank's analytical solution (Eq. 2.10) and attempt to correct its unfulfilled assumptions, in particular the non-zero sensible heats above and below the freezing temperature and

the gradual phase change (ASHRAE, 2006; Pham, 2006, 2014; Wang et al., 2010). Generally, these models include two contributions: the first one consists of a simple empirical correlation for one-dimensional shapes, while the second one considers the multi-dimensional geometrical parameter, using equivalent heat transfer dimensionality (*E*). Normally, the freezing time of a multi-dimensional object is calculated as the ratio of the freezing time of a reference simple geometry (typically an infinite slab) and *E* (Becker & Fricke, 1999).

The correlations to estimate the freezing time of one-dimensional shape product are usually referenced against the infinite slab, infinite cylinder and sphere, and they take into account the average thermal properties of the sample and the conditions (i.e. initial product temperature, cooling air temperature and heat transfer coefficient). One of the most popular methods is a modified Plank's equation developed by Pham (1986) which is accurate to within about ±15% for a wide range of freezing conditions and products (Wang et al., 2010):

$$t_f = \frac{V}{A_s R}\left[\frac{\Delta H_1}{\Delta T_1} + \frac{\Delta H_2}{\Delta T_2}\right]\left[\frac{R}{h} + \frac{R^2}{2k}\right] \tag{2.12}$$

where ΔH_1 (J m^{-3}) and ΔT_1 (K) are the heat released and temperature difference, respectively, for the precooling period, and ΔH_2 (J m^{-3}) and ΔT_2 (K) are those for the combined freezing and post-cooling period, calculated from:

$$\Delta H_1 = \rho c_u \left(T_{in} - T_{fm}\right) \tag{2.13}$$

$$\Delta H_2 = \rho L_f + \rho c_{ff} \left(T_{fm} - T_c\right) \tag{2.14}$$

$$\Delta T_1 = \frac{T_{in} + T_{fm}}{2} - T_a \tag{2.15}$$

$$\Delta T_2 = T_{fm} - T_a \tag{2.16}$$

T_{fm} (K) is the 'mean freezing temperature':

$$T_{fm} - 273.15 = 1.8 + 0.263\left(T_c - 273.15\right) + 0.105\left(T_a - 273.15\right) \tag{2.17}$$

Several models have been proposed to evaluate the equivalent heat transfer dimensionality (Cleland, Cleland, & Earle, 1987a, 1987b; Hossain, Cleland, &

Cleland, 1992a, 1992b, 1992c; Ilicali, Teik, & Shian, 1999; Pham, 1991; Salvadori, Mascheroni, & De Michelis, 1996). The most general equation for a three-dimensional irregular shape is (Hossain et al., 1992b):

$$E=1+\frac{1+2/\mathrm{Bi}}{\beta_1^2+2\beta_1/\mathrm{Bi}}+\frac{1+2/\mathrm{Bi}}{\beta_2^2+2\beta_2/\mathrm{Bi}} \tag{2.18}$$

$$\beta_1=\frac{A_{xs}}{\pi R^2} \tag{2.19}$$

$$\beta_2=\frac{3V}{4\pi\beta_1 R^3} \tag{2.20}$$

$$\mathrm{Bi}=\frac{hR}{k} \tag{2.21}$$

where A_{XS} (m^2) is the smallest cross-sectional area of the food object through the thermal center.

2.4.3 Numerical solutions

The analytical and empirical solutions are useful for situations that can be modelled by convection only at the surface, where h and T_a are constant, and where heat generation is negligible. They are most accurate for regular geometries. In other cases, the problems are best handled by numerical techniques. Numerical methods include finite difference, finite element and finite volume methods. Finite difference (FD) methods are only practical for regular geometries where an orthogonal rectangular grid can be used. Finite element (FE) and finite volume (FV) are easily applied to irregular geometries and foods with heterogeneous structures, which are the basis of most commercial packages designed. Further details about FD, FE and FV methods are provided by (James et al., 2009; Pham, 2006, 2014; Wang et al., 2010).

In the literature, a range of numerical models for the food chilling and freezing applications may be found. For chilling processes, Davey and Pham (1997) developed a multi-region finite-difference model to predict heat loss and weight loss of beef during air blast chilling. The irregular geometry was approximated by cylinders for the leg, rump and foreleg regions, and by slabs for the loin, ribs, shoulder and neck regions. Thermal properties were assumed to be independent of

temperature. The finite-difference model of Davey and Pham (1997) over-predicted the heat removed during the first 2 h of chilling by 12.6% on average. Davey and Pham (2000) introduced a more realistic representation of the beef side using a multi-layered two-dimensional finite element model of a carcass during chilling. Thermal properties were homogenized across the sections. The accuracy of the finite element model was superior to that of the finite difference model developed earlier (Davey and Pham (1997)), with an added advantage that it could predict local temperatures, including surface temperatures.

Wang and Sun (2002) developed a three-dimensional finite element model for rectangular, brick-shaped roasted meat during air blast cooling. The model included the variation in physical properties of meat and operating conditions. Temperature profiles and product weight loss were predicted by this model.

Campañone, Giner, and Mascheroni (2002) developed a generalized numerical model using a finite difference scheme for regularly shaped food refrigerated in air. The model took into account surface water evaporation, and thermal properties were modeled as functions of temperature and composition.

Numerical methods for freezing may be designed to deal with variation in thermal properties, particularly thermal conductivity and specific heat. Huan, He, and Ma (2003) used the finite element method to analyse the freezing of foods. The apparent specific heat method was used to account for the enthalpy of phase change during freezing. The authors highlighted that the food shape and size, freezing air temperature and freezing air velocity are the important factors affecting the freezing rate. Mannapperuma, Singh, and Reid (1994a, 1994b) used a finite difference method based on enthalpy formulation (Mannapperuma & Singh, 1988) to simulate air blast freezing of whole chickens and chicken parts individually and in packages. The experimental temperature histories were compared with simulated results to estimate surface heat transfer coefficients. Fikiin (1996) presented a quasi-one-dimensional numerical solution of unsteady heat transfer during the freezing process. The enthalpy method and the Kirchhoff function were used to deal with the variable specific heat and thermal conductivity. The enthalpy-Kirchhoff approach was also used by Santos, Vampa, Califano, and Zaritzky (2010) to model

the freezing of bakery products. The finite element scheme was used for the spatial discretization. Perussello, Mariani, and do Amarante (2011) developed a finite-difference model to solve the transient heat conduction equation, transformed by the enthalpy and Kirchhoff functions. Food thermal properties were modeled as a function of composition and temperature.

All the above-mentioned works on numerical simulation relied on the implementation of original models by the authors. Given the complexity of the heat transfer phenomena occurring, the models are relatively complex, and their implementation often requires top-level expertise in the field of applied mathematics. This requirement is very frequently not compatible with regular skills of designers of refrigeration equipment.

Another option is the use of commercial numerical simulation packages including computational fluid dynamics (CFD) packages. The CFD approach offers the possibility of coupling the heat transfer inside products with the heat transfer in the surrounding environment, allowing a detailed local analysis of heat transfer phenomena. The development of user-friendly interfaces makes these software packages more straightforward to use, provided that the simulation approach is properly implemented and adapted to the particular case study. Furthermore, the increased calculation speed of modern processors has made the use of commercial CFD packages with personal computers more feasible.

2.5 CFD methodology.

CFD is a computer-based simulation tool for analysing fluid flow and heat transfer problems. The governing equations in CFD simulations are the mathematical formulations of the conservation of mass, momentum and energy which are referred to as the Navier-Stokes equations. In order to provide easy access to their solution power, many commercial CFD packages include sophisticated user interfaces to input problem parameters and to examine the results. Hence, all codes contain three main elements: (i) pre-processing, (ii) solving and (iii) post-processing (Versteeg & Malalasekera, 2007).

2.5.1 Pre-processing

Pre-processing includes determining the computational domain, mesh generation, and definition of material properties and boundary conditions. The computational domain represents the object under investigation. The designer must be fully aware of the physics of the problem and the factors which can influence the airflow. For example, when modelling the forced air chilling of packaged foods, the upstream and downstream sections must be large enough to avoid an influence of the boundary conditions at the inlet and outlet on the airflow in the proximity of the food package. On the other hand, the size of the computational domain can be reduced based on symmetries or periodicity, thereby reducing the computational cost.

Once defined, the computational domain is subdivided into elements to create the 'mesh' for computation. This stage of the process is very important since the reliability of a CFD simulation depends on the size of these elements (the solution is 'gird dependent') (Smale, Moureh, & Cortella, 2006; Zhao, Han, Yang, Qian, & Fan, 2016). As the size of elements decreases, the accuracy of the solution, the computational time and memory requirements all increase. Therefore, an optimal mesh must be achieved to compromise between the calculation accuracy and computational cost.

The properties of the fluids and of the solids involved in the simulation must be specified, the boundary conditions at each interface must be defined, and the initial conditions for all the variables must be provided. Boundary and initial conditions are the constraints applied on the governing equations. They connect the model with the surrounding environment. Inappropriate boundary and initial conditions can lead to misleading results.

2.5.2 Solving

Solving involves using a numerical method to solve the governing equations. The first step of the numerical algorithm is to discretize the governing equation over the mesh to obtain a system of algebraic equations. The discretization scheme can be

finite difference, finite element or finite volume. The finite volume method has become widely used among CFD codes because of its ease of understanding and programming and its high computation efficiency (Norton & Sun, 2006; Versteeg & Malalasekera, 2007; Zhao et al., 2016). The next step is to solve the algebraic equations. The underlying physical phenomena are complex and non-linear, so an iterative solution approach is required. The most popular solution procedure is the SIMPLE algorithm, which ensures correct linkage between pressure and velocity. However, to enhance convergence rates, some improved methods have been proposed, such as SIMPLEC, SIMPLER, and PISO. A comprehensive description of these methods was presented in (Versteeg & Malalasekera, 2007). Calculations continue until a specified accuracy is achieved, usually quantified by evaluating the residuals in the balance of one or more variables (i.e. mass, energy etc.). At this point, the solution is said to converge.

2.5.3 Post-processing

A post-processor is used to analyse the data generated by CFD simulations. Typically, the simulation results can be presented in the form of temperature and velocity maps, vector plots of the velocity field, contour plots of other scalar variables, and animations. In addition to graphics, most CFD packages allow the field data to be exported to third-party software, where they can be further processed.

2.6 CFD modelling approach to simulate packaged products

The goal of this research project is to model forced air chilling and freezing processes of packaged products. Taking into account airflows around and inside packages, complex geometries and spatially-variable properties, developing a model of such a composite domain is a difficult challenge (Smale et al., 2006). The main obstacle that has limited many previous models is the determination of the airflow behaviour around food products; information that is required to determine the values of the local heat transfer coefficients and the local air temperature around each product item. Even in the case of uniformly distributed products, the measurement of the fluid flow within packages using traditional methods is impossible without disturbing the packaging arrangement itself (Ferrua, 2007)

There are two main CFD approaches that have been applied to model packaged food: the porous medium approach and the explicit modelling approach. A brief description of each of these modelling approaches is given below.

2.6.1 Porous medium modelling

A porous medium is a solid matrix with interconnected pores or void spaces, through which a fluid (typically air) can flow. Representing a food package as a porous medium removes the need to account for the complex physical structures when modelling the transport phenomenon within the system (O'Sullivan, 2016). Variables, such as temperature, velocity and moisture content are then averaged over a representative elementary volume of this homogeneous media. The length scale of the representative elementary volume needs to be much larger than the pore scale but still considerably smaller than the entire package structure. The transport equations may be solved by coupling pressure drop relationships, such as the Ergun and Darcy-Forchheimer models, with the energy conservation equations for the solid and air phases. More detail about the development of the porous medium modelling was presented in (Verboven, Flick, Nicolaï, & Alvarez, 2006).

The application of the porous medium approach to heat transfer in food processing operations can be found in the literature (Ambaw et al., 2016; Ambaw et al., 2013; Delele, Ngcobo, Opara, & Meyer, 2013; Delele, Schenk, Ramon, Nicolaï, & Verboven, 2009; Getahun, Ambaw, Delele, Meyer, & Opara, 2017a, 2017b; Hoang, Duret, Flick, & Laguerre, 2015; Zou, Opara, & McKibbin, 2006a, 2006b).

The greatest advantage of the porous medium model is that it allows for the simplification of the mathematical model by using volume-averaged fluid flow properties, thereby reducing computing time and simulation costs. However, despite extensive effort, the accuracy of the porous-medium approach for modelling the airflow and heat transfer within packaging has been questioned, particularly for layered packaging (Zou et al., 2006b). The main disadvantage of this approach is the disregard for temperature and pressure gradients internal to the product. Another limitation of this approach is that the continuous-medium assumption inherent to a

porous media may not be justified when the package-to-product equivalent diameter ratio is less than 10, which is the case for a tray of bulk-packed drumsticks or a tray of whole chickens considered in this study.

For forced-air cooling of packaged products, the airflow and the local cooling behavior inside packages must be accounted for to achieve an optimum design of the cooling process. The increasing calculation power of personal computers means that the greater computation demands of direct simulation compared to the porous medium approximation are becoming less prohibitive.

2.6.2 Direct computational fluid dynamics simulations

In direct CFD simulation, the complex features of the solid geometries (food products and package material) are not simplified to the same extent as in the porous medium approach. Instead, the explicit geometry of packaged product is taken into account in a direct model. The airflow and heat transfer through the system can be simulated by direct solution of the Navier-Stokes equations and the energy equations of the fluid and solid domains (Verboven et al., 2006). Because this approach deals with local properties and variables, it can provide a more fundamental understanding of the complex fluid flow and heat transfer behaviour. By contrast, the geometrical construction of the computational domain and mesh generation can become more challenging due to the explicit geometry considered by the model and this can increase the computational load significantly.

2.7 Application of CFD to foods chilling and freezing

With the advances in numerical modelling and computing power, CFD has been employed as a tool to optimize and develop equipment and processing strategies for the food industry (Norton & Sun, 2006). The detailed information provided by the use of CFD models has facilitated unique opportunities to investigate alternative system designs, without the need for expensive and time-consuming experiments.

For industrial food chilling, Mirade, Kondjoyan, and Daudin (2002) developed a three-dimensional (3D) CFD model to determine the velocity field in a pork chiller

containing 290 carcasses. The 3D geometrical model of a pork carcass was created from the 2D shape of the pork carcass with a thickness of 20 cm. The airflow profile was used to estimate heat and mass transfer coefficients which were then employed in the analytical model developed by Daudin and Kuitche (1996) to calculate chilling kinetics inside pork carcasses. A reasonably good agreement was observed between the calculated and measured air velocities, and the accuracy in temperature and weight loss predictions were 1°C and 0.1% in absolute value, respectively. Pham, Trujillo, and McPhail (2009) presented a simplified, combined model in which CFD software FLUENT was employed to calculate the local heat and mass transfer coefficients, before applying a finite element method to simulate heat transfer on a two-dimensional model of a beef chilling process. The water diffusion was modelled on a fine secondary 1D mesh because water diffusion and heat transfer occurred on very different scales. The supplementary 1D grid used for solving the water diffusion equation was implemented in an additional piece of code programmed via a specific FLUENT user-defined function. The model was verified by wind tunnel tests and industrial chiller tests on heat load, temperatures, weight loss and surface water activity. The agreement between the model and result from wind tunnel tests was very good, while the agreement with the industrial chillers tests was only qualitative. Although the computation time of the simplified combined model was reduced remarkably compared to using CFD for both airflow and heat transfer simulation, it was difficult to use because the user-defined function was written in a different programming language than the CFD code.

For the chilling of horticulture products, Defraeye et al. (2013, 2014) presented a direct CFD approach to model different packaging designs for oranges stacked on a pallet in forced convective cooling. In these studies, cooling performance and energy consumptions of each package design was evaluated. A comparison of the simulation results with experimental data showed good agreement between the two.

The direct CFD approach has also been used by many researchers to simulate the effect of altering the size and location of air vents in horticultural produce packaging and whether these changes can improve the airflow distribution and cooling uniformity within and between the product packages (Berry, Defraeye, Nicolaï, & Opara, 2016; Berry, Fadiji, Defraeye, & Opara, 2017; Han, Zhao, Yang,

Qian, & Fan, 2015; Lu, Chen, & Wang, 2016). In these studies, a fruit stack was assumed to be comprised of regular spheres organized typically in a staggered arrangement. The use of such simplifications can cause large differences between measured and simulated data for local air velocity, convective heat transfer coefficient, and the degree of the cooling uniformity (Gruyters et al., 2018). This difference was larger the less spherical the fruit (e.g. pears did not show good agreement between model and experiment). Therefore, more realistic fruit shapes are preferable. Ferrua and Singh (2009a, 2009b, 2009c, 2009d, 2011) were amongst the first to develop a direct CFD model that used a real product shape to optimise the forced-air cooling of individual clamshell-packaged strawberries. The strawberry geometry was reconstructed from digital images and implemented in the model. The authors found that forcing more air through clamshells was unlikely to increase the cooling rate of the process; however, periodically reversing the airflow direction could improve both the rate and the uniformity of the cooling process. In addition, bypassing half the airflow entering the pallet structure into the second part of the pallet, thus decreasing the temperature of the air being delivered at the warmest points within the system could also improve the uniformity of the cooling process and significantly reduced the airflow resistance in the system.

Recently, Gruyters et al. (2018) presented a CFD model for studying the cooling process of packed apples and pears using 3D fruit shapes generated from X-ray computed tomography images. The Discrete Element Method was employed to generate a randomised fruit stack and the biological variability of the fruit shape was taken into account. The authors demonstrated that improving the accuracy of the geometrical model helped to simulate convective cooling processes more accurately.

In freezing applications, Dima, Santos, Baron, Califano, and Zaritzky (2014) used COMSOL to model heat transfer inside a 2D irregular shape (crab claws) during freezing. In this model, Heaviside and Gaussian functions (Neeper, 2000) which can generate a smooth curve around the phase change were used to describe the abrupt variation of the apparent specific heat of the crab claw meat at the initial freezing temperature. The heat transfer coefficients were determined from independent experiments. Predicted results were validated against experimental

data and the validated model was used to generate a polynomial equation to illustrate the effect of heat transfer coefficients and external fluid temperature on freezing times of crab claws. Kiani and Sun (2018) presented a CFD model to study the ultrasound-assisted freezing process of potato sticks and potato spheres implemented on the OpenFOAM platform. Several thermal conductivities were tested in the model. This study concluded that the choice of a proper thermal conductivity model is crucial for achieving accurate heat transfer predictions, and ultrasound could give better results when applied to processes with low cooling rates. Zilio, Righetti, Pernigotto, and Longo (2018) employed the CFD software STAR-CCM + to estimate the freezing time of chicken breast. In this model, the chicken breast was represented by a 3D finite cylindrical shape and the thermal properties of chicken were introduced as a function of temperature by means of a User Defined Function. The experimental average heat transfer coefficient was used to simplify the model. The model showed good agreement with experimental data with the mean relative error and the mean absolute error for the chicken freezing time of -1.4% and 2.4%, respectively. Recently, Zhao et al. (2020) used COMSOL to model bayberry during quick freezing. The flesh and core of bayberry were described by different thermal properties and simplified by ellipsoidal shapes. The authors concluded that the best freezing rate for maintaining the freshness of postharvest bayberry was 8.51 cm/h at the freezing temperature of -120°C.

2.8 Summary

There has been considerable effort put into modelling heat transfer in refrigerated food applications. Numerical methods are generally considered the most accurate class of modelling methods, when analytical solutions are not available. As access to affordable computational power has increased, so too has the sophistication of these models. CFD simulations have become more frequently employed, as they can provide a detailed understanding of the airflow distribution, heat transfer and temperature gradients within a system.

In spite of advances in numerical analysis, significant errors may still arise in their application to real-life problems due to uncertainties in the food property inputs.

The first part of this research will focus on improving the prediction of food properties during chilling and freezing.

In an industrial chiller, the product load and the air velocity distribution have a significant influence on the food chilling rate. Therefore, a CFD model which can, in principle, provide detailed predictions of airflow and heat transfer for a wide variety of situations should be used. CFD model has been used to model the airflow field in the industrial chilling of pork hindquarter (Mirade et al., 2002) or beef carcass (Pham et al., 2009) but not the heat transfer which was simulated by an analytical or a 2D finite element numerical model. Although these combination techniques may yield predictions in reasonably short time periods, the errors associated with the simplified heat transfer model may preclude development of accurate solutions. In this study, CFD will be used to predict both the airflow velocity profile and the instantaneous rate of heat transfer during a food chilling process, in a manner that mimics the airflow and product arrangement of an industrial cheese chiller.

In addition, although the accuracy of refrigeration models has increased over time, their complexity has also increased, with greater resources required, such as time, computing facilities, and a good working knowledge of mathematics. These models, however, have not always been put into practice by those working in the industry owing to the lack of conceptual understanding and people's perception of them. For this, there needs to be a greater emphasis on simple-to-use, flexible, and fast programs (James et al., 2009). Therefore, the next part of this research will present a simple one-dimensional finite difference numerical simulation for predicting the heat transfer of food chilling and freezing processes for industrial users.

While it is already possible to simulate realistic shapes of product (Ferrua & Singh, 2009c; Gruyters et al., 2018) , there are not any CFD freezing models for any food products that use CT scanning as the geometry input. This research will present the first freezing model using the realistic geometrical model derived from CT scanning for polylined whole chickens or chicken pieces. Chicken products have irregular shapes, and when packed in bulk within a polyliner, air voids typically exist

between individual food items which can have significant effect on the freezing rate. Freezing is accompanied by highly non-linear temperature dependencies of thermophysical properties such as thermal conductivity and specific heat. A direct CFD approach which can incorporate the real shape of chicken products, air voids and packaging structures and at the same time allow for the use of temperature-dependent thermal properties will be used to develop the airflow and heat transfer model for bulk-packed chicken during freezing.

2.9 Research objectives

In this study, the terms model/modelling refer to the original work of author in developing a model (i.e construct a geometrical model and setup a numerical solution in a CFD model) while simulation means using existing models to present a solution for heat transfer problems. The objectives of this projects are as follows:

1) Review thermal property models for foods in the literature to propose the best performing model for thermal processing calculations.

2) Develop a CFD model to simulate the airflow and heat transfer in an industrial cheese chilling process and validate the model with experimental data for a variety of operating conditions.

3) Present a simplified one-dimensional numerical heat transfer simulation of food chilling and freezing and validate the simulation with experimental data of a single block of cheese being chilled.

4) Develop and validate CFD models for forced-air freezing of individual trays of bulk-packed whole chickens and chicken drumsticks. Based on the validated model, simple correlations to estimate the effect of operating conditions on freezing time will be developed to optimise the design of the freezing tunnel for chicken products.

Chapter 3
Improved prediction of thermal property of foods

3.1 Introduction

The objective of this chapter was to propose the best composition-based thermal properties models for generic application to foods, requiring only a knowledge of the food composition, initial freezing temperature (if applicable) and temperature of the food, without the need to perform any measurements. A comparison between several property models in literature and published experimental data was done to determine the most accurate one. In particular, an additive specific heat capacity model incorporating a more accurate means of dealing with the specific heat capacity of water and a previously little-known thermal conductivity model provided improved predictions compared to the models recommended in most refrigeration/food engineering handbooks.

3.2 Specific heat and enthalpy

3.2.1 Specific heat

Specific heat is defined as the energy required to change the temperature of a kilogram of food item by one degree Celsius (ASHRAE, 2006). During freezing (and thawing) processes, the phase transformation of water and fat components releases the latent heat of phase transition. In food, the latent heat is not released or absorbed at a constant temperature as it is in pure substances, but over a range of temperatures. Therefore, an effective specific heat capacity (ESHC) must be employed to account for both the change in sensible heat due to temperature change and in latent heat due to phase transition (ASHRAE, 2006). Since the latent heat of fats only becomes important when the fats start to melt, typically above 30°C, it is reasonable to ignore the latent heat of fusion of fat in the temperature range of interest for food preservation.

There are several ESHC models in the literature (ASHRAE, 2006; Rahman, 2009). For prediction based on composition data, not involving any parameters that must

be measured experimentally, three physical models below were used to estimate the effective specific heat capacity of food item:

- Additive model
- Chen's model
- Schwartzberg's model

The weight additive model can be calculated by adding the contribution of the apparent heat capacity of each component together with the latent heat of fusion of water (Cogné, Andrieu, Laurent, Besson, & Nocquet, 2003; Fikiin, 1996)

$$c_e = x_s c_s + x_{wo}(1-\omega)c_w + x_{wo}\omega c_{ice} - x_{wo}L_f\frac{\partial\omega}{\partial T} \tag{3.1}$$

where

c_e (J kg^{-1} K^{-1}) is the effective specific heat capacity

c_w (J kg^{-1} K^{-1}) is the specific heat of the water fraction

c_{ice} (J kg^{-1} K^{-1}) is the specific heat of the ice fraction

T (K) is the temperature of food

ω is the relative quantity of frozen water, calculated by the ratio of mass fraction of ice (x_{ice}) to mass fraction of water in unfrozen food (x_{wo})

$$\omega = \frac{x_{ice}}{x_{wo}} \tag{3.2}$$

x_s, c_s are the mass fraction and specific heat capacity of solid fractions including ash, protein, fibre, carbohydrate, and fat in food items, calculated by Eqs. 3.3 and 3.4, respectively.

$$x_s = x_p + x_{fa} + x_{CHO} + x_{fi} + x_{ash} \tag{3.3}$$

$$c_s = \frac{x_p c_p + x_{fa} c_{fa} + x_{CHO} c_{CHO} + x_{fi} c_{fi} + x_{ash} c_{ash}}{x_s} \tag{3.4}$$

x_p, x_{fa}, x_{CHO}, x_{fi}, x_{ash} are the mass fraction of protein, fat, carbohydrate, fibre and ash in the food item.

c_p, c_{fa}, c_{CHO}, c_{fi}, c_{ash} (J kg^{-1} K^{-1}) are the specific heat of protein, fat, carbohydrate, fibre and ash components.

L_f (J kg^{-1}) is the latent heat of water solidification/fusion determined by Eq. 3.5.

$$L_f = L_o - \int_T^{273.15} c_w dT + \int_T^{273.15} c_{ice} dT \quad (3.5)$$

L_o (J kg^{-1}) is the latent heat of water solidification/fusion at 0°C, L_o = 333.6×10^3 J kg^{-1}.

Table 3.1 shows empirical models of specific heat capacity of the various major components of the foods as functions of temperature.

Table 3.1: Specific heat capacity and density of major food components as a function of temperature T (°C) ($-40 \le T \le 150$°C) (Choi & Okos, 1986)

Component	**Specific heat capacity, kJ kg^{-1} K^{-1}**
Protein	$c_p = 2.0082 + 1.2089\times10^{-3}T - 1.3129\times10^{-6}T^2$
Fat	$c_{fa} = 1.9842 + 1.4733\times10^{-3}T - 4.8008\times10^{-6}T^2$
Carbohydrate	$c_{CHO} = 1.5488 + 1.9625\times10^{-3}T - 5.9399\times10^{-6}T^2$
Fiber	$c_{fi} = 1.8459 + 1.8306\times10^{-3}T - 4.6509\times10^{-6}T^2$
Ash	$c_{ash} = 1.0926 + 1.8896\times10^{-3}T - 3.6817\times10^{-6}T^2$
Ice	$c_{ice} = 2.0623 + 6.0769\times10^{-3}T$

The specific heat capacity of water was correlated from measurement data performed with a differential scanning calorimeter by Archer and Carter (2000) with an R-square value of 0.98

$$c_w = B_1 + B_2 Y^{0.5} + B_3 Y + B_4 Y^{1.5} + B_5 Y^2 + B_6 Y^{2.5} + B_7 Y^3 + B_8 Y^{3.5} + B_9 Y^4 \quad (3.6)$$

where:

B_1 = 14.99, B_2 = 23.19, B_3 = -1716.75,

B_4 = 14122.09, B_5 = -55963.72, B_6 = 125411.02,

B_7 = -162011.7, B_8 = 112359.99, B_9 = -32309.86.

$Y = \dfrac{T - 228}{228}$, 233.15 K $\le T \le$ 273.15 K

For 273.15 K < $T \leq$ 383.15 K, c_w was calculated by Patek et al's correlated equation (Pátek, Hrubý, Klomfar, Součková, & Harvey, 2009)

$$c_w = -0.4615\left[c_3 + \frac{T}{10}\left(\sum_{i=1}^{3} n_i\left(n_i+1\right)a_i\left(\frac{10}{593-T}\right)^{n_i+2} + \sum_{i=1}^{4} m_i\left(m_i+1\right)b_i\left(\frac{10}{T-232}\right)^{m_i+2}\right)\right] \quad (3.7)$$

where

$n_1 = 4$, $n_2 = 5$, $n_3 = 7$, $m_1 = 2$, $m_2 = 3$, $m_3 = 4$, $m_4 = 5$, $c_3 = -8.983025854$,
$a_1 = -1.661470539\times10^{5}$, $a_2 = 2.708781640\times10^{6}$, $a_3 = -1.557191544\times10^{8}$,
$b_1 = -8.237426256\times10^{-1}$, $b_2 = -1.908956353$, $b_3 = -2.017597384$,
$b_4 = 8.546361348\times10^{-1}$.

The second model used to predict ESHC is Chen's model based on Raoult's Law (ASHRAE, 2006; Chen, 1985)

$$\text{if } T > T_f : c_e = 4.19 - 2.30x_s - 0.628x_s^{3} \quad (3.8)$$

$$\text{if } T \leq T_f : c_e = 1.55 + 1.26x_s - \frac{\left(x_{wo} - x_b\right)L_o\left(T_f - T_o\right)}{\left(T - T_o\right)^2} \quad (3.9)$$

where

T_f (K) is the initial freezing point of food
T_o (K) is the initial freezing point of pure water, T_o = 273.15K
x_b is mass fraction of bound water, x_b =0.4 x_p (ASHRAE, 2006)

Schwartzberg's equation for determining the ESHC of frozen food has the following form (ASHRAE, 2006; Schwartzberg, 1976)

$$c_e = c_u + \left(x_b - x_{wo}\right)\left(c_w - c_{ice}\right) + \frac{18}{M_s}\left(\frac{8.314T_o^2}{18\left(T_o - T\right)^2} - 0.8\left(c_w - c_{ice}\right)\right) \quad (3.10)$$

where c_u is specific heat of foods at temperatures above the freezing point determined by Eq. 3.8, M_s is the molecular weight of dry matter within the food item estimated by Eq. 3.11 below (ASHRAE, 2006):

$$M_s = \frac{0.8314 x_s T_o^2}{-\left(x_{wo} - x_b\right) L_o \left(T_f - T_o\right)} \tag{3.11}$$

3.2.2 Enthalpy

Enthalpy can be obtained by integrating expressions of ESHC with respect to temperature. For the purposes of comparison, the reference temperature, T_r, for zero enthalpy at 233.15K was chosen to match the zero reference temperature of the experimental data of (Pham, Wee, Kemp, & Lindsay, 1994). In the case of the additive model, the enthalpy of foods, H, was calculated by integrating Eq. 3.1.

$$H = x_s \int_{233.15}^{T} c_s dT + x_{wo} \int_{233.15}^{T} c_w dT - \omega x_{wo} L_f + x_{wo} L_{233} \omega_{233} \tag{3.12}$$

where L_{233} and ω_{233} are latent heat of water solidification/fusion and relative quantity of the frozen water at T = 233.15K.

In the same manner, Chen's enthalpy model was obtained by integrating Eq. 3.8 and Eq. 3.9 for the food item at temperatures above and below the initial freezing point, respectively:

$$\text{if } T > T_f : H = H_f + \left(T - T_f\right)\left(4.19 - 2.30 x_s - 0.628 {x_s}^3\right) \tag{3.13}$$

$$\text{if } T \le T_f : H = \left(T - T_r\right)\left(1.55 + 1.26 x_s - \frac{\left(x_{wo} - x_b\right) L_o \left(T_f - T_o\right)}{\left(T - T_o\right)\left(T_r - T_o\right)}\right) \tag{3.14}$$

where H_f is the enthalpy of food at the initial freezing temperature estimated by evaluating Eq. 3.14 at $T = T_f$

Integrating Schwartzberg's ESHC model (Eq. 3.10) leads to the following expression for the enthalpy of frozen food (ASHRAE, 2006; Schwartzberg, 1976):

$$H = \left(T - T_r\right)\left\{c_u + \left(x_b - x_{wo}\right)\left(c_w - c_{ice}\right) + \frac{18}{M_s} x_s \left[\frac{8.314 T_o^2}{18\left(T_o - T_r\right)\left(T_o - T\right)} - 0.8\left(c_w - c_{ice}\right)\right]\right\} \tag{3.15}$$

The Schwartzberg model for enthalpy above the freezing point was estimated with Eq. 3.13; however, H_f was determined by Eq. 3.15 at the initial freezing temperature.

3.3. Thermal conductivity

The thermal conductivity of foods depends on structure, composition and temperature (Fricke & Becker, 2001; Rahman, 2009). It is the dependence of the thermal conductivity of the food on structure that is accounted for by the thermal conductivity models in the literature (ASHRAE, 2006; Carson, 2006; Rahman, 2009). This study only considers models which are functions of the composition of the food and thermal conductivities of the major food components, and do not involve any parameters which must be measured experimentally. Carson et al. (2016) divided the thermal conductivity models for heterogeneous materials into two groups:

- Single-step methods, which predict thermal conductivity using a single model equation
- Multi-step methods, which employ more than one model to predict thermal conductivity.

3.3.1 Single-step method

The simplest models that meet the single-step criteria are the Series, Parallel and Geometric models. The Series model corresponds to the weighted harmonic mean of the thermal conductivities of the food components (Rahman, 2009).

$$k_e = \frac{1}{\sum_i \frac{v_i}{k_i}} \tag{3.16}$$

The Parallel model corresponds to the weighted arithmetic mean of the thermal conductivities of the components (Rahman, 2009)

$$k_e = \sum_i k_i v_i \tag{3.17}$$

The Geometric model is the weighted geometric mean of the thermal conductivity of the components of the foods (Rahman, 2009)

$$k_e = \prod_i k_i^{v_i} \tag{3.18}$$

where k_e (W m^{-1} K^{-1}) is the thermal conductivity of the mixture, k_i (W m^{-1} K^{-1}) is the thermal conductivity of the i^{th} food component, and v_i is the volumetric fraction of the i^{th} food component. v_i was estimated from mass fractions and densities:

$$v_i = \frac{x_i / \rho_i}{\sum (x_i / \rho_i)} \tag{3.19}$$

If the food is porous and the porosity (the volume fraction of air, v_a) has not been measured it may be estimated from the apparent (bulk) density (ρ_e) (ASHRAE, 2006; Carson et al., 2016)

$$\rho_e = \frac{1 - v_a}{\sum \frac{x_i}{\rho_i}} \tag{3.20}$$

Thermal conductivities and densities of major food components as a function of temperature are summarised in Table 3.2.

The Parallel and Series models represent the theoretical bounds of the thermal conductivity of heterogeneous materials, in which the Series model provides the lower limit and the Parallel model provides the upper limit. (Carson et al., 2016)

Two other models that can predict the effective thermal conductivity of a food product in a single step are the Effective Medium Theory model (EMT; Landauer, 1952) :

$$\sum_i v_i \frac{k_e - k_i}{k_i + 2k_e} = 0 \tag{3.21}$$

and the Co-continuous model (CC; Wang, Carson, North, & Cleland, 2008)

$$k_e = \frac{\sum_i \frac{v_i}{k_i}}{2}\left(\sqrt{1+\frac{8\sum_i k_i v_i}{\sum_i \frac{v_i}{k_i}}}-1\right) \tag{3.22}$$

Table 3.2 Thermal conductivities and densities of major food components as a function of temperature T (°C) ($-40 \le T \le 150$°C) (ASHRAE, 2006; Carson, 2011; Choi & Okos, 1986)

Component	**Thermal conductivity, W m^{-1} K^{-1}**	**Density, kg m^{-3}**
Protein	$0.17887+1.1958\times10^{-3}T-2.7178\times10^{-6}T^2$	$1.3299\times10^{3} - 5.1840\times10^{-1}T$
Fat	$0.18071-2.7604\times10^{-3}T-1.7749\times10^{-7}T^2$	$9.2559\times10^{2} - 4.1757\times10^{-1}T$
CHO	$0.20141+1.3874\times10^{-3}T-4.3312\times10^{-6}T^2$	$1.5991\times10^{3} - 3.1046\times10^{-1}T$
Fiber	$0.18331+1.2497\times10^{-3}T-3.1683\times10^{-6}T^2$	$1.3115\times10^{3} - 3.6589\times10^{-1}T$
Ash	$0.32962+1.4011\times10^{-3}T-2.9069\times10^{-6}T^2$	$2.4238\times10^{3} - 2.8063\times10^{-1}T$
Ice	$2.2196-6.2489\times10^{-3}T+1.0154\times10^{-4}T^2$	$9.1689\times10^{2} - 1.3071\times10^{-1}T$
Air	$2.364\times10^{-2}+7.2822\times10^{-5}T$	$353/(T+273.15)$
Water	$0.57109+1.7625\times10^{-3}T-6.7603\times10^{-6}T^2$	$9.9718\times10^{2}+3.1439\times10^{-3}T$ $-3.7574\times10^{-3}T^2$

The Series and Parallel models physically match structures where layers of the components are aligned either perpendicular or parallel to the heat flow direction, as their names imply. The EMT model represents the physical structure where all components are mutually dispersed with each other (co-dispersed) i.e. no component necessarily represents a continuous phase. The CC model represents a physical structure where all of the components are continuous but intertwined and none is dispersed (Carson et al., 2016).

3.3.2 Multi-step methods

Single-step methods offer simplicity and are designed for the specific structures mentioned above. However, food components rarely exist as a single structure (Carson et al., 2016). Therefore, there is potential for the multi-step method, which

combines more than one structure model to produce a better thermal conductivity prediction.

For frozen foods without air voids, Pham and Willix (1989) and Fricke and Becker (2001) recommended the use of Levy's model (Levy, 1981) to account for the presence of ice. In the first step, the thermal conductivity of all the components excluding ice, k_{mix}, was calculated using the Parallel model (Eq. 3.17). Then, in the second step, the thermal conductivity of frozen food without air voids was estimated by Eq. 3.23

$$k_{Levy} = k_{ice}\frac{2k_{ice} + k_{mix} - 2\left(k_{ice} - k_{mix}\right)F}{2k_{ice} + k_{mix} + \left(k_{ice} - k_{mix}\right)F} \tag{3.23}$$

where

k_{Levy} (W m^{-1} K^{-1}) is the thermal conductivity of frozen food without air voids

k_{mix} (W m^{-1} K^{-1}) is the thermal conductivity of all the components excluding ice

k_{ice} (W m^{-1} K^{-1}) is the thermal conductivity of the ice component

$$F = \frac{2/G - 1 + 2\left(1 - v_{ice}\right) - \sqrt{\left[2/G - 1 + 2\left(1 - v_{ice}\right)\right]^2 - 8\left(1 - v_{ice}\right)/G}}{2} \tag{3.24}$$

$$G = \frac{\left(k_{ice} - k_{mix}\right)^2}{\left(k_{ice} + k_{mix}\right)^2 + k_{ice}k_{mix}/2} \tag{3.25}$$

v_{ice} is the volume fraction of the ice component

For porous foods, the air voids must be considered in addition to ice, water, and other components. As the thermal conductivity of air is very low compared to that of the other components, porosity has a large influence on the effective thermal conductivity of foods (Cogné et al., 2003).

In order to incorporate the influence of the air phase on the effective thermal conductivity of frozen foods, if nothing is assumed to be known about its structure, (Carson et al., 2016) recommended a multi-step procedure using the EMT model in the following forms:

$$k_{EMT}^{up} = \frac{(3v_a - 1)k_a + \left[3(1 - v_a) - 1\right]k_{u,np} + \sqrt{\left\{(3v_a - 1)k_a + \left[3(1 - v_a) - 1\right]k_{u,np}\right\}^2 + 8k_{u,np}k_a}}{4} \quad (3.26)$$

$$k_{EMT}^{fp} = \frac{(3v_a - 1)k_a + \left[3(1 - v_a) - 1\right]k_{f,np} + \sqrt{\left\{(3v_a - 1)k_a + \left[3(1 - v_a) - 1\right]k_{f,np}\right\}^2 + 8k_{f,np}k_a}}{4} \quad (3.27)$$

Eqs. 3.26 and 3.27 represent the two-component forms of Eq. 3.21 for unfrozen, porous and frozen, porous foods, respectively (Carson et al., 2016). In these equations, k_a, v_a are the thermal conductivity and volume fraction of the air component, $k_{u,np}$ is the thermal conductivity of the unfrozen, non-porous food determined by the Parallel model (Eq. 3.17) and $k_{f,np}$ is the thermal properties of the frozen, non-porous foods determined by Levy's model (Eq. 3.23).

The Maxwell-Eucken model may be used when a dispersion of one phase forms within a continuous phase (Carson et al., 2016). If air forms a dispersed phase within a food (sponge/foam-like foods), this model has the following form:

$$k_{ME1} = k_{f,np}\frac{2k_{f,np} + k_a - 2\left(k_{f,np} - k_a\right)v_a}{2k_{f,np} + k_a + \left(k_{f,np} - k_a\right)v_a} \quad (3.28)$$

If air forms the continuous phase (particulate foods) then the following form of the Maxwell-Eucken model is employed:

$$k_{ME2} = k_{f,np}\frac{2k_a + k_{f,np} - 2\left(k_a - k_{f,np}\right)\left(1 - v_a\right)}{2k_a + k_{f,np} + \left(k_a - k_{f,np}\right)\left(1 - v_a\right)} \quad (3.29)$$

Dul'nev and Novikov (1991) introduced a procedure to estimate the effective thermal conductivity of any heterogeneous food products. In this model, a food item is considered to consist of water, ice, solids (ash, protein, fibre, carbohydrate and fat), and air. The effective thermal conductivity of the food product is determined by a three-step procedure. In the first step, the thermal conductivity of the solid phase is calculated from the ash, protein, fibre, carbohydrate and fat fractions using

the Parallel model (Eq. 3.17), and the thermal conductivity of the medium that surrounds each i^{th} component is determined using Eq. 3.30:

$$N_i = \frac{\sum_{j \neq i} k_j v_j}{\sum_{j \neq i} v_j} \tag{3.30}$$

In the second step, the thermal conductivities of the binary systems consisting of the i^{th} component (thermal conductivity k_i with volume fraction v_i) and the medium around it (thermal conductivity N_i with volume fraction 1- v_i) are determined using the following relationship (Dul'Nev & Novikov, 1977):

$$K_i = k_{\max} \left\{ c^2 + \lambda (1-c)^2 + \frac{2\lambda c(1-c)}{\lambda c + 1 - c} \right\} \tag{3.31}$$

where, $\lambda = k_{\min} / k_{\max}$, $k_{\min}$ is the minimum value between k_i and N_i and $k_{\max}$ is the maximum value between k_i and N_i, the value of c is related to the volume fraction, m, of the component which has a smaller thermal conductivity determined by Eq. 3.32:

$$c = 0.5 + A \cos \frac{\varphi}{3} \tag{3.32}$$

where:

$$A = \begin{cases} -1, & m \leq 0.5 \\ 1, & m > 0.5 \end{cases}$$

$$\varphi = \begin{cases} 2\pi - X, & X > 0 \\ 2\pi + X, & X \leq 0 \end{cases}$$

$$X = \arctan \sqrt{\frac{1-(2m-1)^2}{|2m-1|}}$$

Finally, the thermal conductivity of the whole system is estimated by Eq. 3.33:

$$k = \sum_i k_i \frac{K_i - N_i}{k_i - N_i} \tag{3.33}$$

3.4. Relative quantity of frozen water

The prediction of the thermal properties of frozen food requires knowledge of the food's ice fraction or the relative quantity of frozen water (ω, Eq. 3.2) which in turn is strongly dependent on temperature. Therefore, a model of the relative quantity of frozen water is required for thermal property prediction.

Models for predicting relative quantity of frozen water can be found in (ASHRAE, 2006; Fikiin, 1998; Rahman, 2009). Many of these require calculations of mole fractions, which in turn requires estimation of molar masses for the macromolecules (proteins and complex carbohydrates). Many contain empirical parameters, and most require knowledge of the amount of bound or un-freezable water. With the requirement that the calculation procedure should not involve parameters that must be determined experimentally, the empirical model proposed by Tchigeov (1979) which based only on total water content and the initial freezing temperature (Eq. 3.34) was chosen to estimate the relative quantity of the frozen water:

$$\omega = \frac{x_{ice}}{x_{wo}} = \frac{1.105}{1 + \frac{0.7318}{\ln\left(T_f - T + 1\right)}} \tag{3.34}$$

Unlike other empirical models that contain parameters which are specific to the food in the question and typically need to be determined from experiments, the empirical parameters in Eq. 3.34 apply generally and do not need to be determined from an ice fraction measurement. Fikiin (1998) stated that Eq. 3.34 can be applied for various products (meat, fish, milk, eggs, fruits, and vegetables) and provides satisfactory accuracy when $228.15\text{K} \le T \le T_f$ and $271.15\text{K} \le T_f \le 272.75\text{K}$. In cases of initial freezing temperature lower than 271.15K, such as cheese product, Carson et al. (2016) recommended to use a more general relationship based on Raoult's law and the Clausius-Clapeyron equation:

$$\omega = \left(1 - \frac{x_b}{x_{wo}}\right)\left(\frac{T - T_f}{T - T_o}\right) \tag{3.35}$$

In this study, Eq. 3.34 and Eq. 3.35 were used for foods with initial freezing point above and below 271.15 K, respectively. Figure 3.1 shows Eqs. 3.34 and 3.35 plotted assuming an initial temperature of 272.15K, a protein mass fraction of 0.2 and a total water mass fraction of 0.75.

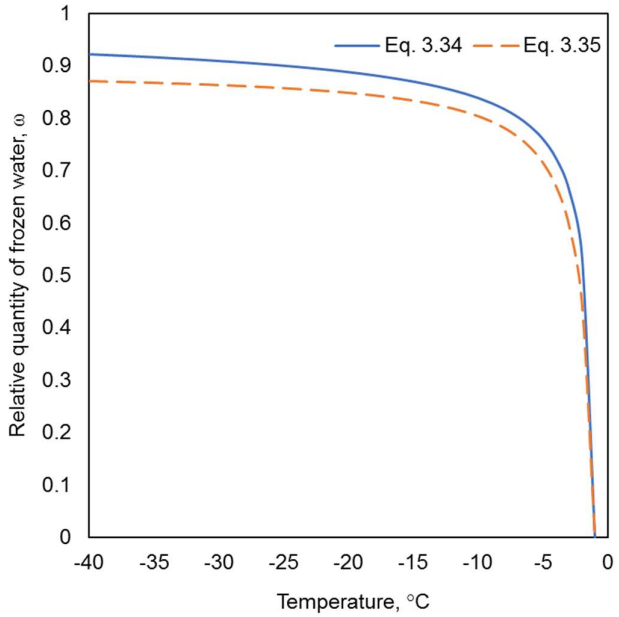

Figure 3.1 Plots of two different relative quantity of frozen water models (Eqs 3.34 and 3.35) with T_f= 272.15K, x_p = 0.2, x_{wo} = 0.75

It is clear from the discrepancy between the prediction results of Eqs 3.34 and 3.35 shown in Figure 3.1, that the selection of relative quantity of frozen water model introduces an extra source of uncertainty. For example, the discrepancy between the thermal conductivity prediction of Dul'Nev & Novikov's model based on relative quantity of frozen water calculated firstly from Eq. 3.34 and secondly from Eq. 3.35 may be as high as 9%, depending on the relative quantity of frozen water. This error occurs independently of any further error that may result from the selection of an unsuitable thermal conductivity model. Ideally, a thermal property model should therefore be tested independently of a relative quantity of frozen water model since, if the relative quantity of frozen water model over-predicts and the thermal property model under-predicts (or vice versa), thermal property predictions may appear to be accurate for a given set of data, but may only be so by coincidence. The most common approach when thermal property models are being compared appears simply to have been to base all thermal property models on a single relative quantity of frozen water model.

3.5 Comparison of model predictions against measured data

The predicted values of the thermal property models discussed in sections 3.2 to 3.4 were compared to experimental data from the literature. Since the mathematical expression for enthalpy of the food item was obtained by integrating the effective specific heat equation, an accurate enthalpy model will mean that the effective specific heat model is also accurate. Therefore, only enthalpy and thermal conductivity predictions have been validated in this study. The criteria for selecting data used in this evaluation were that the food compositions and initial freezing temperature were available, and the measurement methodology was proven to be accurate. The enthalpy data were obtained from Pham et al. (1994), and thermal conductivity data were taken from Willix, Lovatt, and Amos (1998) and Cogné et al. (2003) for non-porous foods, and porous frozen foods, respectively.

The absolute relative error between model predictions and experimental data is defined as

$$\delta = \frac{|exp - mod|}{exp} \times 100\% \tag{3.36}$$

where *mod*, and *exp* are model predicted data and experimental data, respectively.

3.5.1 Enthalpy

Table 3.3 illustrates the mean absolute relative errors between the model predictions and experimental data taken from the literature (Pham et al., 1994) for enthalpy of a variety of foods over the temperature range from -40°C to 40°C. In general, the additive model produced the best predictions with a mean error across all materials of 3.86%, while Chen's model and Schwartzberg's model produced mean errors of 9.30% and 12.85%, respectively. Comparison between experimental data and enthalpy predictions for lean lamb was plotted in Figure 3.2. It also shows good agreement between the predicted results of the additive model and experimental data. Chen's model and Schwartzberg's model tended to be less accurate for non-freezing temperatures than for freezing temperatures.

Table 3.3 Comparision of the mean absolute relative errors between predicted and experimental enthalpy data (Pham et al., 1994) of foods over temperature ranged from -40°C to 40°C.

Material	Mean absolute relative errors, %		
	Additive model	Chen	Schwartzberg
Lean lamb	0.77	9.48	13.19
Lean beef	1.45	10.74	14.57
Lean chicken	4.58	7.64	12.50
Learn pork	3.04	7.94	11.36
Lean venison	1.73	9.27	12.50
Mutton mince, cooked	3.00	5.43	9.25
Ham cooked	4.85	3.50	9.68
Beef hamburgers patties	6.00	8.93	11.16
Gurnard fillets	2.54	9.49	13.48
Terakihi fillets	3.12	8.60	12.96
Mutton liver	4.82	10.45	14.03
Mutton kidney	5.60	15.13	17.65
Mutton brains	2.93	11.29	17.81
Kiwifruit	9.67	12.33	9.74
Mean of all materials	**3.86**	**9.30**	**12.85**

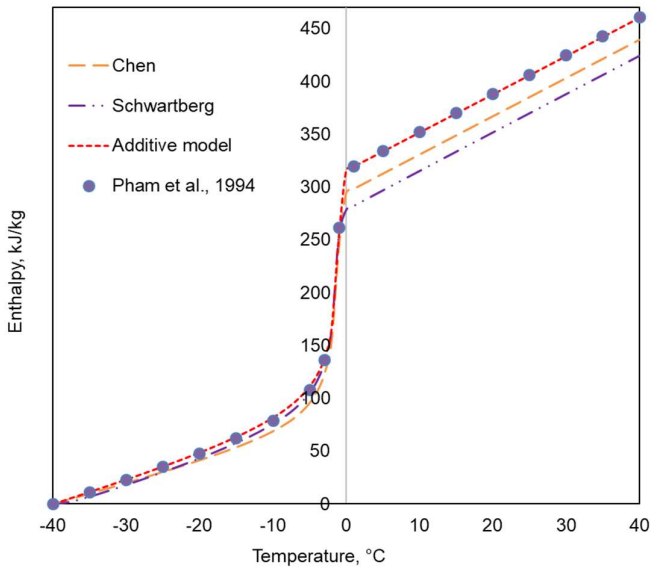

Figure 3.2: Comparision between experimental data (Pham et al., 1994) and enthalpy predictions for lean lamb

3.5.2 Thermal conductivity

3.5.2.1 Non-porous foods

Table 3.4 summarizes the mean absolute relative error between model predictions and experimental data (Willix et al., 1998) for non-porous foods over a range of temperature. On average, Dul'nev & Novikov's model gave the most accurate predictions. The Parallel and Series models produced very high prediction errors, while most of the other models showed reasonable agreement with the experimental data, with the average mean relative error between model prediction and experimental data for all the materials being less than 15%. Figure 3.3 shows plots of thermal conductivity predictions of various models compared to experimental data for lean beef. It can be seen from the figure that the Parallel model significantly over-predicted thermal conductivity, and the Series model significantly under-predicted thermal conductivity. The Levy model and Dul'nev and Novikov model provided better predictions than other models in the freezing range. All thermal conductivity models performed better in the non-freezing temperature than in the freezing temperature.

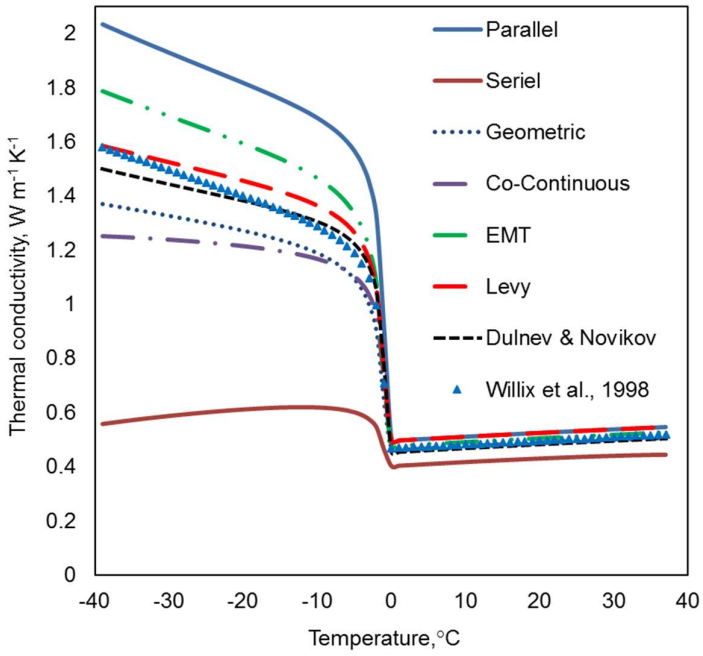

Figure 3.3. Comparison between experimental data (Willix et al., 1998) and the thermal conductivity predictions for lean beef

Table 3.4 Comparison of the absolute relative errors between predicted and experimental thermal conductivity values (Willix et al., 1998) for non-porous foods

Material	Mean absolute relative error, %							Temp. range, °C	
	Parallel	Series	Geometric	Co-Continuous	EMT	Levy	Dulnev & Novikov	Low	High
Lean beef	17.8	35.1	6.2	7.3	7.2	4.6	2.9	-39	37
Beef mince	54.7	30.9	9.2	13.4	30.5	29.5	19.7	-39	38
Boneless Chicken	26.6	41.3	5.5	8.0	13.1	7.8	3.0	-39	16
Pork sausage meat	31.0	37.5	6.6	4.0	10.2	11.8	7.1	-40	37
Venison	27.4	27.1	4.3	6.8	16.4	14.4	7.3	-33	36
Gurnard fillets	12.7	34.3	7.1	9.1	5.1	2.1	4.4	-39	37
Lemon fish fillets	24.9	31.0	5.1	6.6	14.9	11.2	7.6	-38	37
Snapper fillets	24.2	29.5	2.8	5.5	14.3	11.4	4.7	-40	37
Tarakihi fillets	25.0	29.3	2.3	5.1	14.9	12.2	5.3	-39	37
Trevally fillets	15.1	32.9	6.2	8.0	6.0	5.4	3.8	-37	39
Cheddar cheese	14.8	40.3	22.9	10.7	16.2	6.9	10.8	-39	26
Edam cheese	11.1	41.7	23.9	12.8	16.5	11.4	12.5	-38	26
Mozzarella cheese	22.1	45.1	22.9	10.8	12.0	6.1	8.5	-39	22
Mean of all materials	**23.6**	**35.1**	**9.6**	**8.3**	**13.6**	**10.4**	**7.5**		

3.5.2.2 Porous foods

Table 3.5 shows the absolute relative errors between the model prediction and experimental thermal conductivity data of ice cream obtained from Cogné et al. (2003) for different porosities at -20°C and -30°C.

Table 3.5 Comparison of the absolute relative errors between predicted and experimental thermal conductivity values for ice cream (Cogné et al., 2003)

Porosity	Parallel	Series	Geo	CC	EMT	Dul & Nov	Multi-step Method	
							EMT	ME1
-20°C								
0.13	49.71	85.10	35.87	40.25	4.01	0.57	0.32	1.65
0.23	56.07	88.73	47.94	46.05	4.83	0.05	3.04	1.59
0.33	68.47	89.71	55.52	46.05	14.00	3.24	5.70	5.39
0.41	70.26	90.27	62.14	47.11	28.19	0.71	15.16	3.39
0.46	78.90	89.95	63.96	44.85	34.85	3.50	18.95	6.74
0.60	102.46	88.06	67.51	36.19	55.58	9.85	39.58	15.57
0.67	111.29	86.47	68.53	30.85	63.69	10.82	53.19	18.44
Average	**76.7**	**88.3**	**57.4**	**41.6**	**29.3**	**4.1**	**19.4**	**7.5**
-30°C								
0.13	51.62	86.40	36.97	42.22	5.90	0.27	0.20	1.14
0.23	54.63	89.94	50.38	49.04	5.42	3.06	5.69	1.15
0.33	68.62	90.74	57.54	48.55	14.14	1.05	7.46	3.57
0.41	69.85	91.27	64.23	49.73	29.20	1.71	17.19	1.24
0.46	70.36	91.39	67.63	49.97	39.24	3.53	24.65	0.25
0.60	105.97	89.07	69.18	38.13	57.51	9.64	41.06	15.30
0.67	106.25	88.10	71.51	35.64	67.31	6.28	57.10	13.31
Average	**75.3**	**89.6**	**59.6**	**44.8**	**31.2**	**3.6**	**21.9**	**5.1**

Once again, the Dul'nev and Novikov's model showed the best accuracy with an average relative error of less than 4.1%. The Maxell-Eucken model with air as the dispersed phase (ME1) also gave a good agreement with the experimental data. This

can be explained by the fact that the air phase was dispersed in other phases in the structure of ice cream. Figure 3.4 presents a comparison between thermal conductivity predictions generated by Dul'nev and Novikov's model and the experimental data found in (Cogné et al., 2003) at different air porosities. The model provided a better prediction for the thermal conductivity of frozen ice cream (relative errors about 5%) than that for unfrozen ice cream (relative errors around 15%).

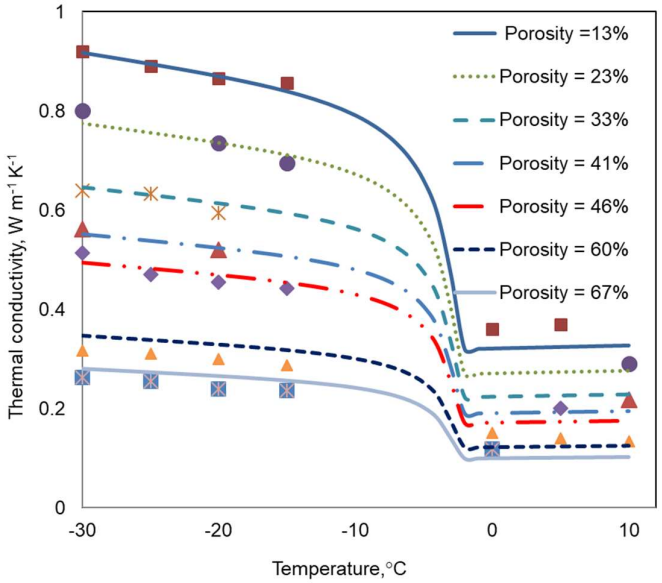

Figure 3.4: Comparison between thermal conductivity data (Cogné et al., 2003) and predictions of Dul'nev and Novikov's model for ice-cream. The predicted results depict in the lines and the experimental data depict in the points.

3.6. Conclusions

An assessment of selected composition-based thermal property models for foods was presented. The effective specific heat capacity predicted by the additive model (Eq. 3.1) with the specific heat of water correlated from experimental data of Archer and Carter (2000) and Pátek et al. (2009), and the thermal conductivity model of Dul'nev and Novikov (Eqs. 3.30-3.33) showed better predictions compared to other models for a wide range of food products. Therefore, the additive model and the Dul'nev and Novikov model are recommended as the best models for prediction of effective specific heat capacity and thermal conductivity for food products, and will be used for thermal properties modelling in all the chilling and freezing models in this thesis.

Chapter 4

Numerical heat transfer model for industrial chilling installations

4.1 Introduction

Food technology continues to develop as new refrigeration equipment becomes available and as consumer preferences continue to change (Bogh-Sorensen, 2006). On the industrial scale, food refrigeration equipment is often made to order for a given end-user and may be designed either for a single type of product or multiple products. With such a high degree of customisation in modern refrigeration equipment, it is necessary to have a design optimisation tool to evaluate the performance of the refrigeration system. The rate of cooling for a given chilling operation depends on the refrigeration air temperature and airflow characteristics (turbulence intensity, velocity profile), packaging, and packing arrangement, as well as the dimensions, morphology and physical properties of the food product (ASHRAE, 2006; O'Sullivan et al., 2014).

Food Product Modeller, FPM, (MIRINZ) is a software tool that is currently being used by a large number of food process equipment manufacturing companies in New Zealand to improve the design of chilling and freezing tunnels. FPM is a finite difference numerical model, which can accurately predict the heat transfer rates within food products. However, it is only for a single product, and not able to predict the flow field in the tunnel. The heat transfer coefficient at the surface of the product has to be supplied to FPM by its user, or estimated by FPM using a correlation based on an air velocity that is supplied by the user. In an industrial chiller, the product load and the air velocity distribution have a significant influence on the food chilling and freezing rate. Therefore, a CFD model which can, in principle, provide accurate predictions of airflow and heat transfer for almost any situation would have some advantages over FPM. CFD has been used to model similar systems such as pork chilling (Mirade et al., 2002) and industrial beef chilling (Kuffi et al., 2016).

This chapter will present a CFD based numerical model for six blocks of agar in a forced air chilling which mimics the airflow and product arrangement in an industrial cheese chiller, and validate that model against experimental data.

4.2 Experimental study

4.2.1 Objective

The aim of the experimental study is to provide data to validate a numerical model of the forced-air chilling of regularly shaped products by proving its ability to predict the temperature profile at certain positions of the test objects. The operating and boundary conditions in the experiments will then be reproduced in the numerical model.

4.2.2 Experimental system

The experimental setup was designed to closely match a commercial chilling tunnel, similar to the one shown in Figure 4.1. The tunnel chills 20-kilogram blocks of cheese wrapped in a plastic liner, each block being within a cardboard carton having dimensions of 190×300×385 mm, from 30°C to 10°C in a 24-hour cooling cycle.

Figure 4.1 The industrial cheese chilling tunnel (photo courtesy of Milmeq)

During the commercial chilling process, the cartons in the tunnel are cooled by a constant stream of air forced through the refrigeration coil at one end of the tunnel,

and then through the food pallet suspended in the upper and lower tiers. On the conveyor, two cartons were placed close to each other to form a block. These blocks were lined up in a row before being transferred to the pallet shelf. The product arrangement in the real tunnel is shown in Figure 4.2a. Spacing between the cartons ensures each block is subjected to the same airflow profile and refrigerated air temperature. The cold air flowed parallel to the longest side of the cartons (the 385 mm dimension).

A laboratory scale forced-air cooling tunnel was designed, as performing experiments at full scale was unfeasible due to the high experimental cost. It was assumed that the cheese carton distribution within the tunnel was uniform and each carton was symmetric about the vertical centre plane along the flow direction. Based on this assumption, only six cartons with four blocks on the two sides of the central pair cut by the symmetry plane were modelled in the experiments (Figure 4.2b).

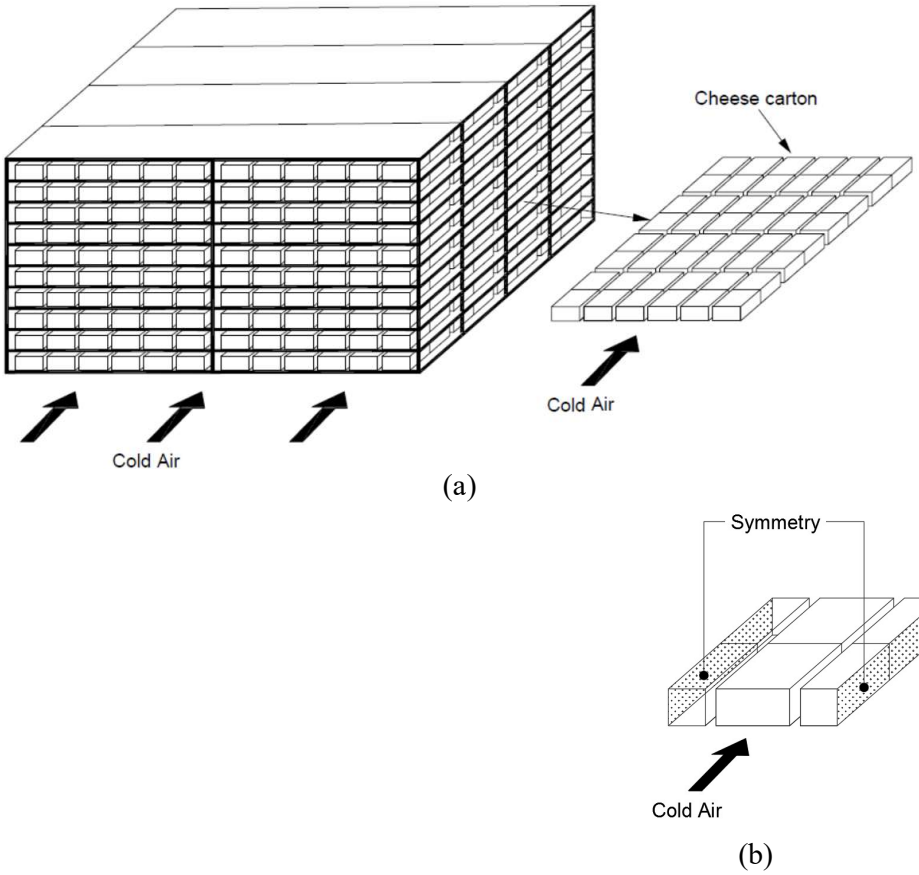

Figure 4.2 a) Products arrangement in the industrial cheese chiller. b) Experimental domain

The sample life of food materials is relatively short due to microbiological spoilage. Therefore, food analogue materials, such as agar gel, are often used in food processing experiments. Agar gel is easily shaped to a desired form and can be reused for many experiments without spoilage. The thermophysical properties of agar gel are also well established. For these reasons, agar gel was used instead of real cheese during chilling experiments. Six blocks of agar gel (5% agar powder, and 95% water on the weight basis) in acrylic plastic boxes were arranged to create an airflow pattern similar to the industrial tunnel (Figure 4.3).

Figure 4.3: Six blocks of agar arrangement

Because of space constraints, the dimensions of the blocks of agar were obtained by scaling all the linear dimensions of the cheese carton by a factor of 0.7, meaning the agar block volume was only 34% that of the actual block of cheese. The dimensions of the two test blocks in the middle were 135×210× 270 mm, while the dimensions of the half blocks on the sides were 135×105×270 mm.

These blocks of agar were then placed in a polystyrene test chamber (PTT; Figure 4.4a) which was in turn placed into an environmental testing chamber (ETC). A transition section (Figure 4.4b) was created to guide the airflow from the inlet through the product due to a suction created by a variable speed fan at the tunnel outlet. A fine net was placed at the upstream end of the tunnel to diffuse the airflow. The experimental set up allowed for precise control of the temperature and velocity of the refrigerated air passing through the PTT.

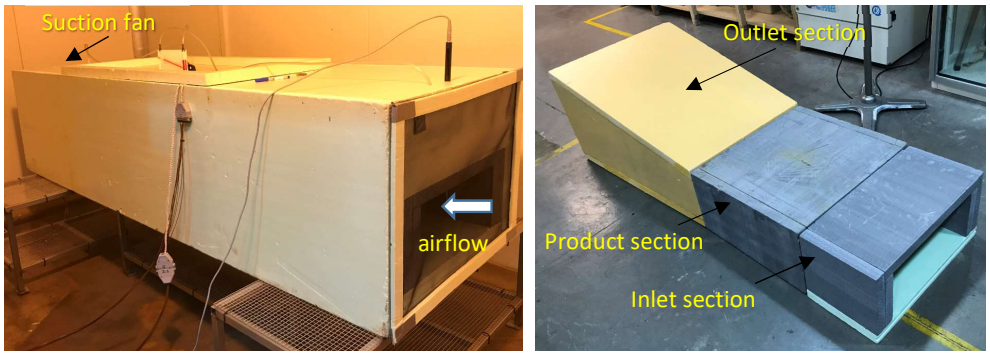

a) b)

Figure 4.4: a) Polystyrene Test Tunnel and b) the transition section

Temperatures were measured with T-type thermocouples connected to a Keysight 24982A data acquisition unit and were recorded every 60 seconds. Figure 4.5 indicates the thermocouple positions in the agar blocks. Thermocouple Numbers 1 and 11 measured the cooling air temperature. Multipoint thermocouple probes supporting thermocouple Numbers 3, 4, 5 and 13, 14, 15 were placed along the shortest axes of Block A and Block B respectively. Thermocouple Numbers 4 and 14 were at the geometric centre of the blocks and the two other thermocouples on each multipoint probe were 2 cm from the geometric centre. The other thermocouples were at the middle of each surface of the agar blocks. The thermocouples were calibrated with an ice-point reference prior to the experiments.

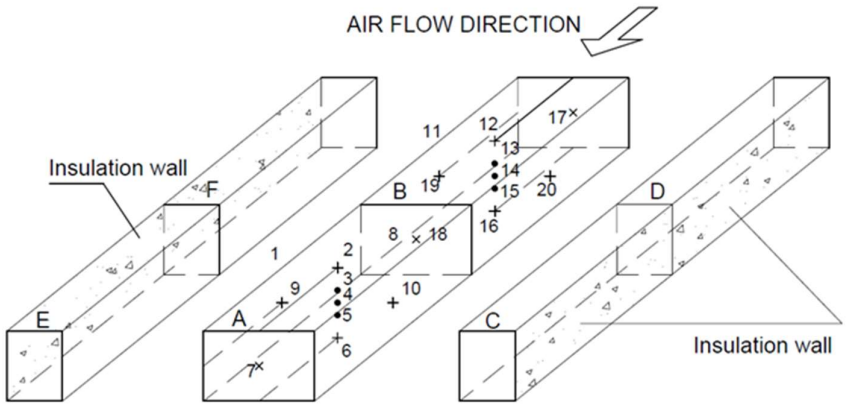

Figure 4.5: Thermocouples position in the six blocks of agar chilling trials (not to scale)

In order to locate the exact position of the geometric centre of the block of agar, a multi-thermocouple probe was inserted into the centre of the block of agar. This was achieved by placing the probe when the plastic container was half-full of agar

(Figure 4.6a). When a half-block of agar was firm, and the mid-point of the multi-thermocouple was rigidly attached to the geometric centre of the block of agar, the remaining volume of the container was then filled with agar (Figure 4.6b).

Surface temperatures were measured by thermocouples that were mounted on a copper plate to increase the area in contact with the surface of the agar block and placed in the middle of each surface of blocks (Figure 4.7).

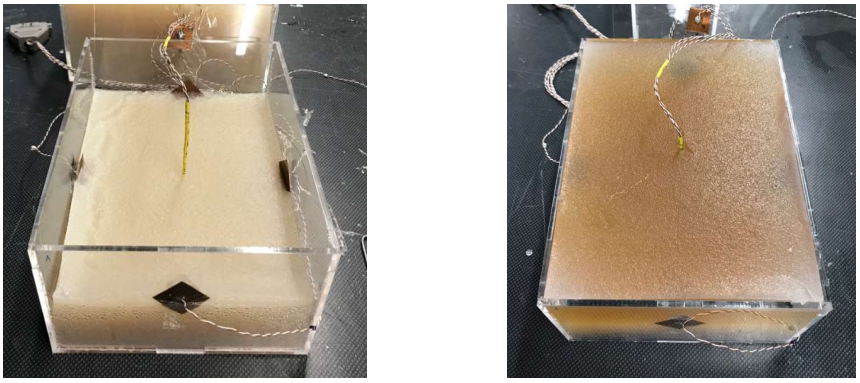

a) b)

Figure 4.6: The process of inserting a multi-thermocouple probe in a block of agar: a) half-full block of agar, b) full block of agar in a plastic box

Figure 4.7: Image of a surface temperature's thermocouple

Prior to each chilling trial, the six blocks of agar were equilibrated at 20°C for at least 24 hours. The agar temperatures were also monitored during the equilibrating process to ascertain all temperatures measured in each block of agar were within 0.5°C of 20°C. The ETC temperature was set and maintained at 0°C during the trials. The initial agar temperature and refrigerated air temperature were chosen to suit the controlled temperature range of the ETC while keeping the same temperature driving force for heat transfer as industrial cheese chilling (30°C to

10°C). The experiment was terminated when all the monitored temperatures fell below 2.5°C, which represents the seven-eighths cooling time (i.e. the time required for the temperature difference to be one-eighth of the initial temperature difference).

The air velocity was kept constant during each experiment. Three different inlet air velocities (1 m s^{-1}, 3 m s^{-1}, 4.5 m s^{-1}) were tested, and each trial was repeated three times. The air velocity was measured by a hot-wire anemometer (DANTEC 54N60 FlowMaster, Figure 4.8a) before and after each trial both at the inlet of the tunnel and at a position 2 cm above the top surface of the test blocks. The sample time of each velocity measurement was five minutes. The inlet and outlet pressures of the airflow through the PTT were measured before and after each trial using an inclined fluid manometer (RS Pro, RS 730-2937, Figure 4.8b).

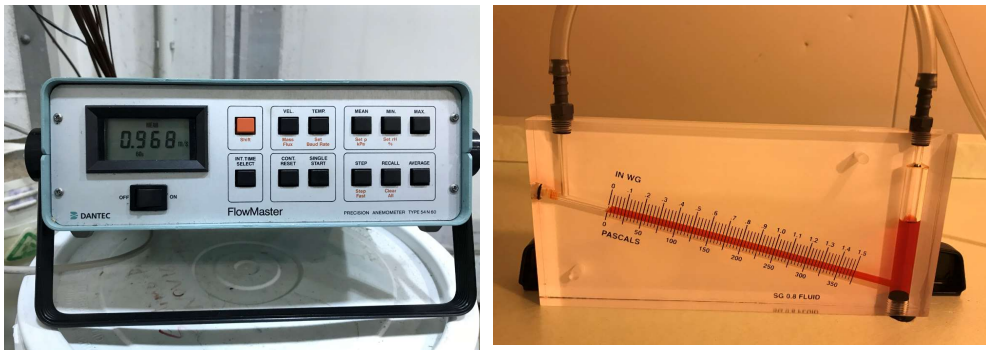

a) b)

Figure 4.8: a) DANTEC anemometer and b) inclined fluid manometer

4.3 CFD model for six blocks of agar chilling

4.3.1 Introduction

In this section, a CFD model for heat transfer in six blocks of agar in a forced-air chiller is presented. In the first step, a steady-state simulation of the airflow and heat transfer was performed to identify the air velocity distribution, and the convective heat transfer coefficient at the product surface. Next, the converged steady-state solution for the airflow was used as an initial condition for an unsteady heat transfer simulation.

4.3.2 Geometrical model

To save the computational cost, the computational domain of the multiple agar block chilling model was reduced by a factor of 2 based on a symmetry plane, (Figure 4.9). The geometrical model was created using Ansys Design Modeller, with half of the centre blocks, and the two half-blocks on the left side included in the geometrical model.

The inlet boundary was located 30 cm upstream from the product section and the outlet boundary was 155 cm downstream of the product section to prevent the inlet and outlet boundary conditions from influencing the airflow distribution over the product section.

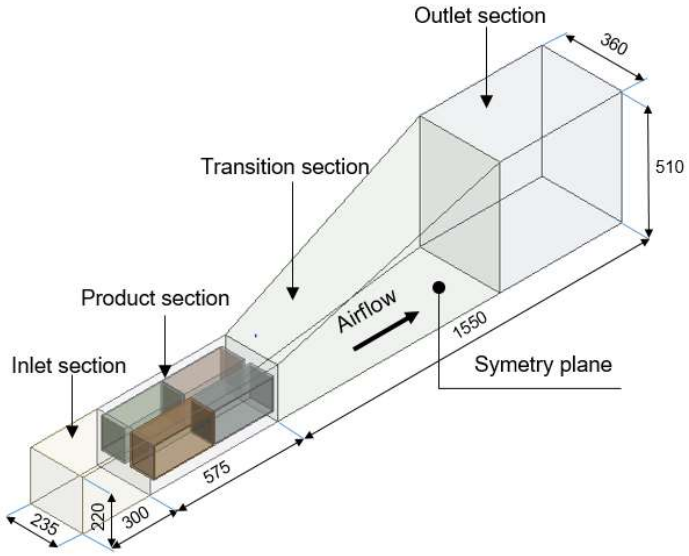

Figure 4.9: The computational domain of the six blocks agar chilling

4.3.3 Transport phenomena and governing equations in the forced air cooling

In the forced air cooling of food materials, the mechanisms for heat transfer can be complicated. Heat is removed by conduction within the product, then at the product surface, convective heat transfer is the main cooling mechanism. Heat also can be lost from the surface of the product by means of moisture loss (evaporation) and thermal radiation. In the agar chilling trials, the agar blocks were enclosed in plastic boxes which were sealed with glue and tape, and therefore, moisture evaporation

can be assumed to be insignificant. Previous studies have concluded that radiation heat transfer has a negligible effect in forced-air cooling of food products (Defraeye, Lambrecht, et al., 2013; Gruyters et al., 2018; O'Sullivan et al., 2016), and thus it was not included in the model.

The airflow field around the agar blocks can be either laminar or turbulent. The Reynolds number for the airflow forced through the cooling tunnel was used to characterise the flow regime. The minimum air velocity in the multiple agar block chilling experiments was 1 m s^{-1} (section 4.2.2). The hydraulic diameter at the inlet of the tunnel was $D_H = 4A/P = 0.3$ m, and the kinematic viscosity of air at 0°C was $\nu = 1.338 \times 10^{-5}$ m^2 s^{-1} (Cengel & Ghajar, 2011). Therefore, the resulting Reynolds number was:

$$\mathrm{Re} = \frac{uD_H}{\nu} = \frac{1 \times 0.3}{1.338 \times 10^{-5}} = 22421 \tag{4.1}$$

The Reynolds number of 22421 at the minimum air velocity confirmed that the flow in the cooling tunnel was within the turbulent regime.

The flow field and heat transfer calculations can be decoupled if there is no temperature-dependence of the air thermal properties or buoyancy force (Fluent, 2017). The thermal properties of air can be considered to be constant due to relatively small temperature change during the process (less than 20°C; Dehghannya et al., 2010; Ferrua & Singh, 2009; Gruyters et al., 2018; Tanner et al., 2002) . The buoyancy effects can be estimated by the ratio between Grashof and Reynolds number squared (Eq. 4.2). If this ratio is lower than unity, the buoyancy force can be neglected (Cengel & Ghajar, 2011; Fluent, 2017).

$$\frac{Gr}{\mathrm{Re}^2} = \frac{g\beta\Delta TL}{u^2} \tag{4.2}$$

where g (m s^{-2}) is the acceleration due to gravity; β (K^{-1}) is the volumetric thermal expansion coefficient; ΔT (K) is the temperature difference between the product surface and the bulk of air; L (m) is the characteristic length; and u (m s^{-1}) is the airflow velocity.

At the beginning of the chilling process, the initial agar temperature is 20°C, the refrigerated air temperature is 0°C. The hydraulic diameter of the two test blocks of agar (Height = 0.135 m, Length = 0.540 m, Width = 0.210 m) is used as the characteristic length, $L = V/A = 0.036$ m, and the thermal expansion coefficient of air at 0°C is estimated from the ideal gas approximation, $\beta = T^{-1} = 3.66\times10^{-3}$ K^{-1}. Substituting these values into Eq. 4.2 for 1 m s^{-1} yields:

$$\frac{Gr}{\mathrm{Re}^2} = \frac{g\beta\Delta TL}{u^2} = \frac{9.81\times 0.00366\times 20\times 0.036}{1^2} = 0.026 \tag{4.3}$$

Since the calculated value of Gr/Re^2 (0.026) is significantly less than unity, buoyancy-driven flows can be neglected in this study.

Under these flow conditions, the airflow around agar blocks can be simulated as steady and incompressible flow (Ferrua & Singh, 2009b; Redding, Yang, Shim, Olatunji, & East, 2016), and the flow within the system can be described by the following forms of the continuity and momentum equations, respectively:

$$\nabla \cdot u = 0 \tag{4.4}$$

$$u \cdot \nabla u = -\frac{\nabla P}{\rho_a} + \nu_a \nabla^2 u \tag{4.5}$$

where u (m s^{-1}) is the velocity vector, P (Pa) is the pressure, ρ_a (kg m^{-3}) is the air density, and ν_a (m^2 s^{-1}) is the kinematic viscosity of air.

The energy transport in the air can include not only conduction and convection but also the diffusion of the water vapour (Ferrua & Singh, 2009b). However, since the agar was contained in sealed boxes, moisture evaporation was insignificant in this study. Hence, the energy equation in the air domain was described by:

$$\rho_a c_a \left(\frac{\partial T_a}{\partial t} + u \cdot \nabla T_a \right) = k_a \nabla^2 T_a \tag{4.6}$$

where c_a (J kg^{-1} K^{-1}), k_a (W m^{-1} K^{-}) and T_a (K) are heat capacity, thermal conductivity and temperature of air, respectively.

The heat transfer equation within solid regions (agar blocks and plastic boxes) was modelled as:

$$\rho_s c_s \left(\frac{\partial T_s}{\partial t} \right) = k_s \nabla^2 T_s \tag{4.7}$$

where t (s) is the processing time; ρ_s (kg m^{-3}), c_s (J kg^{-1} K^{-1}), k_s (W m^{-1} K^{-}) and T_s (K) are the density, heat capacity, thermal conductivity and temperature of solid, respectively.

4.3.4 Numerical setup

4.3.4.1 Thermal physical properties of materials

The thermophysical properties of the agar, acrylic plastic and air are listed in Table 4.1. As discussed above, the thermal properties of air can be assumed to be independent of temperature and were determined based on the thermal properties of the dry air at 0°C found in (Cengel & Ghajar, 2011). The density and specific heat of agar can be estimated from properties of water at the same temperature, found in (Cengel & Ghajar, 2011), while the thermal conductivity of agar was obtained from (Zhang et al., 2010). The thermal properties of acrylic plastic can be found in (EngineeringToolbox). Since the variation of thermal properties of agar and acrylic plastic were less than 4% within the range of temperature used in the experiments (from 20°C to 2.5°C), their properties at the initial temperature of 20°C were chosen in the calculations

Table 4.1: Material thermo-physical properties

Materials	Density (kg m^{-3})	Specific heat (J kg^{-1}K^{-1})	Thermal cond, (W m^{-1} K^{-1})	Dynamic Viscosity (kg m^{-1} s^{-1})
Air	1.292	1006	0.02364	1.729 x 10^{-5}
Acrylic	1190	1470	0.2	-
Agar	998	4182	0.543	-

4.3.4.2 Boundary conditions

The surfaces of the blocks of agar were modelled as no-slip walls with zero roughness. A zero heat flux boundary condition was used for the sidewalls of the PTT. The coupled thermal condition was applied for the interfaces between airflow and acrylic, acrylic and agar, and acrylic and acrylic.

The inlet of the computational domain was defined as the velocity inlet with velocities of 1 m s^{-1}, 3.0 m s^{-1}, and 4.5 m s^{-1} imposed, as for the experiments. The inlet temperature was set to the temperature of the ETC (0°C, section 4.2.2). The low turbulence intensity of 1% was used due to the presence of the fine airflow diffuser.

The outlet of the computational domain was defined as a pressure outlet with an underpressure measured by the inclined manometer to represent the pressure drop created by the suction fan. An outlet pressure of -85, -35 and -5 Pa were imposed for the high, medium and low inlet air velocity, respectively.

4.3.4.3 CFD simulation.

The CFD code used was ANSYS Fluent 18.2, which uses the finite volume technique. The standard k-ε turbulence model was employed, due to its robustness, relative accuracy over the wide range of turbulence flows and CPU efficiency (Fluent, 2017). The Enhanced Wall Treatment (EWT) option which automatically switches from a low-Reynolds-number approach to the wall functions (Fluent, 2017) was enabled for near-wall modelling. The fluid region close to the agar block surface was meshed with a small mesh size to ensure the low y^+ value (the dimensionless wall distance used to describe the flow behaviour) for the low-Reynolds-number approach would be valid. From the surface of the agar blocks outwards, 10 layers of hexahedral elements were placed with the first layer thickness of 0.1 mm and a growth rate of 1.2.

A hybrid mesh with tetrahedral and hexahedral elements was generated using ANSYS mesh generation software. The element size in the product section was 10

mm while the maximum face size was kept as default (36.5 mm). A mesh sensitivity study was performed by running simulations at three different mesh sizes to estimate the spatial discretization error from the difference in the average surface heat transfer coefficient (*SHTC*) of two test blocks of agar (Table 4.2).

The mesh independent solution was determined by Richardson extrapolation (Roache, 1997), and the value of the average *SHTC* was 42.44 $Wm^{-2}\,K^{-1}$. The error of the average *SHTC* for a mesh size of 0.1 mm of 1.2% was considered sufficiently low. Therefore, the mesh with 273258 elements was chosen for these computations.

Table 4.2. Effect of different mesh size on average *SHTC* of two test blocks of agar

Mesh size on product surface (mm)	Number of elements	y^+ (average)	*SHTC* (average) ($W\,m^{-2}\,K^{-1}$)
0.4	262923	5.06	46.05
0.2	266901	2.52	44.12
0.1	273258	1.25	42.94

The pressure-velocity coupling was solved with the SIMPLE scheme. The second-order spatial discretisation was used throughout for pressure, momentum, turbulence kinetic energy, turbulence dissipation rate and energy. The Green Gauss Cell-Based method was employed for the gradient discretization. The default solution controls were used.

Prior to the transient simulation of the chilling process, steady-state simulations of airflow and heat transfer were performed using a constant agar temperature of 20°C (the initial agar temperature, section 4.2.2). These simulations were used to obtain the initial flow field and the heat transfer coefficient on the surface of the agar blocks. Subsequently, transient simulations were performed to predict the temperature history of the agar block during the forced-air chilling. Because the steady-state airflow field was imposed during the transient simulations and buoyancy was not included in the model (section 4.3.3), the flow and turbulence calculations could be turned 'off' to reduce computation time. The transient simulation was run with a time step of 1 minute and a maximum of 20 iterations for

each time step. The computational time for 800 minutes of simulated cooling time was 21 minutes on a 64-bit Intel ® Xeon ® CPU E5-1620, 3.5 GHz, 16 GB RAM.

4.3.5 Results

4.3.5.1 Uncertainty analysis of the experimental data

The temperature profile of the agar blocks was computed by averaging the temperature history of the three replicates of the experimental trials, Eq. 4.8:

$$\overline{T}_i(t) = \frac{\sum_{j=1}^{n} T_{ij}(t)}{n} \tag{4.8}$$

where $\overline{T}_i$ (K) is the average temperature at the i^{th} thermocouple; T_{ij} (K) is the temperature of the i^{th} thermocouple number in the j^{th} trial; n is the number of experimental trials (n =3); and t(s) is the processing time. The experimental uncertainty in $\overline{T}_i(t)$ at 95% confidence interval and a normal distribution, was computed by Eq. 4.9:

$$P_{\overline{T}_i}(t) = \tau_{n-1,0.025} \times \frac{1}{\sqrt{n}} \left[\frac{1}{n-1} \sum_{i=1}^{n} \left(\overline{T}_i - T_{ij} \right)^2 \right]^{1/2} \tag{4.9}$$

where $P_{\overline{T}_i}(t)$ (°C) is the uncertainty in $\overline{T}_i$; $\tau_{n-1,0.025}$ is the student's t-statistic with (n-1) degrees of freedom at a 95% confidence interval.

4.3.5.2 Comparison of measured and predicted temperatures

Figure 4.10 illustrates the comparison between the predicted and experimental temperatures of the two test blocks, in which Block B was at the front and Block A was at the back along the flow direction at the inlet air velocity of 1 m s^{-1}. Results were shown for the geometric center temperatures (T4 and T14) and the top surface temperatures (T2 and T12). The error bars represent the experimental uncertainty at 95% confidence interval. The experimental air temperature was calculated as the

averaged value of three replicated trials (section 4.2). Figure 4.11 and 4.12 show a similar comparison at the inlet air velocity of 3.0 m s^{-1} and 4.5 m s^{-1}, respectively.

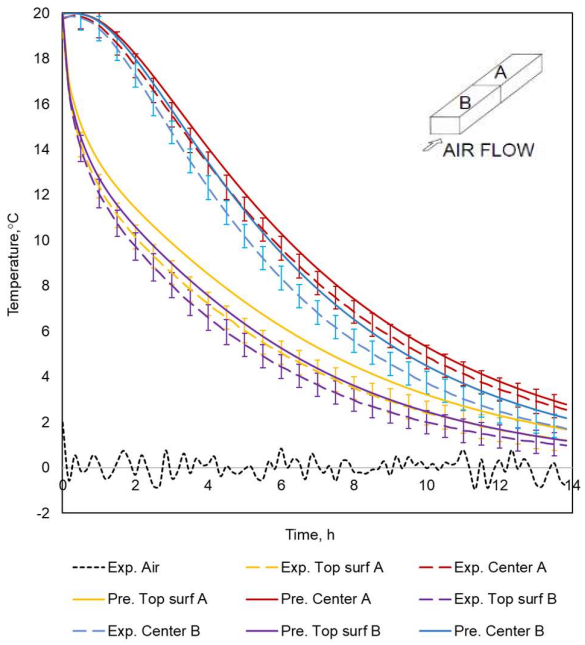

Figure 4.10: Comparison between predicted and experimental temperature of two tested blocks at the inlet velocity of 1 m s^{-1}

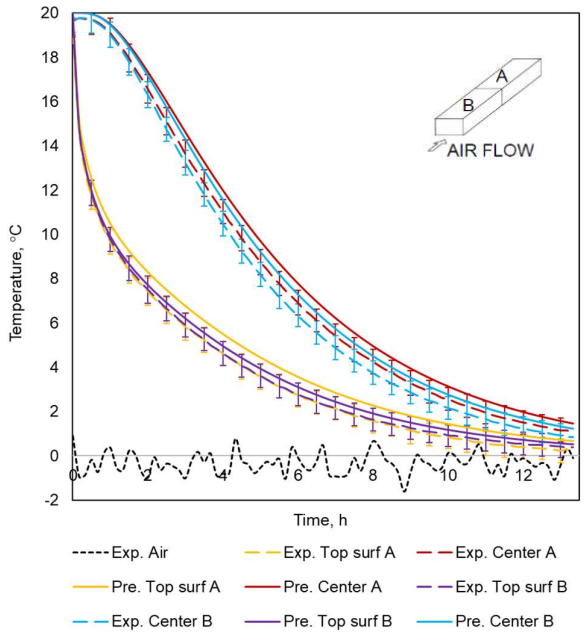

Figure 4.11: Comparison between predicted and experimental temperature of two tested blocks at the inlet velocity of 3 m s^{-1}

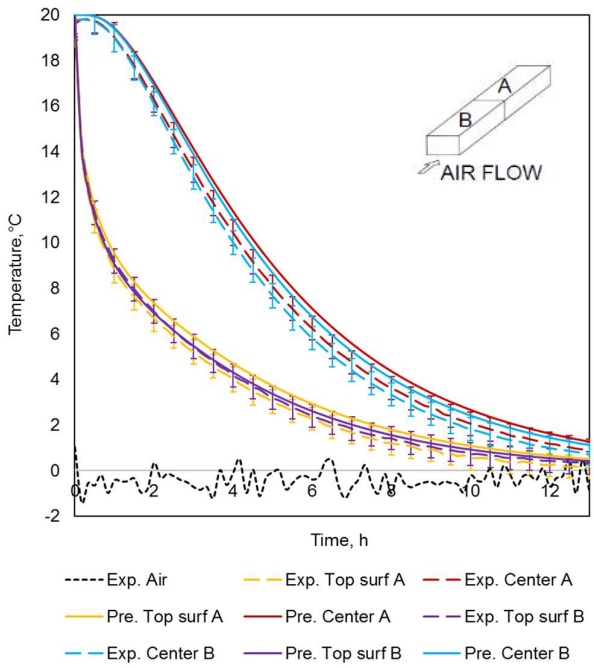

Figure 4.12: Comparison between predicted and experimental temperature of two tested blocks at the inlet velocity of 4.5 m s^{-1}

Figures 4.10 - 4.12 show good agreement between predicted and experimental data. The model tended to underpredict the temperature drop. This could be explained by the model not including the effect of natural convection and thermal radiation.

The accuracy of the temperature predictions of the CFD model was evaluated by the mean absolute temperature difference, ΔT_{mean} as Eq. 4.10 below:

$$\Delta T_{mean} = \frac{\sum_{i=1}^{n} \left| T_{m,i} - T_{p,i} \right|}{n} \tag{4.10}$$

where $T_{m,i}$ (K) and $T_{p,i}$ (K) are the measured and predicted temperature at time point i and n is the number of measured temperature values.

The values of ΔT_{mean} at different measured temperatures are given in Table 4.3. The Biot numbers at each testing conditions was determined by:

$$\mathrm{Bi} = \frac{hL}{k} \tag{4.11}$$

where h (W m^2 K^{-1}) is the surface-averaged heat transfer coefficient of two test blocks (section 4.3.5.3), L (m) is the characteristic dimension, L = 0.036 m (Section 4.3.3), and k (W m^{-1} K^{-1}) is the thermal conductivity of agar, k = 0.543 W m^{-1} K^{-1} (Table 4.1)

Table 4.3: Mean absolute temperature difference at different locations and testing conditions.

Testing conditions		ΔT_{mean} (°C)							
v (m s^{-1})	Bi	T2	T4	T7	T10	T12	T14	T17	T20
1	1.0	1.0	0.5	0.5	0.6	0.8	0.6	0.8	0.2
3	2.2	0.7	0.7	0.1	0.2	0.2	0.7	0.2	0.3
4.5	2.8	0.6	0.7	0.1	0.2	0.1	0.7	0.1	0.3

Overall, the model predictions fit well with the experimental data. The values of ΔT_{mean} were 1.0°C or less for all the monitored temperatures. At the lowest inlet air velocity (1 m s^{-1}), the largest differences between predicted and measured temperatures were at the top surfaces (T2 and T12, Figure 4.5) with ΔT_{mean}= 1.0°C and 0.8°C, respectively. At the highest airspeed (4.5 m s^{-1}), the largest differences were at the centre temperatures (T4 and T14, Figure 4.5), with ΔT_{mean}= 0.7°C for both positions.

At the low air velocity (low Biot number) the uncertainty of the surface heat transfer coefficient (e.g. neglecting natural convection and thermal radiation) is more pronounced. That could be hypothesised to explain the high discrepancies between predicted and experimental surface temperatures.

At higher air velocity (higher Biot number), the system becomes dominated by internal resistance to heat transfer. Therefore, the uncertainty of thermal properties (e.g. assuming a constant thermal properties) is more pronounced. The predicted centre temperatures which are more affected by the thermal property uncertainty would have higher errors compared to predicted surface temperatures.

4.3.5.3 Local surface heat transfer coefficient

The surface heat transfer coefficient (*SHTC*), h (W m^{-2} K^{-1}), was calculated by Eq. 4.12:

$$h = \frac{q_{wall}}{T_{in} - T_{air}} \tag{4.12}$$

where q_{wall} (W m^{-2}) is the initial wall heat flux determined from the steady-state simulation, T_{in} (K) is the initial temperature of the blocks of agar, and T_{air} (K) is the cooling air temperature. Figure 4.13 shows a contour plot of the *SHTC* of two test blocks of agar, at the inlet air velocity of 4.5 m s^{-1}. The *SHTC* across the agar block surface varied by a factor of 5, with the maximum value at the four corners of the surface on the upstream side and minimum values at the opposite surface. The averaged *SHTC* over the agar blocks surface at air velocities of 1 m s^{-1}, 3 m s^{-1}, and 4.5 m s^{-1} were 15.3 W m $^{-1}$ K $^{-2}$, 32.5 W m $^{-1}$ K $^{-2}$ and 42.9 W m $^{-1}$ K $^{-2}$, respectively.

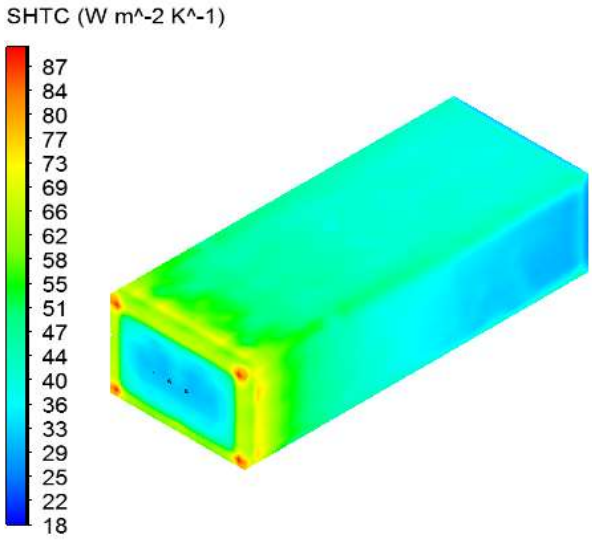

Figure 4.13: *SHTC* of two test blocks of agar at the inlet air velocity of 4.5 m s^{-1}

4.3.5.4 Cooling heterogeneity of two tested blocks of agar

Figure 4.14 illustrates the discrepancies between predicted temperatures at the same positions on the surface (T2 vs T12, T10 vs T20, Figure 4.5) and at the geometrical centre (T4 vs T14, Figure 4.5) of the two test blocks of agar at the inlet air velocity

of 4.5 m s^{-1}. The maximum temperature difference at the surface (1°C) was about two and a half times higher than that at the centre of the two blocks (0.4°C). The temperature decreased faster in block B (in the front with respect to the airflow direction) than in block A (at the back). This trend is more obvious at the surface temperatures at the beginning of the chilling process. This observation was to be expected since the surface heat transfer coefficient decreased along the flow direction (Figure 4.13) and is consistent with heat transfer theory for convection over a flat surface (Cengel & Ghajar, 2011). At the end of the process, the temperature difference between the agar block surface and the air was comparatively small and the temperatures of the two blocks were almost the same.

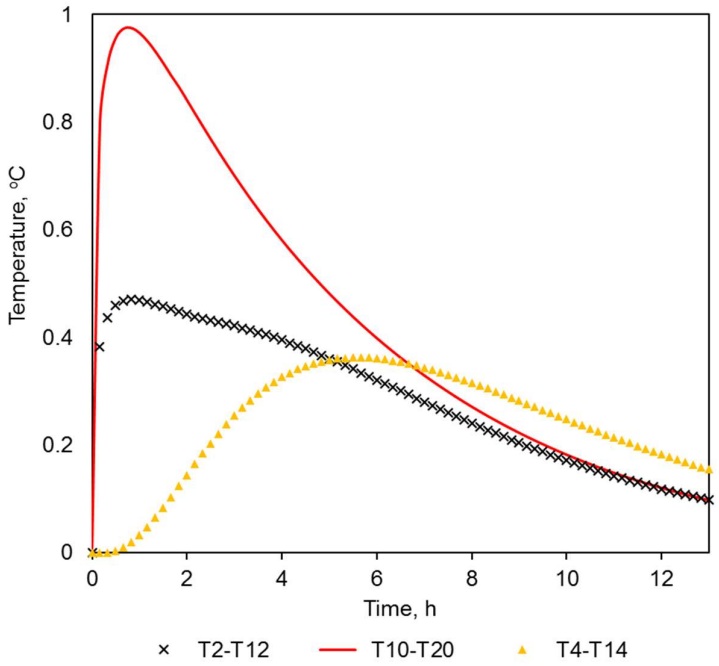

Figure 4.14: Temperature difference of the two test blocks at the same positions at the inlet air velocity of 4.5 m s^{-1}

Figure 4.15 presents the predicted temperature distribution of two test blocks agar at the velocity inlet of 4.5 m s^{-1} after 4.5 hours (the half cooling time). The cooling rate was fastest at the corners, and the slowest cooling position was at the centre of the interface of the two test blocks.

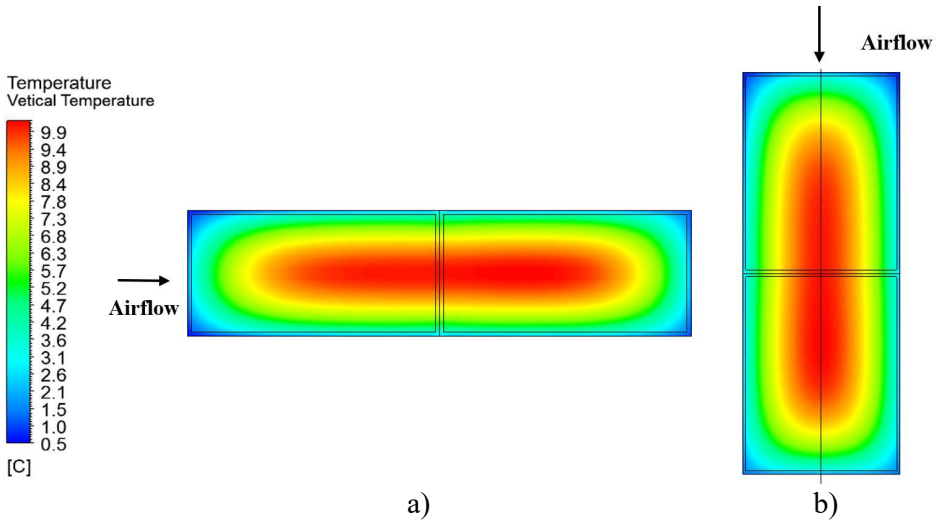

Figure 4.15: Temperature distribution for a) vertical symmetry plane and b) horizontal symmetry plane of the two test blocks agar after 4.5 hours (half cooling time) at the velocity inlet of 4.5 m s^{-1}

4.3.6. Conclusion

The CFD model for the forced air chilling of six agar blocks in an arrangement that was representative of an industrial cheese chiller was presented and validated.

The use of standard k-ε turbulence model with the Enhanced Wall Treatment function can predict to within 1°C compared to experimental data. However, due to model simplification, the model routinely underpredicted the experimentally observed cooling rate.

The model presented in this study can be applied for industrial cheese chilling operations which have a similar airflow pattern and product arrangement as the experiment.

Chapter 5
A simple heat transfer simulation for the forced-air chilling of food products

5.1 Introduction

For industrial use, a quick and reliable solution to predict the chilling time, product temperature distributions and heat flow is useful to have, rather than always spending time to set up a complicated CFD solution. In addition, it is highly unlikely that a company will be prepared to pay for a CFD licence or employ someone who has sufficient expertise to use it if they do not have to. In this chapter, a one-dimensional numerical solution proposed by Ghraizi, Chumak, Onistchenko, and Terziev (1996) has been used with a new thermal properties model and heat transfer coefficients to develop a simplified cooling simulation. This approach uses the partial differential equation describing one-dimensional non-linear unsteady heat conduction inside of the product, and solves it by a finite difference technique. The method can take into account the temperature-dependence of thermal properties of foods and a general shape factor is used to reflect the product geometry. The simulation was applied to a single block of cheese, and agar. Predicted results were compared to experimentally measured temperature profiles as well as to results generated by the commercial FPM software.

5.2 Experimental system

The chilling trials for a single block of cheese and a single block of agar were conducted in the environmental test chamber (ETC) at AgResearch Ltd, Hamilton, New Zealand. The blocks of agar were taken from the six agar blocks experiments (section 4.2). Because access to the ETC was limited, two chilling trials were performed simultaneously, by using two polystyrene test tunnels (PTT, Figure 5.1), in which one agar block was put in the top tunnel and the other block was placed in the bottom tunnel. To increase the air velocity through the PTT, a transition section was made to reduce the cross-sectional area in the product section. The transition section was attached to the original PTT walls by screws and sealed by duct tape to ensure that all the air drawn by the fan passed through the product section.

Figure 5.1: Experimental system for a single block of agar chilling

The modified PTT with a transition section is shown in Figure 5.2, in which the cross-sectional area at the product section was reduced by a factor of 2.4 compared to the original PTT. The cross-sectional area at the inlet and the outlet of the modified tunnel were 510×300 mm and 510×720 mm respectively, while the length of the tunnel was kept at 2400 mm as the original PTT.

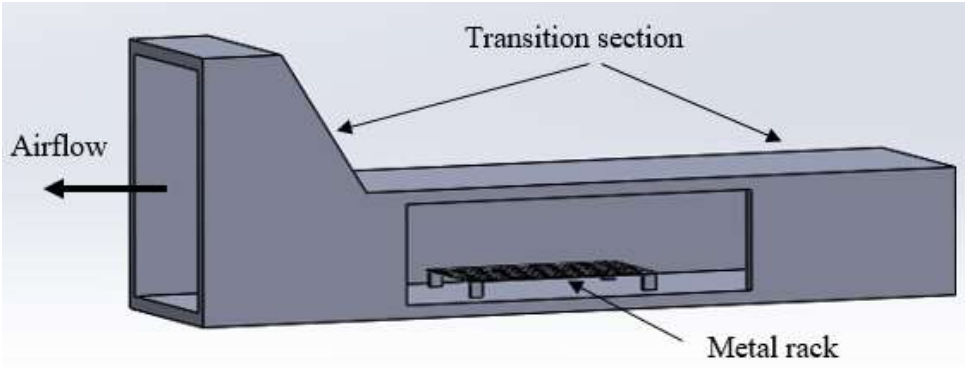

Figure 5.2: The modified PTT with a transition section for the single block of agar experiment

A metal rack was provided to support the test block and allow airflow to sweep the bottom surface of the sample. The configurations of the two tunnels (dimensions, transition section, and suction fan) were identical, making the airflow patterns of the top and the bottom tunnel the same.

The measurements and experimental procedure of the single block of agar experiments were the same as the experiments with six blocks of agar (section 4.2). Inlet air velocities of 1.0 m s^{-1} and 4.0 m s^{-1} were used and three replicate trials were performed at each air velocity.

In the last set of experiments, a real block of cheese measuring 190× 300×385 mm was used (Figure 5.3).

a) b)

Figure 5.3: a) The test sample, and b) a single block of cheese in the chilling tunnel

Figure 5.4 illustrates the thermocouple positions in the block of cheese. The multi-thermocouple probe supporting thermocouple Numbers 11, 12, 13 was placed along the shortest axis. Thermocouple Number 12 was at the geometric centre of the block and the two other thermocouples on the probe were 1.5 cm from the geometric centre. The multi-thermocouple probe supporting thermocouple Numbers 4, 5, 6, which was placed along the longest axis, positioned those thermocouples at 180, 140, 100 mm distance from the front surface in the airflow direction respectively. Thermocouple Numbers 2 and 16 measured the air temperature. The other thermocouples were surface thermocouples located at the centre of each surface outside the carton, except for thermocouple Number 14 and 7, which were placed inside the carton. All thermocouples were connected to the Keysight 24982A data acquisition unit and temperatures were recorded every 60 seconds.

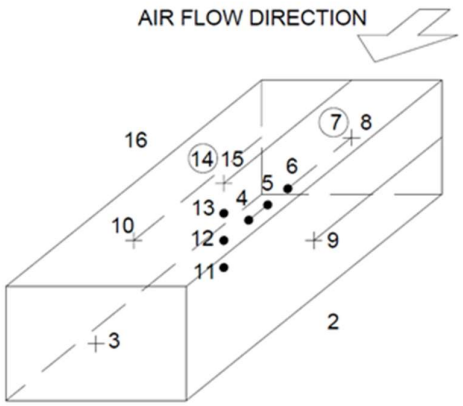

Figure 5.4: Thermocouples position in the single block of cheese chilling trial

The experimental measurements and procedure were similar to the experiment with six blocks of agar. The initial cheese temperature was within 0.5°C of 19.5°C, and the refrigerated air temperature was kept constant at 0°C. To save the experimental time, the experiments were terminated when all the monitored temperatures were fell below 10°C (half-way between the initial cheese temperature and the cooling air temperature). This experiment was conducted at two inlet air velocities, 1.0 and 4.4 m s^{-1} (note that the higher air velocity for the cheese (4.4 m s^{-1}) was greater than that for the agar 4.0 m s^{-1}). Each experiment was repeated twice.

5.3 Numerical solution

The mathematical model of the heat transfer upon symmetric cooling was defined as a non-linear heat conduction equation with the corresponding boundary conditions, as follows (Fikiin, 1996; Ghraizi et al., 1996):

$$C(T)\frac{\partial T(x,t)}{\partial t} = \frac{1}{x^E}\frac{\partial}{\partial x}\left[k(T)x^E\frac{\partial T(x,t)}{\partial x}\right] \tag{5.1}$$

$$T(x,0) = T_{in}(x) \tag{5.2}$$

$$\left.\frac{\partial(x,t)}{\partial x}\right|_{x=0} = 0 \tag{5.3}$$

$$-k(T)\left.\frac{\partial T(x,t)}{\partial x}\right|_{x=R} = h\left[T(R,t) - T_a\right] \tag{5.4}$$

where C (J m^{-3} K^{-1}) is the volumetric heat capacity, E is the shape factor and R (m) is characteristic length determined as the half-thickness of the shortest dimension. Eq. 5.1 is the Fourier heat conduction equation inside food products, Eq. 5.2 is the initial boundary equation, Eq. 5.3 is the symmetric boundary condition and Eq. 5.4 is the third kind boundary condition prescribing the heat flux due to convection on the surface of a food product. The shape factor, E, is used to account for the 'dimensionality' of the heat transfer problem. When the appropriate value for E is inserted into the one-dimensional form of the heat conduction equation (Eq. 5.1), the results will coincide or be satisfactorily close to those obtained by solving the corresponding multidimensional problem (Fikiin, 1996). In the Ghraizi et al., (1996) model the formula of E developed by (Fikiin, 1996), Eq. 5.5, was used:

$$E = \frac{A.R}{V} - 1 \tag{5.5}$$

where A (m^2), V (m^3) are the heat transfer area and the volume of the object, respectively.

The finite difference scheme is shown in Figure 5.5, in which the (i,j)-point corresponding to position i ($x = x_i$) and time j ($t = t_j$) was determined as follows:

$$x_i = x_{i-1} + \Delta x,\ i = 1,2,\ldots,N\ ,\ \Delta x = \frac{R}{N}$$

$$t_j = t_{j-1} + \Delta t,\ j = 1,2\ldots$$

where the time step, Δt (s), and space increment, Δx (m), can be variable and N is the number of nodes. Because of the temperature-dependence of thermal properties, it is necessary to average those quantities in the vicinity (efgh) of each (i,j)-point to make the numerical solution to be more stable (Onishenko, Vjazovsky, & Gnatiuk, 1991). These local average values can be obtained by integrating the governing equation (Eq. 5.1) in the vicinity (efgh, Figure 5.5):

$$\iint_{efgh} x^E C(T) \cdot \frac{\partial T(x,t)}{\partial t} dxdt = \iint_{efgh} \frac{\partial}{\partial x}\left[k(T) \cdot x^E \frac{\partial T(x,t)}{\partial x} \right] dxdt \tag{5.6}$$

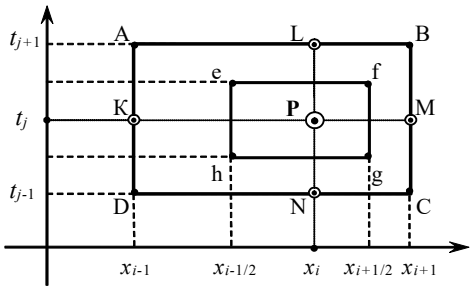

Figure 5.5: The finite different scheme

More details of the finite difference solution of Eq. (5.1-5.4) were presented in (Ghraizi et al., 1996), in which the internal nodes were discretized by the central difference formula, and the boundary nodes were approximated by the three-point backward/forward difference. The approximate system of linear algebraic equations, therefore, has the following form:

$$a_{ij}T_{ij} + b_{ij}T_{i\text{-}1,j} + e_{ij}T_{i+1,j} = d_{ij}, \quad i = 1,2,...,N\text{-}1 \tag{5.7}$$

$$3T_{0j} - 4T_{1j} + T_{2j} = 0 \tag{5.8}$$

$$-k\left(T_{Nj}\right)\frac{3T_{Nj} - 4T_{N\text{-}1,j} + T_{N\text{-}2,j}}{2\Delta x} + h\left[T_a - T_{Nj}\right] = 0 \tag{5.9}$$

where:

$$a_{ij} = \frac{C_{ij}}{E+1}\left[\left(x_i + \frac{\Delta x}{2}\right)^{E+1} - \left(x_i - \frac{\Delta x}{2}\right)^{E+1}\right] + \frac{\Delta t}{2\Delta x}k_{ij}^{\mathrm{II}}\left(x_i + \frac{\Delta x}{2}\right)^{E} + \frac{\Delta t}{2\Delta x}k_{ij}^{\mathrm{I}}\left(x_i - \frac{\Delta x}{2}\right)^{E}$$

$$b_{ij} = -\frac{\Delta t}{2\Delta x}k_{ij}^{\mathrm{I}}\left(x_i - \frac{\Delta x}{2}\right)^{E}$$

$$e_{ij} = -\frac{\Delta t}{2\Delta x}k_{ij}^{\mathrm{II}}\left(x_i + \frac{\Delta x}{2}\right)^{E}$$

$$d_{ij} = \left[\frac{C_{ij}}{E+1}\left\{\left(x_i + \frac{\Delta x}{2}\right)^{E+1} - \left(x_i - \frac{\Delta x}{2}\right)^{E+1}\right\} - \frac{\Delta t}{2\Delta x}\left\{k_{ij}^{\mathrm{II}}\left(x_i + \frac{\Delta x}{2}\right)^{E} + k_{ij}^{\mathrm{I}}\left(x_i - \frac{\Delta x}{2}\right)^{E}\right\}\right]T_{i,j\text{-}1} +$$
$$\frac{\Delta t}{2\Delta x}k_{ij}^{\mathrm{II}}\left(x_i + \frac{\Delta x}{2}\right)^{E}T_{i+1,j\text{-}1} + \frac{\Delta t}{2\Delta x}k_{ij}^{\mathrm{I}}\left(x_i - \frac{\Delta x}{2}\right)^{E}T_{i\text{-}1,j\text{-}1}$$

$C_{ij}, k_{ij}^{\mathrm{I}}, k_{ij}^{\mathrm{II}}$ are the volumetric heat capacity and average thermal conductivities of the *(i,j)*-point, determined as the average values of the adjacent points, and are assumed to be the constant values.

$$C_{ij} = (1/6)\left(C_K + C_P + C_M + C_C + C_N + C_D\right) \tag{5.10}$$

$$k_{ij}^{\mathrm{I}} = (1/6)\left(k_P + k_N + k_D + k_K + k_A + k_L\right) \tag{5.11}$$

$$k_{ij}^{\mathrm{II}} = (1/6)\left(k_P + k_L + k_B + k_M + k_C + k_N\right) \tag{5.12}$$

It may be observed that the system of equations, Eq. (5.7-5.9) has the tridiagonal form, which can be solved by the tridiagonal matrix algorithm. Its solution is illustrated in the form of the recursion formula below:

$$T_{ij} = M_{i+1,j} T_{i+1,j} + N_{i+1,j}; i = 0,1,\ldots, N-1 \tag{5.13}$$

$$M_{i+1,j} = \frac{-e_{ij}}{a_{ij} + b_{ij} M_{ij}};\ i = 1,2,\ \ldots,\ N\text{-}1 \tag{5.14}$$

$$M_{1,j} = \frac{a_1 + 4e_1}{3e_1 - b_1} \tag{5.15}$$

$$N_{i+1,j} = \frac{d_{ij} - b_{ij} N_{ij}}{a_{ij} + b_{ij} M_{ij}};\ i = 1,2,\ \ldots,\ N\text{-}1 \tag{5.16}$$

$$N_{1,j} = \frac{-d_1}{3e_1 - b_1} \tag{5.17}$$

$$T_{Nj} = \frac{d_{N-1,j} - 3T_a b_{N-1,j}\left(\dfrac{2\Delta x h}{3k\left(T_{Nj}\right)}\right) - N_{Nj}\left(a_{N-1,j} + 4b_{N-1,j}\right)}{M_{Nj}\left(a_{N-1,j} + 4b_{N-1,j}\right) + e_{N-1,j} - 3b_{N-1,j}\left(1 + \dfrac{2\Delta x h}{3k\left(T_{Nj}\right)}\right)} \tag{5.18}$$

In the procedure to determine the temperature profile at the j^{th} time step, the algorithm needs to know temperatures at the $(j\text{-}1)^{\text{th}}$, j^{th} and $(j+1)^{\text{th}}$ time step to calculate the average thermal properties of the *(i,j)*-point. Therefore, an iterative "prognosis-correction" regime (Figure 5.6) was required (Ghraizi et al., 1996), in which, K is the number of iterations and the iterations are interrupted when the maximal difference between the temperature profiles, T_{ij}, of two consecutive iterations is less than a given tolerance, ε.

The one-dimensional simulation was programmed in MATLAB (The MathWorks Inc., Natick, MA). In the simulation, the number of nodes was N =100 and the time

step Δt was 10 minutes. The computational time for 18 hours of cheese chilling was 30s on a 64-bit Intel ® Xeon ® CPU E5-1620, 3.5 GHz, 16 GB RAM

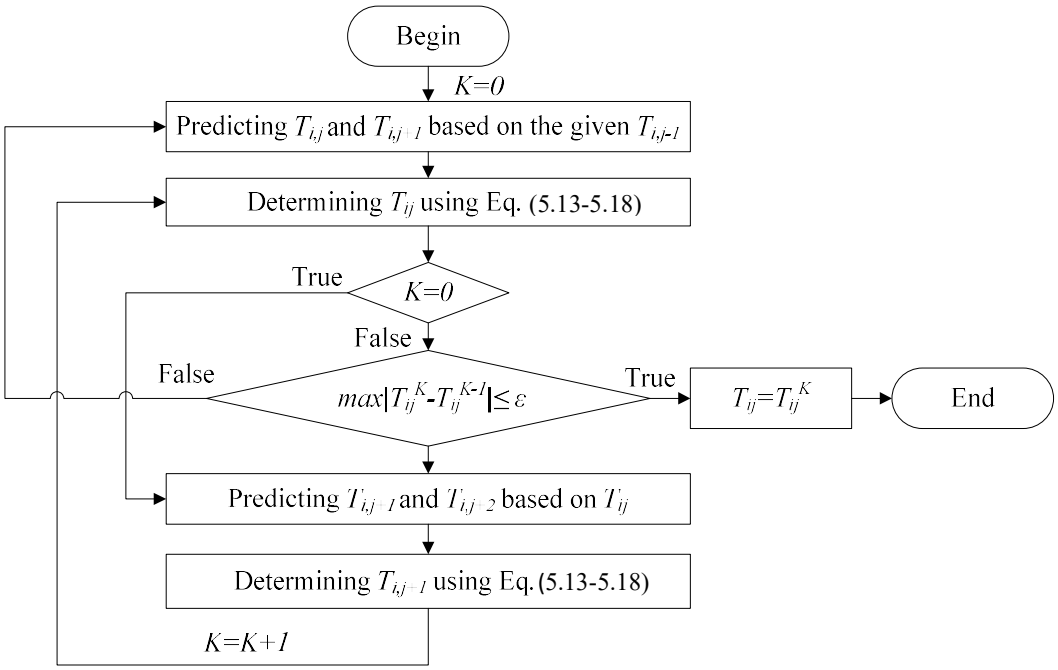

Figure 5.6: "Prognosis-correction" regime to determine T_{ij}

5.4 Thermal properties and heat transfer coefficient model

To apply the Ghraizi et al. (1996) model, the additive effective specific heat capacity model (Eq. 3.1), and the Dul'nev & Novikov thermal conductivity (Eqs. 3.30-3.33) were used as recommended in the chapter 3. The density model was kept as the original (Eq. 3.20). The composition of cheese used in the thermal properties calculation was 36.3% water, 23.5% protein, 34.1% fat, and 3.6% ash, found in (Willix et al., 1998), while agar was assumed to have the thermal properties of water.

The convective heat transfer coefficient was calculated by the correlation equation proposed by (Pham, Lowry, Fleming, Willix, & Reid, 1991) and (A. C. Cleland & Earle, 1976) to approximate convective heat transfer coefficient as function of airflow velocity. The overall heat transfer coefficient between the food package and the cooling medium, h (W m^{-2} K^{-1}), was determined from an estimate of the

convective heat transfer, the thermal resistance of the packaging materials, and the air gap between the food and packaging:

$$\frac{1}{h} = \frac{1}{h_{conv}} + \frac{\delta_{air}}{k_{air}} + \sum \frac{\delta_{pkg}}{k_{pkg}} \tag{5.19}$$

where the convective heat transfer coefficient was calculated as a mean value of the convective heat transfer coefficient correlations proposed by (Pham et al., 1991) and (A. C. Cleland & Earle, 1976):

$$h_{conv} = \frac{(u \times 8.6) + (u \times 4.5 + 6.8)}{2} \times 1.12 \tag{5.20}$$

where u (m s^{-1}) is the air velocity around the food product. Thermal conductivities and thicknesses of the packaging materials and air gaps are shown in Table 5.1.

Table 5.1 Thickness of packaging materials and air gap.

Sample	Thickness, mm			
	Acrylic plastic	Polyethylene	Air gap	Cardboard
	(k=0.2)[b]	(k=0.33)[b]	(k=0.026)[a]	(k=0.078)[a]
Agar	4.5	-	-	-
Cheese	-	0.3	3	3

Source: [a] S. P. Singh, Burgess, and Singh (2008); [b] The Engineering Toolbox (n.d.)

5.5 Results

The results of the one-dimensional numerical simulation, which is named as CFM, were validated by comparison with experimental data, as well as the predicted results of the commercial software FPM version 4 (FPM, AgResearch MIRINZ), using a three-dimensional simulation. The experimental uncertainties at 95% confidence level were estimated by Eqs. 4.8 and 4.9 from the three replicated trials for the single block of agar and from two replicated trials for the block of cheese.

The air velocities at 2 cm above the test sample (u_{above}, Table 5.2) determined in the experiments were used to calculate the heat transfer coefficient in CFM using Eq. 5.19. The Biot number was estimated by Eq. 4.11. The calculated heat transfer coefficient and the equivalent Biot number for each trial were shown in Table 5.2

Table 5.2 The calculated heat transfer coefficient and Biot number for each experiment

Chilling trails	u_{inlet} (m s^{-1})	u_{above} (m s^{-1})	h (W m^{-2}K^{-1})	Biot
Agar	1.0	1.5	11.1	0.6
	4.0	5.5	22.1	1.2
Cheese	1.0	1.5	4.5	0.7
	4.4	7.0	5.8	0.9

5.5.1 Comparison of measured and predicted product temperatures

Figures 5.7 and 5.8 show the comparisons of measured and predicted temperature profiles for the block of cheese at the geometric center and the top surface along the shortest axis at different inlet air velocities. A similar comparison was made for the single agar block shown in Figures 5.9 and 5.10. The error bars in Figures 5.7 to 5.10 were based on the standard deviations of the experimental data. The experimental air temperature was averaged from all replicated experimental trials (section 5.2).

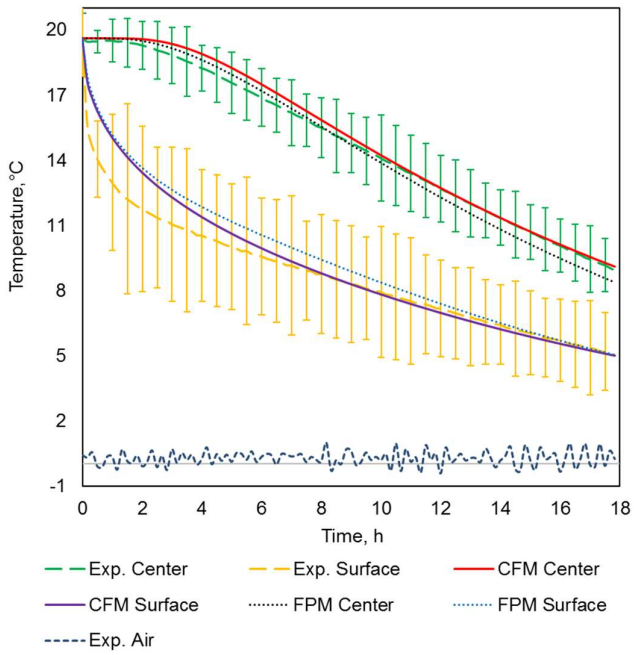

Figure 5.7: Plots of the temperature predictions of CFM, FPM with experimental data for a single block of cheese at the inlet velocity of 1.0 m s^{-1}

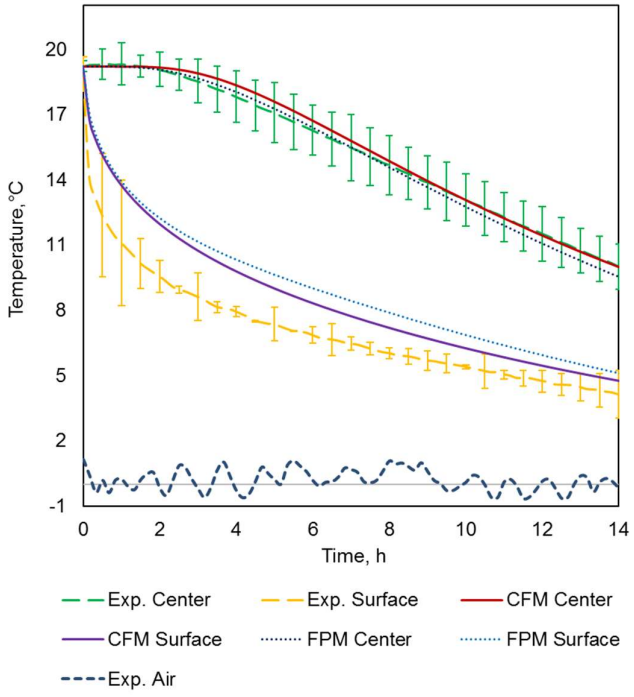

Figure 5.8: Plots of the temperature predictions of CFM, FPM with experimental data for a single block of cheese at the inlet velocity of 4.4 m s^{-1}

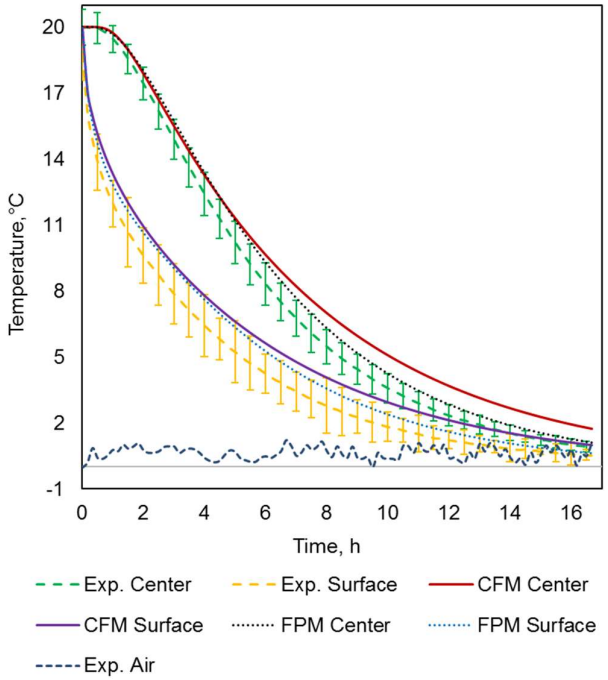

Figure 5.9: Plots of the temperature predictions of CFM, FPM with experimental data for a single block of agar at the inlet velocity of 1 m s^{-1}

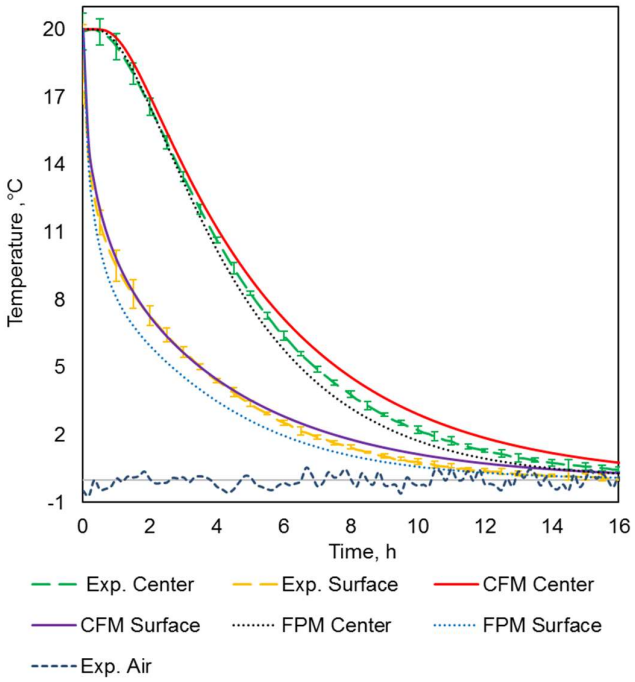

Figure 5.10: Plots of the temperature predictions of CFM, FPM with experimental data for a single block of agar at the inlet velocity of 4 m s^{-1}

In general, the simulation results performed by CFM fit well with the prediction results of FPM and the measured data. For the single block of cheese, both CFM and FPM show a good agreement with experimental data for the centre temperature prediction while big discrepancies can be seen for the surface temperature prediction. This can be explained by the uncertainty of the measurement of the thickness of the air gap underneath the carton on the top surface of the cheese test sample. For the single block of agar, CFM and FPM performed better at the high inlet air velocity. This can be justified by the fact that at the high air velocity (high Biot number) the internal resistance is dominant over the external resistance. Hence, the uncertainties of the overall heat transfer coefficient prediction could be reduced.

The accuracy of the predicted temperatures of the one-dimensional simualtion and FPM was illustrated by the mean absolute temperature difference (ΔT_{mean}, Eq. 4.10). Table 5.3 shows the ΔT_{mean} for the simulation results generated by CFM and FPM at the geometrical centre and surface along the shortest axis of a single block of cheese and a single bock of agar at different testing conditions.

Table 5.3 The mean absolute temperature difference for simulation performed by CFM and FPM at different locations and different Biot numbers

Materials	u_{inlet}, m s^{-1}	Biot number	ΔT_{mean} at surface, °C		ΔT_{mean} at centre,°C	
			CFM	FPM	CFM	FPM
Agar	1.0	0.6	1.1	0.7	1.1	0.6
	4.0	1.2	0.3	0.5	0.5	0.4
Cheese	1.0	0.7	0.5	0.8	0.3	0.3
	4.4	0.9	1.4	1.9	0.2	0.2

It can be seen from Table 5.3 that both CFM and FPM show a good agreement with experimental data with the mean temperature difference no more than 1.9°C

5.5.2 Comparison of experimental and numerical cooling times

The cooling time is a key design parameter when designing the refrigeration system. The accuracy of the numerical model was also assessed by comparing the numerical and experimental half cooling time (HCT), which is defined by the time required for the food products have cooled halfway from the initial temperature to the

cooling air temperature, and determined by the time that the dimensionless temperature (Y, Eq. 5.21) took to equal 0.5:

$$Y = \frac{T(0,t) - T_a}{T_{in} - T_a} \tag{5.21}$$

where $T(0,t)$ (K) is the centre temperature of the block of cheese or block of agar, T_{in} (K) is the initial temperature of food products and T_a is cooling air temperature. The experimental and predicted HCT at each test condition for the block of cheese and the single block of agar are shown in Table 5.4. The relative differences between the HCT predicted by CFM and FPM and the experimental data were lower than 6%, except for the HCT of the agar block with the inlet air velocity of 1 m s^{-1}.

Table 5.4 Comparison of predicted and experimental HCT for cheese and agar chilling

Materials	u_{inlet}, m s^{-1}	Experiments	CFM		FPM	
		HCT, h	HCT, h	Diff, %	HCT, h	Diff, %
Agar	1.0	5.1	5.8	13.7	5.6	9.8
	4.0	4.3	4.5	4.7	4.1	4.7
Cheese	1.0	16.4	16.6	1.2	15.5	5.5
	4.4	14.5	14.6	0.7	13.9	4.1

5.6 Conclusions

A one-dimensional numerical solution developed by Ghraizi et al. (1996) for non-linear unsteady heat transfer of food products in the chilling process was presented, using thermal properties calculated by the methods described in Chapter 3 and the correlation equation of the convective heat transfer coefficient proposed by (Pham et al., 1991) and (A. C. Cleland & Earle, 1976). The simualtion fits well with the experimental results and the predicted data of the three-dimensional simualtion. Therefore, CFM can be used to provide a quick cooling time prediction (the computational time for 18 hours of cheese chilling was 30s on a 64-bit Intel ® Xeon ® CPU E5-1620, 3.5 GHz, 16 GB RAM implemented in MATLAB) with sufficient

confidence in the temperature distribution along the shortest characteristic dimension of a 3-D object, which represents the greatest interest for food engineering investigations (Fikiin, 1996).

Chapter 6

Experimental study on the forced air freezing of whole chicken and bulk packed chicken drumsticks

6.1 Introduction

Many research projects have been conducted into characteristic the refrigeration of chicken products (Anderson, Sun, Erdogdu, & Singh, 2004; James, Vincent, de Andrade Lima, & James, 2006; Mannapperuma et al., 1994a, 1994b). However, they did not appear to present any data for the forced-air freezing of chicken containing a liner bag or polyliner, which is a common feature of the packaging system of the New Zealand chicken industry. This chapter describes laboratory experiments for the forced air freezing of bulk-packed whole chickens and chicken drumsticks within a polyliner, based on the information obtained from an industrial freezing tunnel. The objectives of the experimental work were to investigate the impact of the packing arrangement (or structure) of chicken drumsticks and the presence of a liner bag with the associated air voids between chickens and polyliner on freezing rate. The cooling performance of a tray of whole chickens and a tray of chicken drumsticks at different operating conditions was also evaluated. The experimental data will then be used to validate the prediction results of the CFD model described later in Chapter 7. Therefore, experiments were designed to have clear boundary conditions that could be replicated in a modelling environment; and a number of replications were performed to account for measurement and human error.

6.2 The industrial chicken freezing

The case study of the industrial chicken freezing was a chicken processing plant in Waitoa, Waikato. Under typical operation, the chicken is firstly loaded into either plastic or cardboard trays with open tops (Figure 6.1). The weight of each package ranges from 9 kg to 13 kg depending on the type of chicken products.

Figure 6.1: Typical trays used by the chicken processors (photo courtesy of Milmeq)

Chicken portions (thighs, drumsticks etc.), spend some time in the boning room at 10°C and then up to an hour waiting in the queue to go into the freezing tunnel in a room approximately at 0°C. This means that the temperature distribution in the product is highly unlikely to be uniform before it enters the tunnel, and also that there is likely to be significant variation in temperature between different types of chicken products. For example, trays containing chicken drumsticks may be noticeably cooler than trays containing whole chickens.

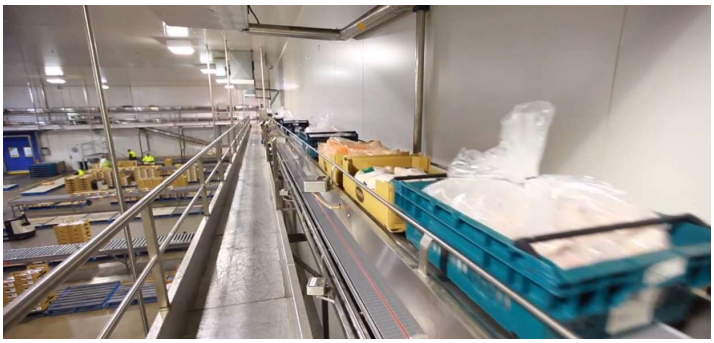

Figure 6.2: Chicken on the conveyors before entering the freezing tunnel (photo courtesy of Milmeq).

Chickens are frozen in the freezing tunnel (Figure 6.3) at -25°C, in which the trays of chicken products are placed on movable shelves. The tunnel design and product arrangement are similar to the industrial cheese chilling tunnel (Figure 4.2). Refrigerated air flows parallel to the longest dimension of the trays with two trays placed one behind the other on a shelf. The clearance between the trays makes sure that all the trays are exposed to a similar airflow profile. Perforations in the shelves allow for airflow to sweep the bottom surface of the tray.

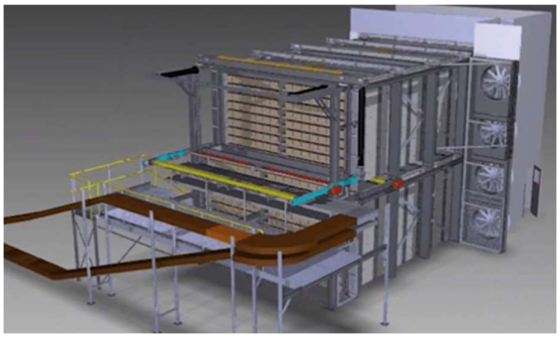

Figure 6.3: A typical freezing tunnel configuration (photo courtesy of Milmeq).

The tunnel can accommodate varying product types and carton sizes that require different freezing times. Shelves within a system are allocated different retention times, and the interfacing conveyors automatically pre-sort and accumulate product types, allowing transfer onto the designated shelf depending on the product retention time.

6.3 Experimental system

The chicken freezing trials were conducted at the AgResearch Ltd, Hamilton facility. Two Polystyrene Test Tunnels (PTT) that were used in the cheese and agar experiments (section 5.2) were reused for these experiments (Figure 6.4). Each PTT consisted of a variable speed suction fan at the downstream end, a fine mesh screen at the upstream end (used to diffuse the airflow), and an open section where the chicken trays were loaded.

Figure 6.4: Experimental system for chicken freezing trials

The two tunnels were put in the Environmental Test Chamber (ETC) allowing for precise control of the temperature of the cooling air being forced through the PTT. A transition section was created by fixing a polystyrene panel as shown in Figure 6.5. This ensured the majority of the airflow generated by the suction fan passed through the product section.

a)

b)

c)

Figure 6.5: Close fit of the transition section to the original tunnel: a) front view, b) back view, c) inside the PTT

a)

b)

Figure 6.6: The cardboard tray in the chicken freezing trials: a) without polyliner, b) with polyliner.

Cardboard trays with open tops, measuring 325 mm × 580 mm × 130 mm and polyliners, as used by chicken processors (Figure 6.6), were used in these experiments. Each tray was loaded with either 1.) seventy-two drumsticks or 2.) eight whole chickens. In each tunnel, a 5-cm height metal platform was used to support the tray of chickens. This arrangement allowed the bottom surface of the cardboard tray to be exposed to refrigerated air.

6.4 Experimental design

There are several experimental variables that are difficult to reproduce in the trials, such as the size, shape and location of individual chicken carcasses or chicken drumsticks within a tray, and the exact location of thermocouples embedded in the monitored products. These could have considerable influence when the measured data are used for numerical model validation purposes (see chapter 7), particularly if specific temperature locations are being compared. Instead, it is more common practice to compare the average of all measured product temperatures with the value predicted by the model (Ambaw, Mukama, & Opara, 2017; Defraeye, Lambrecht, et al., 2013; Ferrua & Singh, 2009b; O'Sullivan et al., 2016). The more temperatures are measured, the more reliable the average chicken temperature becomes; in this study there were 20 temperature logging channels available. Additionally, by carefully sizing and placing whole chickens or chicken drumsticks in the tray, and suitably distributing all the measurement locations within the tray, the effect of product shape and exact location of thermocouples on the average chicken temperature per tray can be minimised (Ferrua, 2007).

6.4.1 Temperature measurement

6.4.1.1 The whole chicken freezing trials

The temperature history of each chicken was monitored at a position 3-cm deep in the breast and in the deepest part of the gastro-intestinal cavity during the freezing trial. The chickens selected for the trials weighed approximately 1.6 kg each (the exact weight of each chicken was recorded before each trial). To replicate the industrial freezing scenario, eight chicken carcasses were placed into a tray; five

chickens (Numbers 1 to 5, Figure 6.7a) were arranged in a portrait orientation in the first row and three chickens (Number 6 to 8, Figure 6.7a) were arranged in a landscape orientation in the second row.

a)

b)

Figure 6.7: Chickens arrangement in a tray a) excluding and b) including the thermocouples

T-type thermocouples with sheath diameter of 4 mm were chosen for the whole chicken freezing trials. The big diameter of the thermocouples helped them to firmly embed in the chickens. Eighteen thermocouples were used for this experiment, with sixteen used to record the breast and cavity temperature of each chicken, one to measure the cooling air temperature, and one to measure air temperature inside the liner bag. Each thermocouple cable was labelled before being manually inserted into the chicken. As much as possible, the positions and the depths to which the thermocouples were inserted were the same for every

chicken. After insertion of thermocouples in all chickens, the polyliner was wrapped and sealed using plastic tape. The thermocouples were then carefully tied to each other and the cardboard tray to make sure they did not move during the freezing trial (Figure 6.8). The cooling air temperature was measured at a position 3 cm above the chicken tray in the tunnel.

Figure 6.8: The completed chicken tray for freezing trials

Temperatures were recorded on a Keysight 24982A data acquisition unit every 60 seconds during the freezing trials. The D type connector, a multiway thermocouple connector, was used to connect the thermocouple to the data logger. This allowed the connection of all the monitored thermocouples to the data logger in one motion rather than individually so that data recording could start as soon as the test samples were loaded in the PTT. The temperature history of chicken changes quickly at the beginning of the freezing process; therefore, it is very important to start recording as soon as possible.

The total cable length from the measuring point to the logger was minimised to keep the loop cable resistance to lower than 100 Ohms to avoid a significant measurement error, as recommended by manufacturer (RS, 2002).

6.4.1.2 Bulk packed chicken drumstick trials

For chicken drumsticks, two freezing trials were run at the same time, with one tray placed in the top tunnel and another tray in the bottom tunnel of the PTT. In each tray, the temperatures of eight selected drumsticks at different locations were measured, with one thermocouple being used to measure the refrigerated air temperature above the tray and one more to measure the air inside the plastic liner bag (20 thermocouples in total).

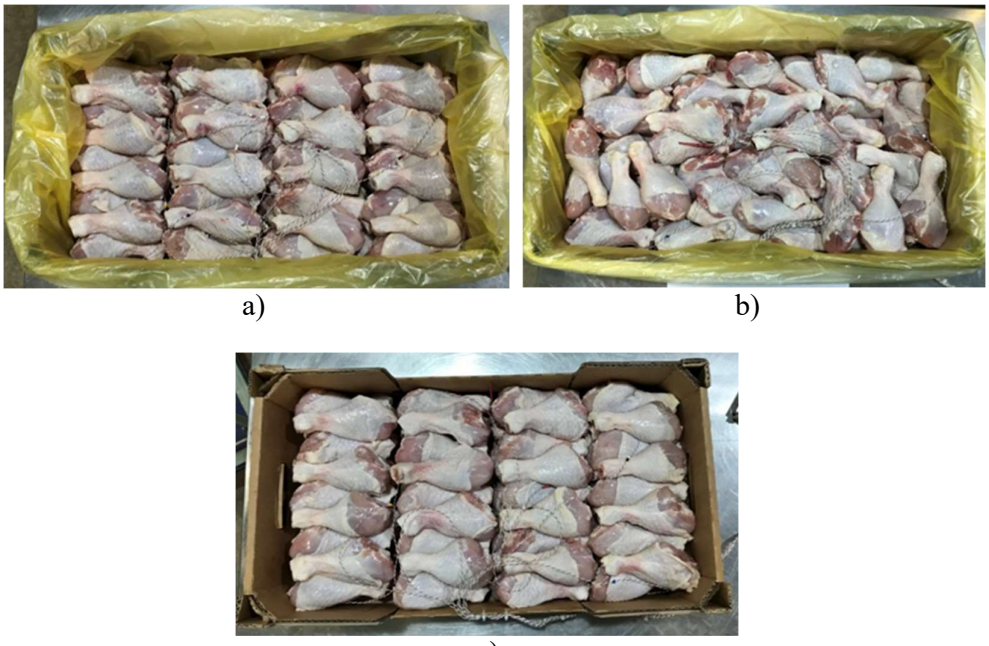

a) b)

c)

Figure 6.9: Bulk packed chicken drumsticks arrangements: a) regularly arranged drumsticks with liner bag, c) randomly arranged drumsticks with liner bag, c) regularly arranged drumsticks without liner bag

Three sets of freezing experiments were conducted on the bulk-packed chicken drumsticks. In the first experiment, the cooling behaviour of a tray of regularly arranged drumsticks within the plastic liner (Fig. 6.9a) was investigated. Seventy-two drumsticks weighing between 140 g to 190 g were arranged in four layers. Eight drumsticks each having a mass of 160 g (the average weight of drumsticks in a tray) distributed along the two diagonals at both high and low, central and peripheral positions were chosen for temperature measurement (Fig. 6.10). In which, drumstick Numbers 1, 3 and 4 are on the bottom layer, drumstick Number 2 is on

the second layer, drumstick Numbers 5, 6 and 8 are on the third layer and the drumstick Number 7 is on the top layer

In the second set of experiments, a tray of drumsticks arranged randomly within the liner bag was used (Fig 6.9b). The drumsticks selected for temperature measurement also weighed 160 g and were carefully placed at similar locations to the measurement positions in the first set of experiments.

In the third experiment, a tray of regularly arranged drumsticks without the plastic bag was used (Fig. 6.9c) and thermocouple placement was the same as for the first set of experiments.

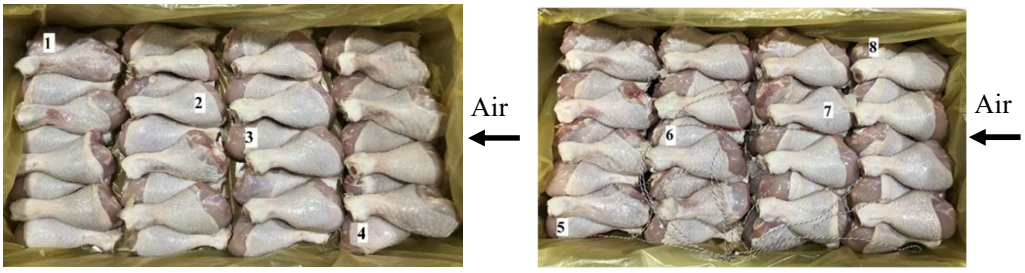

Figure 6.10: Chicken drumsticks distribution: a) the bottom and second layer, b) the third and top layer

The distribution of temperature measurement positions was designed to account for the spatial variation in temperature throughout the tray, bearing in mind that a maximum of eight thermocouples could be placed in each tray. This was done so that the average of the eight measured temperatures could represent the volume average temperature of the bulk-packed drumsticks as closely as possible.

T-type thermocouple wires with the sheath diameter of 2 mm were used to measure the drumstick temperature. Because of the flexibility of the wires, they could go to any position in the tray without making any significant changes in the drumstick arrangement or the airflow pattern in the polyliner bag. The measurement end of each thermocouple was made rigid by enclosing it alongside a plastic rod within a heat shrink tube. This allowed the wire to be easily inserted into the drumsticks to the desired location (approximately 3 cm deep in the thickest part of the leg, Figure

6.11) and helped them to remain in place during the trial. All the thermocouples were calibrated using an ice-point reference before and after the measurements.

The Keysight 24982A data acquisition unit with D-type connector was also used for drumstick freezing trials with temperatures recorded every 60 seconds during the trials.

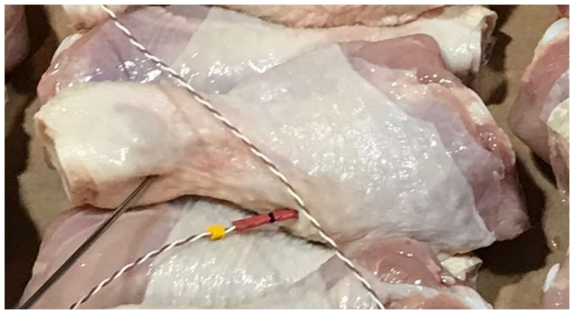

Figure 6.11: Thermocouple placement in chicken drumsticks

6.4.2 Air velocity and pressure measurement

The air velocities at the inlet of the PTT and 5 cm above the chicken tray were measured before and after each trial using a hot-wire anemometer (Dantec 54N60 FlowMaster). The sample time for each velocity measurement was five minutes. The air velocity was held constant during the experiment.

In addition, in order to define the outlet boundary condition in the numerical model (see chapter 7), the pressure drop of the airflow through the PTT created by the suction fan was measured by an inclined fluid manometer (RS Pro, RS 730-2937) before and after each trial.

6.5 Experimental procedure

Chickens were purchased fresh from a local retailer on the day of delivery from the processor. They were then sorted, scaled and positioned individually in the tray and thermocouples were placed as described previously. The plastic liner was then tied to enclose the chicken and thermocouples (other than for the experiments without the plastic liner bag). The loaded trays were subsequently placed in the ETC to

equilibrate at 10°C for 24 hours. The chicken temperatures were monitored during the equilibration process to ascertain when the chicken reached a uniform temperature.

All freezing trials started with chickens at uniform initial temperature of 10°C (equilibration temperature) and the ETC air temperature was maintained at -25°C. The inlet air velocity was adjusted to the desired speed. The whole chicken freezing trials were tested at three inlet air velocities of 1.0 m s^{-1}, 2.5 m s^{-1}, and 4.5 m s^{-1}. The regularly arranged bulk packaged drumsticks (with and without liner bag) freezing trials were run at inlet air velocities of 1.0 m s^{-1}, 2.5 m s^{-1}, and 4.3 m s^{-1}, and the randomly arranged drumstick freezing trials were run at inlet air velocities of 1.0 m s^{-1} and 4.3 m s^{-1}. The thermally equilibrated chicken trays were placed in the tunnels and the trial was started. Each trial was terminated when all the monitored chicken temperatures fell below -21°C (seven-eighths of the difference between initial and cooling air temperatures).

After the freezing process was completed, the samples were thawed for 12 hours at the ambient temperature, before being re-equilibrated in ETC at 10°C for at least 24 hours. Two subsequent trials were performed on each batch of whole chickens or chicken drumsticks, with the exception of the eight drumsticks that contained the thermocouples, which were replaced by fresh 160 g drumsticks for each replicate. No samples were used for more than three trials. The trials were repeated until the standard deviation of the experimental data was lower than a certain value (3.0°C for the average temperature of chicken drumstick, and 2.0°C for the average temperature of chicken breast and chicken cavity). There were at least three replicates at each air velocity for each type of experiment.

6.6 Experimental results

6.6.1 Average temperature of chicken breast and chicken cavity per tray

As discussed in section 6.4, the average temperature of all the monitored chickens per tray could be used to validate a heat transfer model (see chapter 7). Therefore, the time history of the average temperature at two different positions: 3 cm depth in chicken breast and in the chicken cavity, were computed from the experimental

results. In each trial, the average temperature profile of chicken breast and chicken cavity was calculated by averaging temperatures at the same position of all chickens within a tray, Eq. 6.1

$$\overline{T_{x,j}}(t) = \frac{\sum_{i=1}^{N} T_{x,i,j}(t)}{N} \tag{6.1}$$

where:

x indicates the position in a chicken (3 cm deep in the breast or in the cavity)

j indicates the j^{th} trial number

i indicates the individual chicken in a tray

N is the total number of chickens in a tray, $N = 8$

t(s) is the processing time

$\overline{T_{x,j}}$ (K) is the average temperature in the j^{th} trial at the position 'x'

$T_{x,i,j}$ (K) is the temperature of the i^{th} chicken in the j^{th} trial at position 'x'

The average temperature over time of a tray of chicken was computed by averaging the temperature histories of all experimental trials, Eq. 6.2

$$\overline{T_x}(t) = \frac{\sum_{j=1}^{n} T_{x,j}(t)}{n} \tag{6.2}$$

where:

n is the number of the experimental trials (n = 4 at the 1 m s^{-1} freezing trial and n = 5 at the 2.5 m s^{-1} and 4.5 m s^{-1} freezing trials, section 6.5);

$\overline{T_x}$(K) is the average temperature at the position 'x'

The experimental uncertainty in $\overline{T_x}(t)$ at a 95% confidence interval and a normal distribution of the measurements, was computed by Eq. 6.3:

$$P_{\overline{T_x}}(t) = \tau_{n-1,0.025} \times \frac{1}{\sqrt{n}} \left[\frac{1}{n-1} \sum_{j=1}^{n} \left(\overline{T_{x,j}}(t) - \overline{T_x}(t) \right)^2 \right]^{1/2} \tag{6.3}$$

where:

$P_{\overline{T}_x}(t)$ (°C) is the experimental uncertainty in $\overline{T}_x$

$\tau_{n-1,0.025}$ is the student's t-statistic with (n-1) degrees of freedom at a 95% confidence interval.

The experimental average temperature profiles of chicken breast and chicken cavity at the inlet air velocity of 1 m s^{-1}, 2.5 m $^{-1}$ and 4.5 m s^{-1} are compared in Figure 6.12.

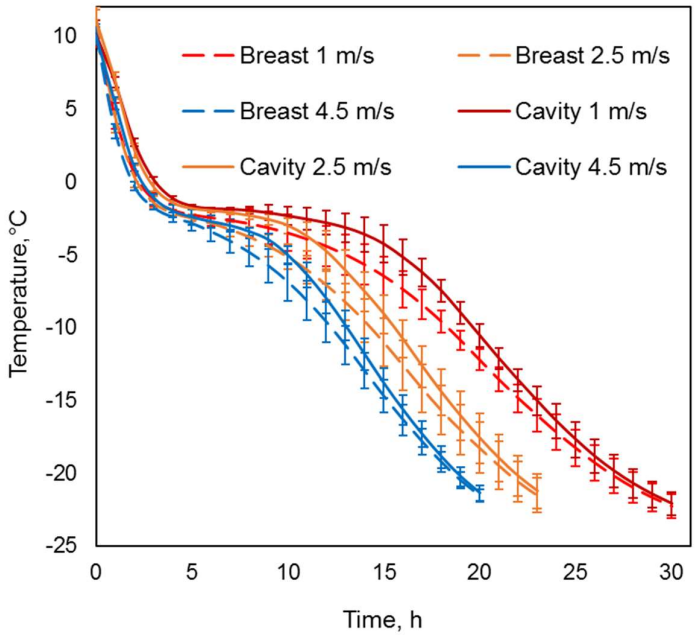

Figure 6.12: The plots of average temperature per tray of chicken breast and chicken cavity during the freezing trial at three tested air velocities. Error bars indicate standard deviation

As expected, the freezing rate was faster at the higher air velocity. Within a tray, the average temperature of chicken cavities was higher than that of chicken breasts, at the same air velocity. That means the slowest cooling point in a tray of chicken in the forced-air freezing will be in the cavity position. The experimental uncertainty of the average chicken temperature was smaller than 1.8°C for all three tested air velocities.

The temperature history of a food product depends on the initial temperature and the cooling air temperature (Defraeye, Lambrecht, et al., 2013) and these were

slightly different between trials. Hence, the seven-eighths cooling time (SECT) (i.e. the time taken for the temperature to reach seven-eighths of the difference between initial and cooling air temperatures) was chosen to compare freezing rates between trials. Using the dimensionless temperature (Y, Eq. 6.4), the SECT of a tray of chicken was determined by the time Y took to equal 0.125

$$Y = \frac{T - T_a}{T_{in} - T_a} \tag{6.4}$$

where T (K) is the average chicken cavity temperature (because the cavity cooled slower than the breast), T_a (K) is the cooling air temperature and T_{in} (K) is the initial temperature of all chicken. The SECT of a tray of chicken at the different air velocities is presented in Table 6.1. The uncertainty of the SECT was calculated using the same formula as the average temperature of chicken with SECT in place of T_x (Eq. 6.3)

Table 6.1: The SECT of a tray of chicken in a freezing trial at different air velocities

Trial number	SECT, h		
	u =1 m s^{-1}	u = 2.5 m s^{-1}	u = 4.5 m s^{-1}
1	27.2	20.4	19.5
2	27.5	23.4	18.9
3	29.0	23.0	19.7
4	27.7	22.3	18.8
5	-	21.6	19.6
Mean	27.8	22.1	19.3
Experimental uncertainty, h	1.2	1.5	0.5

6.6.2 Temperature profile of individual chickens within a tray

Although the size and shape of each chicken, the location of chickens in a tray, and the position of thermocouples within each chicken are random variables, effort was made to minimise this variation between replicates by careful selection of chicken size, placement of chicken in the tray and insertion of thermocouples in each

chicken. The individual chicken temperatures were calculated by averaging temperature histories at the same position for all replicated trials, Eq. 6.5:

$$\overline{T_{x,i}}(t) = \frac{\sum_{j=1}^{n} T_{x,i,j}(t)}{n} \tag{6.5}$$

where

x indicates the position in a chicken (3 cm deep in the breast or in the cavity)

j indicates the j^{th} trial number

i indicates the individual chicken in a tray

n is the number of experimental trials

t(s) is the processing time

$\overline{T_{x,i}}$ (K) is the average temperature at the position 'x' of the i^{th} chicken

$T_{x,i,j}$ (K) is the temperature of the i^{th} chicken in the j^{th} trial at position 'x'

The experimental uncertainty in $\overline{T_{x,i}}(t)$ at a 95% confidence interval and a normal distribution of the measurements, was computed by Eq. 6.6:

$$P_{\overline{T_{x,i}}}(t) = \tau_{n-1,0.025} \times \frac{1}{\sqrt{n}} \left[\frac{1}{n-1} \sum_{j=1}^{n} \left(\overline{T_{x,i}}(t) - T_{x,i,j}(t) \right)^2 \right]^{1/2} \tag{6.6}$$

where

$P_{\overline{T_{x,i}}}(t)$(°C) is the experimental uncertainty in $\overline{T_{x,i}}$

$\tau_{n-1,0.025}$ is the student's t-statistic with (n-1) degrees of freedom at a 95% confidence level.

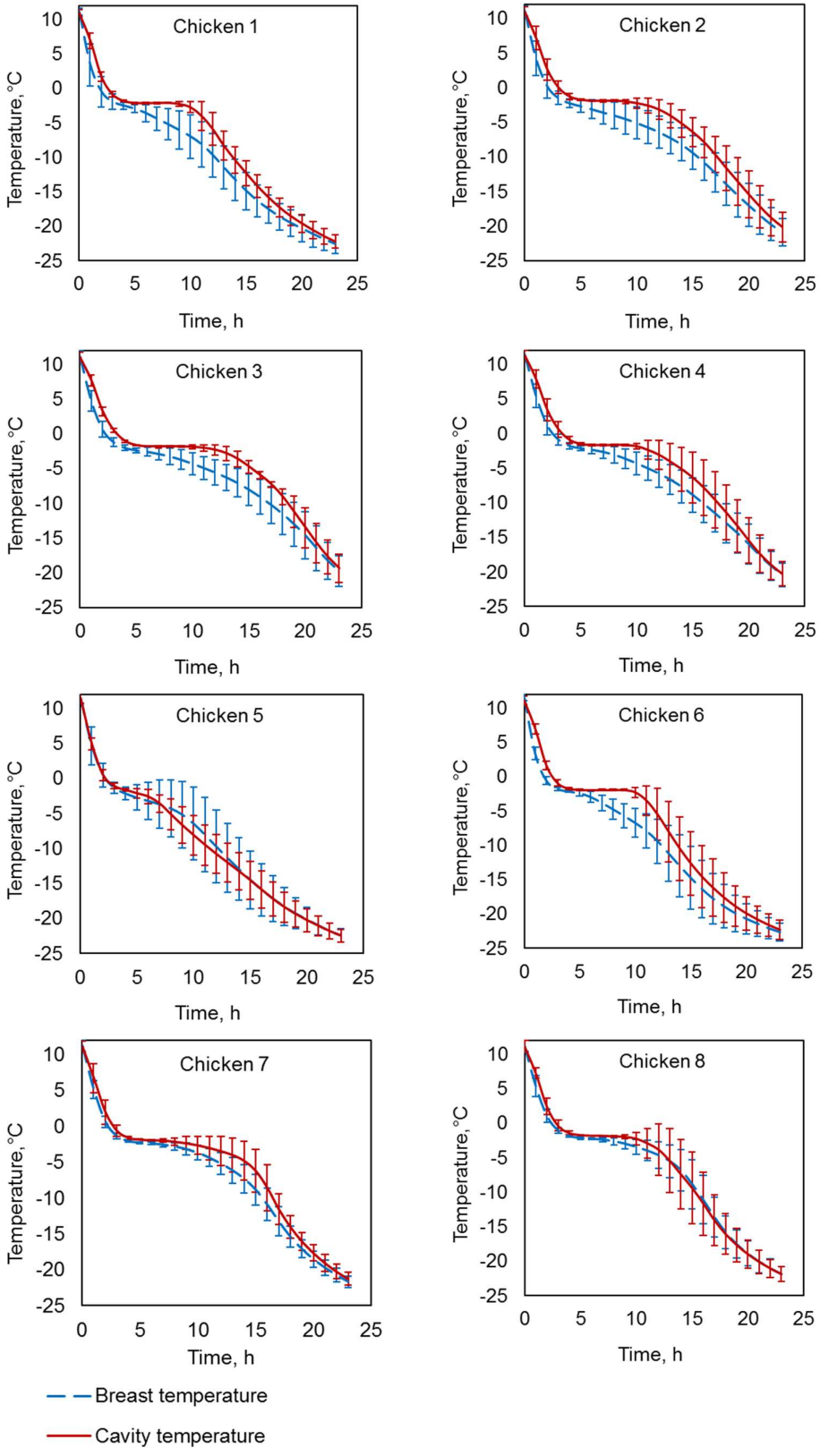

Figure 6.13: Comparison of experimental chicken breast and chicken cavity temperature of individual chicken in the freezing experiment at the inlet air velocity of 2.5 m s^{-1}. Error bars indicate experimental uncertainty

Figure 6.13 illustrates the temperature histories in the breast and in the cavity of individual chickens (averaging from 5 replicated trials) with the error bars indicate experimental uncertainty at an inlet air velocity of 2.5 m s^{-1}. Within a chicken, the cavity temperature was higher than breast temperature except for chicken Numbers 5 and 8 which are close to the tray wall that was against the airflow direction. The experimental uncertainty of all the monitored temperatures was less than 5°C with the greatest uncertainty being in the sub-cooling region. This is reasonable since thermal properties of chicken change significantly in this region.

In order to investigate the cooling heterogeneity within a tray of chicken under forced air freezing, the maximum differences in the breast temperature and cavity temperature of individual chickens within the same tray were calculated for the three tested air velocities (Figure 6.14)

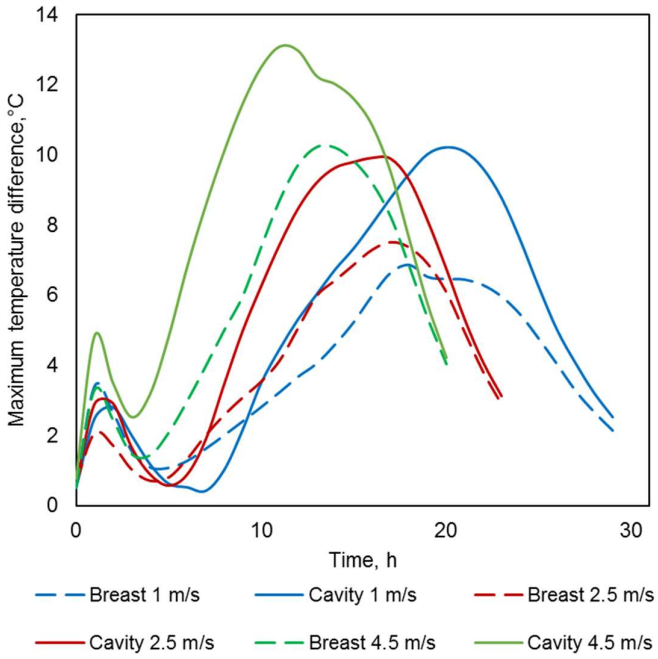

Figure 6.14: The maximum temperature difference profiles of chicken breast and chicken cavity within a tray.

For a given air velocity, the maximum temperature difference of chicken breast of individual chickens within a tray was lower than that for the chicken cavity. The maximum differences at the velocity inlet of 1 m s^{-1}, 2.5 m s^{-1} and 4.5 m s^{-1} were 10.2°C, 9.9°C and 13.1°C obtained after 20 hours, 16 hours, and 11 hours

respectively, which are in the sub-cooling region (Figure 6.12). They were about 30% of the difference between the initial chicken temperature and the cooling air temperature. By the end of the freezing process, the maximum differences decreased for all tested air velocities. The lowest of the maximum differences in the breast temperature and cavity temperature of individual chickens at the finishing point were 2.1°C, and 2.5°C respectively, obtained in the 1 m s^{-1} freezing trials (the finishing point was marked when the average temperature of chicken per tray was -21°C). The results suggest that the lower the cooling air velocity the more uniform of the temperature of chickens within a tray at the end of the process.

6.6.3 The cooling air temperature profile in the whole chicken freezing trials

The average value of the temperature histories of airflow at 3 cm above the chicken tray for each freezing experiment was calculated from all replicated trials and presented in Figure 6.15. The procedure to calculate the experimental uncertainty in the average cooling air temperature was the same as for the individual chicken temperatures (Eq. 6.6). After the initial two hours, the average temperature of the cooling air consistently ranged between -24°C and -25°C.

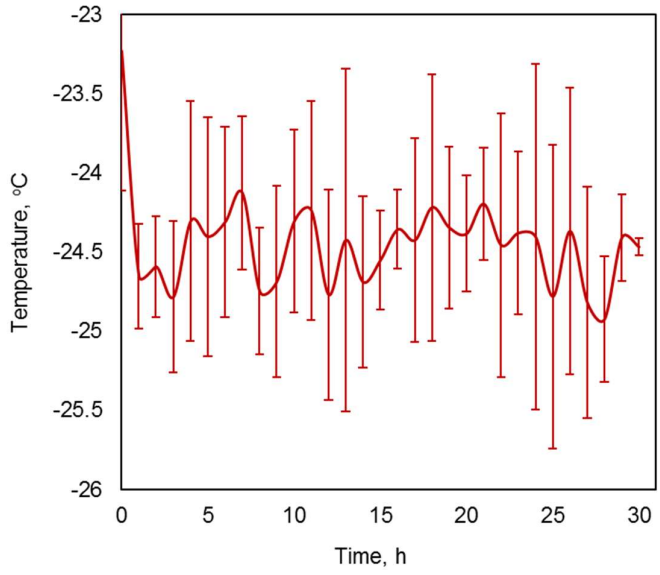

a)

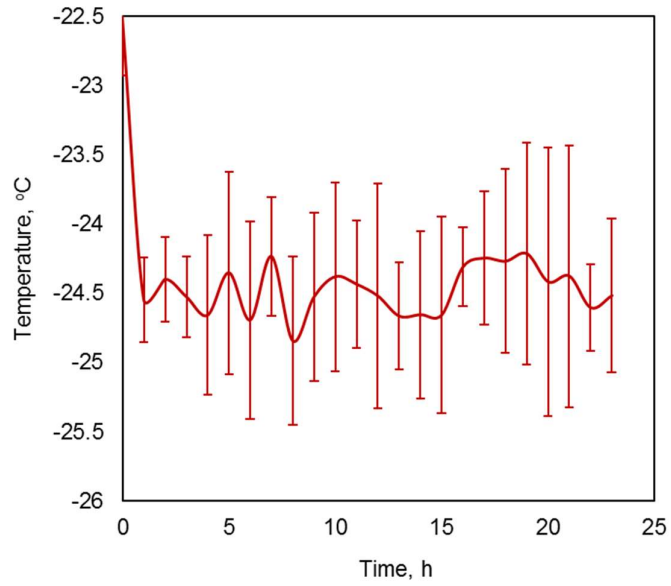

b)

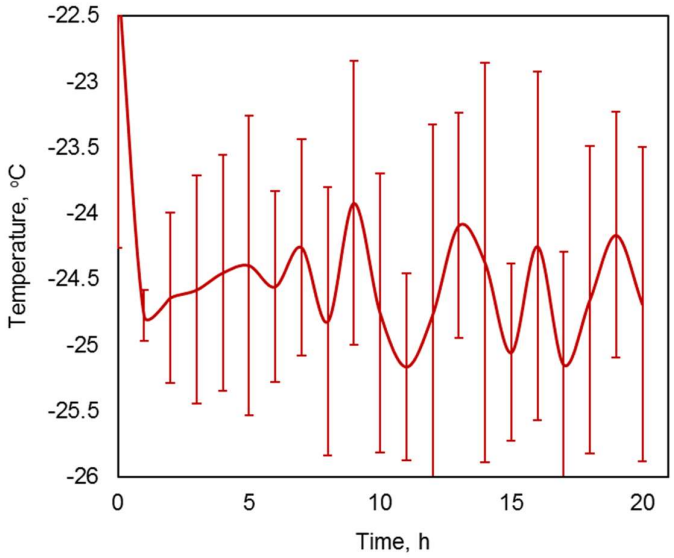

c)

Figure 6.15: The cooling air temperature profiles in whole chicken freezing experiments a) at the air velocity of 1 m s^{-1}, b) at the air velocity of 2.5 m s^{-1} and c) at the air velocity of 4.5 m s^{-1}

6.6.4 The average temperature profile of chicken drumsticks per tray

The average temperature history of chicken drumsticks in a tray was calculated from eight monitored drumsticks. The final average temperature histories of chicken drumsticks during freezing experiments were computed by averaging values from three replicated trials. The experimental uncertainty in these

measurements was determined by the same procedure as for the whole chicken temperatures (Eq. 6.3)

The uncertainty at 95% confidence interval of the average temperature of a tray of drumsticks ranged from 0.5°C to 3.0°C except for the case of the experimental data of the irregularly arranged drumsticks at the inlet air velocity of 4.3 m s^{-1} where the standard deviation was as high as 4.0°C

Figure 6.16 shows the cooling history of the average temperature of drumsticks per tray in the regularly arranged drumstick freezing experiments at three different air velocities. The cooling rate at the inlet air velocity of 1 m s^{-1} was significantly slower than at two other velocities (2.5 m s^{-1} and 4.3 m s^{-1})

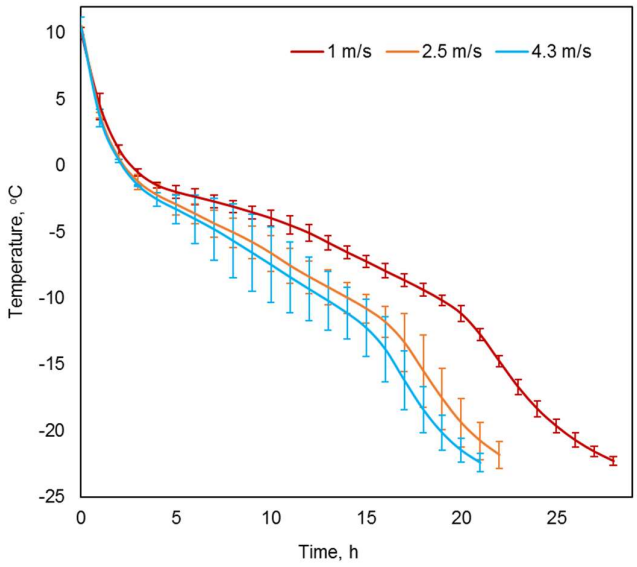

Figure 6.16: Average temperature profiles of chicken drumsticks per tray in the regular arrangement freezing experiments

6.6.5 Comparison of cooling rate between regular and irregular packing of drumsticks

Cooling histories of trays of regularly packed and randomly packed drumsticks were compared in Figure 6.17. The error bars indicate 95% confidence interval of the average temperature of the tray. Although the randomly packed drumsticks appeared to have cooled slightly faster on average than the regularly packed

drumsticks, the difference between the two packing arrangements was less than the uncertainty in the measurements at both low and high air-speeds. This suggests that the packing arrangement and alignment of the leg-bone within the tray did not have a significant impact on freezing time when the drumsticks are contained within the bag. Since the orientation of the drumsticks did not appear to affect freezing time, it is possible that only the total fraction of air voids within the package may be required as model input, with no requirement to account for size or shape of the air voids.

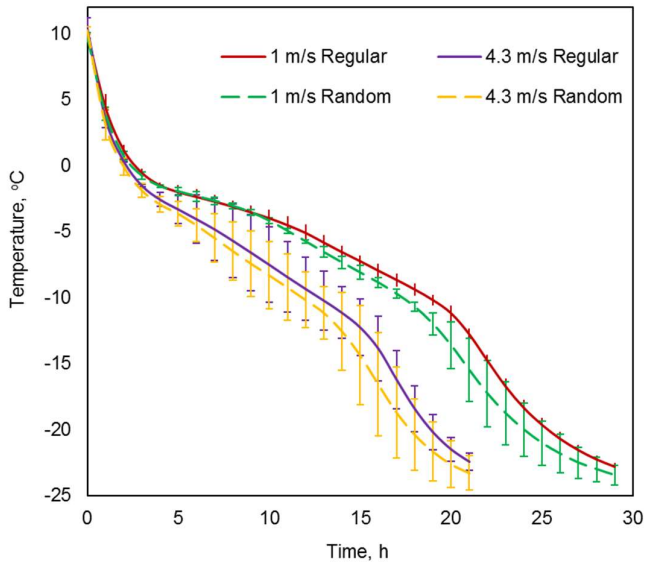

Figure 6.17: Cooling histories of regularly packed and randomly packed drumsticks at different air velocities

6.6.6 Comparison of cooling times of regularly packed drumsticks with and without liner bag

Figure 6.18 shows cooling histories of regularly packed chicken drumsticks with and without the liner bag. As expected, the drumsticks without the liner bag cooled significantly faster than those packed within the liner bag for all three air velocities

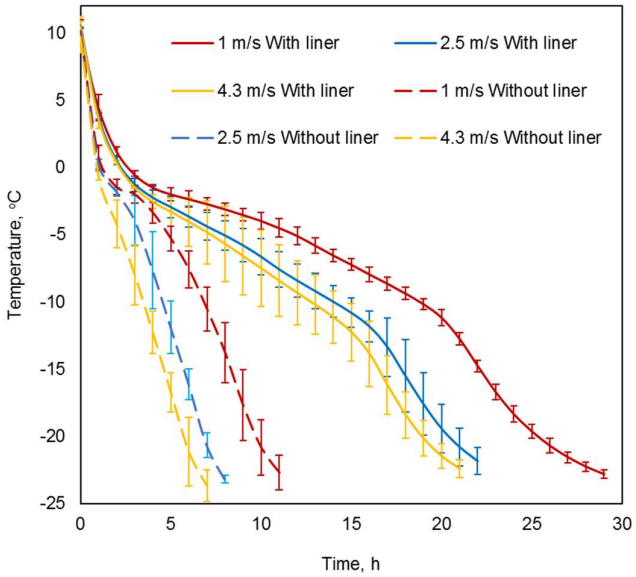

Figure 6.18: Cooling histories of regularly packed drumsticks with and without the liner bag

In order to quantify the effect of the liner bag on cooling time the seven-eighths cooling time (SECT) were calculated, and results are shown in Table 6.2. The effect of the liner bag on cooling time increases as the air velocity increases, the SECT for the plastic lined chicken was more than three times greater than for the unlined case when the air velocity was 4.3 m s^{-1}. The slower cooling of polylined chicken drumsticks can be explained by the insulating effect of the polyliner. Air voids within the polyliner with an intrinsic low thermal conductivity act as an insulating material. With a polyliner, refrigerated air cannot directly interact with the chicken either.

Table 6.2: Experimental SECT of the tray of drumsticks

Air velocity, m s^{-1}	With liner		Without liner	
	SECT, h	Experimental uncertainty, h	SECT, h	Experimental uncertainty, h
1.0	25.9	0.5	9.9	0.8
2.5	20.8	1.2	7.0	0.3
4.3	19.3	0.8	5.9	0.6

For the chicken with liner, the effect of evaporation would be minimal, since any moisture evaporated from chicken surface can be assumed to condense back on cool

surfaces within the polyliner, providing no significant net contribution to the overall heat balance. However, evaporative cooling would have been much more significant for the chicken without the liner (Hu & Sun, 2000; Kuffi et al., 2016), and hence would have contributed to some of the increase in the cooling rate. In the no-liner freezing experiments, the maximum total weight loss of drumsticks (which was at the inlet air velocity of 4.3 m s^{-1}) was 140 g (the weight difference of the bulk-packed drumsticks before each trial and after thawing). The latent heat of evaporation of water is approximately 2500 kJ kg^{-1} (at 0°C) (Cengel & Ghajar, 2011). Hence, the maximum potential contribution by latent heat of evaporation is

$$Q_{eva} = 0.14 \times 2500 = 350 \text{ kJ} \quad (6.7)$$

The enthalpy of chicken at 10°C (initial temperature) and -21°C (final temperature) are 331.2 kJ kg^{-1} and 53.8 kJ kg^{-1}, respectively (Riedel, 1957). Therefore, the total heat load in the freezing process of the 11.5 kg of a tray of drumsticks is:

$$Q_{total} = 11.5 \times (331.2 - 53.8) = 3190 \text{ kJ} \quad (6.8)$$

The potential heat removed from drumsticks by evaporation is 350/3190 ×100 % = 11%. Also, some of the weight loss would have been drip loss, so the actual drying during freezing of drumsticks may contribute to less than 11% of faster cooling in case of no liner.

The liner bag is used to minimise moisture loss during the refrigeration process. The moisture loss could have a detrimental impact on product quality, so it is unlikely that processors would remove the bag to increase throughput. However, these results clearly indicate that the presence of the liner bag has a much greater impact on freezing time than the orientation of the chicken drumsticks within the bag.

6.6.7 Temperature profile of individual drumsticks within a tray

The average temperature histories of individual drumsticks within a tray in the regularly packed drumstick experiments were determined from the three replicated trials. The experimental uncertainties were also computed following the same procedure as for the whole chicken temperatures (Eq. 6.6). It was assumed that the

average cooling history would be a good estimate of the general trend of individual chicken leg temperatures within a tray. Figure 6.19 shows the cooling profile of individual drumsticks within a tray at three different air velocities. In general, a bigger span was observed in the sub-cooling region compared to the pre-cooling region. Drumsticks located at the middle of the tray (drumstick Numbers 2, 3, 6, 7; Figure 6.10) cooled slower than those at the boundary (drumsticks Numbers 1, 4, 5, 8). This is reasonable since the drumsticks at the boundary are closer to the refrigerated air outside.

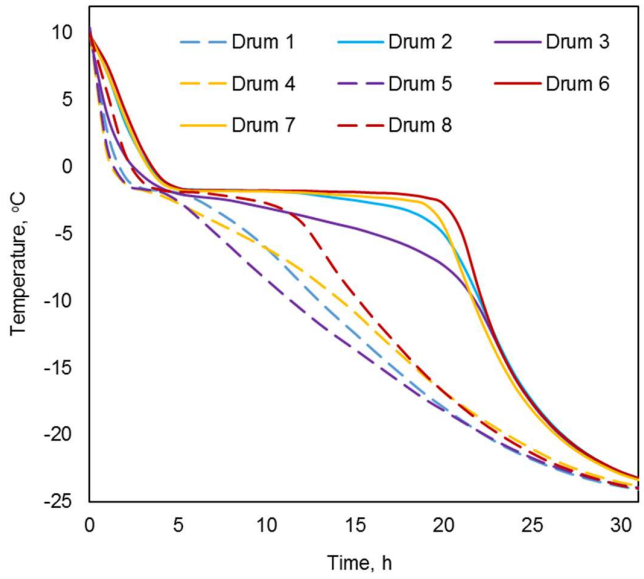

a)

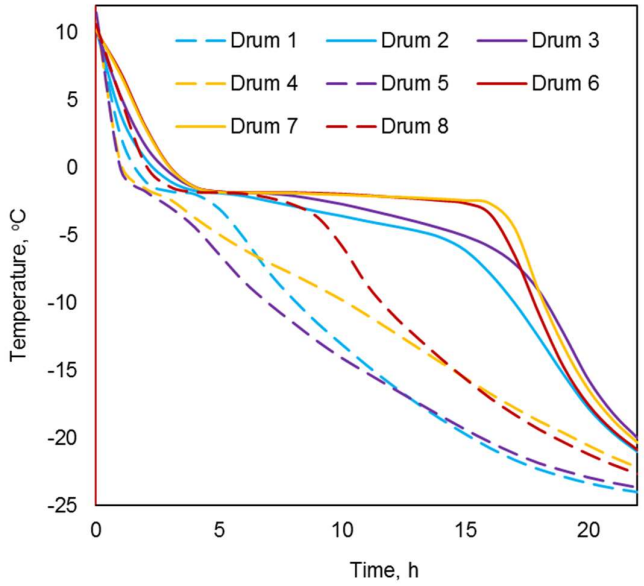

b)

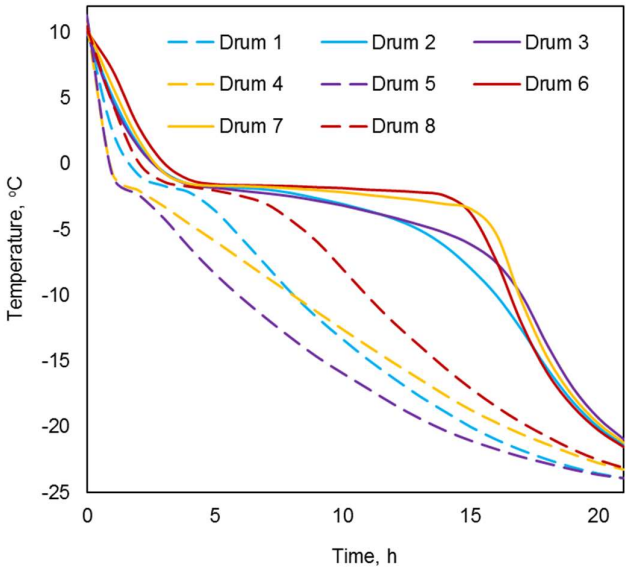

c)

Figure 6.19: Cooling profile of individual drumsticks within a tray in freezing experiment at the inlet air velocity of a) 1.0 m s^{-1}, b) 2.5 m s^{-1} and c) 4.3 m s^{-1}

The cooling heterogeneity in a tray of drumsticks was further investigated by calculating the maximum differences in the temperature of individual drumsticks within a tray (Figure 6.20). Above the initial freezing point, the maximum temperature differences in the 1 m s^{-1}, 2.5 m s^{-1} and 4.3 m s^{-1} freezing experiments were 6.8°C, 7.2°C and 8.1°C, respectively obtained after 1 hour of freezing. In the freezing temperature range, the maximum temperature differences for individual drumsticks rose to 15.4°C, 18.1°C and 17.9°C obtained after 20 hours, 16 hours and 14 hours, respectively. This represented approximately 50% of the difference between the initial and the refrigerated air temperature. By the end of the freezing process, the maximum differences decreased significantly. At the finishing point (marked when the average temperature of drumsticks per tray was -21°C), the 1.0 m s^{-1} freezing experiments showed the lowest difference of 2.5°C compared to 4.0°C and 4.3°C for the 2.5 m s^{-1} and 4.3 m s^{-1} freezing experiments, respectively. These result again confirmed that the lower cooling air velocity led to a more uniform temperature profile of individual chicken pieces within a tray at the end of a freezing process.

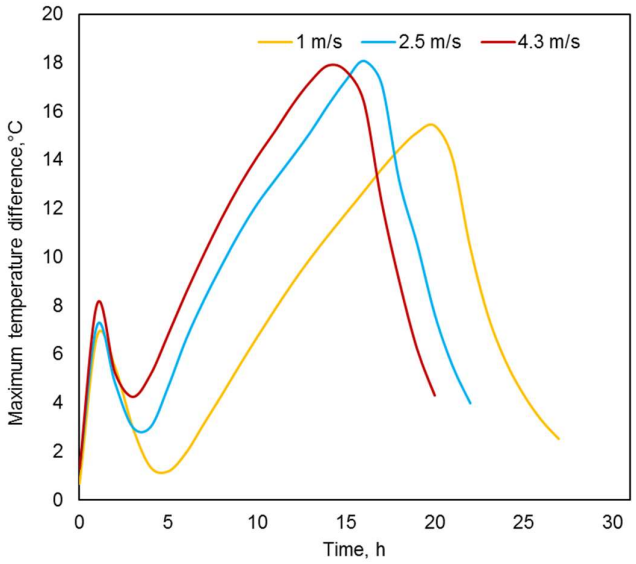

Figure 6.20: The maximum differences in temperatures between individual chicken drumsticks within a tray at different air velocities.

6.6.8 The cooling air temperature profiles in the chicken drumsticks freezing experiments

The temperature histories of the cooling air in the regularly packed drumstick freezing experiments were averaged from the three replicated trials, and the results are shown in Figure 6.21. The experimental uncertainty in these measurements were calculated by the same procedure as for the individual whole chicken temperatures (Eq. 6.6). The average temperature of cooling air varied from -24°C to -25°C in all freezing experiments.

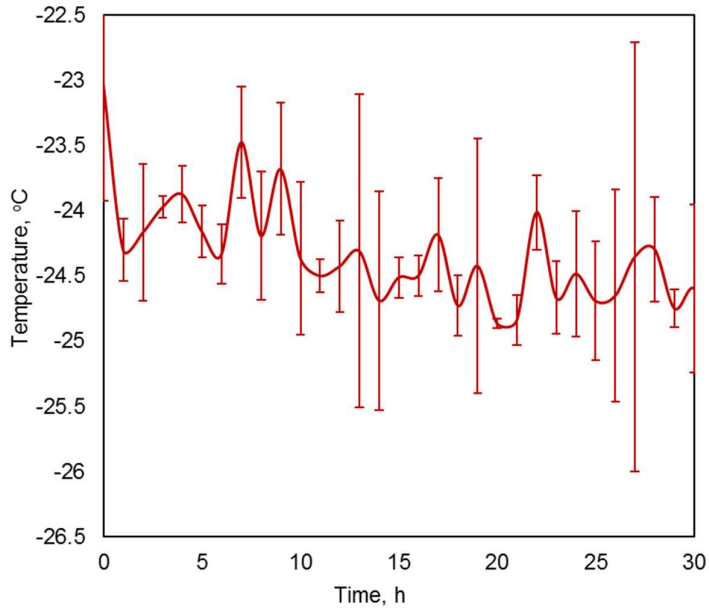
-22.5
-23
-23.5
-24
-24.5
-25
-25.5
-26
-26.5
Temperature, °C
0
5
10
15
20
25
30
Time, h

a)

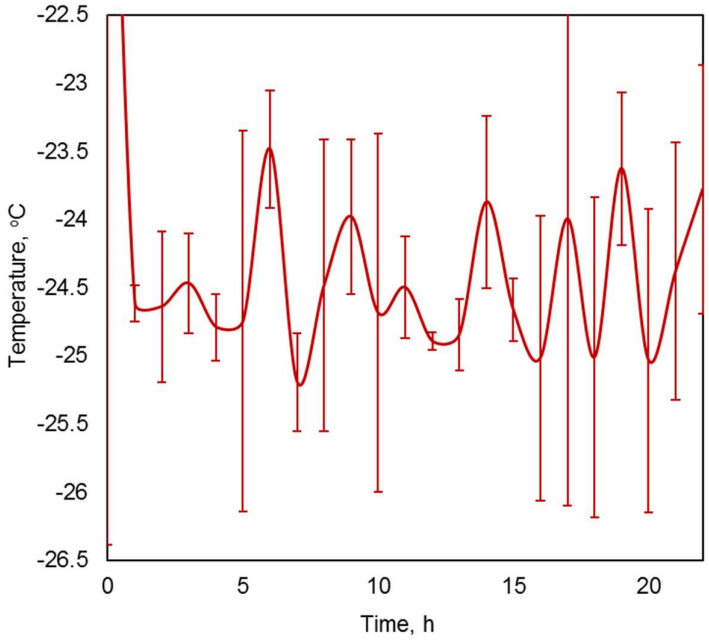
-22.5
-23
-23.5
-24
-24.5
-25
-25.5
-26
-26.5
Temperature, °C
0
5
10
15
20
Time, h

b)

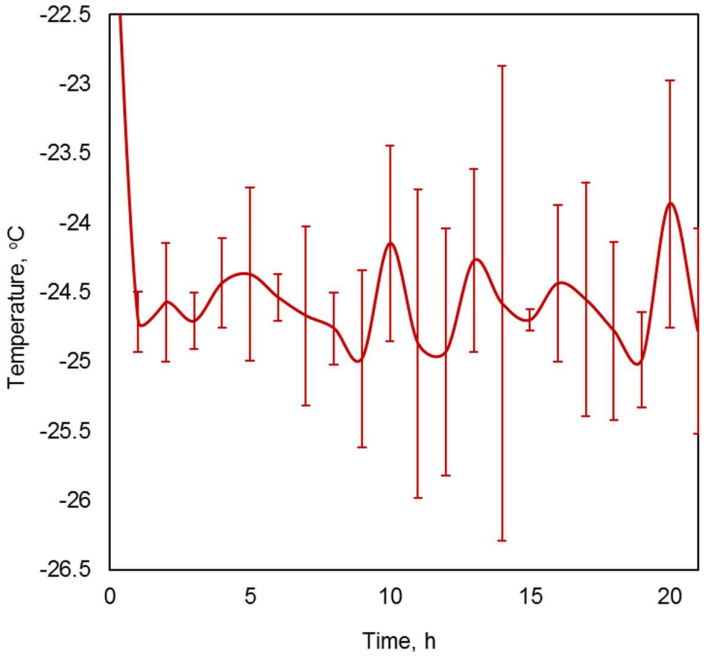

c)

Figure 6.21: The cooling air temperature profiles in regular packed drumsticks freezing experiments a) at the air velocity of 1 m s^{-1}, b) at the air velocity of 2.5 m s^{-1} and c) at the air velocity of 4.3 m s^{-1}

6.7 Conclusions

The freezing trials for a tray of whole chickens and a tray of chicken drumsticks were designed and executed based on information obtained from an industrial chicken freezing operation. Freezing trials were repeated five and three times for chickens and drumsticks, respectively, to collect a validation data set for the modelling of freezing operations.

The results showed a large range in the cooling histories of individual chickens in the sub-cooling region. The maximum difference in the temperatures between individual chickens and chicken legs within a tray were about 30% and 50% of the difference between the initial chicken temperature (10°C) and refrigerated air temperature (-25°C), respectively. The difference decreased towards the end of the process and, the lower the cooling air velocity, the more uniform the chicken temperature near the end.

The packing structure of the chicken drumsticks within the plastic liner bag did not have a significant impact on the freezing rate for any of the air velocities investigated based on a 95% confidence interval. That means the designer doesn't have to know the drumstick orientation when designing the freezer. On the other hand, the presence of the plastic liner bag increased freezing times by more than a factor of 3 at high air velocities. This is because refrigerated airflow can interact directly with the chicken if there is no polyliner, rather than being insulated by air trapped inside the polyliner; and evaporation plays a significant role in the total amount of heat transfer (up to 11% of the total heat load) when there is no polyliner to prevent moisture transfer.

This experimental data will be used as a validation tool for the heat transfer model described in Chapter 7.

Chapter 7

Numerical modelling of the forced air freezing of bulk packed whole chickens and chicken drumsticks

7.1 Introduction

Poultry is the most commonly consumed meat globally, in which chicken meat represents approximately 88 per cent of poultry meat output (ThePoultrySite, 2014). The shelf life of chicken meat is relatively short, all fresh poultry should be consumed within two days of purchasing (Jimenez, Salsi, Tiburzi, Rafaghelli, & Pirovani, 1999), so it is often necessary to freeze chicken to improve food safety and preserve product quality through the supply chain. Benefits of freezing include not only a long shelf life but also an excellent retention of nutrients, sensory qualities and of the prevention of microbial growth (Pham, 2014). An efficient design of freezing equipment is required to maximise the economics. Therefore, it is important that a chicken freezing process be modelled accurately to allow for design optimisation.

On the industrial scale in New Zealand, chicken products are typically cooled within a plastic liner bag (polyliner), which has the effect of restricting air movement within the air voids between the liner and the chickens and results in a larger air void within the bag on top of the chicken. The polyliner increases resistance to heat transfer since it prevents air outside the bag from directly contacting the chicken; however, it serves to reduce moisture loss which is detrimental to product quality and appearance. Despite research to account for the effect of voids on heat transfer rates (Ambaw et al., 2017; Datta, 2007a; James et al., 2006; North, 2000; O'Sullivan et al., 2016) a general approach for dealing with this problem has yet to be established. As such, accounting for voids within food packages remains a significant challenge for designers of industrial refrigeration equipment (Smitheram, 2018).

Several research articles have previously reported chicken freezing process models. Mannapperuma et al. (1994a, 1994b) presented a finite difference numerical method based on enthalpy formulation to simulate the air blast freezing of plastic-

wrapped whole chicken, tray packs of chicken parts and boxed chicken parts. Zilio et al. (2018) used the CFD software STAR-CCM + to model the liquid-solid phase change in the freezing of a chicken breast. The above-mentioned studies approximated the geometry of chicken by using simple shapes and used average heat transfer coefficients to represent the boundary condition over the entire surface of the packaging. None of them accounted for the effect of air voids within packages on the freezing rate. Air voids of different shapes and sizes exist when whole chicken carcasses or chicken drumsticks are packed in bulk, due to the irregular shapes of the products. A more rigorous model for the convective freezing of chicken would provide refrigeration equipment designers with a greater ability to optimise this important industrial process.

In an attempt to reproduce a realistic shape of food product and air voids within packages, many researchers (Ambaw et al., 2017; Ferrua & Singh, 2009b; O'Sullivan et al., 2016) employed a CFD modelling approach. These models were applied to the forced-air chilling of food products. However, modelling the food freezing process could be a greater challenge since thermophysical properties such as the thermal conductivity and specific heat suddenly change around the freezing point, which makes the governing equation becoming highly non-linear and thus difficult to solve (Pham, 2006). In food freezing applications, the CFD approach was successful applied for potatoes (Kiani & Sun, 2018; Kiani, Zhang, & Sun, 2015), pork cuts (Wang & Zou, 2014) and chicken breasts (Zilio et al., 2018).

In this study, the CFD approach would be used to model the forced air freezing of polylined whole chickens and chicken drumsticks packed in bulk. A realistic 3D geometric model of chicken products was obtained empirically from computed tomography images. This represents the first CFD freezing model that uses x-ray tomography to generate a realistic model geometry. The package structure, air voids within packages, and the flow field around the products were included in the model. The prediction results are validated against the experimental data presented in the previous chapter. The model will then be used to investigate the cooling heterogeneity within food packages, airflow distribution in the freezing tunnel and the effect of operating conditions on freezing time.

7.2 Geometrical model

The first step in the development of the CFD model was to construct a 3D geometrical model of a tray of whole chickens and chicken drumsticks in the forced-air freezing tunnel. This model includes the chicken products, the liner bag, the cardboard tray and the airflow domain. Section 7.2.1 to 7.2.3 present the procedure to create a geometrical model of the chicken freezing system.

7.2.1 Reconstruction of bulk packed chicken products geometrical model

Reconstructing a realistic geometrical model of packaged food products is challenging. Ferrua and Singh (2009b) made use of a single realistic strawberry fruit shape in a numerical precooling study. This single fruit shape was used to manually create a geometric model of the stack of identical strawberries in a clamshell. This procedure was also employed by (O'Sullivan et al., 2016) to create a geometrical model of a modular bulk package of kiwifruit. Both generating the single fruit shape and the entire package were very time consuming. With the x-ray computed tomography (CT) image technique, it has recently become possible to quickly generate numerous realistic 3D shapes of bulk-packed chicken products. CT scanning uses x-ray radiation which can penetrate inside objects with sufficient depth depending on the mass density and mass absorption coefficient of the material (Herremans et al., 2013). Therefore, the CT scanning technique can extract with good detail both the outer shape and interior structure (e.g. the gastro-intestinal cavity of chicken carcass) of chicken products packed in bulk. This technique already proved its merit to visualise and model realistic fruit stacks in a non-destructive way (Gruyters, 2019). In this study, CT scanning was used to construct a realistic 3D geometrical model of the empirical shape of bulk-packed chickens.

Whole chicken carcasses and chicken drumsticks were selected for CT scanning and arranged in a tray, following the same procedure as for the experiments (section 6.4). The scans were made by a Philips CT scanner at Massey University School of Veterinary Science, New Zealand (Figure 7.1)

Figure 7.1: Scanning process of a chicken tray

The construction of the chicken model started by creating the 3D surface points (STL geometry file) using the Slicer™ software package. This is an open-source platform for segmentation, registration and 3D visualization of medical imaging data. The first step in the reconstruction of the surface model of the chicken was segmenting CT images into distinct regions (i.e. chicken, cardboard and air). The CT scan data organized into a 3D matrix of volume elements (voxels). Slicer™ uses Otsu's thresholding technique (Otsu, 1979) for the segmentation task. This technique divides the dataset into different classes based on the specify intensity value assigned to each of the voxels. The intensity values used for classifying the dataset are known as thresholds. The mathematical formulation can be described as follows:

$$I = \begin{cases} val_1 & if \ I \le \lambda_1 \\ val_2 & if \ \lambda_1 < I \le \lambda_2 \\ val_n & if \ I > \lambda_{n-1} \end{cases} \tag{7.1}$$

where I is the intensity value, λ is the threshold and n is the number of intensity levels. The main drawbacks of this technique are firstly, the difficulty of finding the most suitable threshold for segmenting of the region of interest on specific dataset; secondly, the sensitivity of the resulting segmentation to noise and intensity of inhomogeneity and thirdly, this technique does not take into account the spatial distribution of the voxel intensities (Benitez Mendieta, 2016).

The segment editor module in Slicer™ allows users to select the threshold range of interest and the resulting 3D surface model will be displayed on the user interface. The selection tools in Slicer were used to remove unwanted structures such as the table on which the tray of chicken sat on during scanning. Figure 7.2 and Figure 7.3 illustrate the final surface reconstructed from CT data of bulk packed whole chickens and chicken drumsticks, respectively

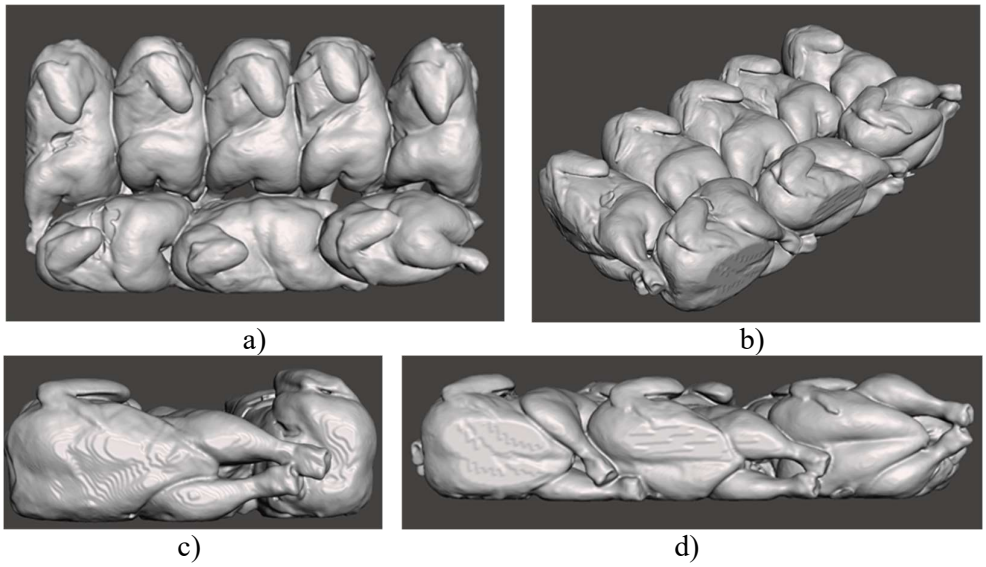

Figure 7.2: Surface reconstruction model of whole chickens a) top view, b) perspective view, c) left side view and d) front view

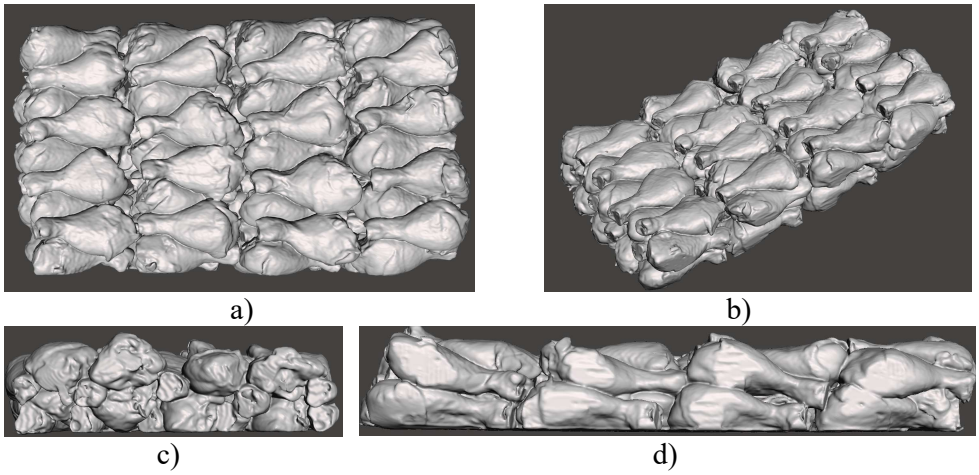

Figure 7.3: Surface reconstruction model of bulk packed chicken drumsticks a) top view, b) perspective view, c) right side view and d) front view

In order to import the CT scan data into the CFD model, the surface geometry of bulk-packed chicken carcasses and chicken pieces needed to be transformed into a

solid. Prior to that, the surface model needs to be clean and smooth to make it possible to convert to solid and avoid the complicated details that can result in highly skewed mesh elements. In the numerical solution, a highly skewed mesh can significantly compromise the accuracy and stability of the model (Ferrua, 2007). Meshmixer™ (Autodesk, Inc) was used for this step because it provides a number of tools dedicated to identifying and correcting errors on imported surfaces (i.e. holes and discontinuities) as well as sculpting, smoothing, and resizing the mesh density.

The final, cleaned reconstructed surfaces (in form of triangle meshes) were converted to quad meshes using ReCap™ Photo (Autodesk, Inc) to make it suitable to transform to solid surface forms (T-spline bodies) using Fusion 360™ (Autodesk, Inc). The summary of the workflow to construct the 3D geometrical model of chicken from CT images is presented in Figure 7.4

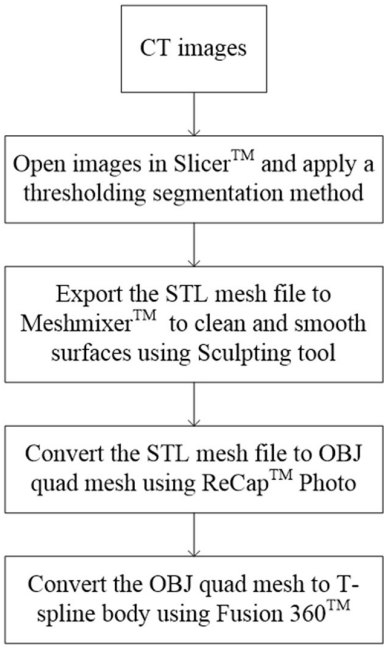

Figure 7.4: The workflow to create a 3D model from CT images

The completed geometrical models of whole chickens and bulk packed chicken drumsticks are depicted in Figure 7.5 and Figure 7.6, respectively. Some simplifications were made to prevent overly complex meshes. The model assumed an ideal thermal contact between the chicken surfaces. In addition, due to the insignificant heat fluxes in the gastro-intestinal cavities of chicken carcass

(confirmed by simulation results), the exact shape of cavities may not affect the freezing rate of bulk-packed whole chickens. Hence, the gastro-intestinal cavities were represented by ellipsoids which closely fit the volume of the reconstructed cavities to reduce the number of finite volumes in the CFD model. Moreover, because of the geometrical similarity of four rows in a tray of drumsticks (eighteen drumsticks in each row, Figure 7.3), the drumstick model was created by a combination of four identical blocks (each block representing one row in bulk-packed drumsticks).

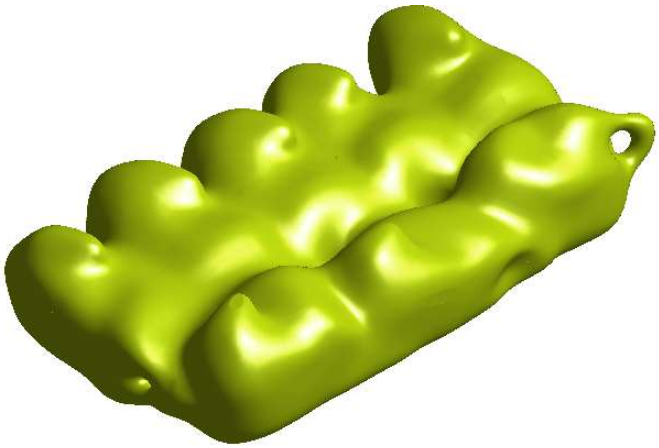

Figure 7.5: Geometrical model of bulk-packed whole chickens

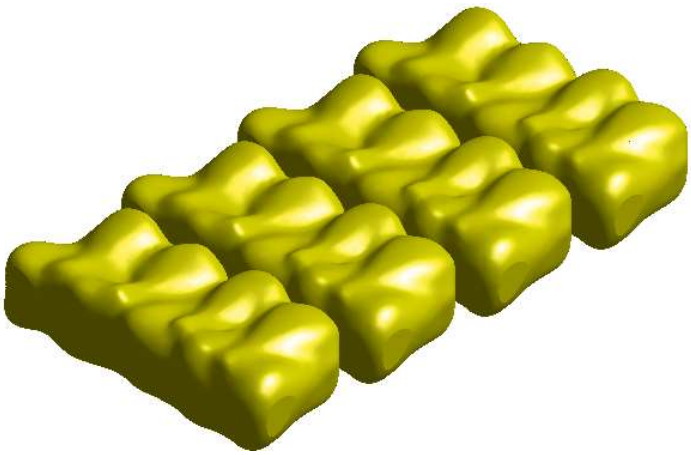

Figure 7.6: Geometrical model of bulk packed chicken drumsticks

The volumes of bulk-packed whole chickens (not considering the gastro-intestinal cavities) and chicken drumsticks geometric models were 11.9×10^{-3} m^3 and 10.8×10^{-3} m^3, respectively. Multiplying the geometric model volumes by the chicken density of 1070 kg m^{-3} (Walters & May, 1963) yields masses of 12.7 kg and 11.5 kg

respectively which are similar to the average weight of a tray of whole chickens (12.8 kg) and chicken drumsticks (11.5 kg) in the experiments (section 6.4).

7.2.2 The cardboard tray and the polyliner model

The geometrical model of the cardboard tray was created manually based on its actual dimensions (580×325×130 mm) using ANSYS Design Modeller (Figure 7.7). The cardboard thickness at bottom, left and right side was 5 mm. The front and the back of the tray were equipped with two handle vents and, on these sides, the cardboard thickness doubled (10 mm).

To simplify the geometric model, the oval handle vents at the end walls were represented by rectangular vents (90×35 mm) which have the same area as the actual vents. The chamfers at four corners of the tray were neglected.

(a)

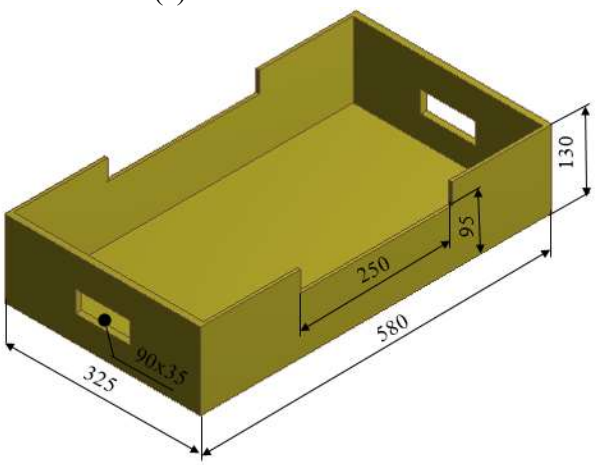

b)

Figure 7.7: Photo of a) the real, and b) the geometrical model construction of the cardboard tray

Bulk-packed chicken products are encased in a liner bag which is in direct contact with chickens at the edges, bottom and top of the tray. However, the single contact points between chicken and polyliner can generate high skewed and distorted meshes in the meat and fluid region inside the liner bag (Ferrua, 2007; O'Sullivan, 2016), that will compromise the accuracy and the stability of the solution. To avoid this problem in the geometric models small air gaps were created between the contact points, effectively placing the polyliner slightly apart from the chicken model. The larger the air gap, the better mesh quality, but the less realistic the thermal contact resistance becomes. The smaller the air gap, the smaller the element sizes must be to discretise the fluid region, increasing the number of mesh elements, the computer resources and computational time needed to perform numerical analysis. A 2 mm clearance between polyliner and chicken model was found to be the minimum distance that could be used to achieve a solution of the numerical model within the computational power constraints (a 64-bit Intel® Xeon® CPU E5-1620, 3.5 GHz, 16 GB RAM).

The artificial air gap placed between the liner and the chicken increases the volume of air inside the polyliner, but this is offset by the volume of air lost when the geometric models of the chickens were built from the CT data (compare Figures 7.2 and 7.3 with Figures 7.5 and 7.6). The experimental results (section 6.6.5) suggested that only the total fraction of air void within package needs to be considered rather than its size and shape when modelling heat transfer of packaged chicken. Moreover, an extra 2 mm gap over the extreme outer points of the chickens was expected to make very little difference when there is already a considerable air gap under much of the liner's surface.

The liner bag was modelled by rectangular blocks close-fitted to the chicken model while ensuring that the minimum gap between liner and chicken was 2 mm. The bottom and lateral surfaces of the liner were assumed to be in direct contact with the cardboard. In the numerical setup, the liner was described as a zero thickness wall. Therefore, it acted as a physical barrier to restrict the airflow inside rather than a thermal barrier to heat transfer. The photos of a tray of whole chickens, chicken drumsticks model were shown in Figures 7.8 and 7.9, respectively.

a)

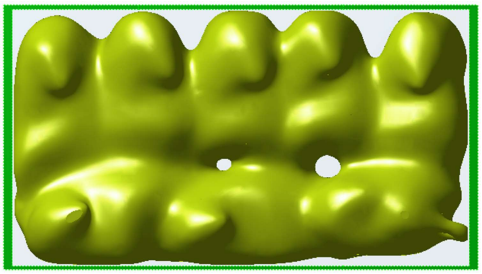

b)

c)

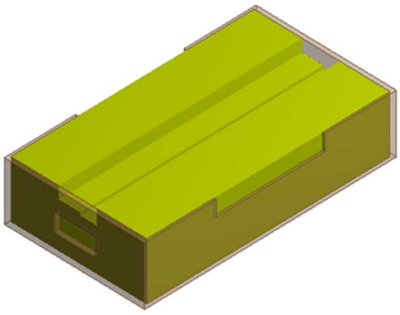

d)

Figure 7.8: a, c) a real tray of whole chickens, b) top view and d) isometric view of 3D model of a tray of chicken containing polyliner

(a)

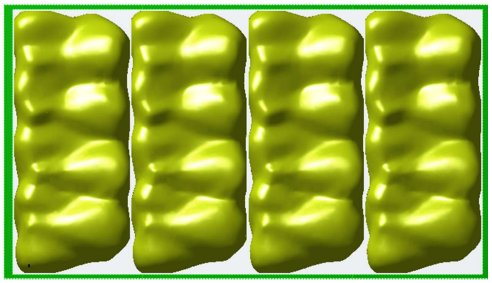

(b)

c)

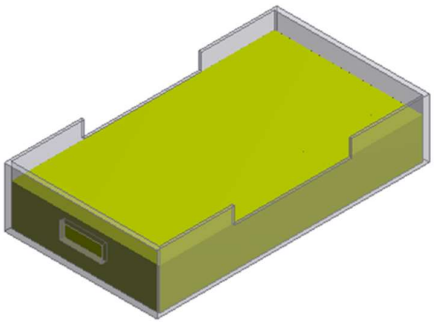

d)

Figure 7.9: a, c) a real tray of drumsticks, b) top view and c) isometric view of 3D model of a tray of drumsticks containing polyliner

7.2.3 The completed computational domain

The computational domain was constructed based on the internal dimensions of the PTT (Section 6.3) with the 3D model of a tray of whole chicken or chicken drumstick placed in the middle section at a distance of 5 cm from the bottom surface as in the experimental setup (Figure 7.10). Transition regions were placed at the inlet and outlet of the tray to aid with mesh refinement. From the inlet to the outlet along the airflow direction, the flow domain was divided into inlet section, transition inlet, product outer section, transition outlet and outlet section with the length of 650, 200, 700, 350, 500 mm, respectively. The inlet and outlet boundaries were both at the distance of 850 mm from the product outer section that was believed long enough to avoid an influence on the flow in the proximity of the product.

The section of the PTT that housed the chicken tray was divided into inner and outer 'product regions'. The product inner region included the air inside the liner bag, the cardboard tray, and the airflow up to 1 cm around the tray. This region was surrounded by the product outer section of the flow domain. The space between product inner and product outer region along the flow direction was kept at 5 cm.

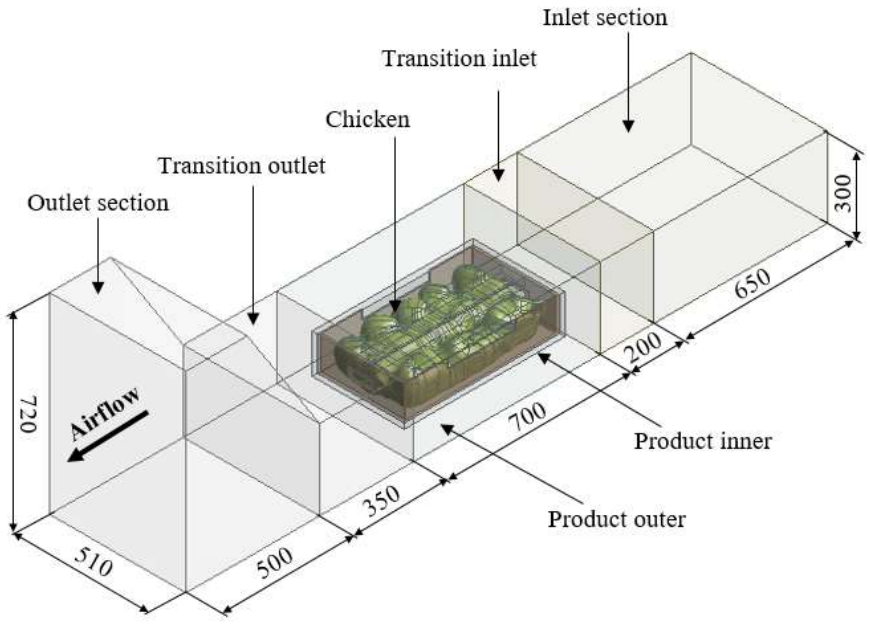

a)

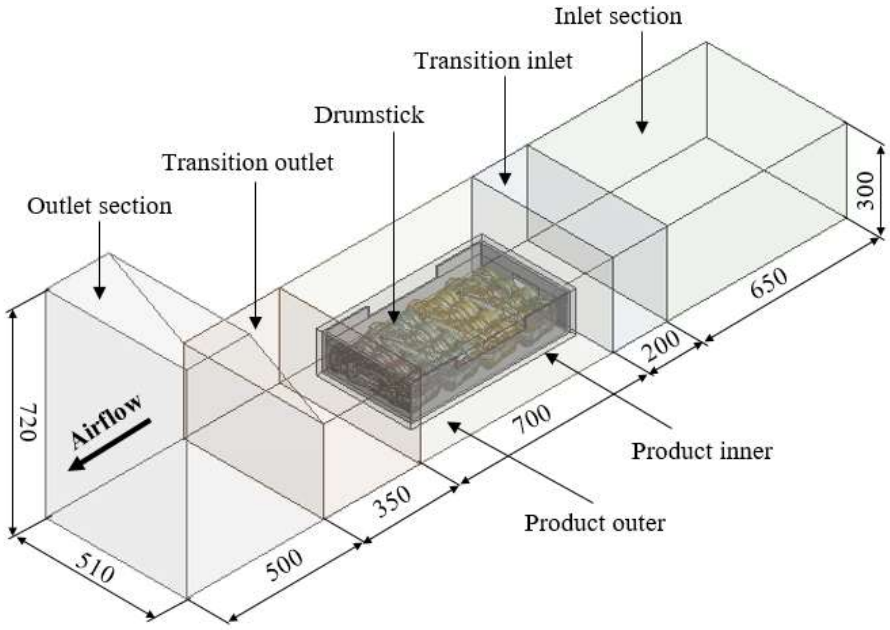

b)

Figure 7.10: Computational domain of a) bulk-packed whole chickens, b) chicken drumsticks in the forced-air freezing model

7.3 Mesh generation

The computational domain was meshed with ANSYS Meshing. Non-uniform mesh sizes were used. The chicken region and product inner region were discretised with the small elements to ensure sufficient definition of the geometrical model of the chicken and small air gap between chicken and polyliner (Figure 7.11 and Figure 7.12). From the product outer section outward the mesh became coarser. The selected element size for each section in the bulk-packed whole chicken model and bulk-packed drumstick model is shown in Table 7.1.

Table 7.1: Element size in the whole chicken model and drumstick model

Section	Whole chicken	Drumstick	Product inner	Product outer	Transition inlet/outlet	Inlet/ Outlet
Element size, mm	8	6	4.2	10	20	40

The mesh was designed to be used for the low-Reynolds number approach to modelling the boundary layer. This approach required high cell density in the wall-

normal direction (Defraeye, Verboven, & Nicolai, 2013). Therefore, in the boundary-layer region of the flow domain from the outer surface of the polyliner and the cardboard onward, 5 layers of prismatic cells were placed, with the first layer thickness of 0.6 mm and the growth rate of 1.2.

A mesh sensitivity study was done by running simulations at three different mesh sizes. Each consecutive mesh was obtained by increasing the number of elements of the previous mesh by 30%. Richardson extrapolation (Roache, 1997) was used to determine the mesh-independent solution. Table 7.2 and Table 7.3 show the effect of different mesh size on the volume-average temperature of whole chickens and drumsticks after 20 hours freezing. The mesh sizing was evaluated at the highest air velocity (4.5 m s^{-1} for whole chicken model and 4.3 m s^{-1} for drumstick model).

Table 7.2: Effect of different mesh size on the volume-average temperature of chicken after 20 hours freezing in the chicken model

Element size on product inner section, mm	Number of elements	$T_{chicken}$ after 20 hours	Mesh Independent solution	Relative error, %
4.8	3184692	-20.5	-19.4	5.2
4.2	4206147	-20.0		2.9
3.7	5593117	-19.8		1.6

Table 7.3: Effect of different mesh size on the volume-average temperature of drumstick after 20 hours freezing in the drumstick model

Element size on product inner section, mm	Number of elements	$T_{drumstick}$ after 20 hours	Mesh Independent solution	Relative error, %
4.8	3458023	-20.6	-19.6	4.9
4.2	4564705	-20.1		2.6
3.7	6047350	-19.9		1.3

With the mesh size of 4.2×10^6 and 4.5×10^6 elements for the whole chicken model and drumstick model respectively, the spatial discretization errors were 2.9% and

2.6% which are common acceptable errors in other studies (A Ambaw et al., 2017; Defraeye, Lambrecht, et al., 2013).Therefore, these grids were used for numerical simulation.

The ranges of orthogonal quality and skewness are from 0 to 1. The higher orthogonal quality and the lower skewness of a mesh the better its quality (Meshing, 2010). The average skewness of the grids for the whole chicken model and drumstick model were 0.24 and 0.23, respectively. For the average orthogonal quality, these figures were the same at 0.76. The worst cells were in the airflow region inside the polyliner. The maximum skewness of the grids of the whole chicken model and the drumstick model were 0.93 and 0.95, which were still lower than the critical value of 0.97 (Ferrua, 2007). The minimum orthogonal quality of these grids were 0.07 and 0.05, respectively. If the orthogonal quality is lower than 0.01 then the grid is unlikely to produce a stable and converging solution (O'Sullivan, 2016)

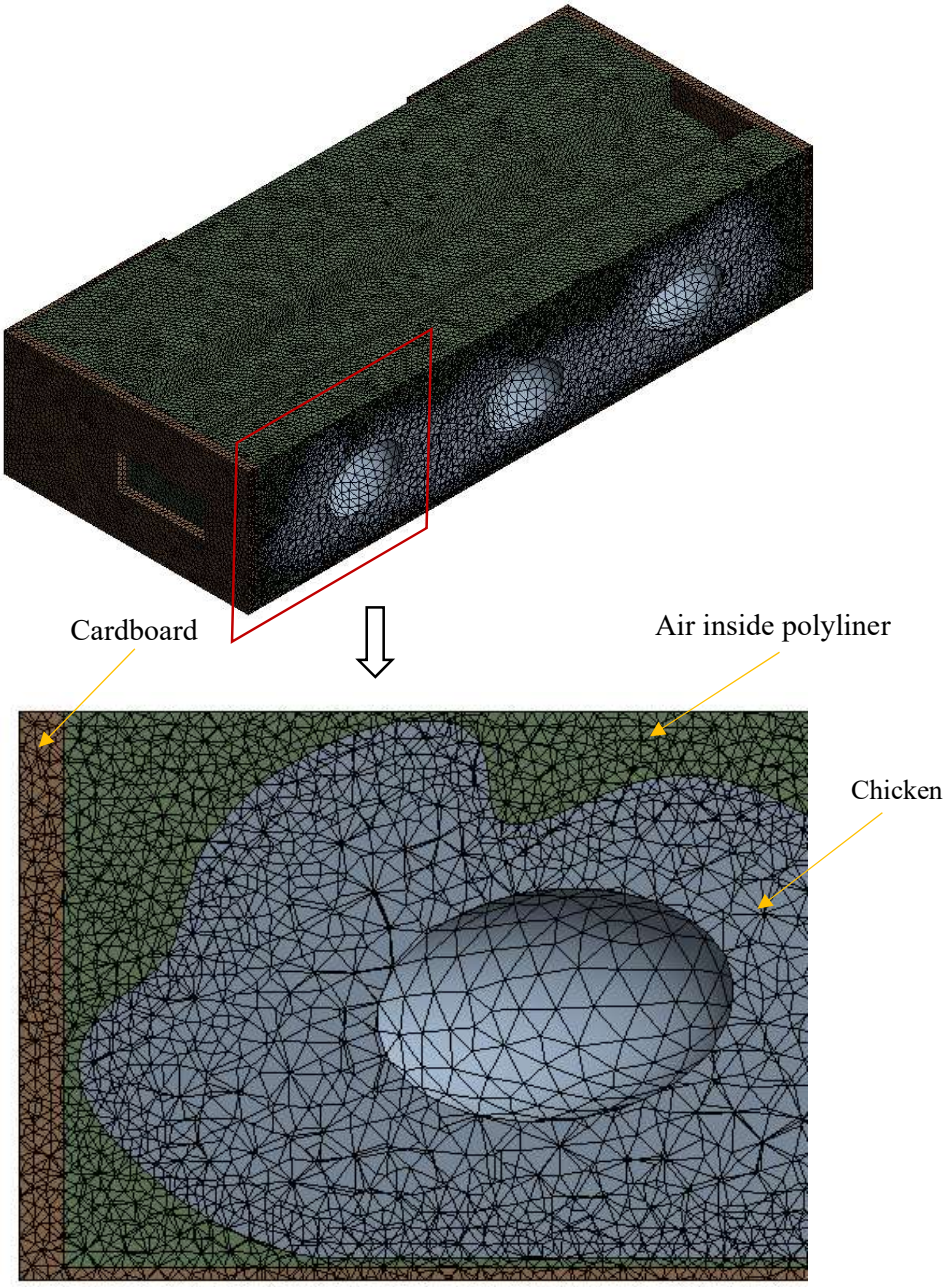

Figure 7.11: a) Mesh of the chickens and air region inside the polyliner b) gap between chickens and polyliner

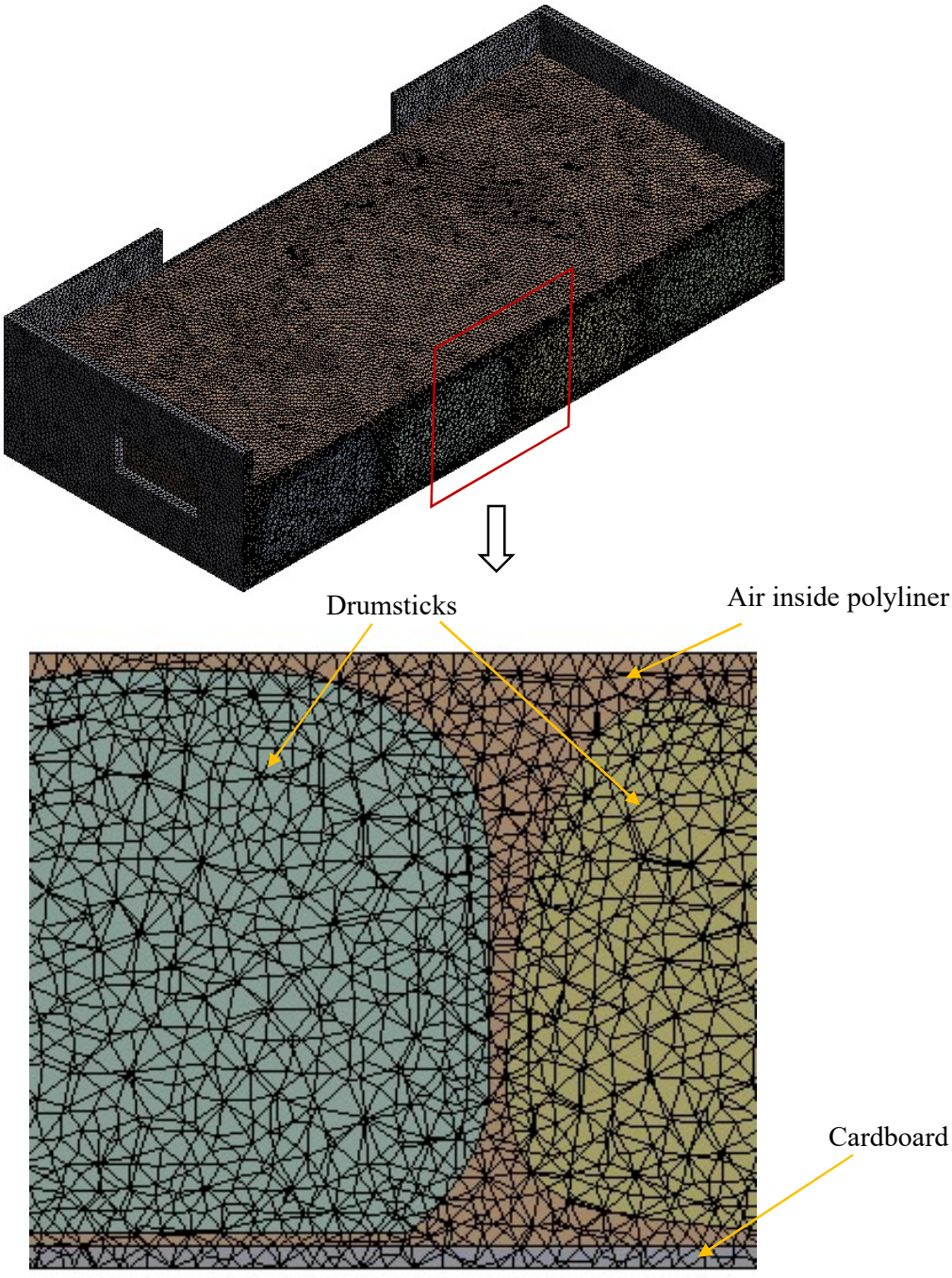

Figure 7.12: a) Mesh of the drumstick and air region inside the polyliner b) gap between drumsticks and polyliner

7.4 Transport equations

During forced-air freezing, chicken products are cooled by two main mechanisms: heat transfer (including conduction, convective and radiation) and mass transfer due to moisture loss from produce surfaces. Previous studies have concluded that radiation and moisture evaporation have a negligible effect in forced air cooling (Defraeye, Lambrecht, et al., 2013; Gowda, Narasimham, & Murthy, 1997; Gruyters et al., 2018; O'Sullivan et al., 2016), and thus they were not included in the freezing model. Typically, for the product in an enclosed space like a liner bag, the effect of natural convection must be accounted for when the Rayleigh number is higher than 1708 (Cengel & Ghajar, 2011). The Rayleigh number for an enclosure is determined from:

$$\mathrm{Ra} = \frac{g\beta\left(T_p - T_l\right)L^3}{\nu^2}\mathrm{Pr} \tag{7.1}$$

where g (m s^{-2}) is gravity; β (K^{-1}) is the volumetric thermal expansion coefficient; T_p and T_l (K) are the temperatures of chicken and polyliner surfaces; L (m) is the characteristic length; ν (m^2 s^{-1}) is the kinematic viscosity and Pr is the Prandtl number. In this model, L is the height of the polyliner (~ 9 cm). T_p and T_l were determined as the initial chicken temperature (10°C) and cooling air temperature (-25°C). The fluid properties are evaluated at the average fluid temperature $T_{avg} = (T_p + T_l)/2$ = -7.5°C, allows β = 3.76 x 10^{-3} K^{-1}, ν = 1.27x 10^{-5} m^2 s^{-1} and Pr = 0.738 (Cengel & Ghajar, 2011). Substituting these variables in Eq.7.1 yields

$$\mathrm{Ra} = \frac{9.81\times 0.00376\times\left(10-\left(-25\right)\right)\times 0.09^3}{\left(1.27\times 10^{-5}\right)^2}\times 0.738 = 4.3\times 10^6 \tag{7.2}$$

Since the calculated value of Ra (4.3 x 10^6) is higher than the critical value (1708), natural convection cannot be neglected in this study. A Ra number less than 10^8 also implies a laminar flow inside the polyliner (ANSYS, 2017)

For the airflow outside the polyliner, the flow regime is characterised by the Reynolds number

$$\mathrm{Re} = \frac{uD_H}{\nu} \tag{7.3}$$

where u (m s^{-1}) is the air velocity, D_H (m) is the hydraulic diameter and v (m^2 s^{-1}) is the kinematic viscosity. To estimate Re, u was taken as the minimum air velocity, u = 1 m/s. The hydraulic diameter at the inlet of the tunnel (300×510 mm) was $D_H = 4A/P$ = 0.378 m, and the kinematic viscosity of the refrigerated-air at -25 ºC was v = 1.128 × 10^{-5} m^2 s^{-1} (Cengel & Ghajar, 2011). Substituting these variables in Eq.7.3 yielded

$$\mathrm{Re} = \frac{1 \times 0.378}{1.128 \times 10^{-5}} = 33510 \tag{7.4}$$

The Reynolds number of 33510 at the minimum air velocity confirmed that the flow outside the polyliner is within the turbulent regime for internal of pipe/duct flow.

Under these conditions, the flow field within the system can be modelled by the following form of the continuity, momentum and energy conservation equations as given in Eqs. 7.5 – 7.9. Gravity was activated in the model and the fluid density was set as a function of temperature to simulate natural convection. No external source terms were included in the model.

The continuity equation was:

$$\frac{\partial \rho_a}{\partial t} + \nabla \cdot (\rho_a u) = 0 \tag{7.5}$$

where ρ_a (kg m $^{-3}$) is the air density, *t(s)* is the time, and u (m s^{-1}) is the velocity vector

The momentum equation was:

$$\frac{\partial (\rho_a u)}{\partial t} + \nabla \cdot (\rho_a u \otimes u) = -\nabla P + \nabla \cdot \tau + \rho g \tag{7.6}$$

where P (Pa) is the pressure, g (m s^{-2}) is the gravity and τ is the stress tensor given by:

$$\tau = \mu_a \left(\nabla u + (\nabla u)^T - \frac{2}{3} \nabla \cdot u \mathrm{I} \right) \tag{7.7}$$

with μ_a (kg m^{-1} s^{-1}) is the dynamic viscosity of air and I is the unit tensor.

The energy conservation equation is:

$$\frac{\partial (\rho_a E)}{\partial t} + \nabla \cdot \left(u \left(\rho_a E + P \right) \right) = \nabla \cdot \left(k_e \nabla T_a \right) \tag{7.8}$$

where k_e (W m^{-1} K^{-1}) is the effective thermal conductivity, E (J kg^{-1}) is the specific energy of fluid defined as:

$$E = H - \frac{P}{\rho} + \frac{u^2}{2} \tag{7.9}$$

where H (J kg^{-1}) is the enthalpy and $u^2/2$ represents the kinetic energy.

In solid regions (chicken products and cardboard tray) the heat transfer equation is given by:

$$\frac{\partial (\rho_s c_s T)}{\partial t} = \nabla \left(k_s \nabla T_s \right) \tag{7.10}$$

where ρ_s (kg m^{-3}), c_s (J kg^{-1} K^{-1}), k_s (W m^{-1} K^{-}) and T_s (K) are the density, heat capacity, thermal conductivity and temperature of solid, respectively

7.5 Numerical model

7.5.1 Thermal properties of materials

Thermal properties of air and packaging materials are presented in Table 7.4. The properties of air were estimated at -25°C (the cooling air temperature), using the data found in Cengel and Ghajar (2011), and were assumed constant throughout the

simulation except for air density inside the polyliner, which was assumed to behave as an ideal gas in order to simulate natural convection. The cardboard properties were the same as those used by (O'Sullivan, 2016; S. P. Singh et al., 2008)

Table 7.4 Thermal properties of air and packaging materials

Properties	Air outside liner	Air inside liner	Cardboard
Density, kg m^{-3}	1.4225	ideal gas	195
Specific heat, J kg^{-1} K^{-1}	1004.5	1004.5	1700
Thermal conductivity, W m^{-1} K^{-1}	0.0217	0.0217	0.078
Dynamic viscosity, kg m^{-1} s^{-1}	1.6×10^{-5}	1.6×10^{-5}	-

The specific heat capacity and thermal conductivity of chicken were set as a function of temperature to account for the sudden change of these properties around the freezing point (Pham, 2006). These properties were estimated from the composition data found in (Sweat, Haugh, & Stadelman, 1973), in which the composition of whole chicken was taken as the white chicken meat with 74.4% water, 0.3% fat and chicken drumstick was considered as dark chicken meat with 76.3% water and 2.5% fat.

The thermal properties prediction method was presented previously in Chapter 3. Since the mathematical expression for enthalpy of a food item was obtained by integrating the specific heat equation, the accuracy of the enthalpy will guarantee the accuracy of the specific heat equations. The comparison between predicted and experimental enthalpy and thermal conductivity data are presented in Table 7.5 and 7.6, respectively. In general, the model gave a better predictions in unfrozen temperature compared to the frozen temperature ranges. The mean relative errors over the temperature range -30°C to 20°C for enthalpy of chicken carcasses and chicken drumsticks were 6.8% and 8.2%, respectively. Those numbers for thermal conductivity prediction were 7.7% and 5.6%. The mean relative errors of less than 10% confirm that the predicted thermal conductivity and enthalpy (or specific heat) of whole chickens and chicken drumsticks are suitable for using in the numerical model.

Table 7.5: Comparison between predicted and experimental enthalpy data for whole chicken and chicken drumsticks. The experimental enthalpy data was obtained from Riedel (1957)

T, °C	Enthalpy, kJ kg^{-1}			Relative error, %	
	Whole Chickens	Drumsticks	Riedel, 1957	Whole Chickens	Drumsticks
-30	20.7	20.9	19.1	8.6	9.4
-20	43.8	44.2	53.8	18.5	17.8
-10	75.4	76.2	74.1	1.7	2.8
-7	91.2	92.3	87.7	4.0	5.2
-5	108.5	110.0	105.7	2.7	4.0
-3	148.8	151.2	137.2	8.5	10.2
-2	223.9	228.2	179.2	24.9	27.3
-1	298.7	304.9	290.4	2.9	5.0
0	302.1	308.3	297.8	1.4	3.5
10	335.0	341.7	331.2	1.2	3.2
20	368.1	375.3	368.3	0.0	1.9
Mean relative error				6.8	8.2

Table 7.6: Comparison between predicted and experimental thermal conductivity data for whole chicken and chicken drumsticks. The experimental thermal conductivity data was taken from Sweat et al. (1973)

T, °C	Thermal conductivity, W m^{-1} K^{-1}				Relative error, %	
	Prediction		Sweat et al. (1973)			
	Whole chickens	Drums	White meat	Dark meat	Whole chickens	Drums
-30	1.58	1.62	1.42	1.49	10.73	8.79
-20	1.50	1.54	1.33	1.39	13.36	10.51
-10	1.41	1.43	1.21	1.28	16.31	12.21
0	0.47	0.48	0.48	0.48	0.34	0.31
10	0.49	0.49	0.48	0.49	1.77	0.59
20	0.51	0.50	0.49	0.50	3.60	1.24
Mean relative error					7.69	5.61

To simplify the model, a constant chicken density of 1070 kg m^{-3}, found in (Walters & May, 1963), was used. Based on the physical properties model, it was predicted that the chicken density varies by only 6% between -25°C (freezing temperature)

and 10°C (initial chicken temperature), suggesting that a constant mid-range density value will be adequate for these simulations.

7.5.2 Boundary and operating conditions

The inlet of the computation domain was defined as the velocity-inlet. The velocities imposed for the whole chicken model were 1 m s^{-1}, 2.5 m s^{-1}, and 4.5 m s^{-1}, and for the drumstick model were 1 m s^{-1}, 2.5 m s^{-1}, and 4.3 m s^{-1}, the same as for the experiments described in Chapter 6. The inlet air temperature was set at -25°C. The low turbulence intensity of 1% was used as the presence of the fine airflow diffuser.

At the outlet of the domain, an under-pressure was imposed to represent the suction pressure of the fan. These values were taken from the experiments and for the high, medium and low inlet air velocity for both whole chickens and drumsticks freezing experiments were -20 Pa, -10 Pa and -5 Pa, respectively. The cardboard, polyliner, chicken products and all other surfaces of the tunnel were modelled as no-slip walls with zero roughness. The initial temperatures of the chicken/drumstick and cardboard were set to the equilibrating temperature at the start of the experiment (approximately 10°C) and differed slightly depending on each experiment. Air volume inside the liner was defined as a laminar zone to simulate natural convection.

7.5.3 Numerical solution

Numerical simulation was performed with CFD code ANSYS Fluent Release 18.2. The standard k-ε turbulence model with the Enhanced Wall Treatment (EWT) option was used. The EWT is the near-wall modelling method that can automatically switch from a low Reynolds number approach (LRNM) to a wall function approach (WF). The LRNM is more accurate than WF in the prediction of convective heat transfer in the boundary layer (Defraeye, Verboven, et al., 2013). However, the restriction that the near-wall mesh must be sufficiently fine everywhere might impose too large a computational requirement. The EWT possesses the accuracy of LRNM for the fine near-wall meshes and, at the same time, will not reduce accuracy for the coarse meshes where the WF is suitable. The

standard k-ε turbulence model is robust, relatively accurate over the wide range of turbulence flows and CPU efficiency (ANSYS, 2017). The combination of standard k-ε turbulence model with EWT for the near-wall modelling was expected to give the best performance for a number of turbulence models (O'Sullivan, 2016)

The SIMPLE algorithm was used for pressure-velocity coupling. The second-order discretization scheme was used for pressure, momentum, turbulent kinetic energy, turbulent dissipation rate and energy. The Green-Gauss Cell Based option was used for gradient discretization, to ensure second-order interpolation, as recommended by ANSYS (2017)

To speed up the calculation, the steady-state flow equation was first solved with the energy equation disabled in order to obtain the initial fluid flow field. Once the steady-state simulation had converged, a transient simulation was performed by solving the flow and energy equations simultaneously to account for the effect of natural convection. The default residuals were used to indicate the converged solution for continuity, x-, y- and z- velocity, energy, k and epsilon. A temporal sensitivity test was performed by running the simulation at three different time steps of 30 s, 60 s and 120 s. The time step-independent solution was determined by Richardson extrapolation (Roache, 1997). The relative errors of the volume-averaged temperature of bulk-packed whole chicken and drumsticks after 20 hours freezing for the time step of 120 s were 0.3 % and 0.6%, respectively. These errors were small enough to justify the use of a time step of 120 s in the numerical simulation. A maximum of 20 iterations per time step was used. The computational times for the whole chicken model and drumstick model for 21 hours freezing were 7.5 hours and 8.0 hours, respectively. The calculations were performed on a 64-bit Intel® Xeon® CPU E5-1620, 3.5 GHz, 16 GB RAM.

7.6 Numerical model validations

The numerical model was first validated by comparing the predicted temperatures with experimental data collected in Chapter 6 for the average temperature history and the SECT of a tray of whole chickens and drumsticks for different refrigerated air velocities. The SECT was calculated following the same method presented in

section 6.6. Subsequently, the measured temperature histories of individual whole chickens or drumsticks within a tray were also compared with the numerical results to assess the accuracy of the developed model in predicting the local cooling behaviour.

7.6.1 Comparison of the numerical and measured average temperature history of chickens per tray.

The predicted average temperatures per tray of chicken breast and chicken cavity were computed by averaging the equivalent temperatures of all chickens. In the numerical model the breast temperature of each chicken was determined at 3 cm depth in the breast along the y-direction (Figure 7.13) to match the thermocouple position in the experiments (Figure 6.7). Since the cavity temperature was measured at an arbitrary position in the cavity, the volume-averaged temperature of the air region within the cavity was chosen as the representative temperature.

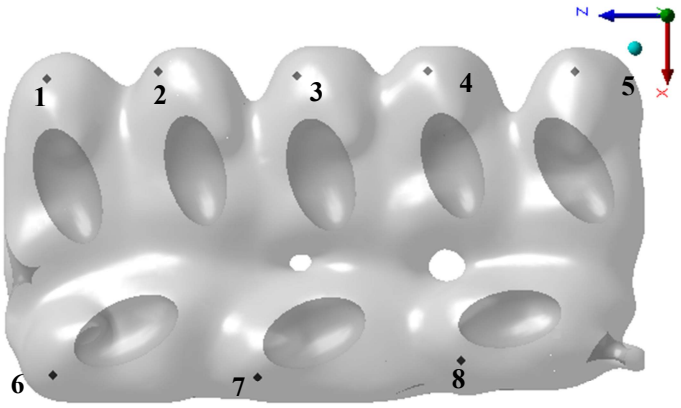

Figure 7.13: Position of virtual breast sensors in chicken model.

Figure 7.14a shows the comparison between the model prediction and experimental average temperatures of chicken breast and chicken cavity at the inlet air velocity of 1 m s^{-1}, with the error bars representing the experimental uncertainty at 95% confidence interval. The same comparisons at inlet air velocities of 2.5 m s^{-1}, and 4.5 m^{-1} are depicted in Figures 7.14 b and 7.14c.

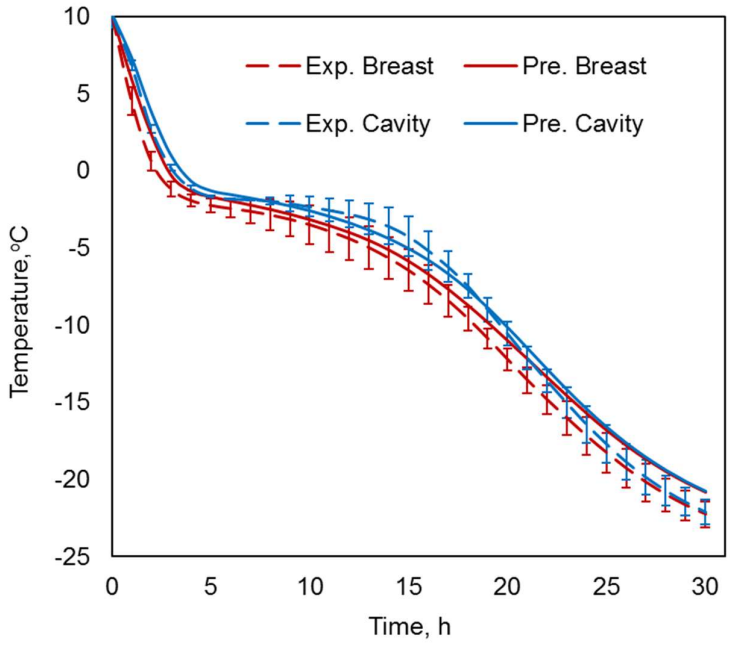
Exp. Breast
Pre. Breast
Exp. Cavity
Pre. Cavity
Temperature, °C
Time, h
10
5
0
-5
-10
-15
-20
-25
0
5
10
15
20
25
30

a)

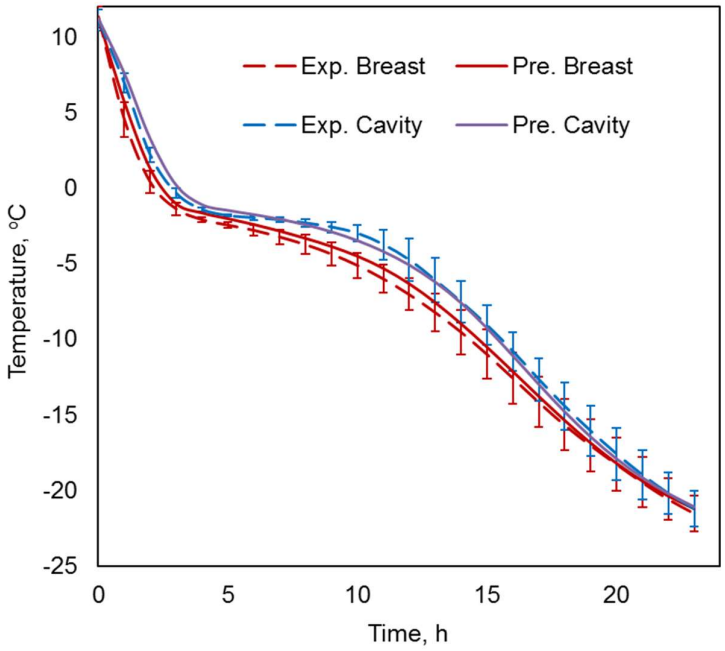
Exp. Breast
Pre. Breast
Exp. Cavity
Pre. Cavity
Temperature, °C
Time, h
10
5
0
-5
-10
-15
-20
-25
0
5
10
15
20

b)

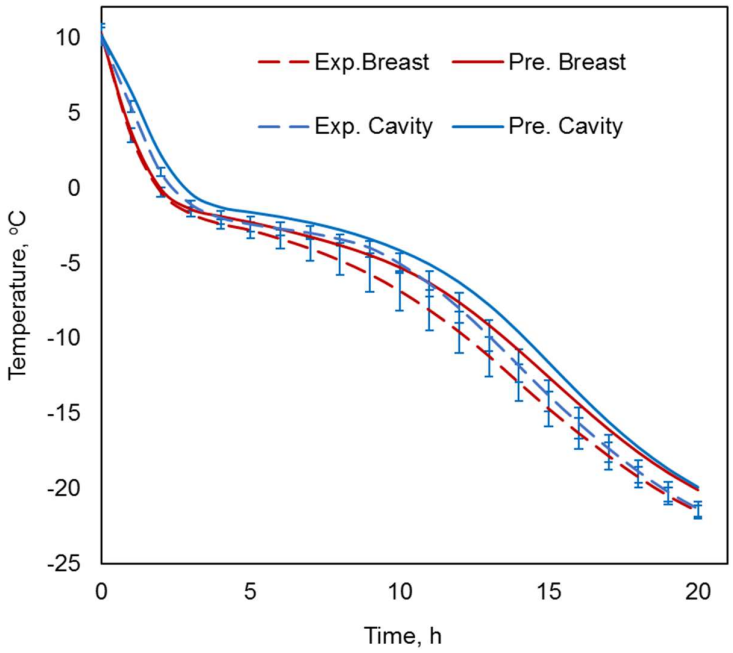

c)

Figure 7.14: Predicted and experimental average temperature of chicken breast and chicken cavity at the air velocity of a) 1 m s^{-1}, b) 2.5 m s^{-1} and c) 4.5 m s^{-1}

The results show good agreement between model predictions and experimental data. The worst prediction was at the air velocity of 4.5 m s^{-1}, with the mean discrepancy between predicted and measured average temperature was 1.3°C for both chicken cavity and chicken breast. At the air velocity of 1 m s^{-1}, the mean temperature differences were 0.9°C and 0.6°C for the breast and cavity temperature, respectively, while they were 0.4°C and 0.3°C for 2.5 m s^{-1}. The worst prediction (under prediction of cooling rate) at the air velocity of 4.5 m s^{-1} may be explained by the possibility that at the high air velocity (high Biot number) the effect of the artificial air gap in the CFD model which increases the internal resistance to heat transfer, has become more pronounced.

7.6.2 Comparison of the numerical and measured SECT of a tray of chickens

The SECT of a chicken tray was determined based on the average temperature history of the chicken cavity. Table 7.7 presents the predicted and experimental SECT (from Chapter 6) for a tray of chicken. The model tends to overpredict the

SECT with the maximum difference between predicted and experimental values of 7.3% at 4.5 m s^{-1}

Table 7.7 Experimental and predicted SECT of a tray of chicken at different air velocities

Air velocity, m s^{-1}	Experimental SECT, h	Experimental uncertainty, h	Predicted SECT, h	Difference, %
1.0	27.8	1.2	29.7	6.8
2.5	22.1	1.5	22.3	0.9
4.5	19.3	0.5	20.7	7.3

7.6.3 Comparison of the numerical and measured temperature history of individual chickens within a tray.

To investigate the performance of the chicken freezing model at specific locations rather than for average temperatures, the experimental and predicted cooling curves were separated on a per chicken basis. The comparison of individual chicken breast and chicken cavity temperature profiles at 1 m s^{-1} air velocity are shown in Figure 7.15. Similar comparisons at 2.5 m s^{-1} and 4.5 m s^{-1} are shown in Figures 7.16 and 7.17, respectively

For the chickens at the corner of the tray (chicken Numbers 1, 5 and 6, Figure 6.7 2) where the thermocouples were close to the contacting points between chickens and the liner bag, the effect of the artificial air gap used in the simulation (which increases the resistance to heat transfer) is most obvious. That is most likely the reason for the under-prediction of the temperature drop of the breast and cavity of these chickens.

The air gap between the top surfaces of chicken Numbers 2, 3, 4, 7 and 8 and the liner in the model can be matched to the presence of thermocouple wires on the top surfaces of the chickens in the experiments (Fig. 6.7). In these chickens, the agreement between predicted and measured temperature history is better for the breast compared to the cavity location. At this point, it is also noteworthy to recall that the chicken cavity geometry was represented by an ellipsoid rather than using their real shape, as derived via CT scanning. In addition, the numerical cavity

temperature was represented by the average temperature of the air volume inside the cavity instead of a single point temperature. Therefore, an error in cavity temperature predictions would be expected. Moreover, it can be hypothesized that the predictions at the breast, which is closer to the chicken surface than the cavity, are less affected by the uncertainty in thermal properties. Hence, the predicted temperatures at these locations closely follow the experimental histories.

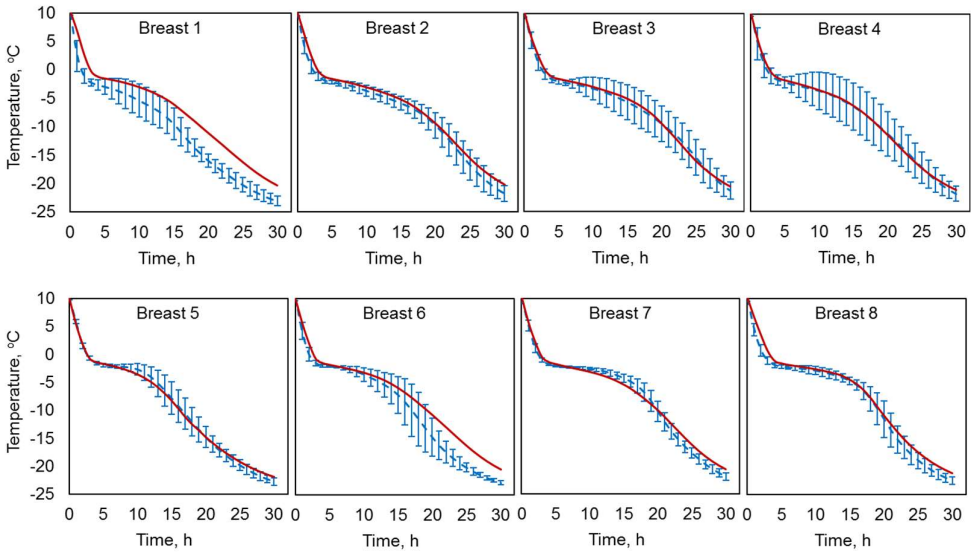

a)

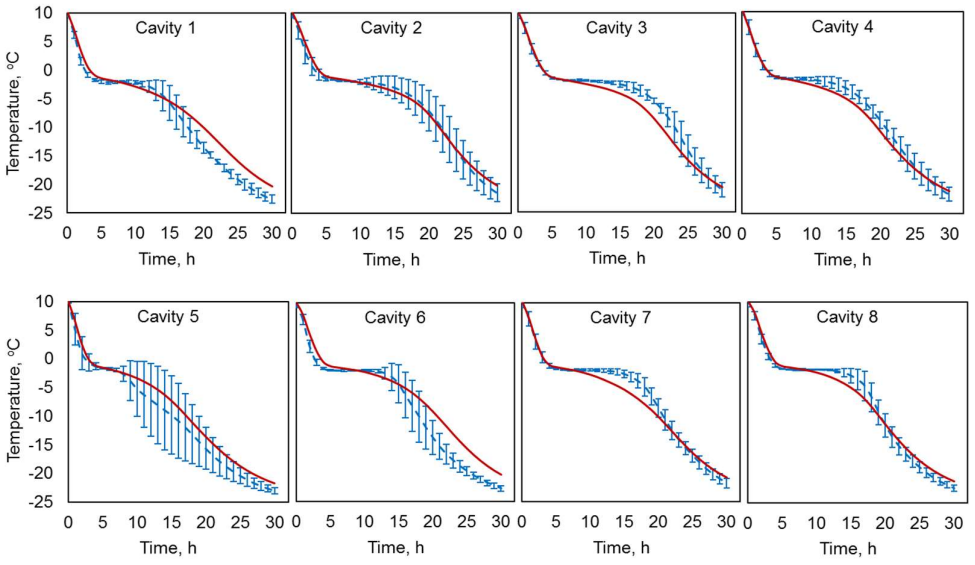

b)

Figure 7.15: Predicted and experimental temperature history of individual a) chicken breasts and b) chicken cavities at the air velocity of 1 m s^{-1}. The numerical temperatures are depicted in red continuous lines; measured values are depicted in blue dash lines

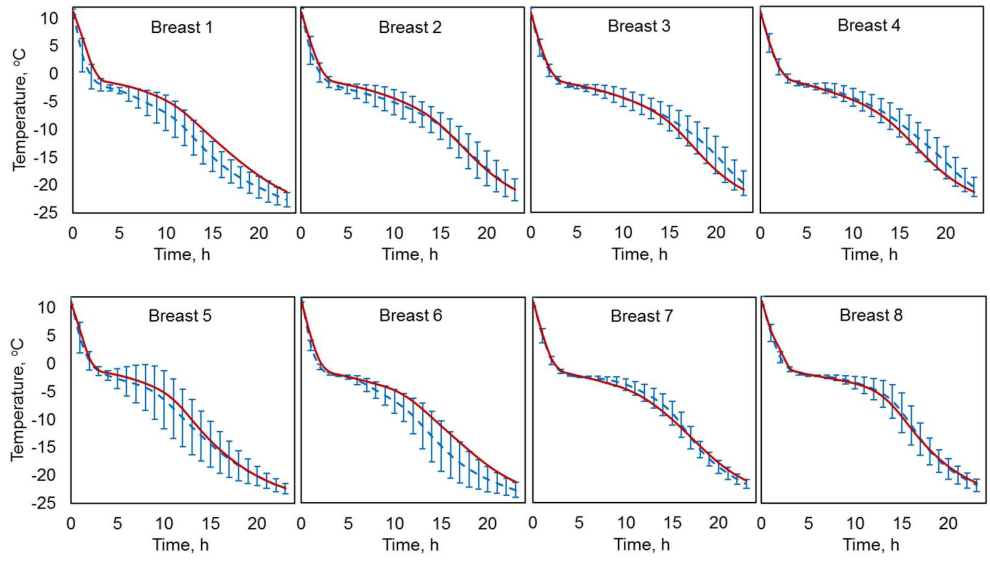

a)

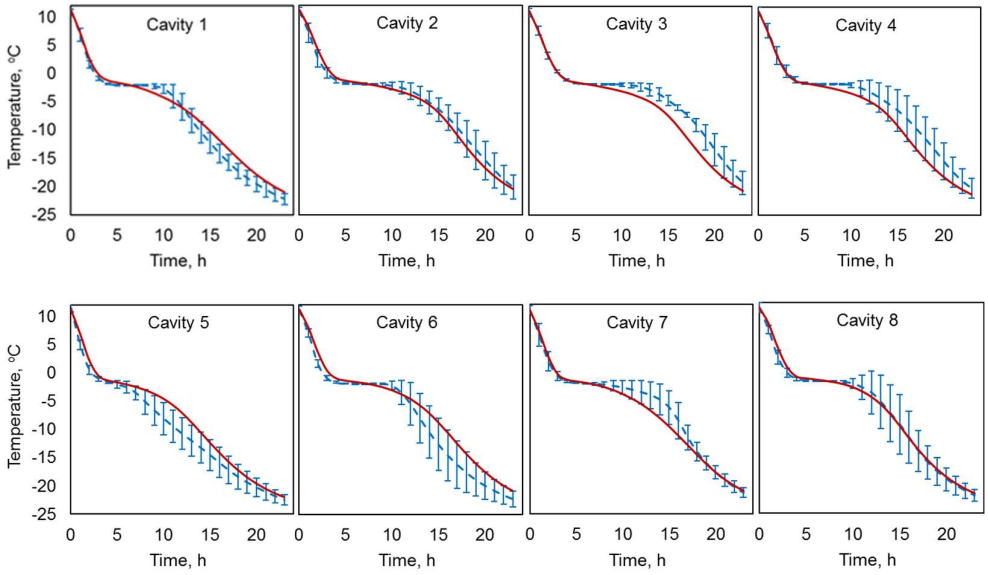

b)

Figure 7.16: Predicted and experimental temperature history of individual a) chicken breasts and b) chicken cavities at the air velocity of 2.5 m s^{-1}. The numerical temperatures are depicted in red continuous lines, measured values are depicted in blue dash lines

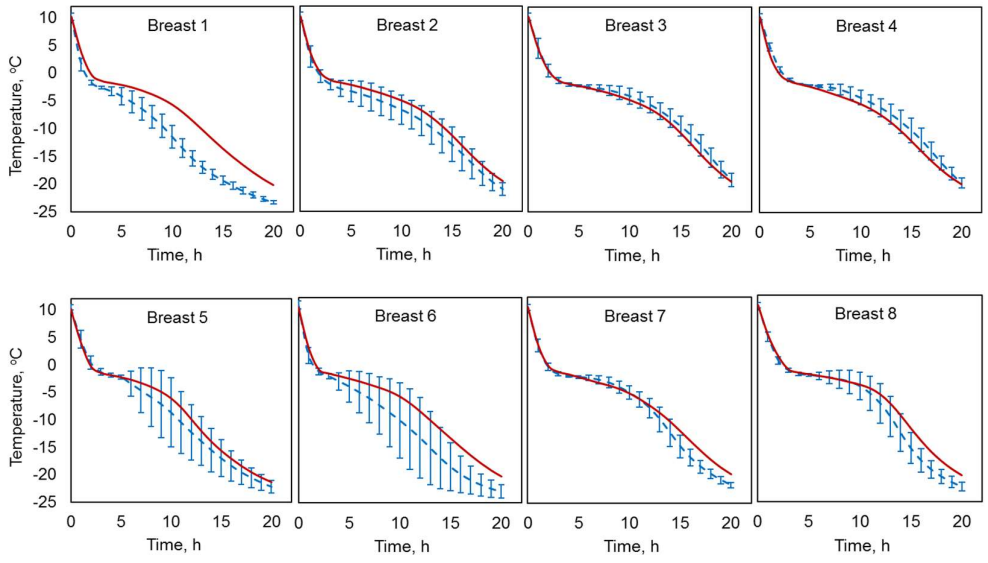

a)

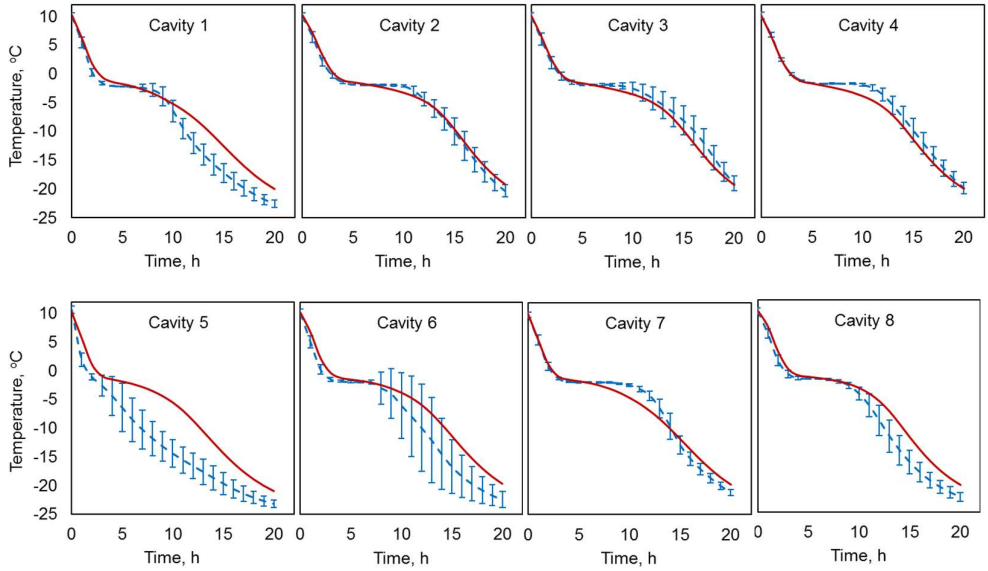

b)

Figure 7.17: Predicted and experimental temperature history of individual a) chicken breasts and b) chicken cavities at the air velocity of 4.5 m s^{-1}. The numerical temperatures are depicted in red continuous lines, measured values are depicted in blue dash lines

7.6.4 Comparison of the numerical and measured average temperature history of chicken drumsticks per tray.

The suitability of the drumstick model was first assessed by comparing the experimental (Chapter 6) and predicted average temperature histories of a tray of

drumsticks. The average predicted temperature was computed by averaging the predicted temperatures at 8 positions (Figure 7.20) which corresponded to the positions of the 8 thermocouples in the experiments. While not shown clearly in Figure 7.18, the depth (y-direction position) of each modelled temperature was also chosen to match the experimental position. Position Numbers 1, 3 and 4 are on the bottom layer, Number 2 is on the second layer, Numbers 5, 6 and 8 are on the third layer and the Number 7 is on the top layer.

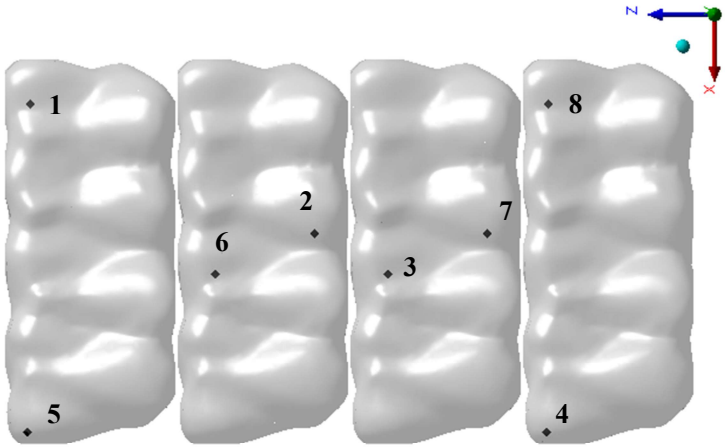

Figure 7.18: Position of virtual sensors in the drumstick model

Figure 7.19 shows the measured and simulated average time-temperature curves per tray of chicken drumsticks. The results show good agreement between the experimental and predicted histories of the drumsticks with mean temperature differences of 0.3°C, 0.9°C and 1.1°C for air velocities of 1 m s^{-1}, 2.5 m s^{-1} and 4.3 m s^{-1} respectively. As can be seen from Figure 7.19, the drumstick model gave a better prediction in the cooling range than in the freezing range. This is reasonable since freezing is a more complicated process than cooling without phase change, because thermal properties highly depend on temperature.

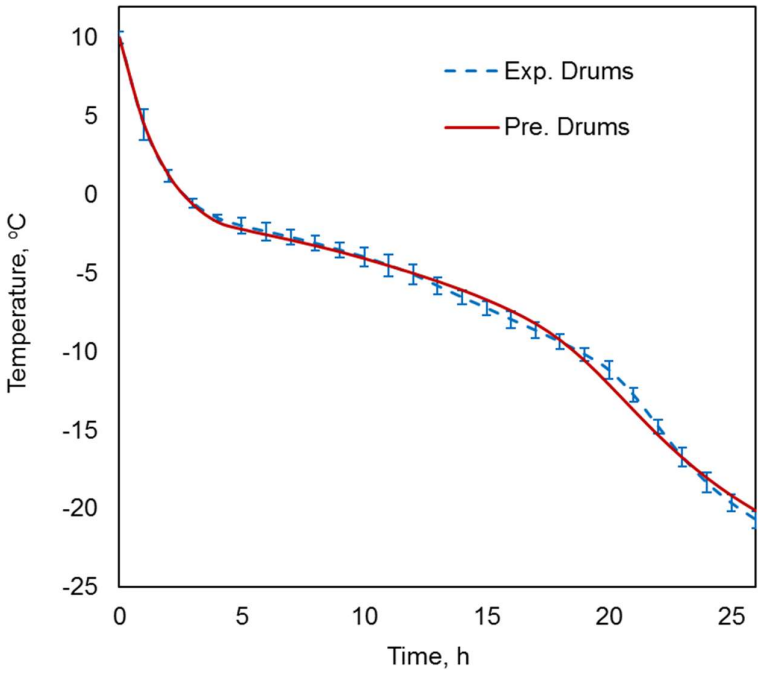
Exp. Drums
Pre. Drums
Temperature, °C
Time, h
10
5
0
-5
-10
-15
-20
-25
0
5
10
15
20
25

a)

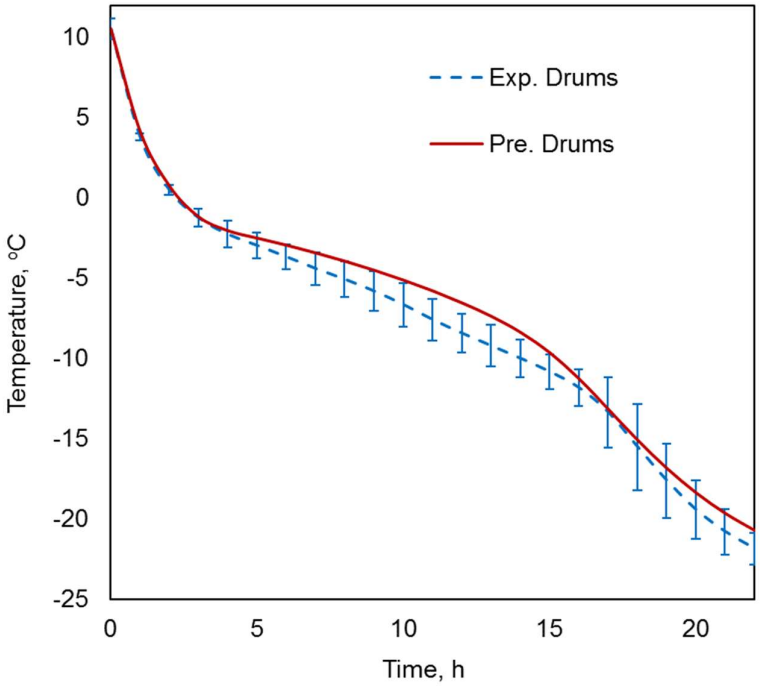
Exp. Drums
Pre. Drums
Temperature, °C
Time, h
10
5
0
-5
-10
-15
-20
-25
0
5
10
15
20

b)

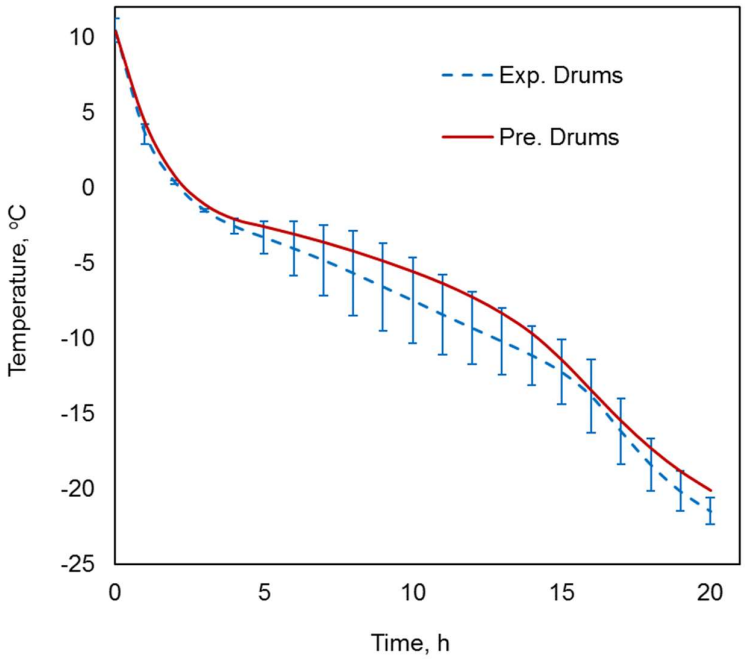

c)

Figure 7.19: Predicted and experimental average temperature of chicken drumsticks per tray at the air velocity of a) 1 m s^{-1}, b) 2.5 m s^{-1} and c) 4.3 m s^{-1}. The numerical temperatures are depicted in red continuous lines, measured values are depicted in blue dash lines.

7.6.5 Comparison of the numerical and measured SECT of a tray of drumsticks

Table 7.8 summarizes the results of predicted and measured SECT of a tray of drumsticks at different air velocities. The SECT was determined based on the average temperature history of a tray of drumsticks. The maximum difference between predicted and experimental SECT was 5.7% at 4.3 m s^{-1}.

Table 7.8 Experimental and predicted SECT of a tray of drumsticks at different air velocities

Air velocity, m s^{-1}	Experimental SECT, h	Experimental uncertainty, h	Predicted SECT, h	Difference, %
1.0	25.9	0.5	26.6	2.7
2.5	20.8	1.2	21.9	5.3
4.3	19.3	0.8	20.4	5.7

7.6.6 Comparison of the numerical and measured temperature histories of individual drumsticks within a tray.

The performance of the drumstick freezing model was further assessed by comparing the predicted and measured temperature histories of specific drumsticks within a tray at the air velocity of 1 m s^{-1} (Figure 7.20), 2.5 m s^{-1} (Figure 7.21), and 4.3 m s^{-1} (Figure 7.22).

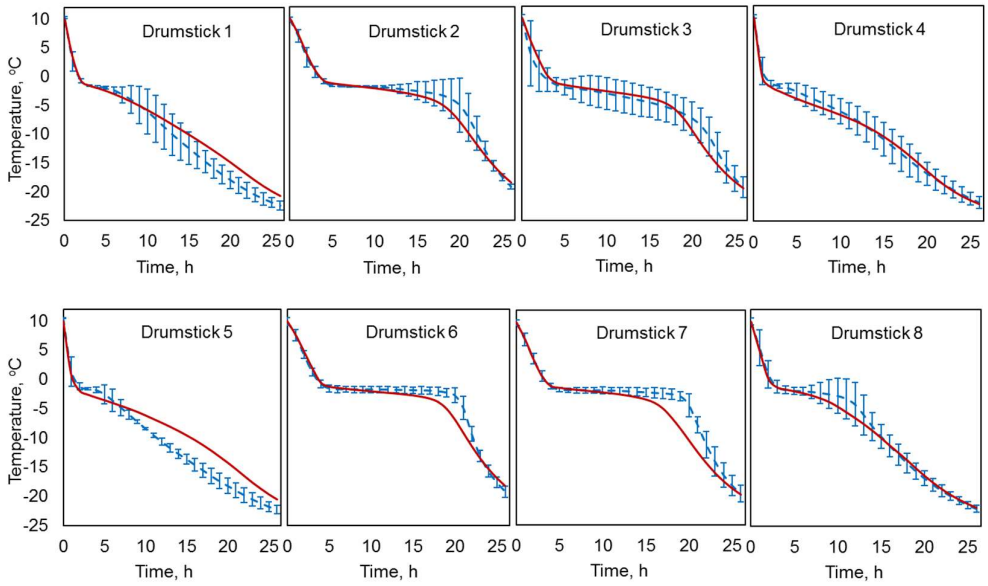

Figure 7.20: Predicted and experimental temperature history of individual drumsticks within a tray at the air velocity of 1 m s^{-1}. The numerical temperatures are depicted in red continuous lines, measured values are depicted in blue dash lines

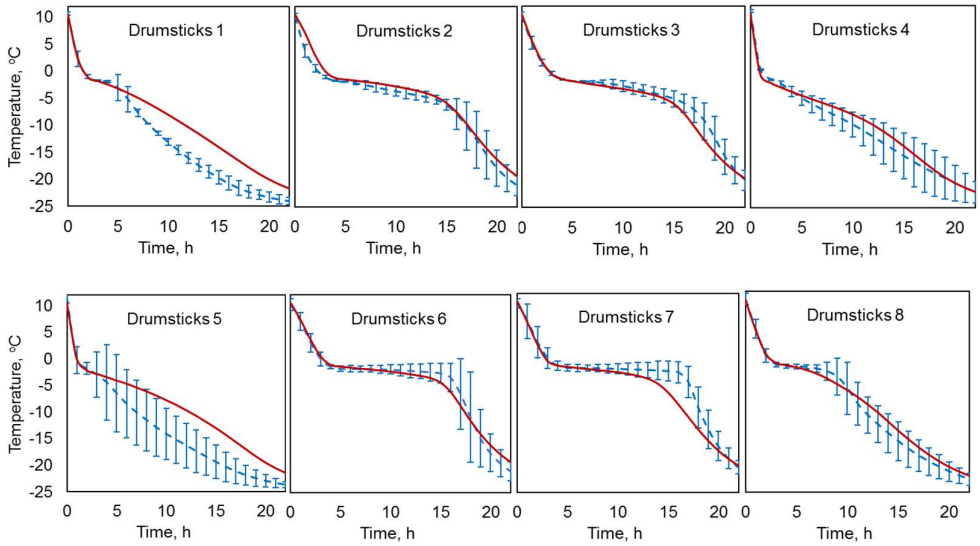

Figure 7.21: Predicted and experimental temperature history of individual drumsticks within a tray at the air velocity of 2.5 m s^{-1}. The numerical temperatures are depicted in red continuous lines, measured values are depicted in blue dash lines

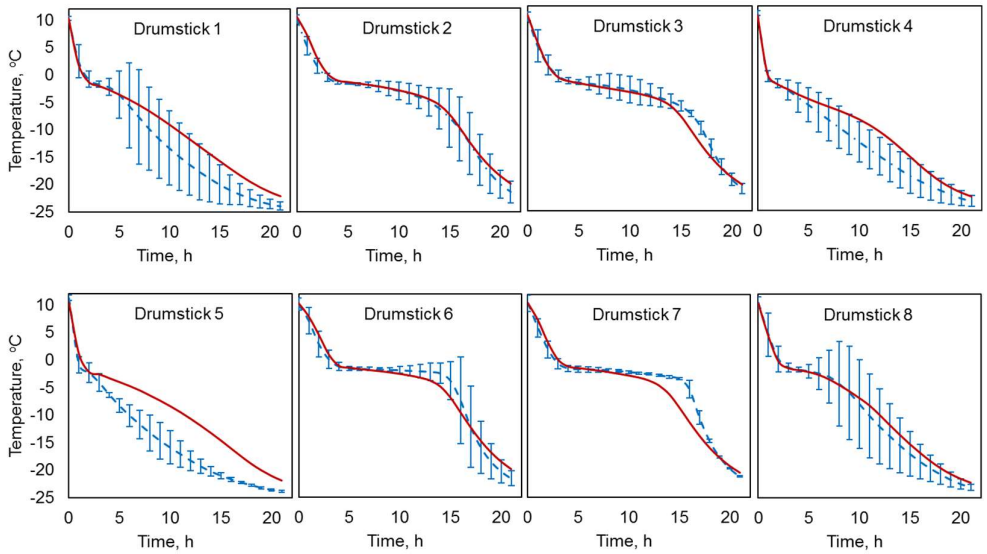

Figure 7.22: Predicted and experimental temperature history of individual drumsticks within a tray at the air velocity of 4.3 m s^{-1}. The numerical temperatures are depicted in red continuous lines, measured values are depicted in blue dash lines

For all tested air velocities, the temperatures predicted by the model followed the same trend as the measured data. Drumsticks located at the edge of the tray

(drumstick Numbers 1, 4, 5 and 8, Figure 7.18) cooled faster than those in the middle (drumstick Numbers 2, 3, 6 and 7).

While the model showed good prediction for temperature histories of drumstick Numbers 2, 3, 4 and 8, it tended to overpredict for drumstick Numbers 1 and 5 and underpredict for drumstick Numbers 6 and 7. This can be explained by the fact that the thermocouple positions of drumstick Numbers 1 and 5 were close to the corner of the tray where the drumsticks are in direct contact with polyliner. Therefore, the effect of the artificial air gap in the model is more obvious in these locations, making the predicted temperatures higher than measured data. On the another hand, the 'bunching' of the polyliner bag where it is tied (with the air gap inside, Figure 7.9c) on the top surface of bulk-packed drumsticks in the experiments can explain the slower cooling in the experimental histories than the modelled temperatures for the drumstick Numbers 6 and 7, which are close to the bunching of the liner bag (Figure 6.10). The over-prediction of temperature of these drumsticks at the end of the freezing process may also be linked to condensation on the drumstick surfaces. Moisture from the air inside the polyliner and moisture evaporated from drumsticks was assumed to condense back on the drumstick surfaces. When the temperature of drumstick surfaces dropped below the freezing point, the condensation would become ice, which has a higher thermal conductivity than chicken at the same temperature (i.e. thermal conductivity of ice at -10°C is 2.3 W m^{-1} K^{-1} (ASHRAE, 2006) while thermal conductivity of chicken at this temperature is only 1.3 W m^{-1} K^{-1}, Sweat et al., 1973). Therefore, the condensed moisture may enhance the heat transfer on drumstick surfaces at the end of the freezing. In addition, the ice layer on the top surface of bulk-packed drumsticks has glued the drumsticks in proximity with the polyliner (drumstick Numbers 6 and 7) and replaced the air voids between them, which could lead to a faster cooling in the experimental temperature of drumstick Numbers 6 and 7 at the end of the freezing process.

7.7 Analysis

7.7.1 Temperature distribution

Figures 7.23 and 7.24 show temperature distributions in a tray of whole chickens and a tray of drumsticks at the inlet air velocity of 2.5 m s^{-1} after 13 hours freezing

(average half cooling time, HCT). The contour plots visualise the temperature of cardboard, air inside the plastic bag, and chickens.

It can be seen from the figures that the temperature of chickens along the edges of the tray was lower than that of the middle one, as would be expected. Along the airflow direction, chickens at the front end cooled faster than those at the back end. The insulation effect of the air layer on top of chicken surfaces was evident from the higher temperature of chickens on top layer compared to those in the bottom layer.

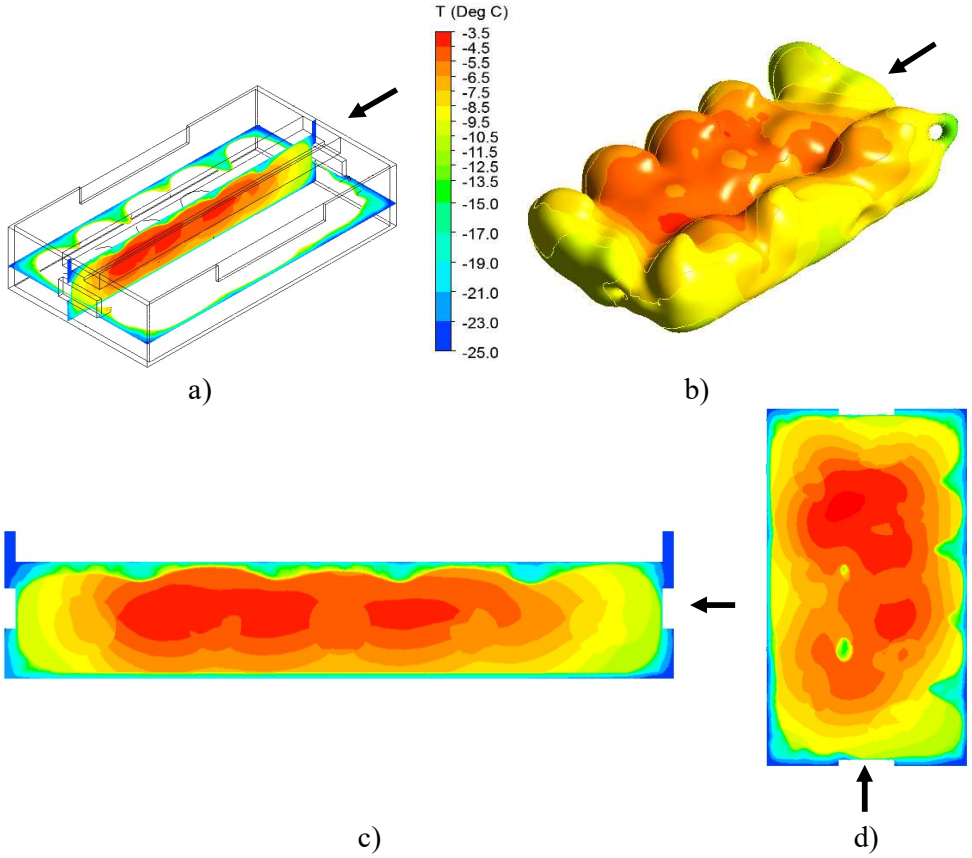

Figure 7.23: a) Location of vertical and horizontal cross-sectional area b) temperature distribution on chicken surfaces, temperature contour along the c) vertical cross-sectional area and d) horizontal cross-sectional area. Results were taken at the air velocity of 2.5 m s^{-1} after 13 hours freezing (average HCT)

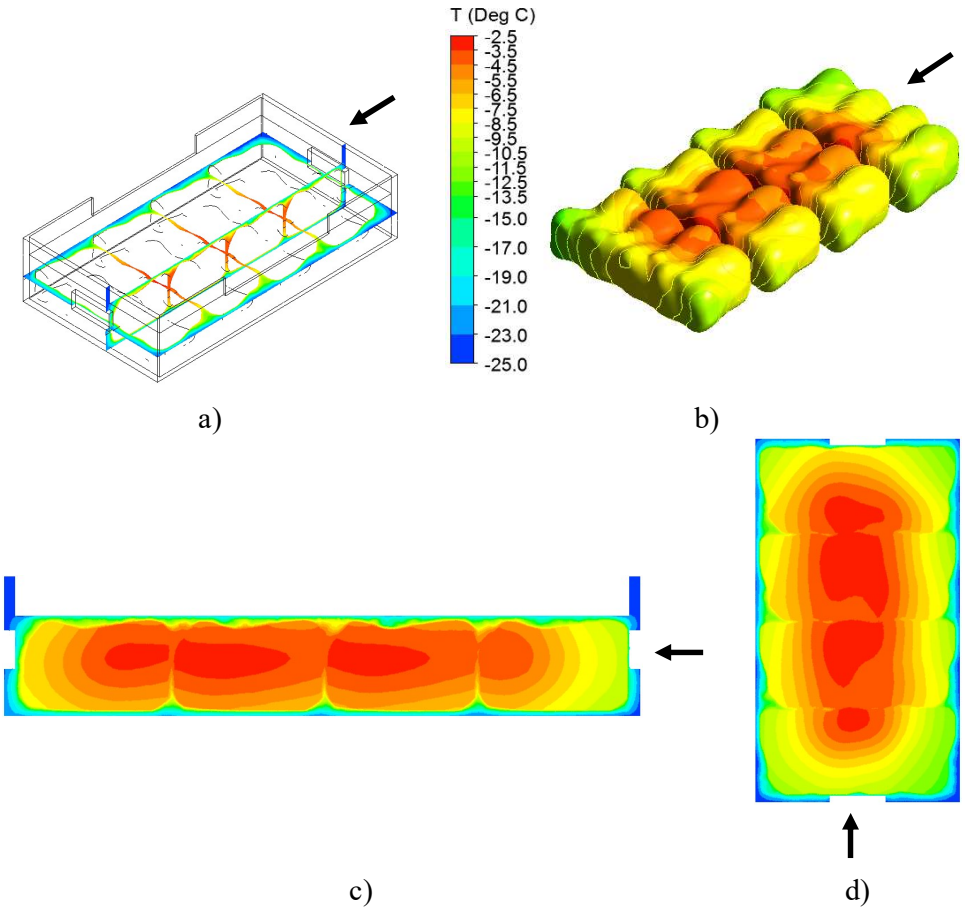

Figure 7.24: a) Location of vertical and horizontal cross-sectional area b) temperature distribution on drumstick surfaces, temperature contour along the c) vertical cross-sectional area and d) horizontal cross-sectional area. Results were taken at the air velocity of 2.5 m s^{-1} after 13 hours freezing (average HCT)

7.7.2 Airflow distribution

Figure 7.25 shows the velocity distribution along the vertical plane (Figure 7.24a) of the airflow in the wind tunnel for the drumstick model at the inlet air velocity of 2.5 m s^{-1}. Since the airflow domain of the whole chicken model is similar to the drumstick model, the flow field in the whole chicken model will be the same as the flow field in Figure 7.25.

The model was based on the actual dimensions of the wind tunnel and the cardboard tray, so the airflow contour was captured as realistically as possible. The high gradient of velocity was observed in the fluid region close to the cardboard and polyliner surfaces. Perpendicular to the direction of the airflow, the air velocity

increased from zero at the cardboard and polyliner surfaces to the maximum value of 4.5 m s^{-1}

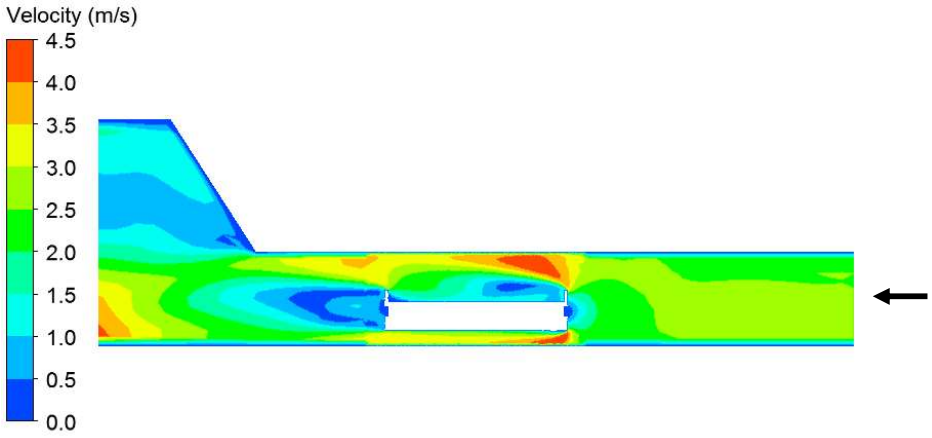

Figure 7.25: Contour along the vertical plane of airflow in the wind tunnel for the drumstick model at the inlet air velocity of 2.5 m s^{-1}

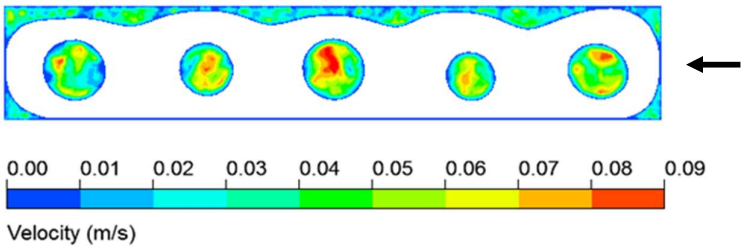

a)

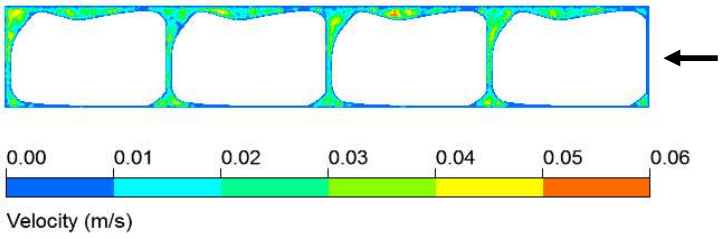

b)

Figure 7.26: Contours along the vertical plane of airflow inside the liner bag of a) chicken model and b) drumstick model. Results were taken at the air velocity of 2.5 m s^{-1} after 13 hours freezing (average HCT)

The velocity fields along the vertical plane inside the polyliner are shown in Figure 7.26a for the whole chicken model and Figure 7.26b for the drumstick model. The effect of natural convection produces a velocity field inside the polyliner with maximum air velocities of 0.09 m s^{-1} and 0.06 m s^{-1} for the whole chickens and drumstick models, respectively. The effect of natural convection is more pronounced at the beginning of the freezing process when the temperature difference between chicken products and refrigerated air inside the polyliner is highest and diminishes toward the end when chicken's temperature closes to refrigerated air temperature.

7.7.3 Effect of operating conditions on freezing time

Having been experimentally validated, the numerical model was used to calculate freezing times under different operating conditions, as presented in Figure 7.27 (for bulk-packed whole chickens) and Figure 7.28 (for bulk-packed drumsticks). For the purposes of this comparison, 'freezing time' is defined as the time taken by the average temperature of chicken (the freezing time of bulk-packed whole chickens was based on the average temperature of the chicken cavity) to reach -18°C.

Figures 7.27 and 7.28 show that the impact of increasing cooling air velocity from 1.0 m s^{-1} to 2.5 m s^{-1} on the freezing time was greater than that when it was raised from 2.5 m s^{-1} to either 4.5 m s^{-1} (for whole chickens) or 4.3 m s^{-1} (for drumsticks), indicating that the relationship between the airflow rate and cooling rate is diminishing. Changing the air temperature from -25°C to -30°C made the freezing time of whole chickens and drumsticks decrease by average 4.9 hours and 4.5 hours respectively, while the reductions were only 3.0 hours and 2.8 hours when the air temperature dropped from -30°C to -35°C. Decreasing the initial temperature from 10°C to 5°C or from 5°C to 0°C resulted in approximately 1 hours faster cooling for both bulk-packed whole chickens and drumsticks.

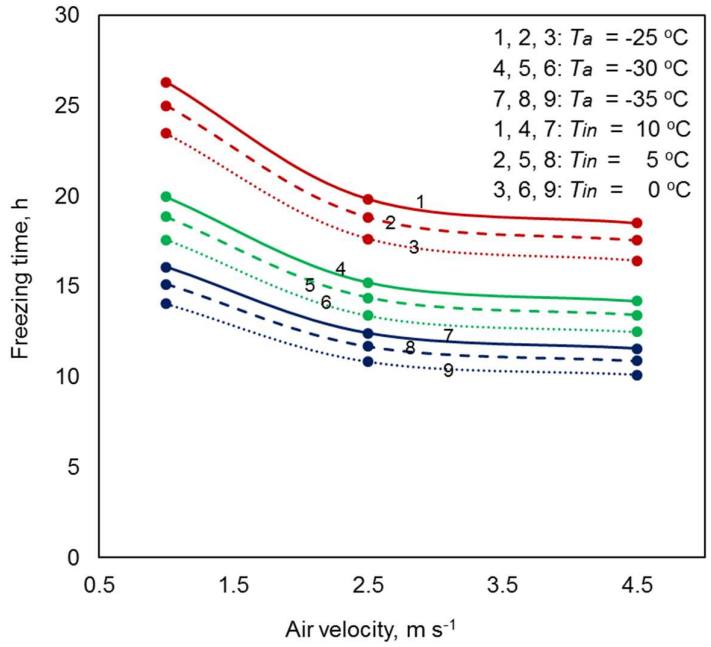

Figure 7.27: Effect of operating conditions on freezing time of bulk-packed whole chickens

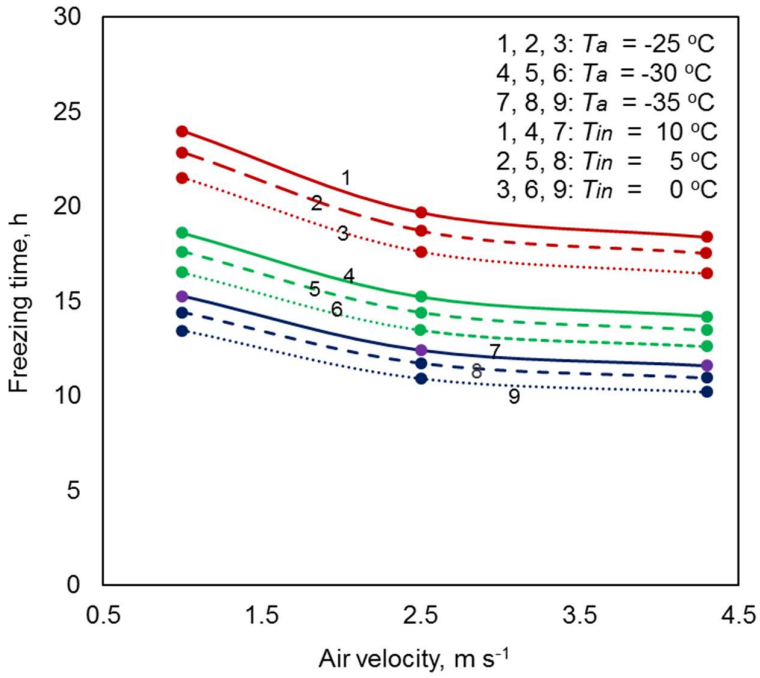

Figure 7.28: Effect of operating conditions on freezing time of bulk-packed drumsticks

The effects of cooling air velocity, cooling air temperature and initial chicken temperature on freezing time were expressed as correlation equations, Eq. 7.11 for bulk-packed whole chickens and Eq. 7.12 for bulk-packed drumsticks, as below:

$$t_c = 8.307u^{-0.233}\left(\frac{-18-T_a}{T_{in}-T_a}\right)^{-0.732} \tag{7.11}$$

$$t_d = 8.077u^{-0.189}\left(\frac{-18-T_a}{T_{in}-T_a}\right)^{-0.702} \tag{7.12}$$

where

t_c, t_d (hours) are the freezing time of bulk-packed whole chickens and bulk-packed drumsticks, respectively

u (m s^{-1}) is the cooling air velocity, ($1 \le u \le 4.5$ m s^{-1} for whole chickens and $1 \le u \le 4.3$ m s^{-1} for drumsticks)

T_a, T_{in} (°C) are the cooling air temperature and the initial chicken temperature, ($-35 \le T_a \le -25$°C, $0 \le T_{in} \le 10$°C)

From the regression statistics, no correlation equation has R-square value lower than 0.95, which indicates a good fit for the correlation equations. Therefore, the correlations developed above can be used to predict the processing time in forced air freezing of bulk-packed chickens and bulk-packed drumsticks in the freezing tunnels where the packages are similar in design to the one considered in this study

7.8 Conclusions

This chapter described a numerical model to simulate the forced-air freezing of bulk-packed whole chickens and drumsticks encased in a polyliner within a carton. The model represents the first case of a CFD food freezing model where the geometry was derived empirically via CT scan data. The polyliner created an enclosed space, consisting of air voids between chicken products and the liner bag. In this space, the effect of natural convection is significant, as shown by the velocity field inside the polyliner of up to 0.09 m s^{-1} for the whole chicken model and 0.06 m s^{-1} for the drumstick model after 13 hours freezing at the air velocity of 2.5 m s^{-}

[1]. Therefore natural convection must be simulated when dealing with polylined food products.

Considering the complexity of the transport phenomena within the system, simplifications and uncertainties required in developing the model as well as the difficulty in identifying the exact position of the thermocouple, reasonable agreement was found between the predicted and experimental temperature histories of individual products. When compared to the freezing history data from Chapter 6, the mean discrepancy in average temperature prediction was less than 1.3°C, and the maximum difference of SECT prediction was 7.3% for both whole chicken and drumstick models. However, in food freezing, the cooling heterogeneity is also of interest since it will affect the quality of individual products. In addition to providing good predictions for average temperatures, the numerical model was also able to predict the temperatures at the specific location within the tray.

The model was used to study the effect of different operational parameters on the freezing rate of the chicken freezing processes. Increasing the refrigerated air velocity above 2.5 m s^{-1}, and decreasing the refrigerated air temperature below -30°C resulted in a diminishing reduction in improvement to freezing time. The proposed correlation equations (Eqs. 7.11 and 7.12) can be used to estimate the freezing time of bulk-packed chickens and bulk-packed drumsticks in the freezing tunnels where the packages are similar in design to the one considered in this study.

Chapter 8
General conclusions and future study

8.1 General conclusions

This research project has developed a numerical model to simulate airflow and heat transfer for industrial cheese chilling and freezing of individual trays of whole chickens and chicken parts. More specifically, a direct CFD approach was used in these models to improve the accuracy of the predictions. The model predictions were validated by experimental data generated as part of the study. Once validated, the model was used to investigate the cooling heterogeneity and the effect of different operating conditions on the processing time. In addition to the CFD model, a simple heat transfer simualtion based on one-dimensional finite difference method was presented for industrial users. Thermal property models in the literature were also reviewed to propose the most suitable choices for thermal processing calculations. The following conclusions were drawn from this research:

1. The effective specific heat capacity predicted by the additive model (Eq. 3.1) with the specific heat of water correlated from experimental data of Archer and Carter (2000) and Pátek et al. (2009), and the thermal conductivity model of Dul'nev and Novikov (Eqs. 3.30-3.33) showed better predictions compared to other models for a wide range of food products. Therefore, the additive model and the Dul'nev and Novikov model are recommended as the best models to predict the effective specific heat capacity and thermal conductivity of food products.

2. The airflow field in the agar chilling model that mimicked the airflow pattern and products arrangement of an industrial cheese chilling process could be numerically modeled as a steady state airflow field and decoupled from energy transport during the transient simulation. The flow and turbulance calculations could be turned off in the transient simulation to reduce computation time.

3. The heat transfer coefficient across the agar block surface varied by factor of 5, with the maximum value at the four corners of the surface on the upstream side and minimum values at the opposite surface.

4. The use of the standard k-ε turbulence model with the Enhanced Wall Treatment in the CFD chilling model of six blocks of agar could predict temperatures to within 1°C compared to experimental data. The model underpredicted the experimentally observed cooling rate routinely, which could be explained by the exclusion of the effect of natural convection, and thermal radiation.

5. The univerality of the one dimensional numerical solution proposed by (Ghraizi et al., 1996) has been improved by incorporating the composition-based thermal property model (the additive effective specific heat capacity model, Eq. 3.1, and the Dul'nev and Novikov thermal conductivity model, Eqs. 3.30 – 3.33) and the correlation equation for the convective heat transfer coefficient proposed by (Pham et al., 1991) and (Cleland & Earle, 1976) . The simulation was validated by experimental temperature histories along the shortest dimension of a single block of agar and a single block of cheese undergoing the chilling process. Additionally, the one-dimensional simulation was compared to results generated by the three dimensional model FPM. The one dimentional simulation fit well with experimental data and the values predicted by FPM. Therefore, the one dimentional simulation can be used to provide a quick cooling time prediction (the computational time was 30s to simulate 18 hours of cheese chilling on a 64-bit Intel ® Xeon ® CPU E5-1620, 3.5 GHz, 16 GB RAM implemented in MATLAB) with sufficient confidence in the temperature distribution along the shortest characteristic dimension of a 3-D object, which represents the greatest interest for food engineers.

6. The freezing experiments showed a large range in the cooling histories of individual chickens in the sub-cooling region. The maximum differences between the temperatures of individual chickens and chicken legs within a tray were about 30% and 50% of the difference between the initial chicken temperature (10°C) and refrigerated air temperature (-25°C), respectively. The difference decreased towards the end of the process, and the lower the cooling air velocity, the more uniform the chicken temperature near the end.

7. The packing structure of the chicken drumsticks within the plastic liner bag did not have a significant impact on the freezing rate for any of the air velocities

investigated, based on a 95% confidence interval. That means the designer doesn't have to know the drumstick orientation when designing the freezer. On the other hand, the presence of the plastic liner bag increased freezing times by more than a factor of 3 at high air velocities. This is because the liner bag prevents refrigerated airflow from directly interacting with the product and evaporation plays a significant role in the total amount of heat transfer (up to 11% of the total heat load) when there is no polyliner to prevent moisture transfer.

8. The CFD model of polylined bulk-packed whole chickens and bulk-packed drumsticks during forced-air freezing based on CT scans of the chicken was validated against experimental freezing data. By using the temperature-dependent thermal properties of chicken meat, the mean differences between the predicted and experimental average chicken temperature was less than 1.3°C for all tested conditions, for both the whole chicken and drumstick model. The maximum difference of SECT prediction was 7.3%. In addition to providing good predictions for average temperatures, the numerical model was also able to predict the temperatures at specific locations within the tray.

9. The simulation results showed the flow field inside the polyliner could reach velocities of up to 0.09 m s^{-1} for the whole chicken model and 0.06 m s^{-1} for drumstick model after 13 hours freezing at the air velocity of 2.5 m s^{-1} which indicates the effect of natural convection is significant during the forced air freezing of polylined bulk-packed chickens and must be included in the simulation.

10. The validated chicken and drumstick model were used to study the effect of different operational parameters on the freezing rate of the chicken freezing processes. The result indicates that increasing the refrigerated air velocity above 2.5 m s^{-1}, and decreasing the refrigerated air temperature below -30°C can lead to a diminishing reduction in improvement to freezing time. The proposed correlation equations (Eqs. 7.11 and 7.12) can be used to estimate the freezing time of bulk-packed chickens and bulk-packed drumsticks in freezing tunnels where the packages are similar in design to the one considered in this study.

8.2 Future study

Although significant progess was made towards the accurate modelling of industrial cheese chilling and chicken freezing processes, several research question remain unanswered and should be considered in the future:

1. In this study the industrial cheese chilling process was modeled as six blocks of agar that mimic the airflow pattern and product arrangement of an industrial chilling tunnel. However, the thermal properties of cheese are different from agar, so the temperature distribution inside blocks of cheese is different from blocks of agar. In a future study, real blocks of cheese should be used instead of blocks of agar. In addition, the product load of the industrial cheese chiller is higher than that in the model, which could make the airflow distribution and cooling rate of the cheese chiller different from the model. Considering the effect of the product load in the cheese chiller, the model for predicting air velocity distribution in a large chiller developed by (Mirade & Picgirard, 2006) could be used in combination with the unsteady heat tranfer simulation of the current model for a more comprehensive analysis of transport phenomena in an industrial cheese chiller.

2. The application of the one-dimensional simulation presented in chapter 5 can be investigated further. Firstly, the simulation can be validated over a wide range of irregular shape food product. In this case, the Biot-number dependent shape factor proposed by (Hossain et al., 1992a, 1992b, 1992c) can be used to account for the irregular shape of the product. Secondly, the simulation can also be applied for the food freezing process since it has already incorporated the temperature-dependent thermal properties of foods.

3. Despite this study presenting the first case of CFD modeling for chicken freezing where the geometry was derived empirically via CT scan data, some simplifications have been made and should be rectified in a future study. Firstly, the 2 mm artificial air gap between chiken and the liner bag was created in the simulation to avoid highly skewed and distorted meshes that can compromise the stability of the solution; however, the artificial air gap will increase the resistance to heat transfer due to the low thermal conductivity of air. Therefore, it would be valuable to

eliminate the artificial air gap in the new model routine. This could be done by using automated methods to generate a realistic polyliner shape for bulk packed product presented in (Olatunji, Love, Shim, & East, 2020). Secondly, the model assumed substantial connection between chicken surfaces that can increase the thermal conductance between chicken products. In this case, a watershed segmentation algorithm for separating the solid objects in the CT scan data could be used. In this algorithm, the Euclidean distance map (EDM) of the CT image is calculated (Danielsson, 1980; Herremans et al., 2013). The EDM can be interpreted as a topographic map of a terrain with mountain peaks (region of solid objects) and local valleys (air regions). If this terrain would be flooded with water, the water would run down the mountain peaks and into local valleys. By marking the local valleys, the mountain peaks can be separated and correspondingly, the solid objects from one another (Esveld, Van Der Sman, Van Dalen, Van Duynhoven, & Meinders, 2012). The watershed algorithm was sussessful applied for a pack of pears (Gruyters, 2019) and could be applied for bulk-packed chicken products. Thirdly, the model assumed homogeneous thermal properties. However, the thermal conductivity of chicken depends on structure (i.e thermal conductivity of chicken meat is different from chicken bone). Considering the spatial variation in thermal properties of chicken could further increase the accuracy of the predictions. This could be achieved by using a geometrical model of the internal structure based on dedicated CT scans that show constrast for muscle, skin and bone.

4. The heterogeneity of the forced air chilling and freezing is strongly influenced by the local airflow behavior within the package system. As this study shows, CFD modelling provides an effective means for predicting and understanding the complexity of the transport of momentum and energy within a packed structure. A logical continuation of this research would be the optimization of the forced air chilling and freezing by using this model. In paticular, CFD can be used as design tool for novel packing system (e.g. adding perforations on liner bags, differences in the geometrical cardboard tray shapes and vent designs), investigating different product arrangements, product weight, and different operating conditions in order to promote a more rapid and uniform cooling of products and increase the energy efficiency.

REFERENCES

Alvarez, G., & Flick, D. (1999). Analysis of heterogeneous cooling of agricultural products inside bins: Part II: thermal study. *Journal of Food Engineering, 39*(3), 239-245.

Ambaw, A., Bessemans, N., Gruyters, W., Gwanpua, S. G., Schenk, A., De Roeck, A., . . . Nicolai, B. M. (2016). Analysis of the spatiotemporal temperature fluctuations inside an apple cool store in response to energy use concerns. *International Journal of Refrigeration, 66*, 156-168.

Ambaw, A., Mukama, M., & Opara, U. L. (2017). Analysis of the effects of package design on the rate and uniformity of cooling of stacked pomegranates: Numerical and experimental studies. *Computers and Electronics in Agriculture, 136*, 13-24.

Ambaw, A., Verboven, P., Defraeye, T., Tijskens, E., Schenk, A., Opara, U. L., & Nicolai, B. M. (2013). Porous medium modeling and parameter sensitivity analysis of 1-MCP distribution in boxes with apple fruit. *Journal of Food Engineering, 119*(1), 13-21.

Anderson, B. A., Sun, S., Erdogdu, F., & Singh, R. P. (2004). Thawing and freezing of selected meat products in household refrigerators. *International Journal of Refrigeration, 27*(1), 63-72.

ANSYS, F. (2017). 18.1, User Guide, ANSYS: Inc.

Archer, D. G., & Carter, R. W. (2000). Thermodynamic properties of the NaCl+ H2O system. 4. Heat capacities of H2O and NaCl (aq) in cold-stable and supercooled states. *The Journal of Physical Chemistry B, 104*(35), 8563-8584.

Arthey, D. (1993). Freezing of vegetables and fruits. *Frozen food technology*

ASHRAE, A. H. (2006). Refrigeration. *American Society of Heating, Refrigerating and Air-Conditioning Engineers, Atlanta, GA*

Becker, B. R., & Fricke, B. A. (1999). Evaluation of semi-analytical/empirical freezing time estimation methods part II: Irregularly shaped food items. *HVAC&R Research, 5*(2), 171-187.

Becker, B. R., & Fricke, B. A. (2004). Heat transfer coefficients for forced-air cooling and freezing of selected foods. *International Journal of Refrigeration, 27*(5), 540-551.

Benitez Mendieta, J. (2016). *An efficient and semiautomatic segmentation method for 3D surface reconstruction of the lumbar spine from Magnetic Resonance Imaging (MRI)*. Queensland University of Technology.

Berry, T. M., Defraeye, T., Nicolaï, B. M., & Opara, U. L. (2016). Multiparameter analysis of cooling efficiency of ventilated fruit cartons using CFD: impact of vent hole design and internal packaging. *Food and Bioprocess Technology, 9*(9), 1481-1493.

Berry, T. M., Fadiji, T., Defraeye, T., & Opara, U. L. (2017). The role of horticultural carton vent hole design on cooling efficiency and

compression strength: a multi-parameter approach. *Postharvest Biology and Technology, 124*, 62-74.

Bogh-Sorensen, L. (2006). *Recommendations for the processing and handling of frozen foods* (4th ed.): International Institute of Refrigeration, Paris.

Campañone, L., Giner, S., & Mascheroni, R. (2002). Generalized model for the simulation of food refrigeration. Development and validation of the predictive numerical method. *International Journal of Refrigeration, 25*(7), 975-984.

Carslaw, H. S., & Jaeger, J. C. (1959). *Conduction of Heat in Solids* (2ed.). Oxford: Clarendon Press.

Carson, J. K. (2006). Review of effective thermal conductivity models for foods. *International Journal of Refrigeration, 29*(6), 958-967.

Carson, J. K. (2011). Predictive modelling of thermal properties of foods. In M. A. Comeau (Ed.), *New topics in food engineering*. New York: Nova Science Publishers, Inc.

Carson, J. K. (2017). Use of simple thermal conductivity models to assess the reliability of measured thermal conductivity data. *International Journal of Refrigeration, 74*, 456-462.

Carson, J. K., Lovatt, S. J., Tanner, D. J., & Cleland, A. C. (2006). Predicting the effective thermal conductivity of unfrozen, porous foods. *Journal of Food Engineering, 75*(3), 297-307.

Carson, J. K., Wang, J., North, M. F., & Cleland, D. J. (2016). Effective thermal conductivity prediction of foods using composition and temperature data. *Journal of Food Engineering, 175*, 65-73.

Cavalier, G., & Tassou, S. (2011). *Sustainable Refrigerated Road Transport, 21st Informatory Note on Refrigerating Technologies*. Retrieved from http://www.iifiir.org/userfiles/file/ publications/notes/NoteTech_21_EN.pdf

Cengel, Y. A., & Ghajar, A. J. (2011). *Heat and mass transfer: fundamentals and applications*

Chen, C. S. (1985). Thermodynamic analysis of the freezing and thawing of foods: Enthalpy and apparent specific heat. *Journal of food science, 50*(4), 1158-1162.

Cheng, S. C., & Vachon, R. I. (1969). The prediction of the thermal conductivity of two and three phase solid heterogeneous mixtures. *International Journal of Heat and Mass Transfer, 12*(3), 249-264.

Choi, Y., & Okos, M. R. (1986). Effects of temperature and composition on the thermal properties of foods. *Food engineering and process applications, 1*, 93-101.

Cleland, A. C., & Earle, R. L. (1976). A new method for prediction of surface heat transfer coefficients in freezing. *Bulletin. Annex-International Institute of Refrigeration (IIR). Refrigeration Science and Technology. 1976-1.*

Cleland, A. C., & Earle, R. L. (1982). A simple method for prediction of heating and cooling cooling in solids of various shapes. *International Journal of Refrigeration, 5*(2), 98-106.

Cleland, D. J., Cleland, A. C., & Earle, R. L. (1987a). Prediction of freezing and thawing times for multi-dimensional shapes by simple formulae Part 1: regular shapes. *International Journal of Refrigeration, 10*(3), 156-164.

Cleland, D. J., Cleland, A. C., & Earle, R. L. (1987b). Prediction of freezing and thawing times for multi-dimensional shapes by simple formulae part 2: irregular shapes. *International Journal of Refrigeration, 10*(4), 234-240.

Cogné, C., Andrieu, J., Laurent, P., Besson, A., & Nocquet, J. (2003). Experimental data and modelling of thermal properties of ice creams. *Journal of Food Engineering, 58*(4), 331-341.

Danielsson, P.-E. (1980). Euclidean distance mapping. *Computer Graphics and image processing, 14*(3), 227-248.

Datta, A. K. (2002). *Biological and bioenvironmental heat and mass transfer*: CRC Press.

Datta, A. K. (2007a). Porous media approaches to studying simultaneous heat and mass transfer in food processes. I: Problem formulations. *Journal of Food Engineering, 80*(1), 80-95.

Datta, A. K. (2007b). Porous media approaches to studying simultaneous heat and mass transfer in food processes. II: Property data and representative results. *Journal of Food Engineering, 80*(1), 96-110.

Daudin, J. D., & Kuitche, A. (1996). Modelling of temperature and weight loss kinetics during meat chilling for time variable conditions using an analytical based method—III. Calculations versus measurements on pork carcass hindquarters. *Journal of Food Engineering, 29*(1), 39-62.

Davey, L. M., & Pham, Q. T. (1997). Predicting the dynamic product heat load and weight loss during beef chilling using a multi-region finite difference approach. *International Journal of Refrigeration, 20*(7), 470-482.

Davey, L. M., & Pham, Q. T. (2000). A multi-layered two-dimensional finite element model to calculate dynamic product heat load and weight loss during beef chilling. *International Journal of Refrigeration, 23*(6), 444-456.

DCANZ. (2018). *About the NZ Dairy Industry.* Retrieved from https://www.dcanz.com/about-the-nz-dairy-industry/

Defraeye, T., Lambrecht, R., Delele, M. A., Tsige, A. A., Opara, U. L., Cronjé, P., . . . Nicolai, B. (2014). Forced-convective cooling of citrus fruit: cooling conditions and energy consumption in relation to package design. *Journal of Food Engineering, 121*, 118-127.

Defraeye, T., Lambrecht, R., Tsige, A. A., Delele, M. A., Opara, U. L., Cronjé, P., . . . Nicolai, B. (2013). Forced-convective cooling of citrus fruit: package design. *Journal of Food Engineering, 118*(1), 8-18.

Defraeye, T., Verboven, P., & Nicolai, B. (2013). CFD modelling of flow and scalar exchange of spherical food products: Turbulence and boundary-layer modelling. *Journal of Food Engineering, 114*(4), 495-504.

Dehghannya, J., Ngadi, M., & Vigneault, C. (2010). Mathematical modeling procedures for airflow, heat and mass transfer during forced convection cooling of produce: a review. *Food Engineering Reviews, 2*(4), 227-243.

Delele, M. A., Ngcobo, M. E., Opara, U. L., & Meyer, C. J. (2013). Investigating the effects of table grape package components and stacking on airflow, heat and mass transfer using 3-D CFD modelling. *Food and Bioprocess Technology, 6*(9), 2571-2585.

Delele, M. A., Schenk, A., Ramon, H., Nicolaï, B. M., & Verboven, P. (2009). Evaluation of a chicory root cold store humidification system using computational fluid dynamics. *Journal of Food Engineering, 94*(1), 110-121.

Dima, J. B., Santos, M. V., Baron, P. J., Califano, A., & Zaritzky, N. E. (2014). Experimental study and numerical modeling of the freezing process of marine products. *Food and Bioproducts Processing, 92*(1), 54-66.

Du-pont, J.-L. (2019). *The role of refrigeration in the global economy, 38th IIR Informatory note on refrigeation technologies*. Retrieved from http://www.iifiir.org/userfiles/file/publications/notes/NoteTech_38_EN.pdf

Dul'Nev, G. N., & Novikov, V. V. (1977). Effective conductivity of systems with interpenetrating components. *Journal of Engineering Physics and Thermophysics, 33*(2), 923-925.

Dul'nev, G. N., & Novikov, V. V. (1991). Transfer processes in inhomogeneous media. *Energoatomizdat, Leningrad, 248*

EngineeringToolbox. Thermal Conductivity of common Materials and Gases. Thermal Conductivity of common Materials and Gases

Esveld, D., Van Der Sman, R., Van Dalen, G., Van Duynhoven, J., & Meinders, M. (2012). Effect of morphology on water sorption in cellular solid foods. Part I: Pore scale network model. *Journal of Food Engineering, 109*(2), 301-310.

FAO. (2018). *The future of food and agriculture Alternative pathways to 2050 (summary version)*. Roma, Italy. Retrieved from http://www.fao.org/3/CA1553EN/ca1553en.pdf

Ferrua, M. J. (2007). *Modeling the forced-air cooling process of fresh horticultural products*: University of California, Davis.

Ferrua, M. J., & Singh, R. P. (2009a). Design guidelines for the forced-air cooling process of strawberries. *International Journal of Refrigeration, 32*(8), 1932-1943.

Ferrua, M. J., & Singh, R. P. (2009b). Modeling the forced-air cooling process of fresh strawberry packages, Part I: Numerical model. *International Journal of Refrigeration, 32*(2), 335-348.

Ferrua, M. J., & Singh, R. P. (2009c). Modeling the forced-air cooling process of fresh strawberry packages, Part II: Experimental validation of the flow model. *International Journal of Refrigeration, 32*(2), 349-358. https://doi.org/10.1016/j.ijrefrig.2008.04.009

Ferrua, M. J., & Singh, R. P. (2009d). Modeling the forced-air cooling process of fresh strawberry packages, Part III: Experimental validation of the energy model. *International Journal of Refrigeration, 32*(2), 359-368. https://doi.org/10.1016/j.ijrefrig.2008.04.011

Ferrua, M. J., & Singh, R. P. (2011). Improved airflow method and packaging system for forced-air cooling of strawberries. *International Journal of Refrigeration, 34*(4), 1162-1173. https://doi.org/10.1016/j.ijrefrig.2011.01.018

Fikiin, K. A. (1996). Generalized numerical modelling of unsteady heat transfer during cooling and freezing using an improved enthalpy method and quasi-one-dimensional formulation. *International Journal of Refrigeration, 19*(2), 132-140.

Fikiin, K. A. (1998). Ice content prediction methods during food freezing: a survey of the Eastern European literature. *Journal of Food Engineering, 38*(3), 331-339.

Fluent. (2017). 18.1, Ansys Fluent User Guide: Inc.

Fricke, B. A., & Becker, B. R. (2001). Evaluation of thermophysical property models for foods. *HVAC&R Research, 7*(4), 311-330.

Getahun, S., Ambaw, A., Delele, M., Meyer, C. J., & Opara, U. L. (2017a). Analysis of airflow and heat transfer inside fruit packed refrigerated shipping container: Part I–Model development and validation. *Journal of Food Engineering, 203*, 58-68.

Getahun, S., Ambaw, A., Delele, M., Meyer, C. J., & Opara, U. L. (2017b). Analysis of airflow and heat transfer inside fruit packed refrigerated shipping container: Part II–Evaluation of apple packaging design and vertical flow resistance. *Journal of Food Engineering, 203*, 83-94.

Ghraizi, J. A., Chumak, I. G., Onistchenko, V. P., & Terziev, G. S. (1996). Mathematical model of various freezing processes of fish and fish-products. *Science et technique du froid*, 379-386.

Gowda, B. S., Narasimham, G., & Murthy, M. K. (1997). Forced-air precooling of spherical foods in bulk: a parametric study. *International journal of heat and fluid flow, 18*(6), 613-624.

Gruyters, W. (2019). *Advanced Computational Fluid Dynamics modelling for a more sustainable and energy efficient postharvest cold chain of pome fruit. Dissertation presented in partial fulfilment of the requirements for the degree of Doctor of Bioscience Engineering (PhD) at KU Leuven*. KU Leuven.

Gruyters, W., Verboven, P., Diels, E., Rogge, S., Smeets, B., Ramon, H., . . . Nicolaï, B. (2018). Modelling Cooling of Packaged Fruit Using 3D Shape Models. *Food and Bioprocess Technology, 11*(11), 2008-2020.

Han, J.-W., Zhao, C.-J., Yang, X.-T., Qian, J.-P., & Fan, B.-L. (2015). Computational modeling of airflow and heat transfer in a vented box during cooling: optimal package design. *Applied Thermal Engineering, 91*, 883-893.

Herremans, E., Bongaers, E., Estrade, P., Gondek, E., Hertog, M., Jakubczyk, E., . . . Spinelli, L. (2013). Microstructure–texture relationships of aerated sugar gels: Novel measurement techniques for analysis and control. *Innovative food science & emerging technologies, 18*, 202-211.

Hoang, H.-M., Duret, S., Flick, D., & Laguerre, O. (2015). Preliminary study of airflow and heat transfer in a cold room filled with apple pallets: Comparison between two modelling approaches and experimental results. *Applied Thermal Engineering, 76*, 367-381.

Hossain, M. M., Cleland, D. J., & Cleland, A. C. (1992a). Prediction of freezing and thawing times for foods of regular multi-dimensional shape by using an analytically derived geometric factor. *International Journal of Refrigeration, 15*(4), 227-234.

Hossain, M. M., Cleland, D. J., & Cleland, A. C. (1992b). Prediction of freezing and thawing times for foods of three-dimensional irregular shape by using a semi-analytical geometric factor. *International Journal of Refrigeration, 15*(4), 241-246.

Hossain, M. M., Cleland, D. J., & Cleland, A. C. (1992c). Prediction of freezing and thawing times for foods of two-dimensional irregular shape by using a semi-analytical geometric factor. *International Journal of Refrigeration, 15*(4), 235-240.

Houska, M., Adam, A., Celba, J., Havlıcek, Z., Jeschke, J., Kubesova, A., . . . Sramek, P. (1997). Thermophysical and Rheological Properties of Foods: Meat, Meat Products and Semiproducts. *Food Research Institute Prague, Prague*

Houska, M., Adam, M., Celba, J., Havlicek, Z., Jeschke, J., Kubesova, A., . . . Sramek, P. (1994). *Thermophysical and Rheological Properties of Foods: Milk, Milk Products and Semiproducts*: Food Research Institute, Prague.

Hu, Z., & Sun, D.-W. (2000). CFD simulation of heat and moisture transfer for predicting cooling rate and weight loss of cooked ham during air-blast chilling process. *Journal of Food Engineering, 46*(3), 189-197. https://doi.org/10.1016/S0260-8774(00)00082-0

Huan, Z., He, S., & Ma, Y. (2003). Numerical simulation and analysis for quick-frozen food processing. *Journal of Food Engineering, 60*(3), 267-273.

IIR. (2009). *The role of refrigeration in worldwide nutrition, 5th informatory note on refrigeration and food*. Retrieved from http://www.iifiir.org/userfiles/file/publications/notes/NoteFood_05_EN.pdf

IIR. (2013). Figuring out frozen food growth rates in Europe. http://www.iifiir.org/clientBookline/service/reference.asp?INSTANCE=EXPLOITATION&OUTPUT=PORTAL&DOCID=IFD_REFDOC_0006712&DOCBASE=IFD_REFDOC_EN&SETLANGUAGE=EN

Ilicali, C., Teik, T. H., & Shian, L. P. (1999). Improved formulations of shape factors for the freezing and thawing time prediction of foods. *LWT-Food Science and Technology, 32*(5), 312-315.

James, C., Ketteringham, L., Palpacelli, S., & James, S. (2009). Prediction of heat transfer during food chilling, freezing, thawing, and distribution. In K. Kristbergsson (Ed.), *Predictive Modeling and RiskAssessment* (pp. 55-78): Springer.

James, C., Vincent, C., de Andrade Lima, T., & James, S. (2006). The primary chilling of poultry carcasses—a review. *International Journal of Refrigeration, 29*(6), 847-862.

Jimenez, S., Salsi, M., Tiburzi, M., Rafaghelli, R., & Pirovani, M. (1999). Combined use of acetic acid treatment and modified atmosphere packaging for extending the shelf-life of chilled chicken breast portions. *Journal of applied microbiology, 87*(3), 339-344.

Kent, M., Christiansen, K., Van Haneghem, I., Holtz, E., Morley, M., Nesvadba, P., & Poulsen, K. (1984). Cost 90 collaborative measurements of thermal properties of foods. *Journal of Food Engineering, 3*(2), 117-150.

Kiani, H., & Sun, D.-W. (2018). Numerical simulation of heat transfer and phase change during freezing of potatoes with different shapes at the presence or absence of ultrasound irradiation. *Heat and Mass Transfer, 54*(3), 885-894.

Kiani, H., Zhang, Z., & Sun, D.-W. (2015). Experimental analysis and modeling of ultrasound assisted freezing of potato spheres. *Ultrasonics sonochemistry, 26*, 321-331.

Kondjoyan, A. (2006). A review on surface heat and mass transfer coefficients during air chilling and storage of food products. *International Journal of Refrigeration, 29*(6), 863-875.

Kuffi, K. D., Defraeye, T., Nicolai, B. M., De Smet, S., Geeraerd, A., & Verboven, P. (2016). CFD modeling of industrial cooling of large beef carcasses. *International Journal of Refrigeration, 69*, 324-339. https://doi.org/10.1016/j.ijrefrig.2016.06.013

Lacroix, C., & Castaigne, F. (1987). Simple method for freezing time calculations for infinite flat slabs, infinite cylinders and spheres. *Canadian Institute of Food Science and Technology Journal, 20*(4), 252-259.

Landauer, R. (1952). The electrical resistance of binary metallic mixtures. *Journal of Applied Physics, 23*(7), 779-784.

Lee-Jones, D. (2019). *New Zealand semi-annual dairy and milk supply report 2019*. Retrieved from https://apps.fas.usda.gov/newgainapi/api/report/downloadreportbyfilename?filename=Dairy%20and%20Products%20Semi-annual_Wellington_New%20Zealand_6-5-2019.pdf

Levy, F. (1981). A modified Maxwell-Eucken equation for calculating the thermal conductivity of two-component solutions or mixtures. *International Journal of Refrigeration, 4*(4), 223-225.

Lin, Z., Cleland, A. C., Cleland, D. J., & Serrallach, G. F. (1993). Prediction of chilling times for objects of regular multi-dimensional shapes using a general geometric factor. *Refrigeration Science and Technology, 1993*(3), 259-267.

Lin, Z., Cleland, A. C., Cleland, D. J., & Serrallach, G. F. (1996a). A simple method for prediction of chilling times for objects of two-dimensional irregular shape. *International Journal of Refrigeration, 19*(2), 95-106.

Lin, Z., Cleland, A. C., Cleland, D. J., & Serrallach, G. F. (1996b). A simple method for prediction of chilling times: extension to three-dimensional irregular shapes. *International Journal of Refrigeration, 19*(2), 107-114.

Lu, L. x., Chen, X. q., & Wang, J. (2016). Modelling and thermal analysis of tray-layered fruits inside ventilated packages during forced-air precooling. *Packaging Technology and Science, 29*(2), 105-119.

Mannapperuma, J. D., & Singh, R. P. (1988). Prediction of freezing and thawing times of foods using a numerical method based on enthalpy formulation. *Journal of food science, 53*(2), 626-630.

Mannapperuma, J. D., Singh, R. P., & Reid, D. S. (1994a). Effective surface heat transfer coefficients encountered in air blast freezing of single plastic wrapped whole turkey. *International Journal of Refrigeration, 17*(4), 273-280.

Mannapperuma, J. D., Singh, R. P., & Reid, D. S. (1994b). Effective surface heat transfer coefficients encountered in air blast freezing of whole chicken and chicken parts, individually and in packages. *International Journal of Refrigeration, 17*(4), 263-272.

Markets and Markets. (2018). *Frozen Food Market by Product (Fruits & Vegetables, Dairy, Meat & Seafood), Type (Raw Material, Half Cooked), Consumption, Distribution Channel, and Region (North America, Europe, Asia Pacific, South America, and MEA) - Global Forecast to 2023.* Retrieved from https://www.marketsandmarkets.com/Market-Reports/global-frozen-and-convenience-food-market-advanced-technologies-and-global-market-130.html

MBIE. (2017). *The investor's guide to the new zealand meat industry 2017.* Retrieved from https://www.mbie.govt.nz/assets/8fdebf6c7b/investors-guide-to-the-new-zealand-meat-industry-2017.pdf

Meshing. (2010). ANSYS Meshing User's Guide: Inc.

Mirade, P.-S., Kondjoyan, A., & Daudin, J.-D. (2002). Three-dimensional CFD calculations for designing large food chillers. *Computers and Electronics in Agriculture, 34*(1), 67-88. https://doi.org/10.1016/S0168-1699(01)00180-6

Mirade, P.-S., & Picgirard, L. (2006). Improvement of ventilation homogeneity in an industrial batch-type carcass chiller by CFD investigation. *Food Research International, 39*(8), 871-881. https://doi.org/10.1016/j.foodres.2006.05.002

MIRINZ. *Food product modeller.* Retrieved from http://mirinz.org.nz/prod/foodprodmod.asp

Neeper, D. (2000). Thermal dynamics of wallboard with latent heat storage. *Solar energy, 68*(5), 393-403.

Nesvadba, P. (2005). Thermal properties of unfrozen foods. In M. A. Rao, S. S. H. Rizvi & A. K. Datta (Eds.), *Engineering properties of foods* (Vol. 3, pp. 149-173).

Newman, A. B. (1936). Heating and Cooling Rectangular and Cylindrical Solids. *Industrial & Engineering Chemistry, 28*(5), 545-548. https://doi.org/10.1021/ie50317a010

North, M. F. (2000). *Prediction of chilling rates for food product packages: PhD thesis, Massey University, New Zealand,* .

Norton, T., & Sun, D.-W. (2006). Computational fluid dynamics (CFD)–an effective and efficient design and analysis tool for the food industry: a review. *Trends in Food Science & Technology, 17*(11), 600-620.

O'Sullivan, J. (2016). *Significant factors affecting the forced-air cooling process of polylined horticultural produce: a thesis presented in partial fulfilment of the requirements for the degree of Doctor of Philosophy in Food Technology at Massey University, Palmerston North, New Zealand*.

O'Sullivan, J., Ferrua, M., Love, R., Verboven, P., Nicolaï, B., & East, A. (2014). Airflow measurement techniques for the improvement of forced-air cooling, refrigeration and drying operations. *Journal of Food Engineering, 143*, 90-101.

O'Sullivan, J., Ferrua, M. J., Love, R., Verboven, P., Nicolaï, B., & East, A. (2016). Modelling the forced-air cooling mechanisms and performance of polylined horticultural produce. *Postharvest Biology and Technology, 120*, 23-35.

Olatunji, J., Love, R., Shim, Y., & East, A. (2020). An automated random stacking tool for packaged horticultural produce. *Journal of Food Engineering*, 110037.

Onishenko, V. P., Vjazovsky, V. P., & Gnatiuk, P. G. (1991. *The calculation of the processes of refrigeration technology at the foodstuff processing on the processing line*. Paper presented at the International Congress of Refrigeration, Montreal, Quebec, Canada

Otsu, N. (1979). A Threshold Selection Method for Gray Level Histograms". IEEE Transactions on System, Man and Cybernetics: January.

Pátek, J., Hrubý, J., Klomfar, J., Součková, M., & Harvey, A. H. (2009). Reference correlations for thermophysical properties of liquid water at 0.1 MPa. *Journal of Physical and Chemical Reference Data, 38*(1), 21-29.

Perussello, C. A., Mariani, V. C., & do Amarante, Á. C. (2011). Combined modeling of thermal properties and freezing process by convection applied to green beans. *Applied Thermal Engineering, 31*(14-15), 2894-2901.

Pflug, I. J. (1965). Developing temperature-time curves for objects that can be approximated by an infinite sphere, an infinite cylinder, or infinite plate. *ASHRAE Trans., 71*, 238-250.

Pham, Q. T. (1991). Shape factors for the freezing time of ellipses and ellipsoids. *Journal of Food Engineering, 13*(3), 159-170.

Pham, Q. T. (2002. *Calculation of processing time and heat load during food refrigeration*. Paper presented at the "Food for Thought - Cool" AIRAH Conference, Darling Harbour, Sydney, Australia

Pham, Q. T. (2006). Modelling heat and mass transfer in frozen foods: a review. *International Journal of Refrigeration, 29*(6), 876-888.

Pham, Q. T. (2008). Modelling of freezing processes. In J. A. Evans (Ed.), *Frozen food science and technology*: Blackwell Publishing.

Pham, Q. T. (2014). *Food freezing and thawing calculations*. New York: Springer.

Pham, Q. T., Lowry, P. T., Fleming, A. K., Willix, J., & Reid, C. M. (1991). Thawing and tempering of cartoned meat and meat cuts. *MIRINZ Technical Report Series (New Zealand)*

Pham, Q. T., Trujillo, F. J., & McPhail, N. (2009). Finite element model for beef chilling using CFD-generated heat transfer coefficients. *International Journal of Refrigeration, 32*(1), 102-113. https://doi.org/10.1016/j.ijrefrig.2008.04.007

Pham, Q. T., Wee, H. K., Kemp, R. M., & Lindsay, D. T. (1994). Determination of the enthalpy of foods by an adiabatic calorimeter. *Journal of Food Engineering, 21*(2), 137-156.

Pham, Q. T., & Willix, J. (1989). Thermal Conductivity of Fresh Lamb Meat, Offals and Fat in the Range-40 to+ 30oC: Measurements and Correlations. *Journal of Food Science, 54*(3), 508-515.

Rahman, M. S. (2009). *Food properties handbook, 2nd ed.* Boca Raton: CRC Press.

Ramaswamy, H., Lo, K., & Tung, M. (1982). Simplified equations for transient temperatures in conductive foods with convective heat transfer at the surface. *Journal of food science, 47*(6), 2042-2047.

Rao, M. A., Rizvi, S. S. H., & Datta, A. K. (2005). *Engineering properties of foods*: CRC press.

Redding, G. P., Yang, A., Shim, Y. M., Olatunji, J., & East, A. (2016). A review of the use and design of produce simulators for horticultural forced-air cooling studies. *Journal of Food Engineering, 190*, 80-93.

Riedel, L. (1957). Calorimetric investigation of the meat freezing process. *Kaltetechnik, 9*(2), 38.

Roache, P. J. (1997). Quantification of uncertainty in computational fluid dynamics. *Annual review of fluid Mechanics, 29*(1), 123-160.

RS. (2002). *Cable selection guide.* Retrieved from https://nz.rs-online.com

Salin, V. (2018). *GCCA Global Cold Storage Capacity Report*. Retrieved from https://www.gcca.org/sites/default/files/2018%20GCCA%20Cold%20Storage%20Capacity%20Report%20final.pdf

Salvadori, V., Mascheroni, R., & De Michelis, A. (1996). Freezing of strawberry pulp in large containers: experimental determination and prediction of freezing times. *International Journal of Refrigeration, 19*(2), 87-94.

Santos, M. V., Vampa, V., Califano, A., & Zaritzky, N. (2010). Numerical simulations of chilling and freezing processes applied to bakery products in irregularly 3D geometries. *Journal of Food Engineering, 100*(1), 32-42.

Schwartzberg, H. G. (1976). Effective heat capacities for the freezing and thawing of food. *Journal of food science, 41*(1), 152-156.

Singh, R. P., & Heldman, D. R. (2009). *Introduction to food engineering*. Elsevier/Academic Press, Amsterdam: Gulf Professional Publishing.

Singh, R. P., & Sarkar, A. (2005). *Thermal Properties of Frozen Foods*. *Engineering properties of foods* (pp. 175-208).

Singh, S. P., Burgess, G., & Singh, J. (2008). Performance comparison of thermal insulated packaging boxes, bags and refrigerants for single-parcel shipments. *Packaging Technology and Science, 21*(1), 25-35.

Smale, N., Moureh, J., & Cortella, G. (2006). A review of numerical models of airflow in refrigerated food applications. *International Journal of Refrigeration, 29*(6), 911-930.

Smitheram, D. (2018). *Design engineer for Milmeq, Personal communication.*

Stafford, K. (Ed.). (2017). *Livestock production in New Zealand*. Auckland, New Zealand: Massey University Press.

Sweat, V. E., Haugh, C., & Stadelman, W. (1973). Thermal conductivity of chicken meat at temperatures between− 75 and 20° C. *Journal of food science, 38*(1), 158-160.

Tanner, D., Cleland, A., & Opara, L. (2002). A generalised mathematical modelling methodology for the design of horticultural food packages exposed to refrigerated conditions Part 2. Heat transfer modelling and testing. *International Journal of Refrigeration, 25*(1), 43-53.

Tchigeov, G. (1979). Thermophysical processes in food refrigeration technology. *Food Industry, Moscow*

ThePoultrySite. (2014). *GLOBAL POULTRY TRENDS 2014.* Retrieved from https://thepoultrysite.com/articles/global-poultry-trends-2014-poultry-set-to-become-no1-meat-in-asia

Tocci, A. M., & Mascheroni, R. H. (1994). Freezing times of meat balls in belt freezers: experimental determination and prediction by different methods. *International Journal of Refrigeration, 17*(7), 445-452.

Verboven, P., Flick, D., Nicolaï, B., & Alvarez, G. (2006). Modelling transport phenomena in refrigerated food bulks, packages and stacks: basics and advances. *International Journal of Refrigeration, 29*(6), 985-997.

Versteeg, H. K., & Malalasekera, W. (2007). *An introduction to computational fluid dynamics: the finite volume method*: Pearson Education.

Walters, R. E., & May, K. (1963). Thermal conductivity and density of chicken breast muscle and skin. *Food Technology, 17*(6), 808-&.

Wang, G., & Zou, P. (2014). Mathematical Modeling of Food Freezing in Air-Blast Freezer. *International journal of materials, mechanics and manufacturing, 2*(4)

Wang, J., Carson, J. K., North, M. F., & Cleland, D. J. (2008). A new structural model of effective thermal conductivity for heterogeneous materials with

co-continuous phases. *International Journal of Heat and Mass Transfer, 51*(9), 2389-2397.

Wang, J., Pham, Q. T., & Cleland, D. J. (2010). Freezing, thawing, and chilling of foods. In mathematical modeling of food processing. In M. M. Farid (Ed.), *Mathematical modeling of food processing*: CRC Press.

Wang, L., & Curtis, W. (2012). Thermophysical properties of frozen foods. In *Handbook of Frozen Food Processing and Packaging* (pp. 101-127): CRC Press/Taylor and Francis Group, Boca Raton/London/New York.

Wang, L., & Sun, D.-W. (2002). Modelling three-dimensional transient heat transfer of roasted meat during air blast cooling by the finite element method. *Journal of Food Engineering, 51*(4), 319-328.

Willix, J., Lovatt, S. J., & Amos, N. D. (1998). Additional thermal conductivity values of foods measured by a guarded hot plate. *Journal of Food Engineering, 37*(2), 159-174.

Zhang, M., Che, Z., Chen, J., Zhao, H., Yang, L., Zhong, Z., & Lu, J. (2010). Experimental Determination of Thermal Conductivity of Water− Agar Gel at Different Concentrations and Temperatures. *Journal of Chemical & Engineering Data, 56*(4), 859-864.

Zhao, C. J., Han, J. W., Yang, X. T., Qian, J. P., & Fan, B. L. (2016). A review of computational fluid dynamics for forced-air cooling process. *Applied energy, 168*, 314-331.

Zhao, Y., Ji, W., Guo, J., Chen, L., Tian, C., Wang, Y., & Wang, J. (2020). Numerical and experimental study on the quick freezing process of the bayberry. *Food and Bioproducts Processing, 119*, 98-107.

Zilio, C., Righetti, G., Pernigotto, G., & Longo, G. A. (2018). Analysis of the freezing time of chicken breast finite cylinders. *International Journal of Refrigeration, 95*, 38-50.

Zou, Q., Opara, L. U., & McKibbin, R. (2006a). A CFD modeling system for airflow and heat transfer in ventilated packaging for fresh foods: I. Initial analysis and development of mathematical models. *Journal of Food Engineering, 77*(4), 1037-1047.

Zou, Q., Opara, L. U., & McKibbin, R. (2006b). A CFD modeling system for airflow and heat transfer in ventilated packaging for fresh foods:: II. Computational solution, software development, and model testing. *Journal of Food Engineering, 77*(4), 1048-1058.

Appendices

Published papers

Journal papers

1. Hoang, D. K., Lovatt, S. J., Olatunji, J. R., & Carson, J. K. (2020). Experimental measurement and numerical modelling of cooling rates of bulk-packed chicken drumsticks during forced-air freezing. *International Journal of Refrigeration* https://doi.org/10.1016/j.ijrefrig.2020.03.012

2. Hoang, D. K., Lovatt, S. J., Olatunji, J. R., & Carson, J. K. (2020). Validated numerical model of heat transfer in the forced air freezing of bulk packed whole chickens. *International Journal of Refrigeration* (Submitted manuscript)

Conference papers

3. Hoang, D. K., Lovatt, S. J., Olatunji, J. R., & Carson, J. K. (2019). *Numerical heat transfer model for industrial chilling installations*. Paper presented at the 25th IIR International Congress of Refrigeration. August 24-30, 2019, Montreal, Quebec, Canada

4. Hoang, D. K., Lovatt, S. J., Olatunji, J. R., & Carson, J. K. (2019). *Experimental study on effects of packing arrangement and plastic liner bag on freezing rates of bulk packed chicken drumsticks*. Paper presented at the 25th IIR International Congress of Refrigeration. August 24-30, 2019, Montreal, Quebec, Canada

5. Hoang, D. K., Lovatt, S. J., & Carson, J. K. (2018). *A quick, reliable solution for modelling cheese chilling process*. Paper presented at the 5th IIR Conference on Sustainability and the Cold Chain. April 4-6, 2018 Beijing, China

6. Hoang, D. K., Lovatt, S. J., & Carson, J. K. (2018). *Improved prediction of thermal conductivity of frozen foods*. Paper presented at the 3rd International Conference on Food Properties (iCFP2018), Sheraton Sharjah Resort and Spa, Sharjah, UAE January 22-24, 2018

International Journal of Refrigeration 114 (2020) 165–174

Contents lists available at ScienceDirect

International Journal of Refrigeration

journal homepage: www.elsevier.com/locate/ijrefrig

Experimental measurement and numerical modelling of cooling rates of bulk-packed chicken drumsticks during forced-air freezing

Duy K. Hoang[a,c,*], Simon J. Lovatt[a], Jamal R. Olatunji[b], James K. Carson[a]

[a] University of Waikato, Private Bag 3105, Hamilton 3240, New Zealand
[b] Massey University, Private Bag 11222, Palmerston North 4442, New Zealand
[c] Hanoi University of Science and Technology, Hanoi, Vietnam

ARTICLE INFO

Article history:
Received 23 December 2019
Revised 10 March 2020
Accepted 13 March 2020
Available online 19 March 2020

Keywords:
Chicken drumsticks
CFD
Experiment
Freezing
Heat transfer

ABSTRACT

The cooling of polylined bulk-packed drumsticks during forced-air freezing was examined experimentally and numerically. The experiments showed that, when contained within the liner bag, the packing arrangement of the chicken drumsticks within the tray did not have a significant impact on freezing rate. However, the presence of the liner bag had a significant impact on freezing times, increasing them by more than a factor of three. A 3D computational fluid dynamics (CFD) model to predict the temperature profile of bulk-packed drumsticks, based on 3D computed tomography images of the chicken, was also developed and validated against the experimental cooling data. By using temperature-dependent thermal properties of chicken meat, the mean differences between the predicted average drumstick temperatures and corresponding experimental results were less than 1.1°C for all tested conditions. Based on the validated model, a correlation was proposed to estimate the effect of operating conditions on freezing time and that correlation may be used to optimise the design of the freezing tunnel for chicken products.

Mesure expérimentale et modélisation numérique des taux de refroidissement de pilons de poulet emballés en vrac soumis au refroidissement par air forcé

Mots clés: Pilons de poulet; CFD; Expérimentation; Congélation; Transfert de chaleur

1. Introduction

Food freezing technology continues to develop as new refrigeration equipment becomes available and as consumer preferences continue to change (Bogh-Sorensen, 2006; Singh & Heldman, 2009). On the industrial scale, food refrigeration equipment is often made to order for a given end user, and may be designed either for a single type of product or multiple products. While modular, mass-produced refrigeration components, such as compressors and condensers, may be incorporated into the overall refrigeration installation, the cold side (evaporator, fans, air flows, etc.) is likely to be highly customised. With such a high degree of customisation, it is important that the freezing process may be modelled accurately to allow for design optimisation.

Factors affecting the freezing time of food products include the refrigerated air temperature and air-flow characteristics (turbulence intensity, velocity), packaging, and packing arrangement, as well as the dimensions, morphology and physical properties of the food product (ASHRAE, 2006; O'Sullivan et al., 2014). Many primary (i.e. minimally processed) products such as meat/poultry cuts, fruit and vegetables have irregular shapes and, when packed in bulk (e.g. within cartons, bag or trays), air voids typically exist between individual food items, which can have a significant effect on freezing rates. Despite research to account for the effect of voids on heat transfer rates (Ambaw et al., 2017; Datta, 2007; North, 2000; O'Sullivan et al., 2016) a general approach for dealing with the problem has yet to be established. As such, accounting

* Corresponding author at: University of Waikato, Private Bag 3105, Hamilton 3240, New Zealand.
E-mail address: hoangduy2702@gmail.com (D.K. Hoang).

https://doi.org/10.1016/j.ijrefrig.2020.03.012
0140-7007/

Nomenclature

Bi	Biot number (dimensionless)
c	specific heat capacity (J kg^{-1} K^{-1})
Fo	dimensionless freezing time
h	heat transfer coefficient (W m^{-2} K^{-1})
H	enthalpy (J kg^{-1})
k	thermal conductivity (W m^{-1} K^{-1})
L	characteristic dimension (m)
St	Stefan number (dimensionless)
T	temperature (°C)
α	thermal diffusivity (m^2 s^{-1})
θ	dimensionless temperature
τ	freezing time (s)

Subscripts

a	property of air
f	initial freezing property
in	initial value

for voids within food packages remains a significant challenge for designers of industrial refrigeration equipment (Smitheram, 2018).

While several research articles report results on the refrigeration of whole chicken carcasses (James et al., 2006; Mannapperuma et al., 1994) there does not appear to be many data for chicken legs (commonly referred to as 'drumsticks'). Chicken legs represent an interesting problem due to their shape and the significance of the bone, which has the potential to act as a conduction pathway to the thermal centre of the drumsticks. Air voids of different shapes and sizes exist when drumsticks are packed in bulk, due to the irregular shapes of the drumsticks. On the industrial scale in New Zealand, chicken portions are typically cooled within a polythene liner bag (polyliner), which has the effect of restricting air movement within the voids and also results in a large air void within the bag on top of the chicken.

The aim of this work was to investigate the forced-convection freezing of bulk-packed drumsticks enclosed in a polyliner within a cardboard tray. Both physical experiments and CFD were used as analysis tools. The CFD model developed in this study was used to investigate the extent to which changes in operating conditions (cooling air velocity and cooling air temperature) could affect the freezing time of a tray of drumsticks.

2. Materials and methods

2.1. Experimental studies

2.1.1. The industrial chicken freezing process

The case study was based on a chicken processing plant in the Waikato Region of New Zealand. Typically, polylined whole chickens or chicken portions are placed on either plastic or cardboard trays with open tops. The weight of the contents of each tray ranges from 9 kg to 13 kg, depending on the type of chicken products. Before entering the freezing tunnel, chicken pieces are cut from the carcass in a room at about 10°C.

In the freezing tunnel, chicken trays are arranged on perforated shelves (Fig. 1) and cooled by refrigerated air at -25°C flowing from the evaporator at one end of the tunnel. The clearance between the top of the trays and the bottom of the shelves ensures that all the trays are exposed to airflow on all sides.

2.1.2. Experimental system

Experimental freezing trials were designed to closely represent the industrial setting and were conducted in the Environmental Test Chamber (ETC) at AgResearch Ltd, Hamilton, New Zealand.

Fig. 1. Product arrangement in an industrial freezing (photos courtesy of Milmeq).

Fig. 2. Experimental system for drumstick freezing trials.

Two polystyrene test tunnels (PTT) 2500 mm long x 720 mm height and 510 mm wide (Fig. 2) were used. Each PTT consisted of a variable speed suction fan at the downstream end, a fine wire mesh at the upstream end (used to diffuse the airflow), and an open tunnel where the chicken trays were loaded. A transition section was placed inside the PTT to guide the airflow and reduce the cross-sectional area to 300 mm x 510 mm. This experimental system allowed for precise control of the temperature and velocity of the cooling air being drawn through the PTT.

Cardboard trays with open tops, measuring 580 mm long x 325 mm wide x 130 mm high, each containing a polyliner as used by chicken processors, were used in these experiments. Each tray was loaded with 11.5 kg of drumsticks. In each run, one tray was placed in the top tunnel and another tray was placed in the bottom tunnel so that two trials could be run at the same time. In each tunnel, a metal platform was used to support the tray of drumsticks. This arrangement allowed the bottom surface of the cardboard tray to be exposed to the cold air, similarly to the industrial arrangement.

2.1.3. Experimental design

Three sets of experiments were conducted for bulk-packed drumsticks (Fig. 3). In the first set, the cooling behaviour of a tray of regularly arranged drumsticks within the plastic liner was investigated. Seventy-two drumsticks weighing from 140 g to 190 g were arranged in four layers. Eight drumsticks each having a mass of 160 g (the average weight of drumsticks in a tray) distributed along the two diagonals at both high and low, central and peripheral positions were chosen for temperature measurement. Drumstick Numbers 1, 3 and 4 are on the bottom layer, drumstick Num-

Fig. 3. Bulk-packed chicken drumsticks arrangements in the freezing trials. The monitored drumsticks were shown for the regular arranged with liner bag experiments.

ber 2 is on the second layer, drumstick Numbers 5, 6 and 8 are on the third layer and the drumstick Number 7 is on the top layer.

The second set of experiments used a tray of drumsticks arranged randomly within the liner bag. The drumsticks selected for temperature measurement in this experiment also weighed 160 g and were carefully placed at similar locations to the measurement positions in the first set of experiments.

The third set of experiments used a tray of regularly arranged drumsticks without the plastic liner bag and thermocouple placement was the same as for the first set of experiments.

T-type thermocouples were inserted in the thickest parts (approximately 3 cm deep) of the eight selected legs. The temperatures were recorded on a Keysight 24982A data acquisition unit every 60 s during the freezing trials. The cooling air temperatures above the tray were also monitored.

The air velocities at the inlet of the PTT were measured before and after each trial using a hot-wire anemometer (Dantec 54N60 FlowMaster). The sample time for each velocity measurement was 5 min. The air velocity was held constant during each trial. In addition, in order to define the outlet boundary condition in the numerical model, the pressure drop of the airflow through the PTT created by the suction fan was measured by an inclined fluid manometer (RS Pro, RS 730-2937) before and after each trial.

2.1.4. Experimental procedure

Chicken drumsticks were purchased fresh from a local retailer on the day of delivery. They were then sorted, weighed and positioned individually in trays and the thermocouples were inserted into the monitored drumsticks. The loaded trays were then placed in the ETC to equilibrate at 10°C (the temperature of chicken pieces before they enter the freezer of a chicken processor) for 24 hours. The drumstick temperatures were monitored during the equilibration process to ascertain when the trays had reached uniform temperatures.

For all freezing trials, the ETC air temperature was maintained at -25°C. The regularly arranged bulk pack of drumsticks (with and without liner bag) freezing trials were tested at inlet air velocities of 1.0 m s^{-1}, 2.5 m s^{-1}, and 4.3 m s^{-1}, and the randomly arranged drumstick freezing trials were tested at inlet air velocities of 1.0 m s^{-1} and 4.3 m s^{-1}. Each trial was terminated when all the monitored chicken temperatures fell below -21°C (seven-eighths of the difference between the initial and cooling air temperatures).

After the freezing process was completed, the drumsticks were thawed for 12 hours before being re-equilibrated at 10°C. Two subsequent trials were performed on each batch of drumsticks, with the exception of the eight drumsticks that contained the thermocouples, which were replaced by fresh 160 g drumsticks for each replicate. Thus, there were three replicates for each air velocity. No drumsticks were used for more than three trials.

2.2. Numerical model

A numerical model was developed for the regularly arranged drumsticks within the liner bag during the freezing process. The overall structure of the contents of the trays (bulk-packed chicken), air voids within the bulk-packed chicken, and the flow field around the products were included in the model.

2.2.1. Geometrical model

CT image reconstruction of bulk-packed drumsticks. Drumsticks were selected for computed tomography (CT) scanning and arranged regularly in a tray, following the same procedure as for the experiments. The scans were made by a Philips CT scanner at Massey University School of Veterinary Science, New Zealand. The CT images were then analysed by Slicer™ software (Slicer, 2019) to generate the 3D surface points (STL geometry file). Slicer™ uses a thresholding technique to segment the dataset into distinct regions (i.e. chicken, cardboard and air). Subsequently, the surface model was sculpted and smoothed by Meshmixer™ (Autodesk, Inc) to smooth complicated physical features which could result in highly skewed and distorted meshes. The 'cleaned', reconstructed surface was finally converted to solid surface form (T-spline body, Fig. 4) using Fusion 360™ (Autodesk, Inc). The volume of bulk-packed drumsticks geometrical model was 10.8×10^{-3} m^3.

Some simplifications were made to prevent overly complex meshes. The model assumed an ideal thermal contact between adjacent drumstick surfaces. In addition, because of the geometrical similarity of 4 rows in a tray of regularly arranged drumsticks (18 drumsticks in each row, Fig. 3), the drumstick model was created by combining 4 identical blocks (each block representing one row of bulk-packed drumsticks).

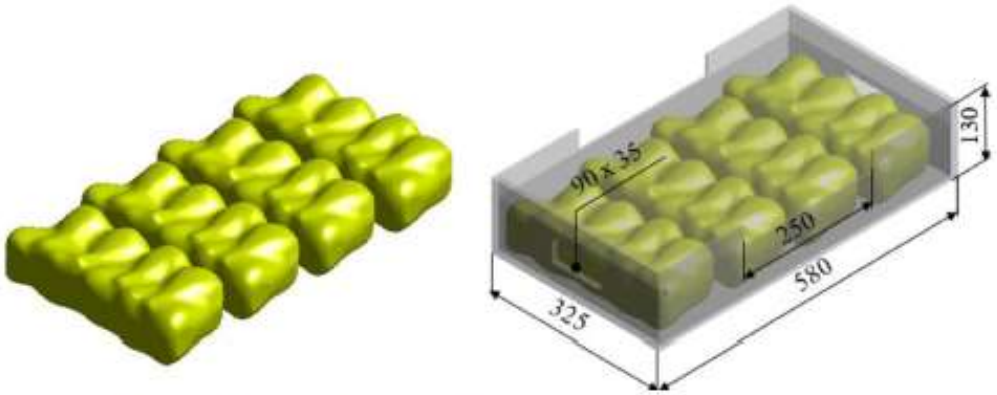

Fig. 4. Geometrical model of bulk-packed chicken drumsticks (on the left) and a tray of drumsticks with a modelled polyliner (on the right).

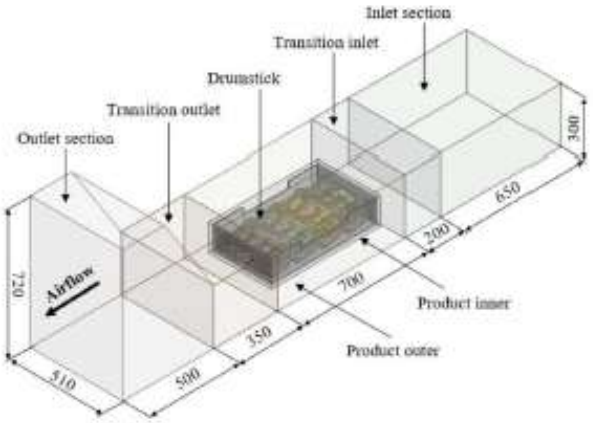

Fig. 5. Computational domain of a tray of drumsticks in the forced-air freezing model.

The cardboard tray and the polyliner model. The geometrical model of the cardboard tray was created based on its actual dimensions using ANSYS Design Modeller. The liner bag was modelled as a rectangular block close-fitted to the bulk-packed drumsticks model while ensuring a minimum gap between liner and chicken of 2 mm (Fig. 4). The minimum 2 mm clearance was created to avoid highly skewed and distorted meshes caused by single contact points between chicken and polyliner (Ferrua & Singh, 2009; O'Sullivan et al., 2016). The bottom and lateral surfaces of the liner were assumed to be in direct contact with the cardboard. In the numerical setup, the liner was described as a zero thickness wall. Therefore, it acted as a physical barrier to restrict the airflow rather than a thermal barrier to heat conduction.

The completed computational domain. The computational domain was constructed based on the internal dimensions of the PTT with the 3D model of a tray of chicken placed in the middle section at a distance of 5 cm from the bottom surface (Fig. 5). Transition regions were placed either side of the tray that aided with mesh refinement. The inlet and outlet boundaries were both at a distance of 850 mm from the product section which was assumed to be far enough to avoid any influence on the flow in the proximity of the product.

2.2.2. Mesh generation

The computational domain was meshed with ANSYS Meshing using a non-uniform mesh. The product inner region which housed the tray of drumsticks (Fig. 5) was discretised with the smallest elements. From the product outer section, the mesh became coarser in the outward direction. The mesh was designed to be used for the low-Reynolds number approach to modelling the boundary layer. This approach required high cell density in the wall-normal direction (Defraeye et al., 2013a). Therefore, in the boundary-layer region of the flow domain from the outer surface of the polyliner and the cardboard onward, 5 layers of prismatic cells were placed with the first layer thickness of 0.6 mm and the growth rate of 1.2.

The total number of elements was 4.5×10^6. The spatial discretisation error was determined by Richardson extrapolation (Roache, 1997), and was about 2.6% for the volume-average temperature of the drumsticks after 20 h freezing.

2.2.3. Numerical simulation

The simulations were performed with ANSYS Fluent 18.2. The airflow was modelled by the Reynolds Averaged Navier Stokes (RANS) equations described in (Fluent, 2017), and the heat transfer was solved using the default settings for the energy equation. The standard k-ε with the Enhanced Wall Treatment (EWT) option was applied for the turbulence model. The SIMPLE algorithm was used for pressure-velocity coupling. A second-order discretization scheme was used throughout. Radiation and moisture evaporation were assumed to have a negligible effect in forced air cooling (Defraeye et al., 2013b; Gowda et al., 1997; Gruyters et al., 2018; O'Sullivan et al., 2016), and thus they were not included in the model. Typically, for the product in an enclosed space like a liner bag, the effect of natural convection must be accounted for when the Rayleigh number is higher than 1708 (Cengel & Ghajar, 2011). For the air region within the polylined drumsticks, the calculated Rayleigh number was 4.3×10^6, which was higher than the critical value. Therefore, natural convection was included in the model. A Rayleigh number less than 10^8 also implies laminar flow inside the polyliner (Fluent, 2017).

Boundary and operating conditions. The inlet of the computation domain was defined as a velocity-inlet with velocities of 1.0 m s^{-1}, 2.5 m s^{-1}, and 4.3 m s^{-1} imposed, as for the experiments. The inlet air temperature was set at -25°C. A low turbulence intensity of 1% was used, due to the presence of the fine airflow diffuser. At the outlet of the computation domain, an under-pressure was imposed to represent the suction pressure of the fan. These values were taken from the experiments and, for the high, medium and low inlet air velocity, were -20 Pa, -10 Pa and -5 Pa, respectively. The cardboard, polyliner, chicken legs and all other surfaces of the tunnel were modelled as non-slip walls with zero roughness. The initial temperatures of solid regions (drumstick and cardboard)

Table 1
Thermal properties of air and packaging materials.

Properties	Air outside liner	Air inside liner	Cardboard
Density, kg m^{-3}	1.4225	ideal gas	195
Specific heat, J kg^{-1} K^{-1}	1004.5	1004.5	1700
Thermal conductivity, W m^{-1} K^{-1}	0.02175	0.02175	0.078
Dynamic viscosity, kg m^{-1} s^{-1}	1.6045×10^{-5}	1.6045×10^{-5}	-

Table 2
Comparison between predicted and experimental enthalpy and thermal conductivity data for chicken drumsticks.

T, °C	Enthalpy, kJ kg^{-1}		Thermal cond., W m^{-1} K^{-1}		Relative error, %	
	Predicted	Riedel, 1957	Predicted	Sweat et al, 1973	Enthalpy	Thermal conductivity
-30	20.9	19.1	1.62	1.49	9.4	8.8
-20	44.2	53.8	1.54	1.39	17.8	10.5
-10	76.2	74.1	1.43	1.28	2.8	12.2
-7	92.3	87.7	1.37		5.2	
-5	110.0	105.7	1.34		4.0	
-3	151.2	137.2	1.12		10.2	
-2	228.2	179.2	0.81		27.3	
-1	304.9	290.4	0.48		5.0	
0	308.3	297.8	0.48	0.48	3.5	0.3
10	341.7	331.2	0.49	0.49	3.2	0.6
20	375.3	368.3	0.50	0.50	1.9	1.2
Mean relative error					8.2	5.6

were set to the equilibrating temperature at the start of the experiment (approximately 10°C) and differed slightly for each experiment. The gravity setting was activated and the air volume inside the polyliner was defined as a laminar zone to simulate natural convection.

Thermal properties of materials. Thermal properties of air and packaging materials are presented in Table 1. The properties of air were estimated at -25°C (the cooling air temperature), using the data found in Cengel and Ghajar (2011), and were assumed to be constant throughout the simulation except for the air density inside the polyliner, which was assumed to behave as an ideal gas in order to simulate the natural convection. The cardboard properties were the same as those used by O'Sullivan, (2016) and Singh et al. (2008).

The specific heat capacity and thermal conductivity of chicken were set as functions of temperature to account for the sudden change of these properties around the freezing point (Pham, 2006). These properties were estimated from the composition data of dark chicken meat found in Sweat et al., 1973, with 76.3% water and 2.5% fat. Temperature-dependent thermal properties were modelled based on a method that has been described previously (ASHRAE, 2006; Carson et al., 2018; Hoang & Nguyen, 2013). Table 2 shows the comparison between experimental enthalpy (Riedel, 1957) and thermal conductivity data (Sweat et al., 1973) and corresponding predicted values. The enthalpy model for chicken was obtained by integrating the specific heat equation. The mean relative errors of less than 10% confirm that the predicted thermal conductivity and specific heat of drumsticks were suitable for use in the numerical model.

Due to the constraint of ANSYS Fluent software that requires the density of solid materials to be constant, the chicken density of 1070 kg m^{-3}, found in (Walters & May, 1963), was used in the model. Based on the physical properties model, it was predicted that the chicken density would vary by only 6% between -25°C (freezing temperature) and 10°C (initial chicken temperature), suggesting that a constant mid-range density value would be adequate for these simulations.

Solution procedure. To speed up the calculation, the steady-state flow equation was first solved with the energy equation disabled in order to obtain the initial fluid flow field. Once the steady-state simulation had converged, a transient simulation was performed by solving the flow and energy equations simultaneously to account for the effect of natural convection. The transient simulation was run at a time step of 120 s, based on a temporal sensitivity analysis. A maximum of 20 iterations per time step was used. The computational time for 21 hours of freezing was 8 hours on a 64-bit Intel® Xeon® CPU E5-1620, 3.5 GHz, 16 GB RAM.

3. Results and discussions

3.1. Experimental results

The impact of packing arrangement and plastic liner bag on freezing rates of bulk-packed drumsticks was assessed by comparing the experimental average temperature history and seven-eight cooling time (SECT) of trays of drumsticks in the three sets of experiments. The SECT was the time taken for the temperature to reach seven-eighths of the difference between initial and cooling air temperatures. The experimental average drumstick temperature per tray was calculated from the eight monitored drumsticks. The SECT of a tray of drumsticks was therefore determined by the time the dimensionless temperature (θ, Eq. (1)), took to equal 0.125:

$$\theta = \frac{T - T_a}{T_{in} - T_a} \tag{1}$$

where T (°C) was the average drumstick temperature, T_a (°C) was the cooling air temperature and T_{in} (°C) was the initial temperature of chicken drumsticks.

3.1.1. Comparison of cooling rate between regular and irregular packings of drumsticks

Cooling histories of trays of regularly packed and randomly packed drumsticks are compared in Fig. 6. The error bars indicate the 95% confidence intervals calculated from three replicated trials. Although the randomly packed drumsticks appeared to have cooled slightly faster on average than the regularly packed drumsticks, the difference between the two packing arrangements was less than the uncertainty in the measurements at both low and high air-speeds. This suggests that the packing arrangement and alignment of the leg-bone within the tray did not have a significant impact on freezing time when the drumsticks were contained

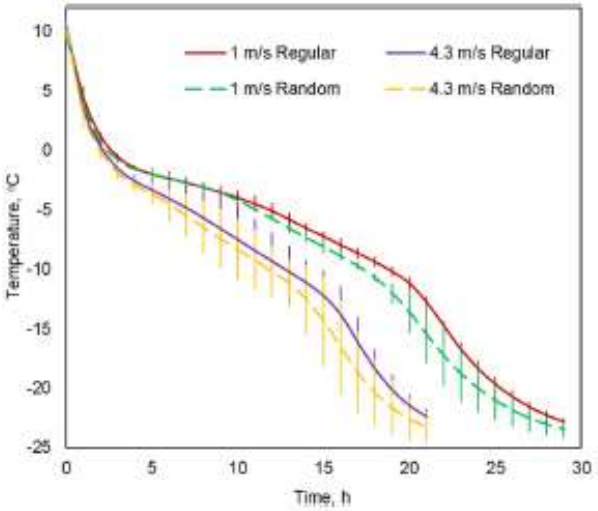

Fig. 6. Average temperature histories of regularly packed and randomly packed drumsticks at different air velocities.

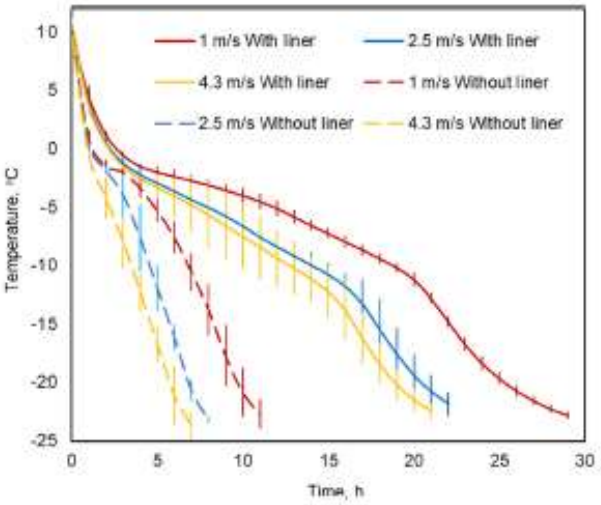

Fig. 7. Average temperature histories of regularly packed drumsticks with and without the liner bag.

within the polyliner bag. Since the orientation of the drumsticks did not appear to affect freezing time, it was possible that only the total fraction of air voids within the package would be required as a model input, with no requirement to account for the sizes or shapes of the air voids.

3.1.2. Comparison of cooling times of regularly packed drumsticks with and without liner bag

Fig. 7 shows cooling histories of regularly packed chicken drumsticks with and without the liner bag. As expected, the drumsticks without the liner bag cooled significantly faster than those packed within the liner bag for all three air velocities.

In order to quantify the effect of the liner bag on cooling time, the seven-eighths cooling time (SECT) was calculated, and results are shown in Table 3. The effect of the liner bag on cooling time increased as the air velocity increased so the SECT for the polylined chicken was more than three times greater than for the unlined case when the air velocity was 4.3 m s^{-1}.

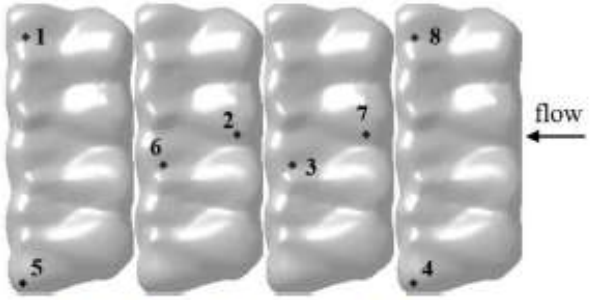

Fig. 8. Position of virtual sensors in the drumstick model.

3.2. Numerical model validations

The numerical model was validated firstly by comparing the predicted temperatures with the experimental data for average temperature history and the seven-eighths cooling time (SECT) of a tray of drumsticks contained in polyliner. Subsequently, the measured temperature histories of specific positions within a tray were also compared with the simulated results to assess the accuracy of the developed model in predicting the local cooling behaviour.

3.2.1. Comparison of the simulated and measured average temperature history of chicken drumsticks per tray

The simulated average temperature was computed by averaging the predicted temperatures at eight positions (Fig. 8) which corresponded to the positions of the eight thermocouples in the experiments. Fig. 9 shows the comparison between measured and simulated average time-temperature curves per tray of chicken drumsticks. The results showed good agreement between the experimental and simulated histories of the drumsticks, with mean temperature differences of 0.3°C, 0.9°C and 1.1°C for air velocities of 1 m s^{-1}, 2.5 m s^{-1} and 4.3 m s^{-1}, respectively. As can be seen from Fig. 9, the drumstick model gave a better prediction of temperatures above the freezing temperature than below the freezing temperature. This was expected because freezing is a more complicated process then cooling without phase change, since thermal properties have a stronger dependence on temperature.

3.2.2. Comparison of the numerical and measured SECT of a tray of drumsticks

Table 4 summarizes the results of predicted and measured SECT of a tray of drumsticks at different air velocities. The maximum difference between predicted and experimental SECT was 5.7% at 4.3 m s^{-1}.

3.2.3. Comparison of the simulated and measured temperature histories of individual drumsticks within a tray

The performance of the drumstick freezing model was further assessed by comparing the simulated and measured temperature histories of specific drumsticks within the tray at 1 m s^{-1} (Fig. 10), 2.5 m s^{-1} (Fig. 11), and 4.3 m s^{-1} (Fig. 12). For all tested air velocities, the temperatures predicted by the model followed the same spatial trend as the measured data. Drumsticks located at the edge of the tray (drumstick Numbers 1, 4, 5 and 8, Fig. 3) cooled faster than those in the middle (drumstick Numbers 2, 3, 6 and 7).

While the model showed good predictions for the temperature histories of drumstick Numbers 2, 3, 4, 6 and 8, it tended to over-predict for drumstick Numbers 1 and 5 and under-predict for drumstick Number 7. This can be explained by the fact that the thermocouple positions of drumstick Numbers 1 and 5 were close to the corner of the tray where the drumsticks are in direct contact with polyliner. Therefore, the effect of the artificial air gap in the

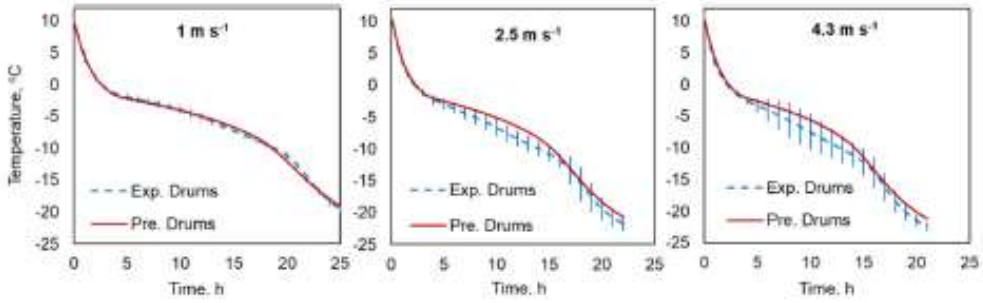

Fig. 9. Simulated and experimental average temperature of chicken drumsticks per tray at all tested air velocities. The simulated temperatures are depicted in red continuous lines; measured values are depicted in blue dashed lines (For interpretation of the references to color in this figure legend, the reader is referred to the web version of this article.).

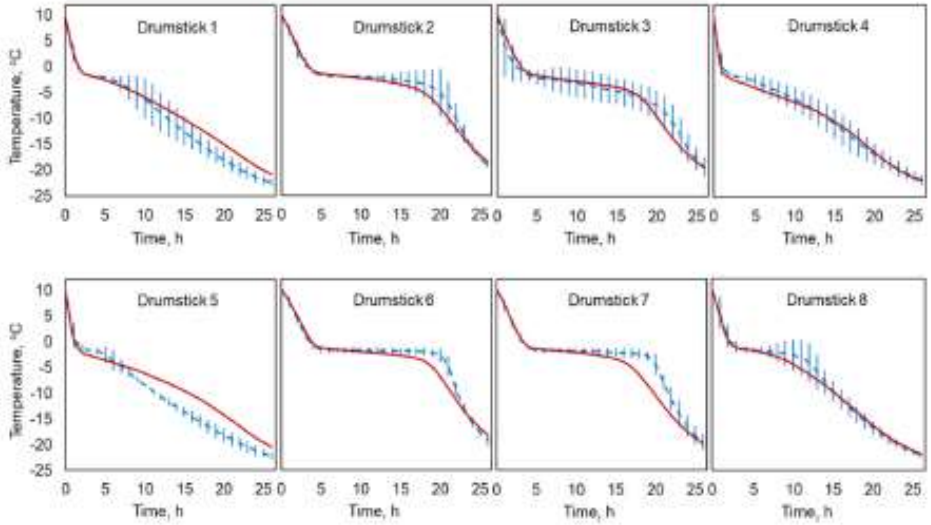

Fig. 10. Simulated and experimental temperature history of individual drumsticks within a tray at the air velocity of 1 m s^{-1}. The simulated temperatures are depicted in red continuous lines, measured values are depicted in blue dashed lines (For interpretation of the references to color in this figure legend, the reader is referred to the web version of this article.).

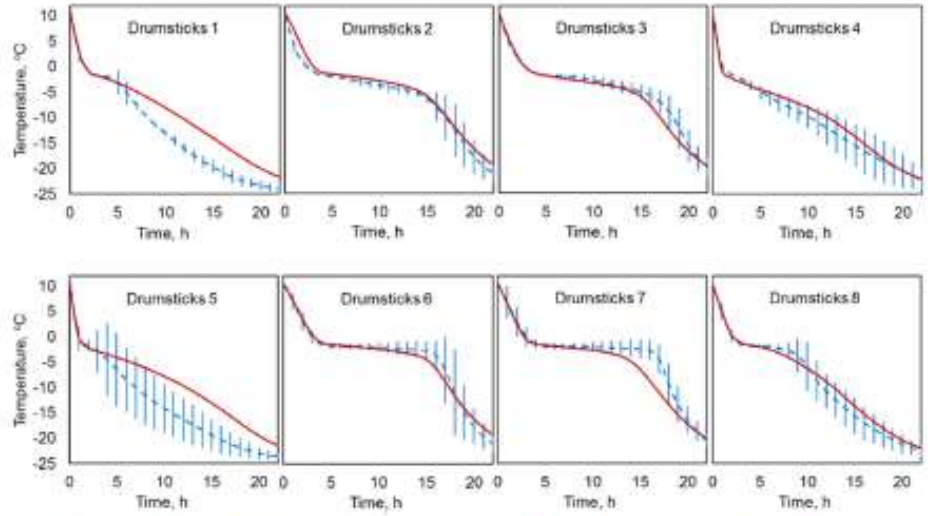

Fig. 11. Simulated and experimental temperature history of individual drumsticks within a tray at the air velocity of 2.5 m s^{-1}. The simulated temperatures are depicted in red continuous lines, measured values are depicted in blue dashed lines (For interpretation of the references to color in this figure legend, the reader is referred to the web version of this article.).

Table 3
Experimental SECT of the tray of drumsticks.

Air velocity	With liner		Without liner	
	SECT, h	Standard deviation, h	SECT, h	Standard deviation, h
1.0 m s^{-1}	25.9	0.5	9.9	0.8
2.5 m s^{-1}	20.8	1.2	7.0	0.3
4.3 m s^{-1}	19.3	0.8	5.9	0.6

Table 4
Experimental and predicted SECT of a tray of drumsticks at different air velocities.

Air velocity, m s^{-1}	Experimental SECT, h	Standard deviation, h	Predicted SECT, h	Difference, %
1.0	25.9	0.5	26.6	2.7
2.5	20.8	1.2	21.9	5.3
4.3	19.3	0.8	20.4	5.7

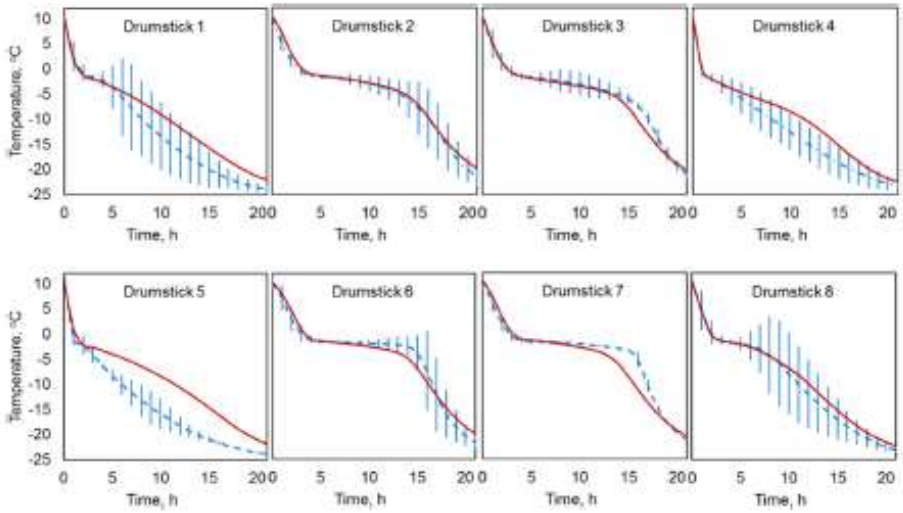

Fig. 12. Simulated and experimental temperature history of individual drumsticks within a tray at the air velocity of 4.3 m s^{-1}. The simulated temperatures are depicted in red continuous lines, measured values are depicted in blue dashed lines (For interpretation of the references to color in this figure legend, the reader is referred to the web version of this article.).

model was more obvious in these locations, making the predicted temperatures higher than measured data.

On another hand, the 'bunching' of the polyliner bag where it was tied (with the air gap inside) on the top surface of bulk-packed drumsticks in the experiments can explain the slower cooling in the experimental histories than the simulated temperatures for the drumstick on the top layer (Number 7). The over-prediction of the temperature of drumstick Number 7 at the end of the freezing process may also be linked to the fusion of condensation on the drumstick surfaces. Moisture from the air inside the polyliner and moisture evaporated from drumsticks was assumed to condense back on the drumstick surfaces. When the temperatures of drumstick surfaces dropped below the freezing point, the condensation would become ice, which has a higher thermal conductivity than chicken at the same temperature (i.e. the thermal conductivity of ice at -10°C is 2.3 W m^{-1} K^{-1} ASHRAE, 2006 while the thermal conductivity of chicken at this temperature is only 1.3 W m^{-1} K^{-1} Sweat et al., 1973). Therefore, the frozen condensed moisture may have enhanced the heat transfer rate on drumstick surfaces towards the end of the freezing process.

3.3. *Effect of operating conditions on freezing time*

Once validated, the numerical model could be used to predict freezing times under different operating conditions as presented in Fig. 13. For the purposes of this comparison, 'freezing time' is defined as the time taken for the average temperature of the chicken to reach −18°C.

Fig. 13 shows that the impact of increasing cooling air velocity from 1.0 m s^{-1} to 2.5 m s^{-1} on the freezing time was greater than that when it was raised from 2.5 m s^{-1} to 4.3 m s^{-1}. Changing the air temperature from -25°C to -30°C made the freezing time decrease by 4.5 hours on average but the reduction was only 2.8 hours when the air temperature dropped from -30°C to -35°C. Decreasing the initial chicken temperature from 10°C to 5°C or from 5°C to 0°C resulted in approximately 1 hour faster cooling.

The predicted average heat transfer coefficient at the inlet air velocity of 4.3 m s^{-1}, 2.5 m s^{-1} and 1 m s^{-1} were 21.4 W m^{-2} K^{-1}, 15.8 W m^{-2} K^{-1} and 9.2 W m^{-2} K^{-1}, respectively (they were not significantly affected by the initial drumstick temperature and cooling air temperature). The Biot number of a tray of drumsticks in forced-air freezing was calculated by Eq. (2):

$$Bi = \frac{hL}{k} \tag{2}$$

where k is the average thermal conductivity of chicken at the tested initial temperatures (0.49 W m^{-1} K^{-1}) and L is the characteristic length determined by volume divided by surface area of a tray of drumstick (0.031 m). Substituting these values into Eq. (2) yields Bi = 0.59, 1.01 and 1.37 at air velocities of 1 m s^{-1}, 2.5 m

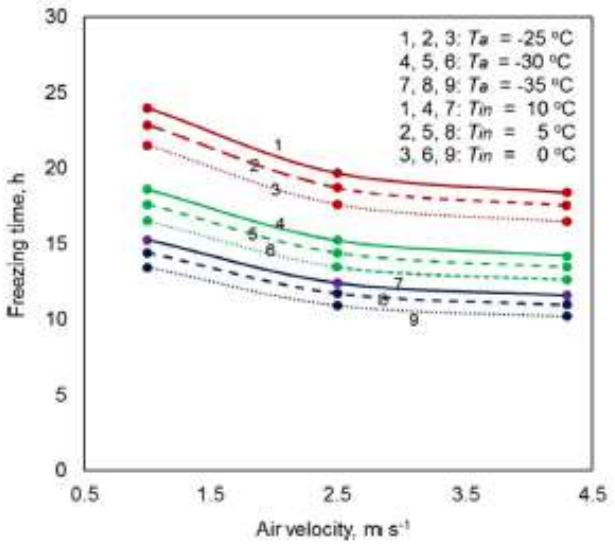

Fig. 13. Effect of operating conditions on freezing time of bulk-packed drumsticks.

s^{-1} and 4.3 m s^{-1}, respectively. The dimensionless Stefan number was calculated from Eq. (3):

$$St = \frac{c_f(T_f - T_a)}{\Delta H_{10}} \quad (3)$$

where c_f is the specific heat of frozen food, determined as specific heat of drumstick at -18°C, (2728 J kg^{-1} K^{-1}); T_f is the initial freezing temperature (-1.7°C, observed from temperature history of chickens in these experiments); T_a is the cooling air temperature (-25°C, -30°C or -35°C) and ΔH_{10} is the enthalpy change of the product between T_f and -10°C (251191 – 76165 = 175026 J kg^{-1}. ΔH_{10} is used instead of the latent heat of freezing to calculate the Stefan numbers, since the latent heat is very difficult to measure independently of the sensible heat. Eq. (3) yields St = 0.36, 0.44, 0.52 at the cooling air temperature of -25°C, -30°C and -35°C, respectively.

The effects of operating conditions on freezing time can be expressed as a function of Bi, St and the dimensionless temperature θ as:

$$Fo = 2.738\ Bi^{-0.326} St^{-0.662} \theta^{-0.387} \quad (4)$$

where Fo is the dimensionless freezing time, $Fo = \alpha\tau/L^2$; α is the average thermal diffusivity of chicken at the tested initial temperatures determined from the thermal properties model (1.34×10^{-7} m^2 s^{-1}); τ (s) is the freezing time and $\theta = (-18\text{-}T_a)/(T_{in} - T_a)$.

The R^2 square value of Eq. (4) was 0.99 indicating a good fit for the correlation equation to the data. This correlation can be used to predict the processing time in forced air freezing of bulk-packed drumsticks in freezing tunnels where the packages are similar in design to the one considered in this study.

4. Conclusions

The cooling performance of polylined bulk-packed drumsticks was investigated by both experiments and CFD simulations. The packing structure of the chicken drumsticks within the plastic liner bag did not have a significant impact on the freezing rate for any of the air velocities investigated, based on a 95% confidence interval of the experimental data. However, the presence of the plastic liner bag increased freezing times by more than a factor of 3 at high air velocities.

A numerical model was developed to simulate the forced-air freezing of regularly packed drumsticks enclosed in a polyliner bag within an open top tray. The model was validated against experimental data for a range of velocities. The mean discrepancy in average temperature prediction was less than 1.1°C, and the maximum difference of the SECT prediction was 5.7%. In addition to providing good predictions for average temperatures, the CFD simulation was also able to predict the temperatures at different locations within the tray. The model could be used to study the effect of different operating conditions on cooling rate, cooling heterogeneity of chickens during freezing in order to optimise operating conditions and avoid freezing injury.

Declaration of Competing Interest

The authors declare that they have no known competing financial interests or personal relationships that could have appeared to influence the work reported in this paper.

Supplementary material

Supplementary material associated with this article can be found, in the online version, at doi:10.1016/j.ijrefrig.2020.03.012.

References

Ambaw, A., Mukama, M., Opara, U.L., 2017. Analysis of the effects of package design on the rate and uniformity of cooling of stacked pomegranates: Numerical and experimental studies. Comput. Electron. Agricul. 136, 13–24.
ASHRAE, A.H., 2006. American Society of Heating, Refrigerating and Air-Conditioning Engineers. Refrigeration *Atlanta, GA*.
Bogh-Sorensen, L., 2006. Recommendations for the Processing and Handling of Frozen Foods, 4th ed. International Institute of Refrigeration, Paris.
Carson, J.K., Lovatt, S.J., Hoang, D.K., 2018. Improved prediction of thermal conductivity of frozen foods. In: Proceedings of the 3rd International Conference on Food Properties (ICFP2018). Sharjah, United Arab Emirates.
Cengel, Y.A., Ghajar, A.J., 2011. Heat and mass transfer: fundamentals and applications. McGraw-Hill, New York, p. 924.
Datta, A.K., 2007. Porous media approaches to studying simultaneous heat and mass transfer in food processes. I: Problem formulations. J. Food Eng. 80 (1), 80–95.
Defraeye, T., Lambrecht, R., Tsige, A.A., Delele, M.A., Opara, U.L., Cronjé, P., Nicolai, B., 2013b. Forced-convective cooling of citrus fruit: package design. J. Food Eng. 118 (1), 8–18.
Defraeye, T., Verboven, P., Nicolai, B., 2013a. CFD modelling of flow and scalar exchange of spherical food products: Turbulence and boundary-layer modelling. J. Food Eng. 114 (4), 495–504.
Ferrua, M.J., Singh, R.P., 2009. Modeling the forced-air cooling process of fresh strawberry packages, Part I: Numerical model. Int. J. Refrig. 32 (2), 335–348.
Fluent, (2017). 18.1, Ansys Fluent User Guide: Inc.
Gowda, B.S., Narasimham, G., Murthy, M.K., 1997. Forced-air precooling of spherical foods in bulk: a parametric study. Int. J. Heat Fluid Flow 18 (6), 613–624.
Gruyters, W., Verboven, P., Diels, E., Rogge, S., Smeets, B., Ramon, H., Nicolaï, B., 2018. Modelling cooling of packaged fruit using 3D shape models. Food Bioprocess Technol. 11 (11), 2008–2020.
Hoang, D.K., Nguyen, D.V., 2013. Effective Specific Heat for Camranh Mango. In: Proceedings of the 3rd International Conference on Sustainable Energy, "RISE towards a Green Future. Ho Chi Minh City, Vietnam.
James, C., Vincent, C., de Andrade Lima, T., James, S., 2006. The primary chilling of poultry carcasses–a review. Int. J. Refrig. 29 (6), 847–862.
Mannapperuma, J.D., Singh, R.P., Reid, D.S., 1994. Effective surface heat transfer coefficients encountered in air blast freezing of single plastic wrapped whole turkey. Int. J. Refrig. 17 (4), 273–280.
North, M.F., 2000. Prediction of chilling rates for food product packages PhD thesis. Massey University, New Zealand.
O'Sullivan, J., Ferrua, M.J., Love, R., Verboven, P., Nicolaï, B., East, A., 2016. Modelling the forced-air cooling mechanisms and performance of polylined horticultural produce. Postharvest Biol. Technol. 120, 23–35.
O'Sullivan, J., Ferrua, M., Love, R., Verboven, P., Nicolaï, B., East, A., 2014. Airflow measurement techniques for the improvement of forced-air cooling, refrigeration and drying operations. J. Food Eng. 143, 90–101.
O'Sullivan, J. (2016). Significant factors affecting the forced-air cooling process of polylined horticultural produce: a thesis presented in partial fulfilment of the requirements for the degree of Doctor of Philosophy in Food Technology at Massey University, Palmerston North, New Zealand.
Pham, Q.T., 2006. Modelling heat and mass transfer in frozen foods: a review. Int. J. Refrig. 29 (6), 876–888.
Riedel, L., 1957. Calorimetric investigation of the meat freezing process. Kaltetechnik 9 (2), 38.

Roache, P.J., 1997. Quantification of uncertainty in computational fluid dynamics. Ann. Rev. Fluid Mech. 29 (1), 123–160.
Singh, R.P., Heldman, D.R., 2009. Introduction to food engineering. Elsevier|Academic Press, Amsterdam Gulf Professional Publishing.
Singh, S.P., Burgess, G., Singh, J., 2008. Performance comparison of thermal insulated packaging boxes, bags and refrigerants for single-parcel shipments. Packag. Technol. Sci. 21 (1), 25–35.
Slicer. (2019). Slicer 4.10.2 released. Retrieved from https://www.slicer.org/.
Smitheram, D., 2018. Design Engineer for Milmeq. Personal communication.
Sweat, V.E., Haugh, C., Stadelman, W., 1973. Thermal conductivity of chicken meat at temperatures between– 75 and 20°C. J. Food Sci. 38 (1), 158–160.
Walters, R.E., May, K., 1963. Thermal conductivity and density of chicken breast muscle and skin. Food Technol. 17 (6) 808-&.

Validated numerical model of heat transfer in the forced air freezing of bulk packed whole chickens

Duy K. HOANG[1, 3, *], Simon J. LOVATT[1], Jamal R. OLATUNJI[2], James K. CARSON[1]

[1] University of Waikato, Private Bag 3105, Hamilton 3240, New Zealand

[2] Massey University, Private Bag 11222, Palmerston North 4442, New Zealand

[3] Hanoi University of Science and Technology, Hanoi, Vietnam

* Corresponding author. Tel: +64 7 838 6460; Fax: +64 7 838 4835

Email: hoangduy2702@gmail.com

ABSTRACT

This study presents a 3D computational fluid dynamics (CFD) model to predict the temperature profile of bulk-packed whole chickens during forced-air freezing based on 3D computed tomography (CT) images of the chicken. The model was validated against experimental cooling data. By using the temperature-dependent thermal properties of chicken meat, the mean differences between the predicted average drumstick temperatures with corresponding experimental results were less than 1.3°C for all tested conditions. Based on the validated model, a correlation was proposed to estimate the effect of operating conditions on freezing time and that correlation may be used to optimise the design of the freezing tunnel for chicken products.

Keywords: *CFD, freezing, heat transfer, whole chicken*

Nomenclature

Bi	Biot number (dimensionless)	*L*	characteristic dimension (m)
c	specific heat capacity (J kg^{-1} K^{-1})	*St*	Stefan number (dimensionless)
Fo	dimensionless freezing time	*T*	temperature (°C)
h	heat transfer coefficient (W m^{-2} K^{-1})	α	thermal diffusivity (m^2 s^{-1})
H	enthalpy (J kg^{-1})	θ	dimensionless temperature
k	thermal conductivity (W m^{-1} K^{-1})	*t*	freezing time (s)

Subscripts

a	property of air
f	initial freezing property
in	initial value

1. Introduction

Poultry is the most consumed meat globally, of which approximately 88 per cent is chicken (ThePoultrySite, 2014). The shelf life of chicken meat is relatively short (Jimenez et al., 1999), so it is necessary to freeze chicken to improve food safety and preserve product quality through the supply chain. Benefits of freezing include not only a long shelf life but also an excellent retention of nutrients, sensory qualities and complete absence of microbial growth (Pham, 2014). An efficient design of freezing equipment is required to maximise the economics. Therefore, it is important that the chicken freezing process be modelled accurately to allow for design optimisation.

On the industrial scale in New Zealand, chicken products are typically cooled within a plastic liner bag (polyliner), which has the effect of restricting air movement within the voids between the liner and the chicken and results in a large air void within the bag on top of the chicken. The polyliner increases resistance to heat transfer since it prevents air outside the bag from directly contacting the chicken; however, it serves to reduce moisture loss which is detrimental to product quality and appearance. Despite research to account for the effect of voids on heat transfer rates (Ambaw et al., 2017; Datta, 2007; James et al., 2006; North, 2000; O'Sullivan et al., 2016) a general approach for dealing with the problem has yet to be established. As such, accounting for voids within food packages remains a significant challenge for designers of industrial refrigeration equipment (Smitheram, 2018).

Mannapperuma et al., (1994) presented a finite difference numerical method based on enthalpy formulation to simulate the air blast freezing of plastic-wrapped whole chickens, packed trays of chicken parts and boxed chicken parts. Zilio et al., (2018) used the CFD software STAR-CCM + to model the liquid-solid phase change in the freezing of chicken breast. The above mentioned studies approximated the geometry of chicken by simple shapes and used average heat transfer coefficients to represent the boundary condition over the entire surface of the packaging. None of them accounted for the effect of air voids within the packaging on the freezing rate. Air voids of different shapes and sizes exist when chicken carcasses are packed in bulk, due to the irregular shapes of the products. A more rigorous model for the convective freezing of chicken would provide refrigeration equipment designers a greater ability to optimise this important industrial process.

This research focused on developing a CFD model for the forced-air freezing of bulk-packed whole chickens encased in a polyliner within a cardboard tray and validating the model against experimental data. The overall structure of the contents of the trays (bulk-packed chickens), air voids within the bulk-packed chickens, and the flow field around the products were included in the model. CT scanning was used to create a geometry that was similar to the empirical shape of bulk packed chickens. The model was then used to investigate the effect of operating conditions on the freezing time of a tray of whole chickens.

2. Materials and methods

2.1 Experimental studies

2.1.1 Experimental system

Experimental freezing trials were conducted in the Environmental Test Chamber (ETC) at AgResearch Ltd, Hamilton, New Zealand. The experimental system were designed to closely represent the industrial setting previously presented in Hoang et al. (2020). A polystyrene test tunnel (PTT) 2500 mm long x 720 mm height and 510 mm wide (Fig. 1) was used. The PTT consisted of a variable speed suction fan at the downstream end, a fine wire mesh at the upstream end (used to diffuse the airflow), and an open tunnel where the chicken trays were loaded. A transition section was placed inside the PTT to guide the airflow and reduce the cross sectional area to 300 mm x 510 mm. The experimental system allowed for precise control of the temperature and velocity of the cooling air being drawn through the PTT.

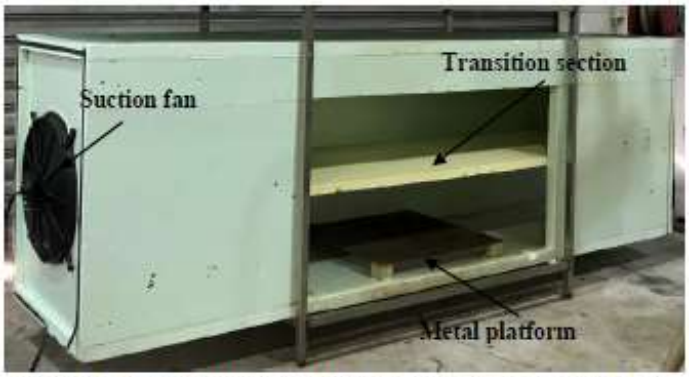

Figure 1: A polystyrene test tunnel for chicken freezing trials

Cardboard trays with open tops, measuring 580 mm long x 325 mm wide x 130 mm high, each containing a polyliner as used by chicken processors, were used in these experiments. Each tray was loaded with eight whole chickens. In the PTT, a metal platform was used to support the tray

of chickens. This arrangement allowed the bottom surface of the cardboard tray to be exposed to refrigerated air, similar to what occurs in the industrial arrangement.

2.1.2 Experimental design

The temperature history of each chicken was monitored at a position 3 cm deep in the breast and in the deepest part of the gastro-intestinal cavity during the freezing trial. The chickens selected for the trials weighed approximately 1.6 kg each. To replicate the industrial case, eight chicken carcasses were placed into a tray; five chickens (Numbers 1 to 5, Fig. 2) were arranged in a portrait orientation in the top row, and three chickens (Numbers 6 to 8, Fig. 2) were arranged in a landscape orientation in the bottom row.

Figure 2: Chickens arrangement within a tray

T-type thermocouples were used for the temperature measurement. As much as possible, the positions and the depths to which the thermocouples were inserted were the same for every chicken. The cooling air temperature was measured at a position 3 cm above the chicken tray in the tunnel. Temperatures were recorded on a Keysight 24982A data acquisition unit every 60 seconds during the freezing trials.

The air velocities at the inlet of the PTT were measured before and after each trial using a hot-wire anemometer (Dantec 54N60 FlowMaster). The sample time for each velocity measurement was 5 minutes. The air velocity was held constant during the experiment. In addition, in order to define the outlet boundary condition in the numerical model, the pressure drop of the airflow through the PTT created by the suction fan was measured by an inclined fluid manometer (RS Pro, RS 730-2937) before and after each trial.

2.1.3 Experimental procedure

Chickens were purchased fresh from a local retailer on the day of delivery. They were then sorted, weighed and positioned individually in the tray and the thermocouples were inserted. The plastic liner was then tied to enclose the chickens and thermocouples. The loaded trays were subsequently placed in the ETC to equilibrate at 10°C (replicating the temperature of chicken in the boning room of a processor) for 24 hours. The chicken temperatures were monitored during the equilibration process to ascertain when the trays had reached uniform temperatures.

For all freezing trials the ETC air temperature was maintained at -25°C. Three different air velocities (1 m s^{-1}, 2.5 m s^{-1} and 4.5 m s^{-1}) were tested. Each trial was terminated when all the monitored chicken temperatures fell below -21°C (seven-eighths of the difference between initial and cooling air temperatures).

After the freezing process was completed, the chickens were thawed for 12 hours before being re-equilibrated at 10°C. Two subsequent trials were performed on each batch of chickens before they were replaced by fresh ones. Five trials were performed for the 2.5 m s^{-1} and 4.5 m s^{-1} freezing experiments and four trials were performed for the 1.0 m s^{-1} freezing experiments

2.2 Numerical model

2.2.1 Geometrical model

2.2.1.1 CT image reconstruction of bulk-packed drumsticks

Chickens were selected for CT scanning and arranged in a tray, following the same procedure as for the experiments. The scans were made by a Philips CT scanner at Massey University School of Veterinary Science, New Zealand. The CT images were then analysed by Slicer™ software (Slicer, 2019) to generate the 3D surface points (STL geometry file). Slicer™ uses the Otsu's thresholding technique (Otsu, 1979) to segment the scan data into distinct regions (i.e. chicken, cardboard and air). Subsequently, the surface model was sculpted and smoothed by Meshmixer™ (Autodesk, Inc) to smooth the complicated physical features which could result in highly skewed and distorted meshes. The 'cleaned', reconstructed surface was finally converted to solid surface form (T-spline body, Fig. 3) using Fusion 360™ (Autodesk, Inc). The volume of bulk-packed whole chickens geometrical model (not considering the gastro-intestinal cavities) was 11.9×10^{-3} m^3.

Some simplifications were made to prevent overly complex meshes. The model assumed an ideal thermal contact between adjacent chicken surfaces, resulting in Fig. 3. The gastro-intestinal cavities of the chickens were represented by ellipsoids which closely fitted to the volume of the reconstructed cavities (see Fig. 5).

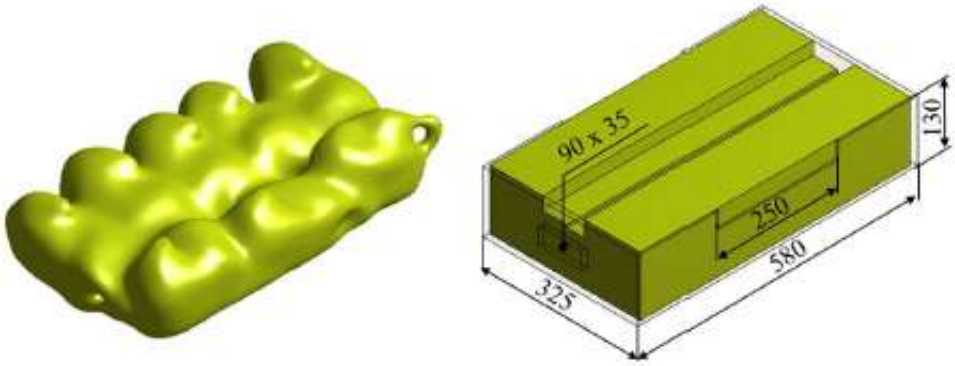

Figure 3. Geometrical model of bulk packed whole chickens (on the left) and a tray of chicken with a modelled polyliner (on the right)

2.1.1.2 The cardboard tray and the polyliner model

The geometrical model of the cardboard tray was created based on its actual dimensions using ANSYS Design Modeller (Fig. 3). The liner bag was modelled as a rectangular block close fitted to the bulk-packed whole chicken model, while ensuring a minimum gap between liner and chicken of 2 mm. The 2 mm clearance was created to avoid highly skewed and distorted meshes caused by the single contact points between chicken and polyliner (similar approaches were used in Ferrua & Singh, 2009 and O'Sullivan et al., 2016). The bottom and lateral surfaces of the liner were assumed to be in direct contact with the cardboard. In the numerical setup, the liner was described as a zero thickness wall. Therefore, it acted as a physical barrier to restrict the bulk airflow from interacting directly with the chicken inside.

2.1.1.3 The completed computational domain

The computational domain was constructed based on the internal dimensions of the PTT with the 3D model of a tray of chicken placed in the middle section at a distance of 5 cm from the bottom surface (Fig. 4). Transition regions were placed at the inlet and outlet of the tray to aid with mesh refinement. The inlet and outlet boundaries were both at a distance of 850 mm from the product section, which was assumed to be far enough to avoid any influence on the flow in the proximity of the product.

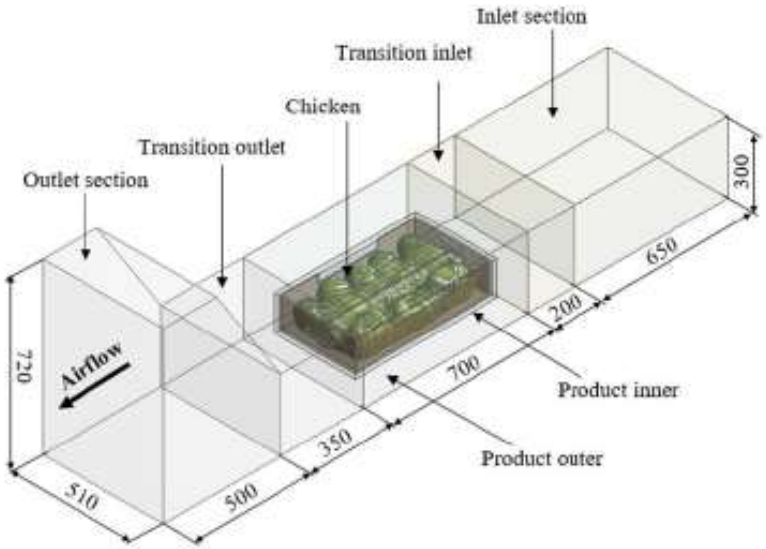

Figure 4: Computational domain of a tray of whole chickens in the forced-air freezing model

2.2.2 Mesh generation

The computational domain was meshed with ANSYS Meshing using non-uniform mesh. The product inner region which housed the chicken tray (Fig.4) was discretised with the smallest element size. From the product outer section, the mesh became coarser with distance in the outward direction. The mesh was designed to be used for the low-Reynolds number approach to modelling the boundary layer. This approach required high cell density in the wall-normal direction (Defraeye et al., 2013a). Therefore, in the boundary-layer region of the flow domain from the outer surface of the polyliner and the cardboard onward, 5 layers of prismatic cells were placed, with the first layer thickness of 0.6 mm and the growth rate of 1.2.

The total number of elements was 4.2×10^6. The spatial discretisation error was determined by Richardson extrapolation (Roache, 1997), and was approximately 2.9% for the volume-average temperature of chickens after 20 hours freezing.

2.2.3 Numerical simulation

The simulations were performed with ANSYS Fluent 18.2. The airflow was modelled by the Reynolds Averaged Navier Stokes (RANS) equations described in (Fluent, 2017), and the heat transfer was solved using the default settings for the energy equation. The standard k-ε turbulence model with the Enhanced Wall Treatment (EWT) option was applied. The SIMPLE

algorithm was used for pressure-velocity coupling and the second-order discretization scheme was used throughout. Radiation and moisture evaporation were assumed to have a negligible effect in forced air cooling (Defraeyeet al., 2013b; Gowda et al., 1997; Gruyters et al., 2018; O'Sullivan et al., 2016), and thus they were not included in the model. Typically, for a product in an enclosed space like a liner bag, the effect of natural convection must be accounted for when the Rayleigh number is higher than 1708 (Cengel & Ghajar, 2011). For the air region within polylined chickens the calculated Rayleigh Number was 4.3×10^6 and therefore natural convection was included in the model. A Rayleigh Number less than 10^8 also implies laminar flow inside the polyliner (Fluent, 2017)

2.2.3.1 Boundary and operating conditions

The inlet of the computation domain was defined as the velocity-inlet with velocities of 1 m s^{-1}, 2.5 m s^{-1}, and 4.5 m s^{-1} imposed, as for the experiments, and the inlet air temperature was set at -25°C. A low turbulence intensity of 1% was used due to the presence of the fine airflow diffuser (O'Sullivan et al., 2016).

At the outlet of the computation domain, an under-pressure was imposed to represent the suction pressure of the fan. These values were taken from the experiments and for the high, medium and low inlet air velocity were -20 Pa, -10 Pa and -5 Pa, respectively. The cardboard, polyliner, chicken products and all other surfaces of the tunnel were modelled as non-slip walls with zero roughness.

The initial temperatures of solid regions (chicken and cardboard) were set to the equilibrating temperature at the start of the experiment (approximately 10°C) and differed slightly depending on each experiment. The gravity setting was activated and the air volume inside the liner was defined as a laminar zone to simulate natural convection.

2.2.3.2 Thermal properties of materials

The thermal properties of air and packaging materials are presented in Table 1. The properties of air were estimated at -25°C (the cooling air temperature), using the data found in Cengel and Ghajar (2011), and were assumed to be constant throughout the simulation except for air density inside the polyliner, which was assumed to behave as an ideal gas in order to simulate the natural convection. The cardboard properties were the same as those used by O'Sullivan, 2016; and Singh et al., 2008.

Table 1: Thermal properties of air and packaging materials

Properties	Air outside liner	Air inside liner	Cardboard
Density, kg m^{-3}	1.4225	ideal gas	195
Specific heat, J kg^{-1} K^{-1}	1004.5	1004.5	1700
Thermal conductivity, W m^{-1} K^{-1}	0.02175	0.02175	0.078
Dynamic viscosity, kg m^{-1} s^{-1}	1.6045×10^{-5}	1.6045×10^{-5}	-

The specific heat capacity and thermal conductivity of chicken were set as functions of temperature to account for the sudden change of these properties around the freezing point (Pham, 2006). These properties were estimated from the composition data of white chicken meat found in Sweat et al. (1973), with 74.4% water and 0.3% fat.

Temperature-dependent thermal properties were modelled based on a method that has been described previously in ASHRAE (2006), Carson et al. (2018) and Hoang & Nguyen (2013). Table 2 shows the comparison between experimental enthalpy (Riedel, 1957), thermal conductivity data (Sweat et al., 1973) and the predicted values using the aforementioned method. The enthalpy model of chicken was obtained by integrating the specific heat equation. The mean relative errors of less than 8% confirm that the predicted thermal conductivity and specific heat of chicken are suitable for use in the numerical model.

Table 2: Comparison between predicted and experimental enthalpy and thermal conductivity data for chicken drumsticks.

T, °C	Enthalpy, kJ kg^{-1}		Thermal cond., W m^{-1} K^{-1}		Relative error, %	
	Predicted	Riedel, 1957	Predicted	Sweat et al, 1973	Enthalpy	Thermal conductivity
-30	20.7	19.1	1.58	1.42	8.6	10.73
-20	43.8	53.8	1.50	1.33	18.5	13.36
-10	75.4	74.1	1.41	1.21	1.7	16.31
-7	91.2	87.7	1.35		4.0	
-5	108.5	105.7	1.28		2.7	
-3	148.8	137.2	1.11		8.5	
-2	223.9	179.2	0.80		24.9	
-1	298.7	290.4	0.47		2.9	
0	302.1	297.8	0.47	0.48	1.4	0.34
10	335.0	331.2	0.49	0.48	1.2	1.77
20	368.1	368.3	0.51	0.49	0.0	3.60

Mean relative error	6.8	7.7

To simplify the model, a constant chicken density of 1070 kg m^{-3}, found in (Walters & May, 1963), was used. Based on the physical properties model, it was predicted that the chicken density varies by only 6% between -25°C (freezing temperature) and 10°C (initial chicken temperature), suggesting that a constant mid-range density value will be adequate for these simulations.

2.2.3.3 Solution procedure

To speed up the simulation time, the steady-state flow equation was first solved with the energy equation disabled in order to obtain the initial fluid flow field. Once the steady-state simulation had converged, a transient simulation was performed by solving the flow and energy equations simultaneously to account for the effect of natural convection. The transient simulation was run at a time step of 120 s based on a temporal sensitivity analysis. A maximum of 20 iterations per time step were used. The computational times for 21 hours freezing was 7.5 hours on a 64-bit Intel® Xeon® CPU E5-1620, 3.5 GHz, 16 GB RAM.

3. Results and discussions

3.1 Numerical model validations

The numerical model was first validated by comparing the predicted temperatures with the experimental data for the average temperature history and the seven-eighths cooling time (SECT) of a tray of chickens. Subsequently, the measured temperature histories of specific positions within a tray were also compared with the numerical results to assess the accuracy of the numerical model in predicting the cooling behaviour at different locations within the tray.

The experimental average temperature of chicken breast and chicken cavity were calculated by averaging temperatures at the same position of all chickens within a tray. The SECT is the time taken for the temperature to reach seven-eighths of the difference between initial and cooling air temperatures. Using the dimensionless temperature (θ, Eq. 1), the SECT of a tray of chickens was determined by the time θ took to equal 0.125

$$\theta = \frac{T - T_a}{T_m - T_a} \quad (1)$$

where T (°C) is the average temperature of chicken cavity (because the cavity cooled slower than the breast, Figs 6-8), T_a (°C) is the cooling air temperature and T_{in} (°C) is the initial temperature of chicken.

3.1.1 Comparison of the simulated and measured average temperature history of chickens per tray.

The simulated average temperatures per tray of chicken breast and chicken cavity were computed by averaging the corresponding temperatures of all chickens. In the numerical model the breast temperature of each chicken was determined at 3 cm depth in the breast along the y-direction (Fig. 5) to match the thermocouple position in the experiments (Fig. 2). Since the position of the cavity temperature measurement was difficult to determine precisely, the volume-averaged temperature of the air region within the cavity was chosen as the representative temperature.

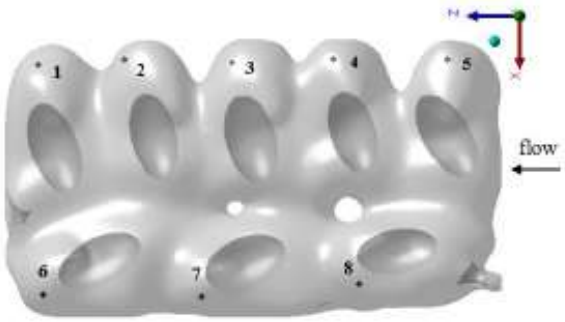

Figure 5: Position of virtual sensors in the chicken model

Fig. 6a shows the comparison between the model prediction and experimental average temperatures of chicken breast and chicken cavity at the inlet air velocity of 1 m s^{-1}, with the error bars representing the experimental uncertainty at 95% confidence interval. The same comparisons at inlet air velocities of 2.5 m s^{-1}, and 4.5 m^{-1} are depicted in Figs. 6b and 6c

The results show good agreement between model predictions and experimental data. The worst prediction result was at the air velocity of 4.5 m s^{-1}, with mean discrepancies between simulated and measured average temperatures of 1.3°C for both chicken cavity and chicken breast. At the air velocity of 1 m s^{-1}, the mean temperature differences were 0.9°C and 0.6°C for the breast and cavity temperature respectively, while they were 0.4°C and 0.3°C respectively at 2.5 m s^{-1}.

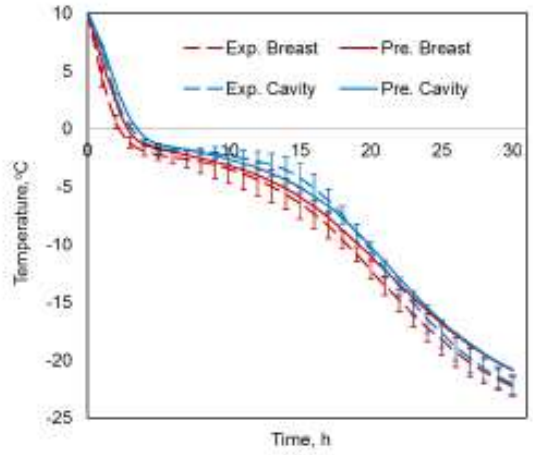

a)

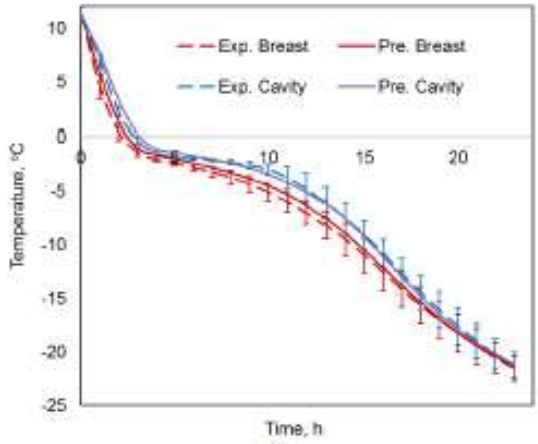

b)

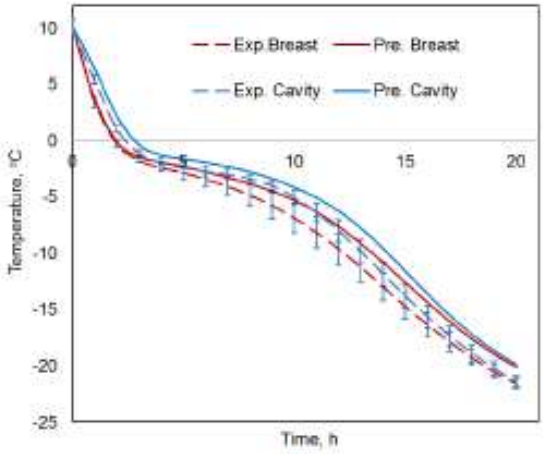

c)

Figure 6: Simulated and experimental average temperature of chicken breast and chicken cavity at the air velocity of a) 1 m s^{-1}, b) 2.5 m s^{-1} and c) 4.5 m s^{-1}

3.1.2 Comparison of the numerical and measured SECT of a tray of chickens

Table 3 presents the predicted and experimental SECT for a tray of chicken at different air velocities. The maximum difference between predicted and experimental values was 7.3% at 4.5 m s^{-1}

Table 3: Experimental and predicted SECT of a tray of chicken at different air velocities

Air velocity, m s^{-1}	Experimental SECT, h	Standard deviation, h	Predicted SECT, h	Difference, %
1.0	27.8	1.2	29.7	6.8
2.5	22.1	1.5	22.3	0.9
4.5	19.3	0.5	20.7	7.3

3.1.3 Comparison of the simulated and measured temperature history of individual chickens within a tray.

To investigate the performance of the chicken freezing model at specific locations, the experimental and simulated cooling curves were separated on a per chicken basis. The comparisons of individual chicken breast and chicken cavity temperature profiles at 1 m s^{-1} are shown in Fig. 7. Similar comparisons at 2.5 m s^{-1} and 4.5 m s^{-1} are shown in Figs. 8 and 9, respectively. For the chickens at the corner of the tray (chicken Numbers 1, 5 and 6, Fig. 2) where the thermocouples were close to the contacting points between chickens and the liner bag, the effect of the artificial air gap used in the simulation (which increases the resistance to heat transfer) is most obvious. That is most likely the reason for the under-prediction of the temperature drop of the breast and cavity of these chickens.

The air gap between the top surfaces of chicken Numbers 2, 3, 4, 7 and 8 and the liner in the model can be matched to the presence of thermocouple wires on the top surfaces of the chickens in the experiments (Fig. 2). In these chickens, the agreement between simulated and measured temperature history is better for the breast compared to the cavity location. It should be noted again that the chicken cavity geometry was represented by an ellipsoid rather than their real shape, as derived via CT scanning. In addition, the numerical cavity temperature was monitored by the average temperature of the air volume inside the cavity instead of a single point temperature. Therefore, some error in cavity temperature predictions would be expected. Moreover, it can be hypothesized that the predictions at the breast location, which is closer to the

chicken surface than the cavity, are less affected by the uncertainties in thermal properties. Hence, the predicted temperatures at these locations closely follow the experimental histories.

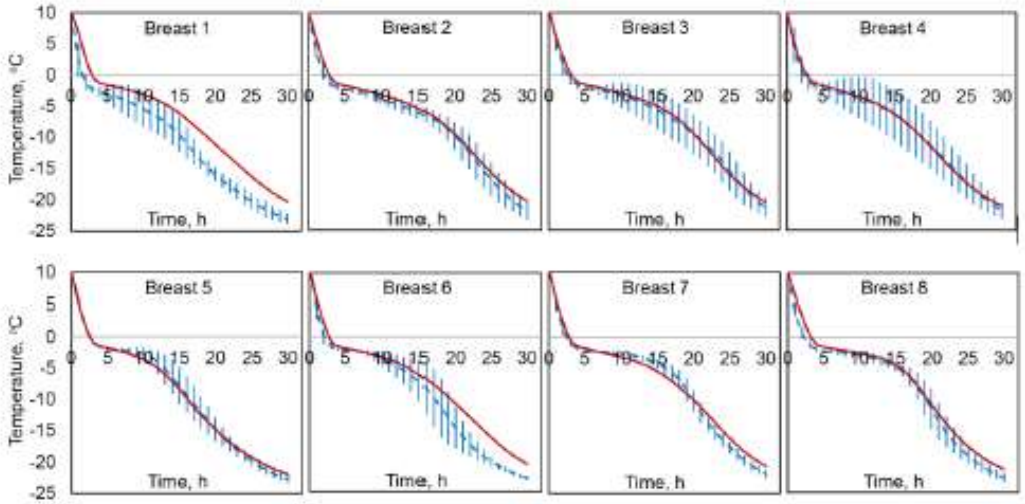

a)

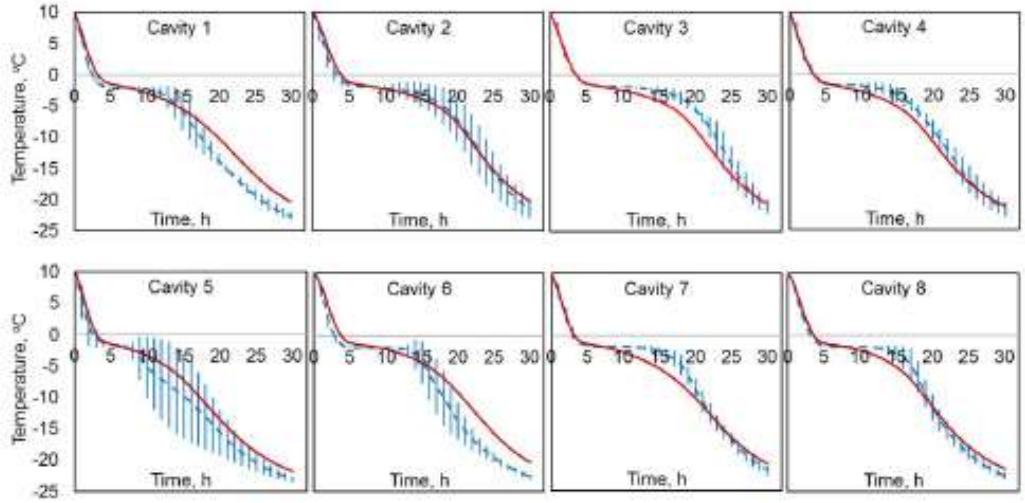

b)

Figure 7: Predicted and experimental temperature history of individual a) chicken breasts and b) chicken cavities at the air velocity of 1 m s^{-1}. The numerical temperatures are depicted in red continuous lines; measured values are depicted in blue dash lines

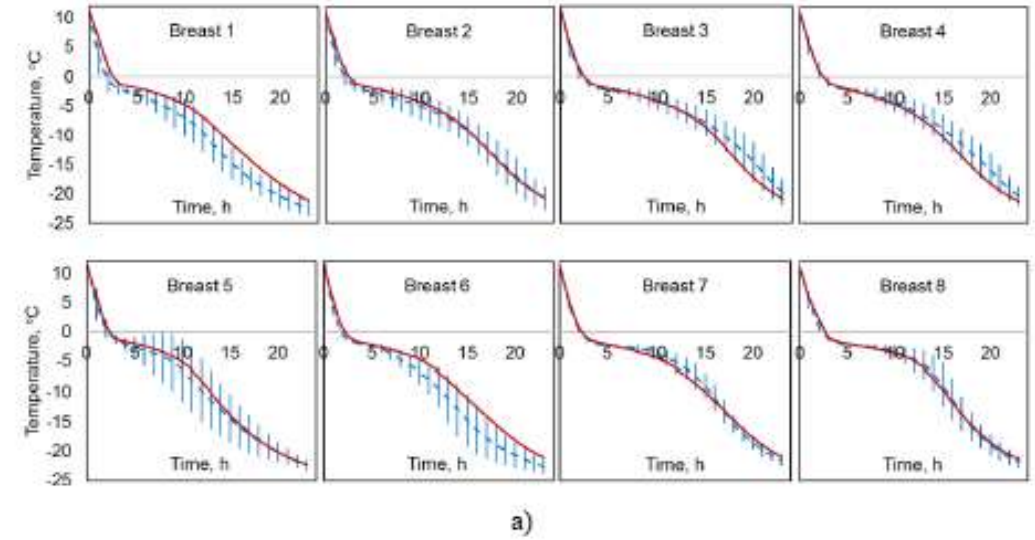

a)

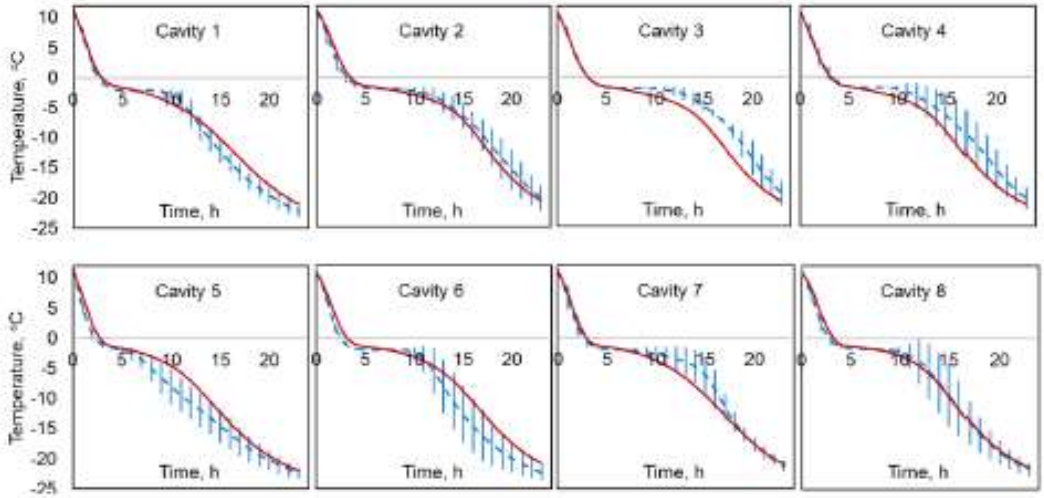

b)

Figure 8: Predicted and experimental temperature history of individual a) chicken breasts and b) chicken cavities at the air velocity of 2.5 m s^{-1}. The numerical temperatures are depicted in red continuous lines, measured values are depicted in blue dash lines

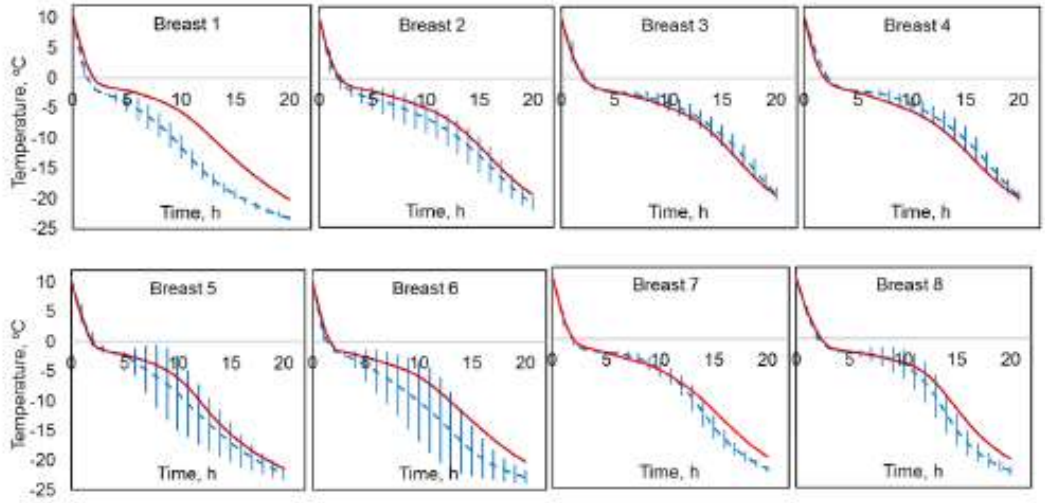

a)

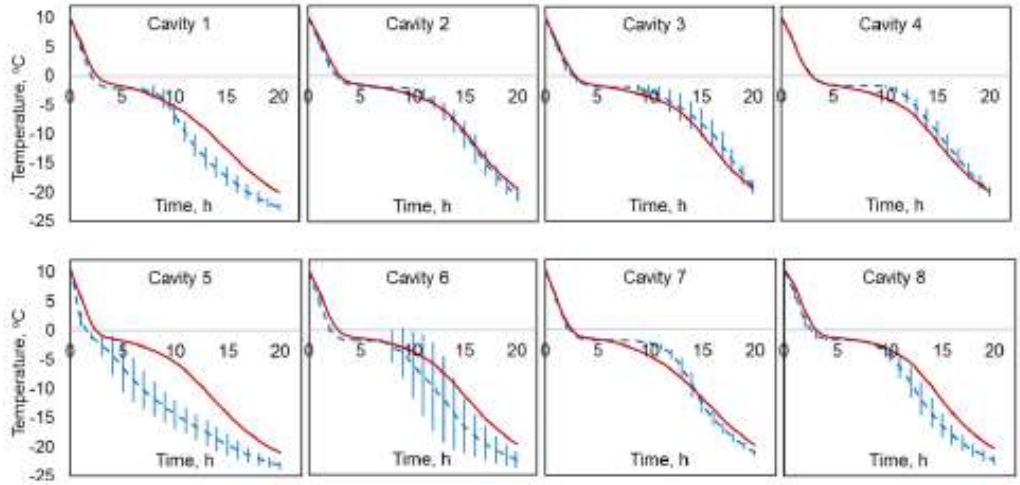

b)

Figure 9: Predicted and experimental temperature history of individual a) chicken breasts and b) chicken cavities at the air velocity of 4.5 m s^{-1}. The numerical temperatures are depicted in red continuous lines, measured values are depicted in blue dash lines

3.2 Effect of operating conditions on freezing time

Having been experimentally validated, the numerical model was used to calculate freezing times under different operating conditions as presented in Fig. 10. For the purposes of this comparison, 'freezing time' is defined as the time taken by the average temperature of chicken cavity to reach -18°C.

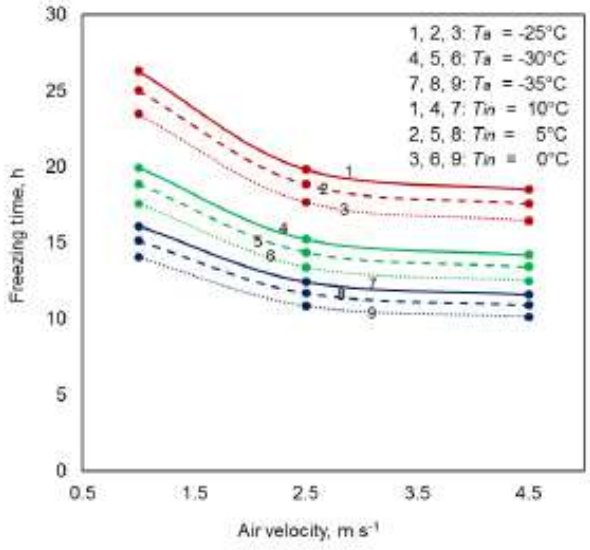

Figure 10: Effect of operating conditions on freezing time of bulk-packed whole chickens

Fig. 10 shows that the impact of increasing the cooling air velocity from 1.0 m s^{-1} to 2.5 m s^{-1} on the freezing time was greater than that when it was raised from 2.5 m s^{-1} to 4.5 m s^{-1}, indicating that the relationship between the airflow rate and cooling rate is diminishing. Changing the air temperature from -25°C to -30°C made the freezing time decrease by 4.9 hours on average, while the reduction was only 3.0 hours when the air temperature dropped from -30°C to -35°C. Decreasing the initial chicken temperature from 10°C to 5°C or from 5°C to 0°C resulted in approximately 1 hour faster cooling.

The numerical model can be used to develop a new dimensionless correlation for the freezing of chickens. First, the Biot number was calculated. The predicted average heat transfer coefficients at the inlet air velocity of 4.5 m s^{-1}, 2.5 m s^{-1} and 1 m s^{-1} were 19.3 W $m^{-2}K^{-1}$, 14.0 W $m^{-2}K^{-1}$ and 8.0 W $m^{-2}K^{-1}$ respectively (they were not significantly affected by the initial drumstick temperature and cooling air temperature). The Biot number of a tray of drumsticks in forced-air freezing was therefore calculated by Eq. 2:

$$Bi = \frac{hL}{k} \tag{2}$$

where k is the average thermal conductivity of chicken at the tested initial temperatures (0.48 W $m^{-1}K^{-1}$) and L is the characteristic length determined by volume divided by surface area of a tray of chicken (0.04 m). Substituting these values into Eq.2 yields Bi = 0.66, 1.17 and 1.60 at air

velocities of 1 m s^{-1}, 2.5 m s^{-1} and 4.5 m s^{-1} respectively. Next, the dimensionless Stefan number was calculated from Eq. 3 (Pham, 2014):

$$St = \frac{c_f(T_f - T_a)}{\Delta H_{10}} \quad (3)$$

where c_f is the specific heat of chicken at -18°C, (2697 J kg^{-1} K^{-1}); T_f is the initial freezing temperature (-1.7°C, observed from temperature history of chickens in these experiments); T_a is the cooling air temperature (-25°C, -30°C or -35°C) and ΔH_{10} is the enthalpy change of the product between T_f and -10°C (246324 – 75353 = 170971 J kg^{-1}). ΔH_{10} is used instead of the latent heat of freezing to calculate the Stefan numbers (Pham, 2014), since the latent heat is very difficult to measure independently of the sensible heat. Eq.3 yields St = 0.36, 0.44, 0.52 at the cooling air temperature of -25°C, -30°C and -35°C, respectively.

The effects of operating conditions on freezing time can be expressed as a function of Bi, St and the dimensionless temperature θ as:

$$Fo = 1.765\, Bi^{-0.399} St^{-0.672} \theta^{-0.412} \quad (4)$$

where Fo is the dimensionless freezing time, $Fo = \alpha t/L^2$; α is the average thermal diffusivity of chicken at the tested initial temperatures determined from the thermal properties model (1.34×10^{-7} m^2 s^{-1}); t (s) is the freezing time and $\theta = (-18\text{-}T_a)/(T_{in} - T_a)$.

The R^2 square value of Eq. 4 was 0.99, indicating a good fit for the correlation equation to the simulation data. This correlation can be used to predict the processing time in forced air freezing of bulk-packed chickens in freezing tunnels where the packages are similar in design to the one considered in this study.

4 Conclusions

This study presented a CFD model for the forced-air freezing of a tray of bulk-packed chickens that was validated against experimental data for a range of cooling air velocities. The geometry of the chickens and packaging was derived empirically via CT scan data, allowing for greater geometrical accuracy than previous models. The mean discrepancy between measured and simulated average temperature prediction was less than 1.3°C, and the maximum difference between measured and simulated SECT was 7.3%. In addition to providing good predictions for average temperatures, the numerical model was also able to predict the temperatures at different

locations within the tray. The model could be used to study the effect of different operating conditions on cooling rate, cooling heterogeneity of chickens during freezing in order to optimise operating conditions and avoid freezing injury.

Acknowledgment

The authors would like to acknowledge the assistance and support of Shane Leath and Robert Wieliczko at AgResearch Ltd, Robert Kemp of Robert Kemp Consulting Ltd, and Ross Clarke and Dave Smitheram both formerly at MilMeq. This work has received funding from Vietnamese government scholarship for Duy Hoang's PhD study.

References

Ambaw, A., Mukama, M., & Opara, U. L. (2017). Analysis of the effects of package design on the rate and uniformity of cooling of stacked pomegranates: Numerical and experimental studies. *Computers and Electronics in Agriculture, 136*, 13-24.

ASHRAE, A. H. (2006). Refrigeration. *American Society of Heating, Refrigerating and Air-Conditioning Engineers, Atlanta, GA*

Carson, J. K., Lovatt, S. J., & Hoang, D. K. (2018). *Improved prediction of thermal conductivity of frozen foods*. Paper presented at the 3rd International conference on Food Properties (ICFP2018), Sharjah, United Arab Emirates

Cengel, Y. A., & Ghajar, A. J. (2011). *Heat and mass transfer: fundamentals and applications*

Datta, A. (2007). Porous media approaches to studying simultaneous heat and mass transfer in food processes. I: Problem formulations. *Journal of food engineering, 80*(1), 80-95.

Defraeye, T., Lambrecht, R., Tsige, A. A., Delele, M. A., Opara, U. L., Cronjé, P., . . . Nicolai, B. (2013b). Forced-convective cooling of citrus fruit: package design. *Journal of Food Engineering, 118*(1), 8-18.

Defraeye, T., Verboven, P., & Nicolai, B. (2013a). CFD modelling of flow and scalar exchange of spherical food products: Turbulence and boundary-layer modelling. *Journal of Food Engineering, 114*(4), 495-504.

Ferrua, M. J., & Singh, R. P. (2009). Modeling the forced-air cooling process of fresh strawberry packages, Part I: Numerical model. *International Journal of Refrigeration, 32*(2), 335-348.

Fluent. (2017). 18.1, Ansys Fluent User Guide: Inc.

Gowda, B. S., Narasimham, G., & Murthy, M. K. (1997). Forced-air precooling of spherical foods in bulk: a parametric study. *International journal of heat and fluid flow, 18*(6), 613-624.

Gruyters, W., Verboven, P., Diels, E., Rogge, S., Smeets, B., Ramon, H., . . . Nicolaï, B. (2018). Modelling Cooling of Packaged Fruit Using 3D Shape Models. *Food and Bioprocess Technology, 11*(11), 2008-2020.

Hoang, D. K., Lovatt, S. J., Olatunji, J. R., & Carson, J. K. (2020). Experimental measurement and numerical modelling of cooling rates of bulk-packed chicken drumsticks during forced air freezing *International Journal of Refrigeration (accepted manuscript)*

Hoang, D. K., & Nguyen, D. V. (2013). *Effective Specific Heat for Camranh Mango*. Paper presented at the The 3rd International Conference on Sustainable Energy, "RISE towards a Green Future", Ho Chi Minh City, Vietnam

James, C., Vincent, C., de Andrade Lima, T., & James, S. (2006). The primary chilling of poultry carcasses—a review. *International Journal of Refrigeration, 29*(6), 847-862.
Jimenez, S., Salsi, M., Tiburzi, M., Rafaghelli, R., & Pirovani, M. (1999). Combined use of acetic acid treatment and modified atmosphere packaging for extending the shelf- life of chilled chicken breast portions. *Journal of applied microbiology, 87*(3), 339-344.
Mannapperuma, J. D., Singh, R. P., & Reid, D. S. (1994). Effective surface heat transfer coefficients encountered in air blast freezing of whole chicken and chicken parts, individually and in packages. *International journal of refrigeration, 17*(4), 263-272.
North, M. F. (2000). *Prediction of chilling rates for food product packages: PhD thesis, Massey University, New Zealand,* .
O'Sullivan, J., Ferrua, M. J., Love, R., Verboven, P., Nicolaï, B., & East, A. (2016). Modelling the forced-air cooling mechanisms and performance of polylined horticultural produce. *Postharvest Biology and Technology, 120*, 23-35.
Otsu, N. (1979). A Threshold Selection Method for Gray Level Histograms". IEEE Transactions on System, Man and Cybernetics: January.
Pham, Q. T. (2006). Modelling heat and mass transfer in frozen foods: a review. *International Journal of Refrigeration, 29*(6), 876-888.
Pham, Q. T. (2014). *Food freezing and thawing calculations*. New York: Springer.
Riedel, L. (1957). Calorimetric investigation of the meat freezing process. *Kaltetechnik, 9*(2), 38.
Roache, P. J. (1997). Quantification of uncertainty in computational fluid dynamics. *Annual review of fluid Mechanics, 29*(1), 123-160.
Slicer. (2019). *Slicer 4.10.2 released.* Retrieved from https://www.slicer.org/
Smitheram, D. (2018). *Design engineer for Milmeq, Personal communication.*
Sweat, V. E., Haugh, C., & Stadelman, W. (1973). Thermal conductivity of chicken meat at temperatures between− 75 and 20° C. *Journal of food science, 38*(1), 158-160.
ThePoultrySite. (2014). *GLOBAL POULTRY TRENDS 2014.* Retrieved from https://thepoultrysite.com/articles/global-poultry-trends-2014-poultry-set-to-become-no1-meat-in-asia
Walters, R. E., & May, K. (1963). Thermal conductivity and density of chicken breast muscle and skin. *Food Technology, 17*(6), 808-&.
Zilio, C., Righetti, G., Pernigotto, G., & Longo, G. A. (2018). Analysis of the freezing time of chicken breast finite cylinders. *International Journal of Refrigeration, 95*, 38-50.

Manuscript ID: 450
DOI: 10.18462/iir.icr.2019.0450

Numerical heat transfer model for industrial chilling installations

Duy K. HOANG [a], Simon J. LOVATT [a], Jamal R. OLATUNJI [b], James K. CARSON [a]

[a] University of Waikato, Private Bag 3105, Hamilton 3240, New Zealand
[b] Massey University, Private Bag 11222, Palmerston North 4442, New Zealand

ABSTRACT

A computational fluid dynamics (CFD) simulation was developed to model heat transfer of six blocks of agar in a forced air chilling process. The flow field was solved at steady-state and decoupled from the heat transfer processes. The six blocks of agar were placed in a polystyrene test chamber that mimics the airflow and product arrangement in an industrial cheese chilling tunnel. Temperatures were measured at the surfaces and the geometric centre of the tested blocks of agar. Good agreement was observed between predicted and experimental data. The local heat transfer coefficient across blocks of agar surface varied by a factor of five at the high air velocity.
Keywords: CFD, heat transfer, chilling, industrial application.

1. INTRODUCTION

Food technology continues to develop as new refrigeration equipment becomes available and as consumer preferences continue to change (Bogh-Sorensen, 2006). On the industrial scale, food refrigeration equipment is often made to order for a given end user, and may be designed either for a single type of product or multiple products. With such a high degree of customisation in modern refrigeration equipment, it is necessary to have a design optimisation tool to evaluate the performance of the refrigeration system. The rate of cooling for a given chilling operation depends on the refrigeration air temperature and airflow characteristics (turbulence intensity, velocity), packaging, and packing arrangement, as well as the dimensions, morphology and physical properties of the food product (ASHRAE, 2006; O'Sullivan et al., 2014).

The experimental assessment of the cooling performance of different package systems is not only costly and time consuming, but also limited in scope. The growth of computer power in recent years has led to an increased use of numerical models to the predict airflow patterns and cooling profiles of food products during forced-air cooling (Defraeye, Verboven, & Nicolai, 2013; Ferrua & Singh, 2009; Gruyters et al., 2018; Kuffi et al., 2016; O'Sullivan et al., 2016). The use of numerical modelling provides detailed information on the local airflow behaviour and temperature profile within the product at different operating conditions. This assists the design process and improves cooling performance of food processing equipment.

This paper details a CFD based numerical model for six blocks of agar in a chilling tunnel. The model was then validated using measured temperatures profile of agar at different air velocities.

2. MATERIALS AND METHODS

2.1 Experiments

Chilling experiments were conducted at AgResearch Ltd. Six blocks of agar gel (food analogue) were place in a polystyrene test chamber (PTT) (Fig. 1a) which was in turn in an environmental testing chamber (ETC). A transition section (Fig. 1b) was created to guide the air flow from the inlet

through the product due to suction created by a fan at the tunnel outlet. The experimental system allowed for precise control of the temperature and air velocity of the cooling air passing through the PTT.

Figure 1a: The Styrene Test Chamber

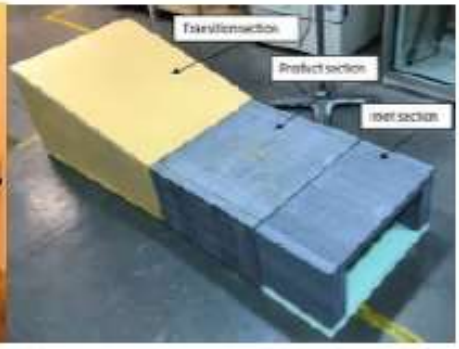

Figure 1b: The transition section

Six blocks of agar were placed in the PTT, arranged (Fig. 2) to create an airflow pattern similar to an industrial cheese chilling tunnel. The four blocks on the two sides of the central pair were cut by the symmetry plane and were bordered by insulated walls to reduce the air flow cross-section. The dimensions of the two test blocks in the middle were 135 x 210 x 270 mm, while the dimensions of the half blocks on the sides were 135 x 105 x 270 mm.

Figure 2: Six blocks of agar arrangement

Temperatures were measured with T-type thermocouples connected to a Keysight 24982A data acquisition unit and were recorded every 60 seconds. Fig. 3 indicates the thermocouple positions in the agar blocks. Thermocouple Numbers 1 and 11 measured the cooling air temperature. The multipoint thermocouple probes supporting thermocouple Numbers 3, 4, 5 and 13, 14, 15 were placed along the shortest axes of Block A and Block B respectively. Thermocouple Numbers 4 and 14 were at the geometric centre of the blocks and the two other thermocouples on the multipoint probes were 2 cm from the geometric centre. The other thermocouples were at the middle of each surface of the agar blocks. The thermocouples were calibrated with an ice-point reference prior to the experiments.

Prior to each chilling trial the six blocks of agar were equilibrated at 20 °C for 24 hours. The ETC temperature was set and maintained at 0 °C during the trials. Three different inlet air velocities (1 m s^{-1}, 3 m s^{-1}, 4.5 m s^{-1}) were tested, and each trial was repeated three times.

Air velocity was measured by a hot-wire anemometer (Dantec 54N60 FlowMaster) before and after each trial at the inlet of the tunnel and at 2 cm above the top surface of the test blocks. The sample time of each velocity measurement was five minutes. The air velocity was kept constant during

each experiment. The inlet and outlet pressures of the airflow through the PTT were measured before and after each trial using an inclined fluid manometer (RS Pro, RS 730-2937)

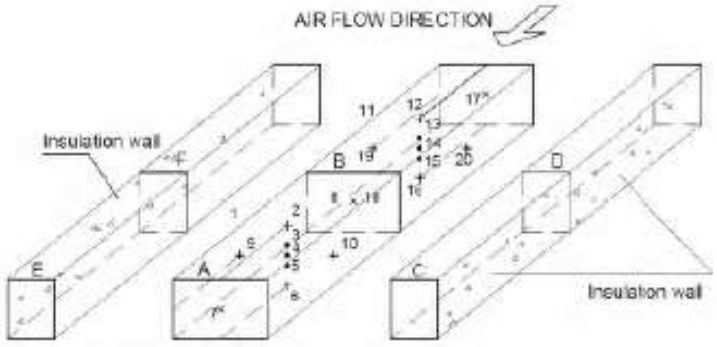

Figure 3: Thermocouples position in the agar chilling trials

2.2 Numerical CFD Model

2.2.1 Geometrical model

Based on a symmetry plane, the computational domain of the agar chilling model was reduced by a factor of 2 (Fig. 4). The geometrical model was created using Ansys Design Modeller, with half of the centre blocks, and the two half-blocks on the left side included in the geometrical model.

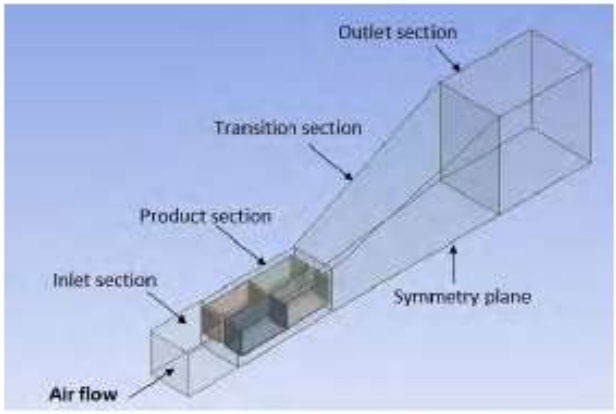

Figure 4: The computational domain of agar chilling

The inlet boundary was located 30 cm upstream of the product section and the outlet boundary was 155 cm downstream of the product section to prevent the inlet and outlet boundary conditions from influencing the airflow distribution over the product section.

2.2.2 Numerical setup

Heat transfer mechanisms during agar chilling include: forced convection between the refrigerated air flow and the blocks of agar surface, conduction inside the blocks of agar, and radiation between the blocks of agar surface and the insulated walls. Typically, in the forced air cooling of food product, the influence of radiation is expected to be small compared to the convective heat transfer (Defraeye, Lambrecht, et al., 2013). Therefore, radiation was neglected in the CFD model.

The momentum and energy transport equations were solved using the Reynolds-averaged Navier-Stokes equations (Versteeg & Malalasekera, 2007). The turbulence model used was the standard k-ε combined with the Enhanced Wall Treatment function.

The thermo-physical properties of the agar, plastic boxes and air are listed in Table 1, and were kept constant throughout the simulation, since they have negligible dependence on temperature in the range between 0°C (cooling air temperature) and 20°C (the initial agar temperature) (Ferrua & Singh, 2009; O'Sullivan et al., 2016). Air properties were evaluated at 0°C while agar and plastic properties were evaluated at 20 °C.

Table 1. Material thermo-physical properties

Materials	Density kg m $^{-3}$	Specific heat J kg $^{-1}$K $^{-1}$	Thermal cond, Wm^{-1}K^{-1}	Dynamic Viscosity kg m^{-1} s $^{-1}$	Reference
Air	1.292	1006	0.02364	1.729 x 10^{-5}	(Yunus & Afshin, 2011)
Plastic	1190	1470	0.2	-	(EngineeringToolbox)
Agar	998	4182	0.543	-	(Zhang et al., 2010)

A hybrid mesh with tetrahedral and hexahedral elements was generated using ANSYS mesh generation software. The element size in the product section was 10 mm while the maximum face size was kept as default (36.5 mm). The fluid region close to the agar block surface was meshed with a small mesh size. From the surface of the agar blocks outwards, 10 layers of hexahedral element were placed with the first layer thickness of 0.1 mm and the growth rate of 1.2. A mesh sensitivity study was performed by running simulations at three different mesh sizes to estimate the spatial discretization error from the difference in the average surface heat transfer coefficient (*SHTC*) of two test blocks of agar (Table 2).

The mesh independent solution was determined by Richardson extrapolation (Roache, 1997), and the value of the average *SHTC* was 42.44 Wm^{-2}K^{-1}. The error of the average *SHTC* for a mesh size of 0.1 mm of 1.2% was considered sufficiently low. Therefore, the mesh with 273258 elements was chosen for these computations.

Table 2. Effect of different mesh size on average SHTC of two test blocks of agar

Mesh size on product surface, mm	Number of elements	Y plus (average)	SHTC (average), W m^{-2} K^{-1}
0.4	262923	5.06	46.05
0.2	266901	2.52	44.12
0.1	273258	1.25	42.94

The surfaces of the blocks of agar were modelled as no-slip walls with zero roughness. A zero heat flux boundary condition was used for the side walls of the PTT. The coupled thermal condition was applied for the interfaces between air flow and plastic, plastic and agar, and plastic and plastic. The inlet of the computational domain was modelled with a uniform velocity boundary condition with a turbulence intensity of 1%. The outlet of the computational domain was defined as a pressure outlet with an underpressure measured by the inclined manometer to represent the pressure drop created by the suction fan. The outlet pressure of -85, -35 and -5 Pa produced inlet velocities of 4.5 m s^{-1}, 3 m s $^{-1}$ and 1 m s^{-1}, respectively.

In this study, the simulations were performed with the ANSYS fluent 18.2 software which uses the finite volume technique. Second-order discretisation was used throughout. The SIMPLE algorithm was used for pressure-velocity coupling. To speed up the simulation, the momentum equations were decoupled from heat transfer equations. A converged steady-state solution for airflow was used as an initial condition for the transient heat transfer equations. The transient simulation was run with a time step of 60 s. The computational time for 800 minutes cooling took 33 minutes on a 64 bit Intel ® Xeron ® CPU E5-1620, 3.5 GHz, 16 GB RAM.

3. RESULTS AND DICUSSIONS

3.1 Local surface heat transfer coefficient

In this study, the surface heat transfer coefficient (*SHTC*) was calculated from Eq. (1):

$$SHTC = \frac{q_{wall}}{T_{in} - T_{air}} \quad \text{Eq. (1)}$$

where q_{wal} (W m^{-2}) is the steady state wall heat flux, T_{in} (K) is the initial temperature of the blocks of agar, and T_{air} (K) is the cooling air temperature. Fig. 5 shows a contour plot of the heat transfer coefficient on the surface of two test blocks of agar, at the inlet air velocity of 4.5 m s^{-1}. The *SHTC* across the agar block surface varied by factor of 5, with the maximum value at the four corners of the surface on the upstream side and minimum values at the opposite surface. The surface-averaged *SHTC* over the agar blocks at inlet air velocities of 1 m s^{-1} , 3 m s^{-1}, and 4.5 m s^{-1} were 15.3 W m^{-1} K^{-2}, 32.5 W m^{-1} K^{-2} and 42.9 W m^{-1} K^{-2} respectively.

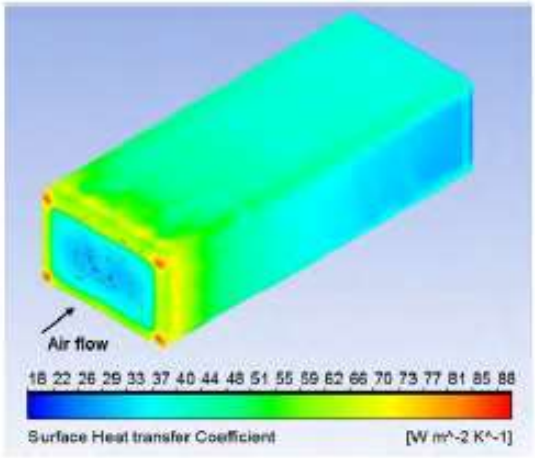

Figure 5: Surface heat transfer coefficient distribution on the surface of two test blocks of agar at the inlet air velocity = 4.5 m s^{-1}

3.2 Comparison of measure and predicted temperature

3.2.1 Uncertainty analysis of the empirical data

The temperature profile of the agar blocks of was computed by averaging the temperature history of the three replicates of the experimental trials Eq. (2):

$$\overline{T_i}(t) = \frac{\sum_{j=1}^{n} T_{i,j}(t)}{n} \quad \text{Eq. (2)}$$

The experimental standard deviation in $\overline{T_i}(t)$ at 95% confidence level and a normal distribution, was computed by Eq. (3):

$$P_{\overline{T_i}} = t_{n-1,0.025} \times \frac{1}{\sqrt{n}} \left[\frac{1}{n-1} \sum_{j=1}^{n} \left(\overline{T_i} - T_{i,j} \right)^2 \right]^{1/2} \quad \text{Eq. (3)}$$

In general, the standard deviation of all monitored temperatures was lower than 0.5°C, except for the surface temperatures (T8 and T18) at the interface of the two test blocks. This could be explained by the imperfect thermal contact of the two test blocks, as there was a small air gap between them.

3.2.2 Comparison of measured and predicted temperatures

Fig. 6 shows the comparison between the predicted and experimental temperatures of the two test blocks, in which Block B was at the front and Block A was at the rear along the flow direction. Overall, the model predictions fit well with the experimental data.

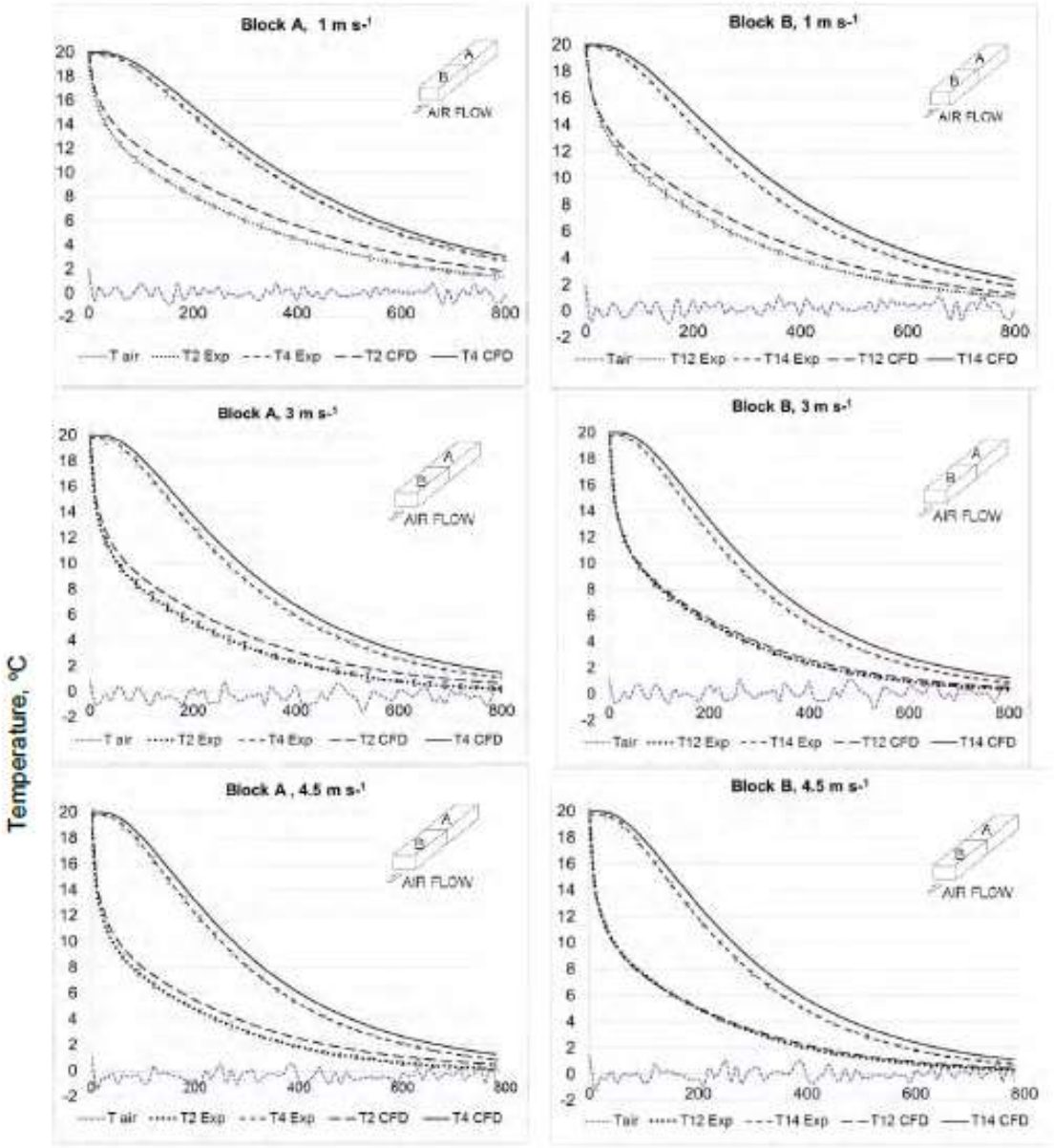

Figure 6: Comparison between predicted and measured temperatures in the two test blocks

For the three air velocities tested, the mean absolute differences between the measured and predicted temperatures (ΔT_{mean}) during the chilling process were lower than 1.0 °C. At the lowest inlet air velocity (1 m s^{-1}), the largest difference between predicted and measured temperatures was at the top surface (T2 and T12) with ΔT_{mean}= 0.98 °C and 0.77 °C, respectively. At the highest

air speed (4.5 m s^{-1}), the largest differences were at the centre temperatures (T4 and T14), with ΔT_{mean}= 0.68 °C and 0.69 °C, respectively.

At low air velocity (low Reynolds number) the contribution of natural convection, and radiation (which were not included in the model) to the overall heat transfer between the air flow and the product surface would have been more significant than that at the high air velocity, which could explain why the agreement between measured and modelled temperature was better at higher air velocities.

Fig. 7 illustrates the predicted temperature differences at the same positions on the surface (T2 vs T12, T10 vs T20) and at the geometrical center (T4 vs T14) of the two test blocks of agar at the inlet air velocity of 4.5 m s^{-1}. The temperature decreased faster in block B (in the front along the air flow direction) than in block A (at the back along the air flow direction). This trend is more obvious at the surface temperatures at the beginning of the chilling process. This observation was to be expected since the *SHTC* decreased along the flow direction (Fig. 5). At the end of the process, the driving force of the heat transfer process (temperature difference between the product surface and the refrigerated air) was decreased and the temperature of the two blocks was almost the same.

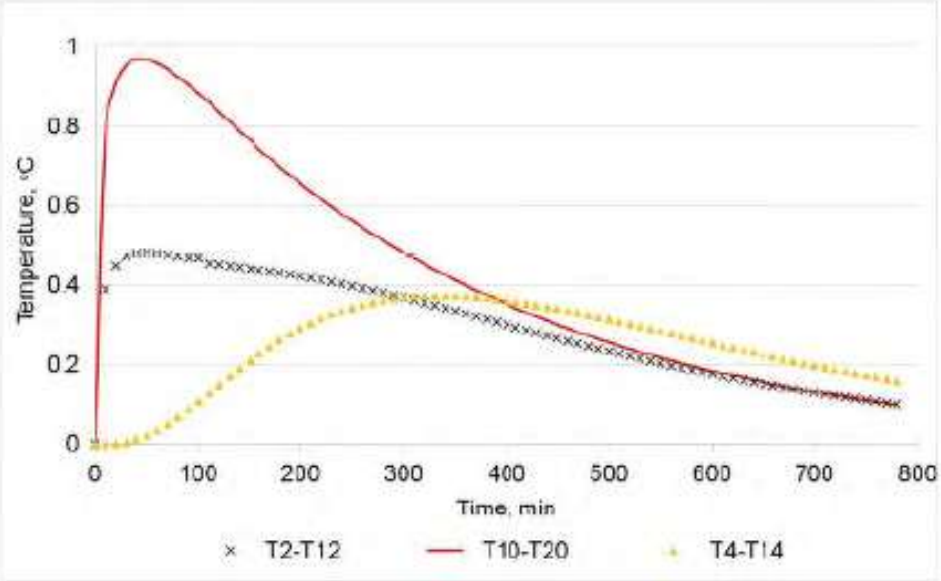

Figure 7: Temperature difference of the two test blocks at the same positions at the inlet air velocity of 4.5 m s^{-1}

5. CONCLUSIONS

The use of standard k-ε turbulence model with the Enhanced Wall Treatment function can predict, to within 1 °C, the forced air chilling of agar blocks in an arrangement that was representative of an industrial cheese chiller. The model presented in this study can be used to evaluate the cooling performance at different operating conditions of the cheese chilling which has similar airflow pattern and products arrangement as the experiment.

NOMENCLATURE

$P_{\overline{T}}$	Standard deviation in $\overline{T_i}(t)$ (K)	T_{air}	The cooling air temperature (K)
q_{wall}	The steady state wall heat flux (W m^{-2})	$\overline{T_i}$	Average temperature at thermocouple

			number *i*-th (K)
t	Time (s)	T_{ij}	Temperature thermocouple number *i*-th in the *j*-th trial (K)
$t_{n-1,\ \alpha/2}$	Student's t-statistic with (*n*-1) degrees of freedom at a (1-α) confidence level	n	Number of the experimental trial, $n = 3$
T_{in}	The initial temperature of the blocks of agar (K)	$SHTC$	Surface heat transfer coefficient (W m^{-2} K^{-1})

REFERENCES

ASHRAE, A. H. (2006). Refrigeration. *American Society of Heating, Refrigerating and Air-Conditioning Engineers, Atlanta, GA*

Bogh-Sorensen, L. (2006). *Recommendations for the processing and handling of frozen foods* (4th ed.): International Institute of Refrigeration, Paris.

Defraeye, T., Lambrecht, R., Tsige, A. A., Delele, M. A., Opara, U. L., Cronjé, P., . . . Nicolai, B. (2013). Forced-convective cooling of citrus fruit: package design. *Journal of Food Engineering, 118*(1), 8-18.

Defraeye, T., Verboven, P., & Nicolai, B. (2013). CFD modelling of flow and scalar exchange of spherical food products: Turbulence and boundary-layer modelling. *Journal of Food Engineering, 114*(4), 495-504.

EngineeringToolbox. Thermal Conductivity of common Materials and Gases. Thermal Conductivity of common Materials and Gases

Ferrua, M., & Singh, R. (2009). Modeling the forced-air cooling process of fresh strawberry packages, Part I: Numerical model. *International Journal of Refrigeration, 32*(2), 335-348.

Gruyters, W., Verboven, P., Diels, E., Rogge, S., Smeets, B., Ramon, H., . . . Nicolaï, B. (2018). Modelling Cooling of Packaged Fruit Using 3D Shape Models. *Food and Bioprocess Technology, 11*(11), 2008-2020.

Kuffi, K. D., Defraeye, T., Nicolai, B. M., De Smet, S., Geeraerd, A., & Verboven, P. (2016). CFD modeling of industrial cooling of large beef carcasses. *International Journal of Refrigeration, 69*, 324-339. 10.1016/j.ijrefrig.2016.06.013

O'Sullivan, J., Ferrua, M., Love, R., Verboven, P., Nicolaï, B., & East, A. (2014). Airflow measurement techniques for the improvement of forced-air cooling, refrigeration and drying operations. *Journal of Food Engineering, 143*, 90-101.

O'Sullivan, J., Ferrua, M. J., Love, R., Verboven, P., Nicolaï, B., & East, A. (2016). Modelling the forced-air cooling mechanisms and performance of polylined horticultural produce. *Postharvest Biology and Technology, 120*, 23-35.

Roache, P. J. (1997). Quantification of uncertainty in computational fluid dynamics. *Annual review of fluid Mechanics, 29*(1), 123-160.

Versteeg, H. K., & Malalasekera, W. (2007). *An introduction to computational fluid dynamics: the finite volume method*: Pearson Education.

Yunus, C. A., & Afshin, J. G. (2011). Heat and mass transfer: fundamentals and applications. *Tata McGraw-Hill, New Delhi, India*

Zhang, M., Che, Z., Chen, J., Zhao, H., Yang, L., Zhong, Z., & Lu, J. (2010). Experimental Determination of Thermal Conductivity of Water− Agar Gel at Different Concentrations and Temperatures. *Journal of Chemical & Engineering Data, 56*(4), 859-864.

Manuscript ID: 451
DOI: 10.18462/iir.icr.2019.0451

Experimental study on effects of packing arrangement and plastic liner bag on freezing rates of bulk packed chicken drumsticks

Duy K. HOANG[a], Jamal R. OLATUNJI[b], Simon J. LOVATT[a], James K. CARSON[a]

[a] University of Waikato, Private Bag 3105, Hamilton 3240, New Zealand
[b] Massey University, Private Bag 11222, Palmerston North 4442, New Zealand

ABSTRACT

Accounting for voids within food packages remains a significant challenge for designers of industrial refrigeration equipment. The aim of this work was to assess the impact of the packing arrangement (regular arrangement versus random/irregular arrangement) and the presence of a carton liner bag on freezing rates of trays of chicken legs ('drumsticks'). The freezing experiments showed that when contained within the liner bag, the packing arrangement of the chicken drumsticks within the tray did not have a significant impact on freezing rate for any of the air velocities investigated based on a 95 % confidence interval. However, the presence of the liner bag had a significant impact on freezing times, increasing them by more than a factor of three at high air velocity (4.3 m s^{-1}).

Keywords: Industrial Refrigeration, Food Freezing, Chicken

1. INTRODUCTION

Food freezing technology continues to develop as new refrigeration equipment becomes available and as consumer preferences continue to change (Bogh-Sorensen, 2006; Singh & Heldman, 2009) On the industrial scale, food refrigeration equipment is often made to order for a given end user, and may be designed either for a single type of product or multiple products. While modular, bulk-produced refrigeration components such as compressors and condensers may be incorporated into the overall refrigeration installation, the cold side (evaporator) is likely to be highly customised. With such a high degree of customisation, it is important that the freezing process may be modelled accurately to allow for design optimisation.

Factors affecting freezing time of food products include the refrigeration air temperature and air-flow characteristics (turbulence intensity, velocity), packaging, and packing arrangement, as well as the dimensions, morphology and physical properties of the food product (ASHRAE, 2006; O'Sullivan et al., 2014). Many primary (i.e. minimally processed) products such as meat/poultry cuts, fruit and vegetables have irregular shapes and, when packed in bulk (e.g. within cartons, bag or trays) air voids typically exist between individual food items, which can have a significant effect on freezing rates. Despite research to account for the effect of voids on heat transfer rates (Datta, 2007; James, Vincent, de Andrade Lima, & James, 2006; North, 2000; O'Sullivan, 2016; O'Sullivan et al., 2016) a general approach for dealing with the problem has yet to be established. As such, accounting for voids within food packages remains a significant challenge for designers of industrial refrigeration equipment (Smitheram, 2018).

While several research articles report results on the refrigeration of whole chicken carcasses (James et al., 2006; Mannapperuma, Singh, & Reid, 1994), there does not appear to be as many data for chicken pieces (portions) and none on chicken legs (commonly referred to as 'drumsticks') in particular. Chicken legs represent an interesting problem due to their shape and the significance

of bone, which has the potential to act as a conduction pathway to the thermal centre of the drumstick. Air voids of different shapes and sizes exist when drumsticks are packed in bulk, due to the irregular shapes of the drumsticks. On the industrial scale, chicken portions are typically cooled within a plastic carton liner bag, which has the effect of restricting air movement within the voids and also results in a larger air void within the bag on top of the chicken (Delele, Ngcobo, Opara, & Meyer, 2013; O'Sullivan, 2016). This research focused on the effects of air voids in bulk-packed chicken drumsticks on freezing times. The aim was to determine the extent to which the packing arrangement (or structure) of chicken drumsticks (and associated voids) and the presence of a liner bag affect freezing rates.

2. METHODS AND MATERIALS

2.1 Experimental Systems

Freezing trials were conducted in the Environmental Test Chamber (ETC) at AgResearch Ltd, Hamilton, New Zealand. Two polystyrene test tunnels (PTT) 2500 mm long x 720 mm height and 510 mm wide (Fig. 1) each with a variable speed fan at the downstream end and a fine mesh at the upstream end to act as a flow diffuser were used. A transition section was placed inside the PTT to guide the air-flow and reduce the cross sectional area to 300 mm x 510 mm. The experimental setup allowed for precise control of the temperature and velocity of the cooling air being forced through the PTT.

Figure 1: Polystyrene Test Tunnels (PTT) in the Environmental Testing Chamber (ETC)

Cardboard trays, as used by chicken processors, measuring 320 mm x 590 mm x 150 mm with open tops (Fig. 2a) were used in this study. Each tray was loaded with 11.5 kg of drumsticks. In each run, one tray was put in the top tunnel and another tray was put in the bottom tunnel such

that two trials could be run at the same time. In each tunnel a metal platform was used to support the tray of drumsticks. This arrangement allowed the bottom surface of the cardboard tray to be exposed to the cold air.

In the first set of experiments, a tray of regularly arranged drumsticks within the plastic liner (Fig. 2b) was frozen at three different air velocities (1 m s^{-1}, 2.5 m s^{-1}, and 4.3 ms^{-1}). Seventy two drumsticks weighing from 140 g to 190g were arranged in four layers. Eight drumsticks each having a mass of 160 g (the average weight of drumsticks in a tray) distributed along the two diagonals at both high and low, central and peripheral positions were chosen for temperature measurement (Fig. 3). In the second set of experiments, a tray of drumsticks arranged randomly within the liner bag was used (Fig 2c). The drumsticks selected for temperature measurement also weighed 160 g and were carefully placed at similar locations to the measurement positions in the first set of experiments. In the third experiment, a tray of regularly arranged drumsticks without the plastic bag was used (Fig. 2d) and thermocouple placement was selected as for the first set of experiments.

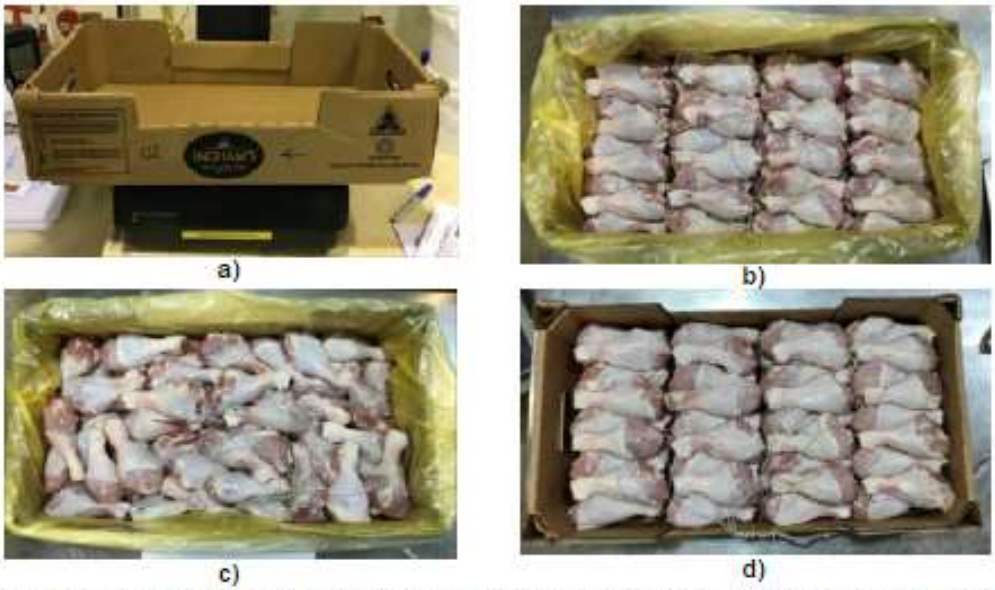

Figure 2: Cardboard trays and chicken used in freezing experiments: a) empty tray, b) regularly arranged drumsticks with liner bag, c) randomly arranged drumsticks with liner bag, d) regularly arranged drumsticks without liner bag

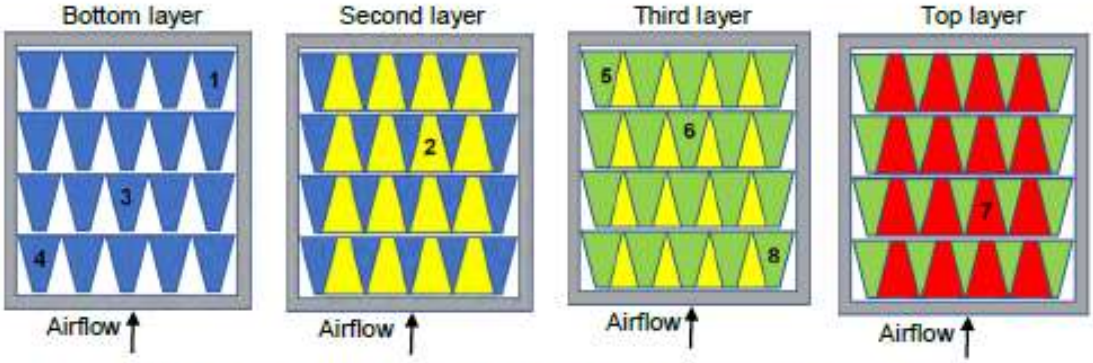

Figure 3: Chicken drumsticks distribution and thermocouple location in a tray

2.2 Measurements

T-type thermocouples were placed at in the thickest part (approximately 3 cm deep, Fig. 4) of the leg at the eight selected locations within the tray. All the thermocouples were calibrated using ice-point reference before and after the measurements. The temperatures were recorded on a Keysight 24982A data acquisition unit every 60 seconds during the freezing trials. The cooling air temperatures above the tray, and the air temperature inside the plastic liner bag were also monitored during the experiments.

The air velocities at the inlet of the PTT and at a position 5 cm above the tray of drumsticks were measured before and after each trial using a hot-wire anemometer (Dantec 54N60 FlowMaster). The sample time for each velocity measurement was five minutes. The air velocity was held constant during the experiment.

Figure 4: Thermocouple placement in chicken drumstick

2.3 Procedure

Chicken drumsticks were purchased fresh from a local retailer on the day of delivery. The drumsticks were then sorted, scaled and positioned individually in the tray and the thermocouples were inserted into the selected drumsticks. The plastic liner was then tied to enclose the drumsticks and thermocouples (other than for the experiments without the plastic liner bag). The loaded trays were then placed in the ETC to equilibrate at 10°C for 24 hours. The drumstick temperatures were monitored during the equilibration process to ascertain when the trays reached uniform temperatures.

All freezing trials started with chicken at uniform initial temperature of 10°C (equilibration temperature) and the ETC air temperature was maintained at -25°C. The inlet air velocity was adjusted to the desired speed (1 m s^{-1}, 2.5 m s^{-1}, or 4.3 ms^{-1}). The thermally equilibrated drumstick trays were placed in the tunnels and the trial was started. Each trial was terminated when all the monitored drumstick temperatures fell below -20°C.

After the freezing process was completed, the drumsticks were thawed for 12 hours, before being re-equilibrated at 10°C. Two subsequent trials were performed on the each batch of drumsticks, with the exception of the eight drumsticks that contained the thermocouples, which were replaced by fresh 160 g drumsticks for each replicate. Thus there were three replicates for each air velocity for each type of experiment (regular arrangement in liner bag, irregular arrangement in liner bag and regular arrangement without liner bag). No drumsticks were used for more than three trials.

3. RESULTS AND DICUSSION

3.1 Uncertainty Analysis

The average temperature profile of a tray of drumsticks during each of the three replicated trials was computed by averaging the temperature history of all monitored drumsticks within the tray (Eq. 1)

$$T_j(t) = \frac{\sum_{i=1}^{N} T_{i,j}(t)}{N} \quad \text{Eq. (1)}$$

The final average-temperature of the tray of drumsticks was computed by averaging the temperature history of the three replicated experimental trials Eq. (2)

$$\overline{T}(t) = \frac{\sum_{j=1}^{n} T_j(t)}{n} \quad \text{Eq. (2)}$$

The experimental standard deviation in $\overline{T}(t)$at a 95% confidence level and a normal distribution of the measurements, was computed by Eq. (3):

$$P_{\overline{T}} = t_{n-1,0.025} \times \frac{1}{\sqrt{n}} \left[\frac{1}{n-1} \sum_{j=1}^{n} \left(\overline{T} - T_j \right)^2 \right]^{\frac{1}{2}} \quad \text{Eq. (3)}$$

In general, the standard deviation of the average temperature of a tray of drumsticks ranged from 0.5°C to 3.0°C except for the case of the experimental data of the irregular arrangement at the inlet air velocity of 4.3 m s^{-1}.

3.2 Temperature profile of individual drumsticks within a tray

Fig. 5 shows the heterogeneity of the freezing process within the tray in case of regularly packed drumsticks at the medium inlet air velocity (2.5 m s^{-1}). The temperature profile of the individual drumsticks were determined by averaging temperature of the three replicated trials. The maximum difference between individual drumsticks increased at the beginning of the process until the first phase change happened in the drumstick number 5, and reach the first peak of 7°C. This value then decreased until the last phase change period started in drumstick number 7, before raised up again and accomplished a second peak of 17°C when the last phase-change period ended in drumstick number 7. The maximum difference temperature declined when the sub-cooling period started at all of the monitored drumsticks.

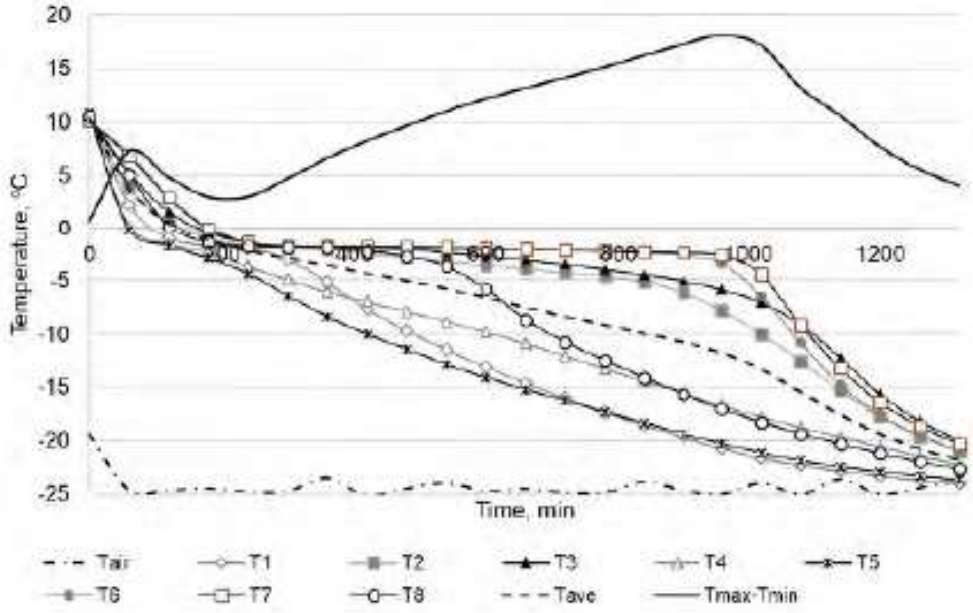

Figure 5: Temperature profile of the monitored drumsticks and the maximum temperature difference between individual drumsticks (the continuous line) within a tray at the air velocity inlet of 2.5 m s^{-1}

3.3 Comparison of Cooling Times between Regular and Irregular Packing of Drumsticks

Fig. 6 shows cooling histories of trays of regularly packed and randomly packed drumsticks, where error bars indicate 95% confidence intervals of the average temperature of the tray. Although the randomly packed drumsticks appeared to have cooled slightly faster on average than the regularly packed drumsticks, the difference between the two packing arrangements was less than the uncertainty in the measurements at both low and high air-speeds. This suggests that the packing arrangement and alignment of the leg-bone within the drumstick did not have a significant impact on freezing time when the drumsticks are contained within the bag. Consequently, it is probable that accounting for packing structure in chicken drumsticks is unnecessary when modelling freezing times.

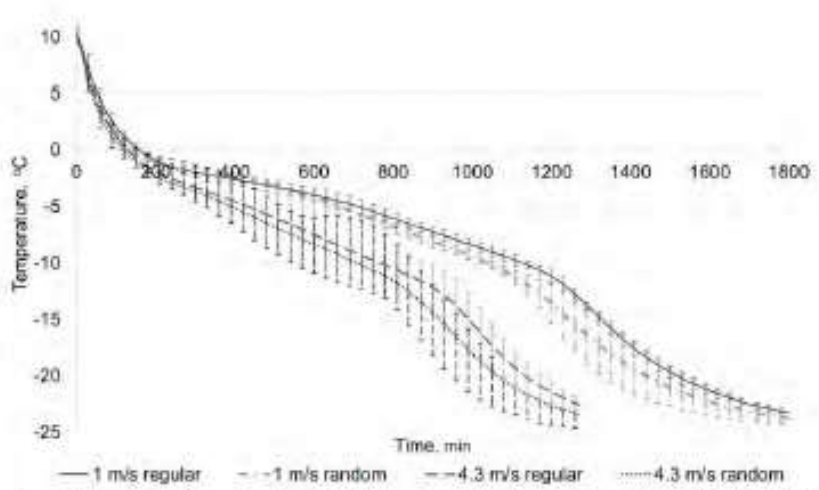

Figure 6: Cooling histories of regularly packed and randomly packed drumsticks at different air velocities

3.4 Comparison of Cooling Times of Regularly Packed Drumsticks with and without Liner Bag

Fig. 7 shows cooling histories of regularly packed chicken drumsticks both with and without the liner bag. As expected, the drumsticks without the liner bag cooled significantly faster than those packed within the liner bag for all three air velocities.

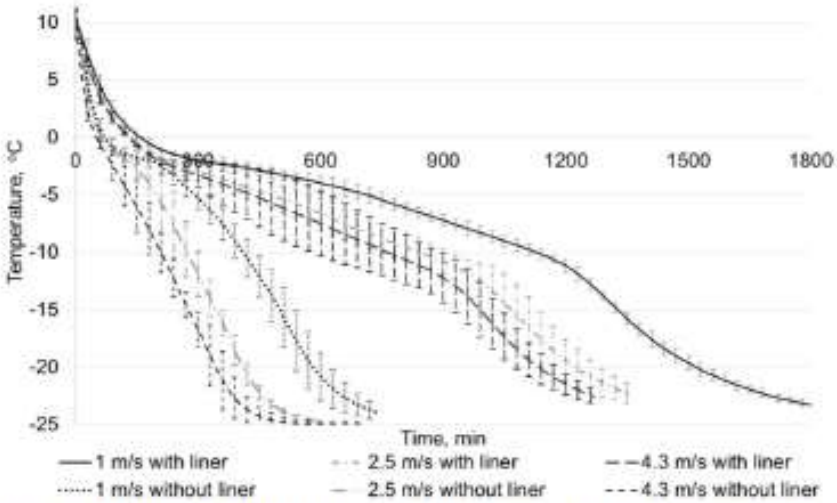

Figure 7: Cooling histories of regularly packed drumsticks with and without the liner bag

In order to quantify the effect of the liner bag on cooling time the seven-eighths cooling time (SECT) (i.e. the time required for the temperature to reach seven eighths of the difference between initial and cooling air temperatures) were calculated, and results are shown in Table 1. The effect of the liner bag on cooling time increases as the air velocity increases, the SECT for the plastic lined chicken more than three times greater than for the unlined case when the air velocity was 4.3 m s^{-1}.

Table 1. Experimental SECT of the tray of drumsticks

Configuration	SECT, min		
	1m s^{-1}	2.5 m s^{-1}	4.3 m s^{-1}
With liner	1520	1250	1160
Without liner	600	420	350

Evaporative cooling would have been much more significant for the chicken without the liner, and hence would have contributed to some of the increase in the cooling rate. However, it was estimated that the effect of evaporation accounted for less than 11 % of the total cooling. The liner bag is required to minimise moisture loss during the refrigeration process, which could have a detrimental impact on product quality, so it is unlikely that processors would remove the bag to increase throughput. However, these results clearly indicate that the presence of the liner bag has a much greater impact on freezing time than the orientation of the chicken drumsticks within the bag. Since the orientation of the drumsticks did not appear to affect freezing time, it is possible that only the total fraction of air voids within the package may be required as a model input, with no requirement to account for size or shape of the air voids.

4. CONCLUSIONS

The freezing experiments showed that the packing structure of the chicken drumsticks within the plastic liner bag did not have a significant impact on freezing rate for any of the air velocities investigated based on a 95% confidence interval. However, the presence of the plastic liner bag increased freezing times by more than a factor of 3 at high air velocities.

NOMENCLATURE

$P_{\bar{T}}$	Standard deviation in $\bar{T}(t)$ (K)	$\overline{T_j}$	Average temperature of a tray of drumsticks during the j-th trial (K)
t	Time (s)	$T_{s,j}$	Temperature of drumstick – s within the tray (K)
$t_{n-1,\,\alpha/2}$	Student's t-statistic with (n-1) degrees of freedom at a (1-α) confidence level	n	Number of the experimental trial, n = 3
$\bar{T}$	Average temperature of a tray of drumsticks (K)		

REFERENCES

ASHRAE, A. H. (2006). Refrigeration. *American Society of Heating, Refrigerating and Air-Conditioning Engineers, Atlanta, GA*.

Bogh-Sorensen, L. (2006). *Recommendations for the processing and handling of frozen foods* (4th ed.): International Institute of Refrigeration, Paris.

Datta, A. (2007). Porous media approaches to studying simultaneous heat and mass transfer in food processes. I: Problem formulations. *Journal of Food Engineering, 80*(1), 80-95.

Delele, M. A., Ngcobo, M. E., Opara, U. L., & Meyer, C. J. (2013). Investigating the effects of table grape package components and stacking on airflow, heat and mass transfer using 3-D CFD modelling. *Food and Bioprocess Technology, 6*(9), 2571-2585.

James, C., Vincent, C., de Andrade Lima, T., & James, S. (2006). The primary chilling of poultry carcasses—a review. *International Journal of Refrigeration, 29*(6), 847-862.

Mannapperuma, J., Singh, R., & Reid, D. (1994). Effective surface heat transfer coefficients encountered in air blast freezing of single plastic wrapped whole turkey. *International Journal of Refrigeration, 17*(4), 273-280.

North, M. F. (2000). *Prediction of chilling rates for food product packages: PhD thesis, Massey University, New Zealand, .*

O'Sullivan, J. (2016). *Significant factors affecting the forced-air cooling process of polylined horticultural produce: PhD thesis. Massey University, New Zealand.*

O'Sullivan, J., Ferrua, M., Love, R., Verboven, P., Nicolaï, B., & East, A. (2014). Airflow measurement techniques for the improvement of forced-air cooling, refrigeration and drying operations. *Journal of Food Engineering, 143*, 90-101.

O'Sullivan, J., Ferrua, M. J., Love, R., Verboven, P., Nicolaï, B., & East, A. (2016). Modelling the forced-air cooling mechanisms and performance of polylined horticultural produce. *Postharvest Biology and Technology, 120*, 23-35.

Singh, R. P., & Heldman, D. R. (2009). *Introduction to food engineering*. Elsevier/Academic Press, Amsterdam Gulf Professional Publishing.

Smitheram, D. (2018). *Design engineer for Milmeq, Personal communication.*

PAPER ID: 0034
DOI: 10.18462/iir.iccc.2018.0034

A QUICK, RELIABLE SOLUTION FOR MODELLING CHEESE CHILLING PROCESS

Duy HOANG, Simon LOVATT, James CARSON

University of Waikato
Private Bag 3105, Hamilton 3240, New Zealand, hoangduy2702@gmail.com

ABSTRACT

Optimisation of the refrigerating system for cheese processing requires an accurate prediction of chilling time, product temperature distributions and heat flow. Many existing CFD models can provide the best predictions by directly solving the three-dimensional heat transfer problem within the product and for air flow around the product; however, they are time-consuming and not suitable for routine use. A one-dimensional numerical solution proposed by Ghraizi, Chumak, Onistchenko, and Terziev (1996) has been used to provide the quick answer to food processing engineers with a good accuracy. In this method, the partial differential equation describing one-dimensional non-linear unsteady heat conduction inside the product has been solved by a finite difference technique. The method can take into account the temperature-dependence of thermal properties of foods and a general shape factor was used to reflect the product geometry. The model was applied to a single block of cheese, and agar. Predicted results are compared to experimentally-measured temperature profiles as well as to results generated by the Food Product Modeller, FPM, software.

Keywords: Modelling, chilling, heat transfer, cheese.

1. INTRODUCTION

Chilling is one of the most important part of the cold chain. Modelling heat transfer in the chilling process has a vital role in food process design and in improving food quality. Foods being processed are normally heterogeneous and have irregular shape. Thermoproperties are functions of food compositions and temperature. Therefore, the partial differential equation governing transient heat transfer is highly non-linear and difficult to solve. The accurate determination of the boundary conditions, especially the surface heat transfer coefficient, is also not easy.

The methods to model the heat transfer problem can be classified into analytical, empirical, and numerical solutions. Analytical techniques produce exact results when their underlying assumptions are fulfilled, but that is rarely the case. Their main usefulness is in providing benchmark results to verify other methods. Empirical formulas are derived with the objective of providing quick answers, with accuracy (usually ±10%) good enough for most industrial users. However, they are limited to situations similar to those used to derive and validate the formulas. Numerical methods can, in principle, provide near-exact predictions for almost any situation, although in practice their accuracy is limited by inadequate knowledge of the problem's parameters (product properties, geometry, flow characteristics) (Pham, 2008). In this research, we propose to use the one-dimensional numerical solution of (Ghraizi et al., 1996) to model heat transfer in the chilling processes of a single block of cheese and a block of agar.

2. MATERIAL AND METHODS

2.1 Experiments

A single block of cheese from Open Country Dairy and a block of agar (5% of agar powder, and 95% water) were selected for chilling experiments. The experiments were conducted in the chilling room at the AgResearch Ltd, Hamilton facility. The samples were placed in a styrene test chamber with a variable speed fan at the downstream end, and a fine net at the upstream end to even out the air flow.

In the first experiment, a block of agar in an acrylic plastic box having dimension of 135 x 270 x 210 mm was used. In the second experiment, a block of cheese having dimension of 180 x 360 x 280 mm, was tested in two different cases: with and without the carton (still in the polyethylene bag). Test samples were kept in a controlled temperature chamber to make them a uniform initial temperature before conducting chilling trials. Temperature was measured at the surfaces, and geometric center with T-type thermocouples connected to a Keysight 24972A data acquisition unit to record every one minute. The thermocouples were calibrated with the ice-point reference before and after measurements.

The cooling air temperature was measured by two different thermocouples placed above, and below the test block. Air velocity was measured at the data sampling frequency of 1 Hz using a hot-wire anemometer (Dantec 54N60 FlowMaster). The velocity sensor was placed at 5 cm above the middle of the top surface of the test blocks. The air velocity was kept constant during the experiment.

Figure 1: Experimental setup for temperature measurement
(a) agar, (b) cheese with carton, (c) cheese without carton

2.2 Numerical solution

The mathematical model of the heat transfer upon symmetric cooling was defined as a non-linear heat conduction equation with the corresponding boundary conditions, as follows: (Fikiin, 1996; Ghraizi et al., 1996)

$$C(T)\cdot\frac{\partial T(x,t)}{\partial t}=\frac{1}{x^{\Gamma}}\cdot\frac{\partial}{\partial x}\left[k(T)\cdot x^{\Gamma}\frac{\partial T(x,t)}{\partial x}\right] \tag{1}$$

$$T(x,0)=T_{in}(x) \tag{2}$$

$$\left.\frac{\partial(x,t)}{\partial x}\right|_{x=0}=0 \tag{3}$$

$$-k(T)\left.\frac{\partial T(x,t)}{\partial x}\right|_{x=R}=h\cdot\left[T(R,t)-T_a\right] \tag{4}$$

where, Eq. (1) is the Fourier heat conduction equation inside food products, Eq. (2) is the initial boundary equation, Eq. (3) is the symmetric boundary condition, and Eq. (4) is the third kind boundary condition. The shape factor, Γ, was generated based on the idea of substituting it into the governing equation of the one-dimensional solution, Eq. (1), such that, the numerical results will coincide or be satisfactory close to those obtained by solving the corresponding multidimensional problem. Fikiin (1996) proposed the formula of Γ as follows:

$$\Gamma=\frac{A\cdot R}{V}-1 \tag{5}$$

where, the characteristic length, R, is the half thickness of the shortest dimension. A, V are the heat transfer surface and the volumetric of the object, respectively.

The finite difference scheme is shown in Fig. 2, in which the (i,j)-point corresponding to $x = x_i$, $t = t_j$ is determined as follows:

$$x_i = x_{i-1} + \Delta x, \quad i = 1,2,\ldots,N, \quad \Delta x = \frac{R}{N}$$

$$t_j = t_{j-1} + \Delta t, \; j = 1,2\ldots$$

where the time step, Δt, and space increment, Δx, can be variable. Because of the temperature-dependence of thermoproperties, it is necessary to average those quantities in the vicinity (efgh) of each (i,j)-point to make the numerical solution to be more stable (Onishenko, Vjazovsky, & Gnatiuk, 1991). These local average values can be obtained by integrating the governing equation in the vicinity (efgh)

$$\iint_{efgh} x^{\Gamma} C(T) \cdot \frac{\partial T(x,t)}{\partial t} dx dt = \iint_{efgh} \frac{\partial}{\partial x}\left[k(T) \cdot x^{\Gamma} \frac{\partial T(x,t)}{\partial x} \right] dx dt \tag{6}$$

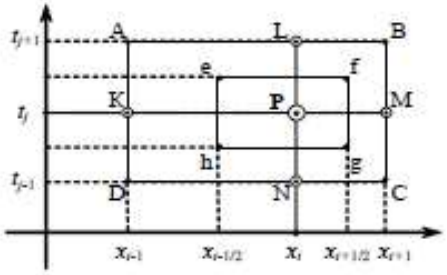

Figure 2: The finite different scheme

More details of the finite difference solution of Eq. (1-4) are presented in (Ghraizi et al., 1996), in which, the internal nodes were discretized by the central difference fomula, and the boundary nodes were approximated by the three-point backward/forward difference. The approximate system of linear algebraic equations therefore has the following form:

$$a_{ij} T_{ij} + b_{ij} T_{i-1,j} + e_{ij} T_{i+1,j} = d_{ij}, \quad i = 1,2,\ldots,N-1 \tag{7}$$

$$3T_{0j} - 4T_{1j} + T_{2j} = 0 \tag{8}$$

$$-k(T_{Nj}) \cdot \frac{3T_{Nj} - 4T_{N-1,j} + T_{N-2,j}}{2\Delta x} + h\left[T_a - T_{Nj}\right] = 0 \tag{9}$$

where

$$a_{ij} = \frac{C_{ij}}{\Gamma+1}\left[\left(x_i + \frac{\Delta x}{2}\right)^{\Gamma+1} - \left(x_i - \frac{\Delta x}{2}\right)^{\Gamma+1}\right] + \frac{\Delta t}{2\Delta x} k_{ij}^{2}\left(x_i + \frac{\Delta x}{2}\right)^{\Gamma} + \frac{\Delta t}{2\Delta x} k_{ij}^{1}\left(x_i - \frac{\Delta x}{2}\right)^{\Gamma}$$

$$b_{ij} = -\frac{\Delta t}{2\Delta x} k_{ij}^{1}\left(x_i - \frac{\Delta x}{2}\right)^{\Gamma}$$

$$e_{ij} = -\frac{\Delta t}{2\Delta x} k_{ij}^{2}\left(x_i + \frac{\Delta x}{2}\right)^{\Gamma}$$

$$d_{ij} = \left[\frac{C_{ij}}{\Gamma+1}\left\{\left(x_i+\frac{\Delta x}{2}\right)^{\Gamma+1}-\left(x_i-\frac{\Delta x}{2}\right)^{\Gamma+1}\right\}-\frac{\Delta t}{2\Delta x}\left\{k_{ij}^2\left(x_i+\frac{\Delta x}{2}\right)^{\Gamma}+k_{ij}\left(x_i-\frac{\Delta x}{2}\right)^{\Gamma}\right\}\right]T_{i,j-1}+$$
$$\frac{\Delta t}{2\Delta x}\lambda_{ij}^2\left(x_i+\frac{\Delta x}{2}\right)^{\Gamma}T_{i+1,j-1}+\frac{\Delta t}{2\Delta x}k_{ij}^1\left(x_i-\frac{\Delta x}{2}\right)^{\Gamma}T_{i-1,j-1}$$

C_{ij}, k_{ij}^1, k_{ij}^2 are the average volumetric heat capacity and thermal conductivities of the (i,j)-point, and are assumed to be the constant values

$$C_{ij} = (1/6)(C_K + C_P + C_M + C_C + C_N + C_D)$$

$$k_{ij}^1 = (1/6)(k_P + k_N + k_D + k_K + k_A + k_L)$$

$$k_{ij}^2 = (1/6)(k_P + k_L + k_B + k_M + k_C + k_N)$$

It can be noticed that the system of equations, Eq. (7-9) has the tridiagonal form, which can be solved by the tridiagonal matrix algorithm. Its solution is illustrated in the form of the recursion formula below:

$$T_{ij} = M_{i+1,j}T_{i+1,j} + N_{i+1,j}; i = 0,1,\ldots,N-1 \tag{10}$$

$$M_{i+1,j} = \frac{-e_{ij}}{a_{ij}+b_{ij}M_{ij}}; \; i = 1,2,\ldots,N-1 \tag{11}$$

$$M_{1,j} = \frac{a_1+4e_1}{3e_1-b_1} \tag{12}$$

$$N_{i+1,j} = \frac{d_{ij}-b_{ij}N_{ij}}{a_{ij}+b_{ij}M_{ij}}; \; i = 1,2,\ldots,N-1 \tag{13}$$

$$N_{1,j} = \frac{-d_1}{3e_1-b_1} \tag{14}$$

$$T_{Nj} = \frac{d_{N-1,j}-3T_a b_{N-1,j}\left(\frac{2\Delta xh}{3k(T_{Nj})}\right)-N_{Nj}\left(a_{N-1,j}+4b_{N-1,j}\right)}{M_{Nj}\left(a_{N-1,j}+4b_{N-1,j}\right)+e_{N-1,j}-3b_{N-1,j}\left(1+\frac{2\Delta xh}{3k(T_{Nj})}\right)} \tag{15}$$

In the procedure to determine the temperature profile at the j-th time layer, the algorithm needs to know temperatures at the $(j-1)$th, j-th and $(j+1)$th time layer to calculate the average thermoproperties of the (i,j)-point. Therefore, an iterative "prognosis-correction" regime (Fig. 3) was required (Ghraizi et al., 1996), in which, K is the number of iterations and the iterations are interrupted when the maximal difference between the temperature profiles, T_{ij}, of two consecutive iterations is less than a given tolerance, ε.

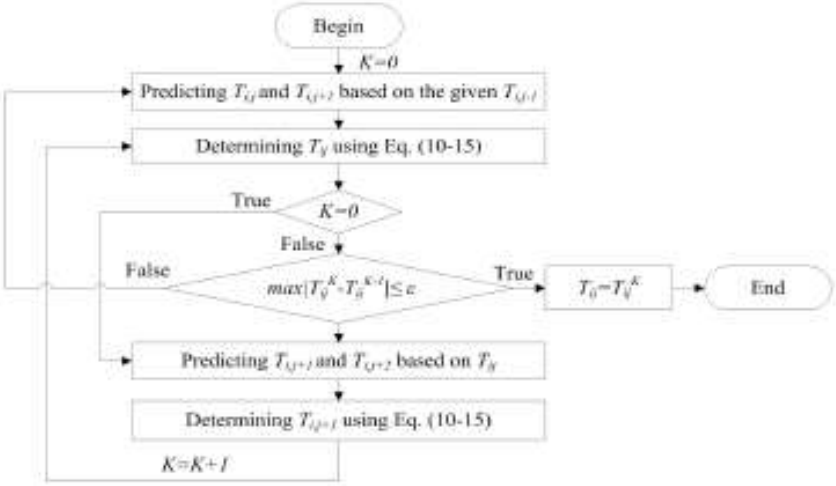

Figure 3: "Prognosis-correction" regime to determine T_{ij}

2.3 Thermal properties and heat transfer coefficient model

Thermoproperties of the test materials were determined as functions of food compositions and temperature. The thermal conductivity model was presented in (Dul'Nev & Novikov, 1977; Dul'nev & Novikov, 1991), the effective specific heat model was presented in (Hoang & Nguyen, 2013), and the density model was obtained from (ASHRAE, 2002). The compositions of cheese using in this calculation were 36.3% water, 23.5% protein, 34.1% fat, and 3.6% ash, while agar was assumed as the pure water.

The heat transfer coefficient, h, was determined from an estimate of the convective heat transfer that occurs between the surface of the food item and the cooling medium, and the thermal resistance of the packaged materials, and the air gap:

$$\frac{1}{h}=\frac{1}{h_{conv}}+\frac{\delta_{air}}{k_{air}}+\sum\frac{\delta_{pkg}}{k_{pkg}} \tag{16}$$

where the convective heat transfer coefficient was determined as a mean value of the convective heat transfer coefficients proposed by Pham, Lowry, Fleming, Willix, and Reid (1991) and Cleland and Earle (1976):

$$h_{conv}=\frac{(v\times 8.6)+(v\times 4.5+6.8)}{2}\times 1.12 \tag{17}$$

Thermal conductivities and thicknesses of the packaging materials and air gaps are shown in Table 1, and the predicted heat transfer coefficient in each chilling trial are shown in Table 2

Table 1.Thickness of packaging materials and air gap.

Sample	Thickness, mm			
	Acrylic plastic	Polyethylene	Air gap	Cardboard
	(k=0.2 $Wm^{-1}K^{-1}$)[a]	(k=0.33 $Wm^{-1}K^{-1}$)[a]	(k=0.026 $Wm^{-1}K^{-1}$)[b]	(k=0.078 $Wm^{-1}K^{-1}$)[b]
Agar	4.5	-	-	-
Cheese without carton	-	0.3	-	-
Cheese with carton	-	0.3	3	3

Source: [a]Singh, Burgess, and Singh (2008); [b] The Engineering Toolbox (n.d.)

3. RESULTS AND DISCUSSION

We conducted 4 trials with a single block of cheese and agar at the initial temperature, T_{in} = 20°C, the cooling air temperature, T_a = 0°C, and different air velocities. The simulated results of the one-dimensional numerical model (CFM) were compared to the predicted results of Food Product Modeller version 4 (FPM, AgResearch MIRINZ), using a three-dimensional simulation, and measured data. The surface temperature and the center temperature along the shortest axis were taken into this assessment exercise. Table 2 illustrates the mean absolute errors between measured and predicted data using CFM and FPM at different temperatures. The absolute errors were calculated by Eq. (18):

$$\Delta T = \left| T_{exp} - T_{mod} \right| \tag{18}$$

Table 2: Average absolute errors between measured data and predicted results

Chilling trials	R, m	Γ	v, ms^{-1}	h, Wm^{-2}K^{-1}	mean ΔT_{surf}		mean ΔT_{center}	
					CFM	FPM	CFM	FPM
Agar	0.063	1.100	3	16.3	0.14	0.73	0.73	0.43
Cheese without carton	0.090	1.143	2	18.2	1.99	1.11	0.64	0.58
Cheese with carton	0.090	1.143	1	4.1	-	-	0.35	0.18
			2	4.8	-	-	0.50	0.32

In general, the predicted results generated by CFM slightly worse than FPM. This is reasonable since FPM is the three-dimensional model while CFM is only the one-dimensional model. However, it was compensated by the much shorter solution time, since its number of nodes was much less than that of the three-dimensional FPM model. The maximum deviations between the measured temperatures and calculated values using CFM and FPM for single block of agar were 1.1°C and 1.0°C, respectively. For the single block of cheese, those numbers were 2.2°C and 1.4°C. Taking into account the uncertainty of the temperature sensors, those numbers are acceptable.

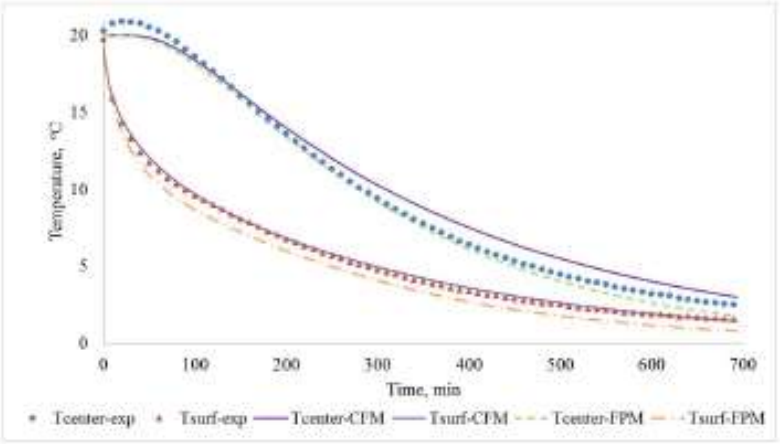

Figure 4: Plots of the temperatures predictions of CFM, FPM with experimental data for single block of agar

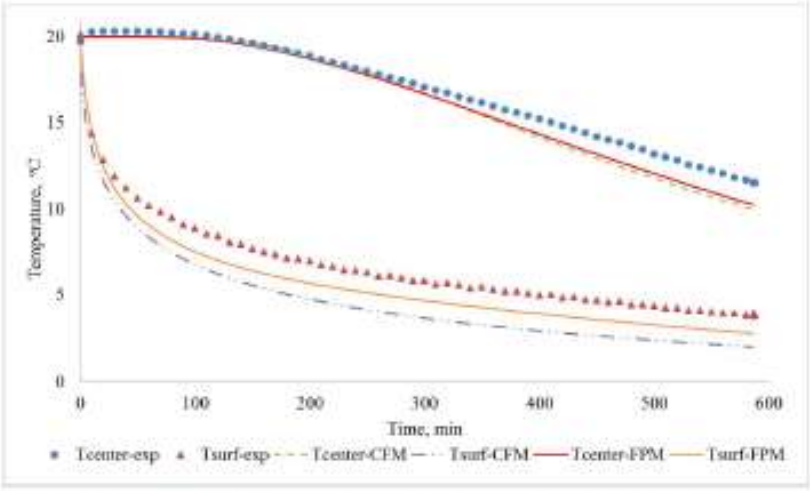

Figure 5: Plots of the temperatures predictions of CFM, FPM with experimental data for single block of cheese without carton

Fig. 4, and Fig. 5 illustrate comparisons between simulated results and experimental data for the chilling process of agar and cheese without the carton. The figures showed the good agreement between the prediction of CFM and the experimental data and the predicted values of FPM. Therefore, the one-dimensional numerical model (CFM) can be used to provide a quick answer with a sufficient confidence about the temperature distribution along the shortest characteristic dimension of a 3-D object, which represents the greatest interest for food engineering investigation. (Fikiin, 1996)

4. CONCLUSIONS

A one-dimensional numerical model for non-linear unsteady heat transfer of food products in the chilling process was presented. The model fits well with the experimental results and the predicted data of the three-dimensional model. Therefore, CFM could be a useful tool for food process design.

NOMENCLATURE

A	area of heat transfer surface (m^2)	R	characteristic length (m)
C	volumetric heat capacity ($Jm^{-3}K^{-1}$)	V	object volume (m^3)
k	thermal conductivity ($Wm^{-1}K^{-1}$)	v	air velocity (ms^{-1})
h	surface heat transfer coefficient ($Wm^{-2}K^{-1}$)	x	position (m)
T	temperature (K)	Δx	space increment (m)
t	time (s)	Γ	shape factor
Δt	time step (s)		
	Subscripts		
air	air gap	i	ith coordinate
a	ambient	j	jth time layer
cov	convective heat transfer	mod	model
exp	experiment	pkg	packaging
in	initial		

REFERENCE

ASHRAE. (2002). Handbook of Refrigeration. American Society of Heating, Refrigerating, and Air Conditioning Engineers, Atlanta.

Cleland, A. C., & Earle, R. L. (1976). A new method for prediction of surface heat transfer coefficients in freezing. Bulletin. Annex-International Institute of Refrigeration (IIR). Refrigeration Science and

Technology. 1976-1.

Dul'Nev, G. N., & Novikov, V. V. (1977). Effective conductivity of systems with interpenetrating components. Journal of Engineering Physics and Thermophysics, 33(2), 923-925.

Dul'nev, G. N., & Novikov, V. V. (1991). Transfer processes in inhomogeneous media. Energoatomizdat, Leningrad, 248.

Fikiin, K. A. (1996). Generalized numerical modelling of unsteady heat transfer during cooling and freezing using an improved enthalpy method and quasi-one-dimensional formulation. International Journal of Refrigeration, 19(2), 132-140.

Ghraizi, J. A., Chumak, I. G., Onistchenko, V. P., & Terziev, G. S. (1996). Mathematical model of various freezing processes of fish and fish-products. Science et technique du froid, 379-386.

Hoang, K. D., & Nguyen, V. D. (2013). Effective Specific Heat for Camranh Mango. Paper presented at the The 3rd International Conference on Sustainable Energy, "RISE towards a Green Future", Ho Chi Minh City, Vietnam.

Onishenko, V. P., Vjazovsky, V. P., & Gnatiuk, P. G. (1991). The calculation of the processes of refrigeration technology at the foodstuff processing on the processing line. Paper presented at the International Congress of Refrigeration, Montreal, Quebec, Canada.

Pham, Q. T. (2008). Modelling of freezing processes. In J. A. Evans (Ed.), Frozen food science and technology: Blackwell Publishing.

Pham, Q. T., Lowry, P. D., Fleming, A. K., Willix, J., & Reid, C. M. (1991). Thawing and tempering of cartoned meat and meat cuts. MIRINZ Technical Report Series (New Zealand).

Singh, S. P., Burgess, G., & Singh, J. (2008). Performance comparison of thermal insulated packaging boxes, bags and refrigerants for single - parcel shipments. Packaging Technology and Science, 21(1), 25-35.

Improved prediction of thermal conductivity of frozen foods

Duy K Hoang, Simon J Lovatt, James K Carson
University of Waikato, Private Bag 3105, Hamilton, New Zealand

Abstract

Thermal conductivity is an important physical property for performing heat transfer calculations. The thermal conductivity of foods has a strong dependence on temperature during the freezing process, which has posed a challenge to those attempting to develop a generic model that can be applied to any food likely to be frozen. Ideally, thermal property models should not incorporate any empirical parameters whose value would need to be determined by a thermal conductivity measurement (since this may defeat the purpose of the model). Instead it should be possible to perform a prediction based only on composition data, in terms of the major food components. Previously, prediction methods incorporating Levy's effective thermal conductivity model have been recommended for modelling thermal conductivity in the freezing range, particularly for meat products. However, in this study the thermal conductivity predictions from a little-known model developed by Russian researchers have been compared to predictions by other models (including Levy's model) against measured thermal conductivity data over a range of temperatures. On average, the Russian model provided the most accurate thermal conductivity predictions.

Keywords
Thermal conductivity, frozen foods

1. Introduction
Thermal conductivity is a key thermal parameter for modelling freezing process, since it influences the rate of heat transfer from the center to the surface of the product. Although there are many reports on thermal conductivity data for some particular foods in the literature [1, 12, 13, 14, 17], there can be high variation in reported data. This may be due to the different conditions at which the property was measured and the differences due to the origin, composition, and structure of the food that may not be included with the measured thermal conductivity data [11]. This can make it difficult to match literature data to foods for which thermal conductivity data are required for process design purposes, or to find literature data that covers the temperature range required for design. Therefore, it is often preferable to use prediction models to estimate the thermal conductivity of foods. There are literally hundreds of thermal conductivity models in the literature, many of which are purely empirical, which limits their range of applicability. Others have theoretical bases but contain some empirical parameters whose values must be determined empirically [2,15]. Relatively few solely require the food's composition data and thermal conductivities of the major food components as inputs for the model [2]. The aim of this paper is to introduce an effective thermal conductivity model for a wide range of food products that is based on composition data and provides a significant improvement in prediction accuracy in comparison to other methods.

2. Thermal conductivity models.
The simplest models that meet the criteria of this study are the Series, Parallel and Geometric models. The Series model corresponds to the weighted harmonic mean of the thermal conductivities of the food components [14]:

$$k_s = \frac{1}{\sum_i \frac{v_i}{k_i}} \quad (1)$$

where k_i is the thermal conductivity of the ith components; and v_i is the volumetric fraction of the ith food component estimated from mass fractions and densities:

$$v_i = \frac{\frac{x_i}{\rho_i}}{\sum_i \frac{x_i}{\rho_i}} \quad (2)$$

Thermal conductivities and densities of major food components as a function of temperature (°C) are shown in Table 1 [18]. The Parallel model corresponds to the weighted arithmetic mean of the thermal conductivities of the components [15].

$$k_e = \sum_i k_i v_i \tag{3}$$

The Geometric model is the weighted geometric mean of the thermal conductivity of the components of the foods [15]

$$k_e = \prod_i k_i^{v_i} \tag{4}$$

Table 1: Thermal conductivities and densities of major food components (-40 ≤ t ≤ 150°C) [1,2,18]

Component	Thermal conductivity, W m^{-1} K^{-1}	Density, kg m^{-3}
Protein	k_p =0.17887+1.1958×10^{-3}t–2.7178×10$^{-6}t^2$	ρ_p = 1.3299×10^3–5.1840×10^{-1}t
Fat	k_f =0.18071-2.7604×10^{-3}t–1.7749×10$^{-7}t^2$	ρ_f = 9.2559×10^2t–5.1757×10^{-1}t
Carbohydrate	k_{CHO} = 0.20141+1.3874×10^{-3}t–4.3312×10$^{-6}t^2$	ρ_{CHO} = 1.5991×10^3t–3.1046×10^{-1}t
Fiber	k_{fi} = 0.18331+1.2497×10^{-3}t–3.1683×10$^{-6}t^2$	ρ_{fi} = 1.3115×10^3t–3.6589×10^{-1}t
Ash	k_{ash} = 0.32962+1.4011×10^{-3}t–2.9069×10$^{-6}t^2$	ρ_{ash} = 2.4238×10^3t–2.8063×10^{-1}t
Water	k_w = 0.57109+1.7625×10^{-3}t–6.7603×10$^{-6}t^2$	ρ_w= 9.9718×10^2+3.1439×10^{-3}t–3.7574×10$^{-3}t^2$
Ice	k_{ice} = 2.2196-6.2489×10^{-3}t+1.0154×10$^{-4}t^2$	ρ_{ice}= 9.1689×10^2–1.3071×10^{-1}t
Air	k_{Air} = 2.364×10^{-2} +7.2822×10^{-5}t	ρ_{Air}= 353/(t+273.15)

The Parallel and Series model represent the theoretical bounds of the thermal conductivity of heterogeneous materials such as foods[4], in which the Series model provides the lower limit and the Parallel model provides the upper limit.

Two other models that can predict the effective thermal conductivity of a food product based only on food composition are the Effective Medium Theory model (EMT) [9]:

$$\sum_i v_i \frac{k_i - k_e}{k_i + 2k_e} = 0 \tag{5}$$

and the Co-continuous model (CC) [16]:

$$k_e = \frac{\sum_i \frac{v_i}{k_i}}{2}\left(\sqrt{1+\frac{8\sum_i k_i v_i}{\sum_i \frac{v_i}{k_i}}}-1\right) \tag{6}$$

The EMT model represents a structure where all components are mutually dispersed while the CC model represents a structure where all components form continuous phases [4].

For frozen foods without air voids, Pham and Willix [13] and Fricke and Becker [8] recommended the use of Levy's model [10] to account for the presence of ice:

$$k_{Levy} = k_{ice}\frac{2k_{ice}+k_{mix}-2(k_{ice}-k_{mix})F}{2k_{ice}+k_{mix}+(k_{ice}-k_{mix})F} \tag{7}$$

$$F = \frac{2/G-1+2(1-v_{ice})-\sqrt{[2/G-1+2(1-v_{ice})]^2-8(1-v_{ice})/G}}{2} \tag{8}$$

$$G = \frac{(k_{ice}-k_{mix})^2}{(k_{ice}+k_{mix})^2+k_{ice}k_{mix}/2} \tag{9}$$

where, k_{mix}, is thermal conductivity of all the components excluding ice, calculated using the Parallel model (Eq. 3).

For, porous foods, the air void must be considered in addition to ice, water, and other components. As the thermal conductivity of air is very low compared to that of the other components, porosity has a large influence on the effective thermal conductivity of foods, especially frozen foods [5]. In order to incorporate the influence of the air phase on the effective thermal conductivity of frozen foods if nothing is assumed to be known about its structure, Carson et al [4] recommended a multi-step procedure using the EMT model in the following forms:

$$k_{EMT}^{up} = \frac{(3v_a-1)k_a + \left[3(1-v_a)-1\right]k_{u,np} + \sqrt{\left\{(3v_a-1)k_a + \left[3(1-v_a)-1\right]k_{u,np}\right\}^2 + 8k_{u,np}k_a}}{4} \quad (10)$$

$$k_{EMT}^{fp} = \frac{(3v_a-1)k_a + \left[3(1-v_a)-1\right]k_{f,np} + \sqrt{\left\{(3v_a-1)k_a + \left[3(1-v_a)-1\right]k_{f,np}\right\}^2 + 8k_{f,np}k_a}}{4} \quad (11)$$

Equations (10) and (11) represent the two-component forms of Eq.(5) for the unfrozen, porous and the frozen, porous foods respectively [4], in which, $k_{u,np}$ is the thermal conductivity of the unfrozen, non-porous food determined by the Parallel model and $k_{f,np}$ is the thermal properties of the frozen, non-porous foods determined by Levy's model.

The Maxwell-Eucken model may be used when a dispersion of one phase forms within a continuous phase [4]. If air forms a dispersed phase within a food, this model has the following form:

$$k_{ME1} = k_{f,np}\frac{2k_{f,np} + k_a - 2\left(k_{f,np} - k_a\right)v_a}{2k_{f,np} + k_a + \left(k_{f,np} - k_a\right)v_a} \quad (12)$$

If air forms the continuous phase then the following form of the Maxwell-Eucken model is employed

$$k_{ME2} = k_{f,np}\frac{2k_a + k_{f,np} - 2\left(k_a - k_{f,np}\right)(1-v_a)}{2k_a + k_{f,np} + \left(k_a - k_{f,np}\right)(1-v_a)} \quad (13)$$

Dul'nev and Novikov [7] introduced a procedure to estimate the effective thermal conductivity of any heterogeneous material (such as a food product) in which components are considered to be "mutually penetrating". In this model, a food is considered to consist of water, ice, solids (ash, protein, fiber, carbohydrate and fat), and air. The effective thermal conductivity of the food product is determined by a three-step procedure. In the first step, the thermal conductivity of the solid phase is calculated from the ash, protein, fiber, carbohydrate and fat fractions using the Parallel model (Eq. 3), and the thermal conductivity of the medium that surrounds each *i*th component is determined using Eq. (14):

$$L_i = \frac{\sum_{j\neq i} k_j v_j}{\sum_{j\neq i} v_j} \quad (14)$$

In the second step, the thermal conductivities of the binary systems consisting of the *i*th component (thermal conductivity k_i with volume fraction v_i) and the medium around it (thermal conductivity L_i with volume fraction $1\text{-}v_i$) are determined using the following relationship [6]

$$K_i = k_{max}\left\{c^2 + \lambda(1-c)^2 + \frac{2\lambda c(1-c)}{\lambda c + 1 - c}\right\} \quad (15)$$

where, $\lambda = k_{min} / k_{max}$, $k_{min} = \min(k_i, L_i)$, $k_{max} = \max(k_i, L_i)$, and the value of c is related to the volume fraction, m, of the component which has a smaller thermal conductivity by Eq. (16):

$$c = 0.5 + A\cos\frac{\varphi}{3} \quad (16)$$

where:

$$A = \begin{cases} -1, & m \le 0.5 \\ 1, & m > 0.5 \end{cases}$$

$$\varphi = \begin{cases} 2\pi - X, & X > 0 \\ 2\pi + X, & X \le 0 \end{cases}$$

$$X = \arctan\sqrt{\frac{1-(2m-1)^2}{|2m-1|}}$$

Finally, the thermal conductivity of the whole system is estimated by Eq. (17):

$$k = \sum_i k_i \frac{K_i - L_i}{k_i - L_i} \tag{17}$$

3. Comparison of model predictions and measured data

The criteria for selecting data used in this evaluation were that the food composition and initial freezing temperature were available, and the measurement methodology was proven to be accurate. The thermal conductivity data for non-porous foods were obtained from Willix et al. [17] and the data for porous frozen foods were taken from Cogné et al. [5]. The reliability of those data was assessed using a method described by Carson [3].

3.1 Non-porous foods

Table 2 shows the mean absoulute relative error (Eq. 18) between model predictions and experimental data for non-porous foods over a range of temperatures.

$$\delta = \frac{\left|k_{exp} - k_{mod}\right|}{k_{exp}} \times 100\% \tag{18}$$

Table 2: Comparison of the absolute relative errors between predicted and experimental thermal conductivity values for non-porous foods (experimental data from Willix et al. [17])

Material	Mean absolute relative error, %							Temp. range, °C	
	Parallel	Series	Geometric	Co-Continuous	EMT	Levy	Dulnev & Novikov	Low	High
Lean beef	17.8	35.1	6.2	7.3	7.2	4.6	2.9	-39	37
Beef mince	54.7	30.9	9.2	13.4	30.5	29.5	19.7	-39	38
Boneless Chicken	26.6	41.3	5.5	8.0	13.1	7.8	3.0	-39	16
Pork sausage meat	31.0	37.5	6.6	4.0	10.2	11.8	7.1	-40	37
Venison	27.4	27.1	4.3	6.8	16.4	14.4	7.3	-33	36
Gurnard fillets	12.7	34.3	7.1	9.1	5.1	2.1	4.4	-39	37
Lemon fish fillets	24.9	31.0	5.1	6.6	14.9	11.2	7.6	-38	37
Snapper fillets	24.2	29.5	2.8	5.5	14.3	11.4	4.7	-40	37
Tarakihi fillets	25.0	29.3	2.3	5.1	14.9	12.2	5.3	-39	37
Trevally fillets	15.1	32.9	6.2	8.0	6.0	5.4	3.8	-37	39
Cheddar cheese	14.8	40.3	22.9	10.7	16.2	6.9	10.8	-39	26
Edam cheese	11.1	41.7	23.9	12.8	16.5	11.4	12.5	-38	26
Mozzarella cheese	22.1	45.1	22.9	10.8	12.0	6.1	8.5	-39	22
Mean of all materials	**23.6**	**35.1**	**9.6**	**8.3**	**13.6**	**10.4**	**7.5**		

On average the Dul'nev & Novikov model provided the most accurate predictions. The Parallel and Series models produced very large average prediction errors, while most of the other models showed good agreement with the experimental data, with the average mean relative error between model prediction and experimental data for all the materials not exceeding 15%.

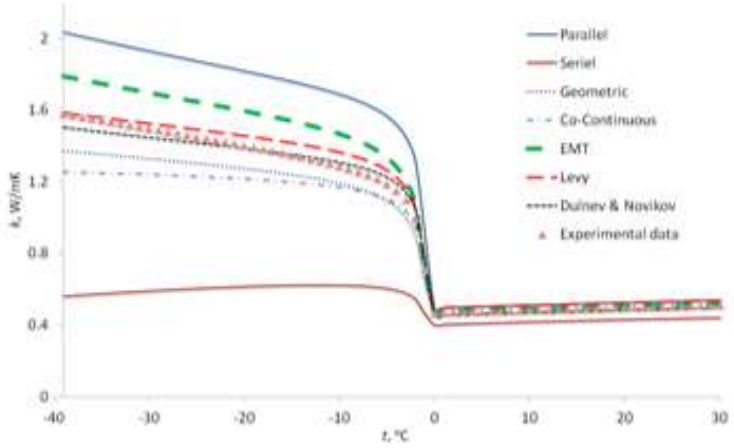

Figure 1. Comparison between experimental data and the thermal conductivity predictions of different models for lean beef

Figure 1 shows plots of thermal conductivity predictions of the models compared with experimental data for lean beef. It can be seen from Figure 1 that the Parallel model significantly over-predicted thermal conductivity, while the Series model significantly under-predicted thermal conductivity. The Levy model and Dul'nev and Novikov model provided better predictions than other models in the freezing range. All models predicted thermal conductivity with greater accuracy in the unfrozen domain than in the frozen domain.

3.2 Porous foods

Table 3 shows the differences between the model predictions and experimental thermal conductivity data of ice cream [5] with different porosities at -20°C and -30°C.

Table 3: Comparison of the differences between predicted and experimental thermal conductivity values for ice cream (experimental data from Cogné et al. [5])

Porosity	Parallel	Series	Geometric	Co-continuous	EMT	Dul & Nov	Multi-step Method [4]	
							EMT	ME1
				-20 °C				
0.13	49.71	85.10	35.87	40.25	4.01	0.57	0.32	1.65
0.23	56.07	88.73	47.94	46.05	4.83	0.05	3.04	1.59
0.33	68.47	89.71	55.52	46.05	14.00	3.24	5.70	5.39
0.41	70.26	90.27	62.14	47.11	28.19	0.71	15.16	3.39
0.46	78.90	89.95	63.96	44.85	34.85	3.50	18.95	6.74
0.6	102.46	88.06	67.51	36.19	55.58	9.85	39.58	15.57
0.67	111.29	86.47	68.53	30.85	63.69	10.82	53.19	18.44
Average	**76.7**	**88.3**	**57.4**	**41.6**	**29.3**	**4.1**	**19.4**	**7.5**
				-30 °C				
0.13	51.62	86.40	36.97	42.22	5.90	0.27	0.20	1.14
0.23	54.63	89.94	50.38	49.04	5.42	3.06	5.69	1.15
0.33	68.62	90.74	57.54	48.55	14.14	1.05	7.46	3.57
0.41	69.85	91.27	64.23	49.73	29.20	1.71	17.19	1.24
0.46	70.36	91.39	67.63	49.97	39.24	3.53	24.65	0.25
0.6	105.97	89.07	69.18	38.13	57.51	9.64	41.06	15.30
0.67	106.25	88.10	71.51	35.64	67.31	6.28	57.10	13.31
Average	**75.3**	**89.6**	**59.6**	**44.8**	**31.2**	**3.6**	**21.9**	**5.1**

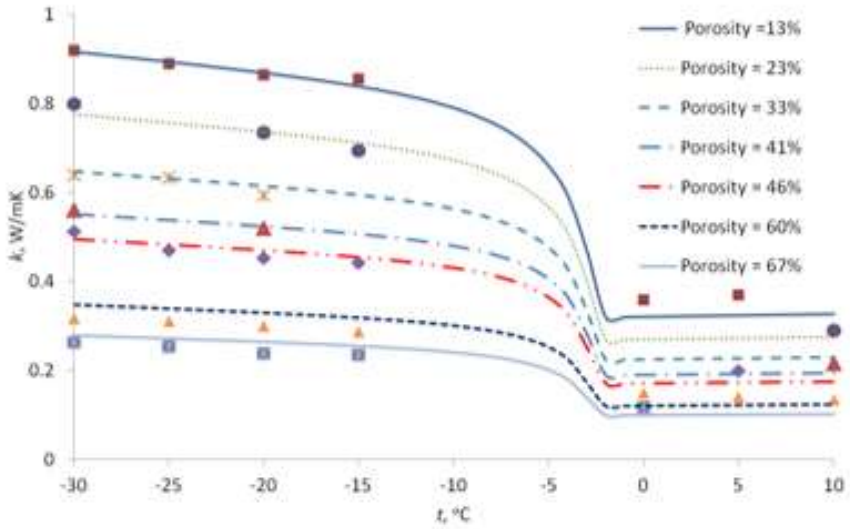

Figure 2: Comparison between thermal conductivity data and predictions of Dulnev and Novikov model for ice cream

Once again the Dul'nev and Novikov model provided the greatest accuracy with an average relative error of 4.1 %. The Maxell-Eucken model with air as the dispersed phase also gave a good agreement with the experimental data. This can be explained by the fact that the air phase was dispersed in other phases in the structure of ice cream. Figure 2 presents a comparison between Dul'nev and Novikov model predictions and the experimental data of Cogné et al. [5] as a function of temperature and different air porosities. The model tended to predict the thermal conductivity of frozen ice cream (relative errors about 5%) with less error than that with unfrozen ice cream (relative errors around 15%).

4. Conclusions.

An assessment of selected composition-based thermal conductivity models for foods was presented. Compared to other models, the Dul'nev and Novikov model has shown superior performance in thermal conductivity predictions for both porous and non-porous foods. Therefore, it is recommended as the best model for thermal conductivity for food products.

References

1. ASHRAE. (2002). Handbook of Refrigeration. *American Society of Heating, Refrigerating, and Air Conditioning Engineers, Atlanta*
2. Carson, J. K. (2011). Predictive modelling of thermal properties of foods.
3. Carson, J. K. (2017). Use of simple thermal conductivity models to assess the reliability of measured thermal conductivity data. *International Journal of Refrigeration, 74*, 456-462.
4. Carson, J. K., Wang, J., North, M. F., & Cleland, D. J. (2016). Effective thermal conductivity prediction of foods using composition and temperature data. *Journal of Food Engineering, 175*, 65-73.
5. Cogné, C., Andrieu, J., Laurent, P., Besson, A., & Nocquet, J. (2003). Experimental data and modelling of thermal properties of ice creams. *Journal of Food Engineering, 58*(4), 331-341.
6. Dul'Nev, G., & Novikov, V. (1977). Effective conductivity of systems with interpenetrating components. *Journal of Engineering Physics and Thermophysics, 33*(2), 923-925.
7. Dul'nev, G., & Novikov, V. (1991). Transfer processes in inhomogeneous media. *Energoatomizdat, Leningrad, 248*
8. Fricke, B. A., & Becker, B. R. (2001). Evaluation of thermophysical property models for foods. *HVAC&R Research, 7*(4), 311-330.
9. Landauer, R. (1952). The electrical resistance of binary metallic mixtures. *Journal of Applied Physics, 23*(7), 779-784.

10. Levy, F. (1981). A modified Maxwell-Eucken equation for calculating the thermal conductivity of two-component solutions or mixtures. *International Journal of Refrigeration, 4*(4), 223-225.
11. Nesvadba, P. (2005). Thermal properties of unfrozen foods. *Engineering properties of foods, 3*, 149-173.
12. Nesvadba, P., Houška, M., Wolf, W., Gekas, V., Jarvis, D., Sadd, P., & Johns, A. (2004). Database of physical properties of agro-food materials. *Journal of Food Engineering, 61*(4), 497-503.
13. Pham, Q., & Willix, J. (1989). Thermal Conductivity of Fresh Lamb Meat, Offals and Fat in the Range -40 to +30 °C: Measurements and Correlations. *Journal of Food Science, 54*(3), 508-515.
14. Rahman, M., & Al-Saidi, G. (2009). Thermal conductivity prediction of foods. *Food properties handbook, 2nd ed. Rahman, MS (ed.). CRC Press, Boca Raton, FL*
15. Rahman, M. S. (2009). *Food properties handbook*: CRC press.
16. Wang, J., Carson, J. K., North, M. F., & Cleland, D. J. (2008). A new structural model of effective thermal conductivity for heterogeneous materials with co-continuous phases. *International journal of heat and mass transfer, 51*(9), 2389-2397.
17. Willix, J., Lovatt, S., & Amos, N. (1998). Additional thermal conductivity values of foods measured by a guarded hot plate. *Journal of Food Engineering, 37*(2), 159-174
18. Choi, Y., and Okos. M. R., 1986, "Effects of Temperature and Composition on the Thermal Properties of Foods." In Food Engineering and Process Applications 1:93-101. London: Elsevier Applied Science Publishers.